UNIVERSITY OF CAMBRIDGE

Human Parainfluenza Virus 3: Genetic Diversity, Virulence and Antiviral Susceptibility

This dissertation is submitted for the degree of Doctor of Philosophy

Anna Alexandra Smielewska
Division of Virology
Department of Pathology
University of Cambridge

Lucy Cavendish College

Date:
June 2018

Human parainfluenza virus 3: genetic diversity, virulence and antiviral susceptibility

Anna Alexandra Smielewska

Human parainfluenza 3 (HPIV3) is a member of the *Paramyxoviridae*, a single strain negative-sense non-segmented RNA virus in the order *Mononegavirales*. It is a respiratory pathogen with a broad spectrum of presentations for which there is currently neither a vaccine nor licensed treatment for HPIV3.

To date most research on HPIV3 has been conducted using significantly culture adapted reference strains. Therefore, minimally adapted clinical strains were grown in two cell culture systems: immortalised and primary. Plaque phenotype, growth kinetics and inflammatory response triggered were evaluated and it was found that there is a range of phenotypes exhibited by clinical strains with potential implications *in vivo*.

To examine the genetic diversity of circulating strains of HPIV3 in the UK, a new amplicon based sequencing pipeline for whole genome sequencing of HPIV3 was developed and validated. A short hypervariable region in the HPIV3 genome was identified and evaluated as a potential candidate for subsequent phylogenetic analysis compared to whole genome data. This method was then applied to tracking an HPIV3 outbreak that took place on a paediatric oncology ward. It was found to be a point-source outbreak and the clinical impact in this setting, as well as the infection control procedures involved were evaluated.

Finally a robust *in vitro* model for the evaluation of potential therapeutic candidates for HPIV3, based on a panel of minimally passaged clinical strains as well as a culture-adapted reference strain, was set up. This model was applied to three potential inhibitors of HPIV3: ribavirin, favipiravir and zanamivir. The results showed that clinical strains were at least as susceptible to ribavirin and favipiravir as the laboratory reference strain and significantly more susceptible to zanamivir. This indicates that further work on minimally adapted clinical strains is essential to further the understanding of this important virus.

Copyright statement

This dissertation is the result of my own work and includes nothing, which is the outcome of work done in collaboration except as declared in the Preface and specified in the text.

It is not substantially the same as any that I have submitted, or, is being concurrently submitted for a degree or diploma or other qualification at the University of Cambridge or any other University or similar institution except as declared in the Preface and specified in the text. I further state that no substantial part of my dissertation has already been submitted, or, is being concurrently submitted for any such degree, diploma or other qualification at the University of Cambridge or any other University or similar institution except as declared in the Preface and specified in the text

It does not exceed the prescribed word limit for the relevant Degree Committee.

Publication arising from this thesis

Smielewska, A. et al. (2018) 'In vitro sensitivity of human parainfluenza 3 clinical isolates to ribavirin, favipiravir and zanamivir', Journal of Clinical Virology. Elsevier, 102(January), pp. 19–26. doi: 10.1016/j.jcv.2018.02.009.

Acknowledgements

First and foremost I would like to thank Public Health England (PHE) for funding me, and University of Cambridge for giving me the opportunity to conduct this research.

I would like to thank my supervisors for all their support and guidance over these years: Professor Ian Goodfellow for the scientific acumen and uncompromising approach to my work and Dr Hamid Jalal for his help in grounding my work in a clinical context and encouraging me to pursue research in the first place.

I would particularly like to thank Dr Edward Emmott for teaching me the practical skills needed for my research, for showing me the ropes, for his unending patience and understanding and above all for being an invaluable friend.

I would also like to thank all the members of the Goodfellow lab and the Division of Virology. A particular mention should go to Dr Frederic Sorgeloos for his knowledge and advice, as well as his unparalleled skills with the 3D printer, which allowed him to make the plastic plate inserts that were used for all my plaque imaging.

Next generation sequencing was conducted by Dr Kim Brugger, Medical Genetics, CUH, and this project would not have been possible without his help. I am very grateful to him.

Dr Kyriaki Ranellou and Dr Kate Rolfe conducted the pilot project that preceded my PhD and I am very grateful to them for giving me a head start.

Dr Lauren Parker from the Barclay Lab, Imperial College London taught me how to handle human airway epithelial cells and kindly shared some of her protocols that allowed me to complete my work with the primary cell line.

Dr Rainer Doffinger and Dr Sophie Davies from the Department of Immunology (CUH) guided me through the process of cytokine measurements and I am indebted to them for their time and their patience.

Callum Pearson and the rest of the team Eastern Field Epidemiology Unit, Institute of Public Health, CUH, conducted the outbreak transmission mapping; it was a privilege to learn from the experts.

The paediatric oncology and infection control teams, Addenbrooke's Hospital, were involved in the management of the outbreak in the summer of 2017. I would like to thank them for their time and dedication.

Additionally I am very grateful to my tutor Dr Jane Greatorex for her wisdom and support, as well as to my college, Lucy Cavendish over the last three years. I would also like to thank my mentor, Dr Chris Smith for his unwavering encouragement.

Last but not least, I have to thank my family, who have always reminded me of the truly important things in life.

Table of contents

Table of figures

Table of tables

Abbreviations

293T	Human embryonic kidney cell line
A549	Human lung carcinoma epithelial cell line
aa	Amino acid
ABGD	Automatic Barcode Gap Discovery
AGKM	African Green Kidney Monkey cell line
ALCL	Anaplastic large cell lymphoma
ALL	Acute lymphocytic leukaemia
AML	Acute myeloid leukemia
ASPV	Atlantic salmon parainfluenza virus
BEK	Bovine embryonic kidney cell line
bp	Base pair
BPIV	Bovine parainfluenza virus
BSC-1	Monkey African green kidney epithelial cell line
BVDV Npro	Bovine viral diarrhoea virus N-terminal protease fragment
CCHF	Congo Crimean Haemorragic Fever
CD46	Membrane cofactor protein (inhibitory complement receptor)
CD55	Complement decay accelerating factor (also known as DAF)
CF	Cystic fibrosis
CHEQS	Clever Health Environment Quality & Safety
CNS	Central nervous system
CO_2	Carbon dioxide
COPD	Chronic obstructive pulmonary disease
cp45	Cold passage 45 (vaccine strain of HPIV3)
CPE	Cytopathic effect
CUH	Cambridge University Hospitals
CV-1	Normal African Green Monkey Kidney Fibroblast Cells
D	Structural domain of F protein of HPIV3
DAB	3,3′-Diaminobenzidine

DAS181	A sialidase fusion protein inhibitor
DD gate	Doublet Discrimination
DMEM	Dulbecco's Modified Eagle's Medium
dpi	Dots per inch
EC_{50}	Effective concentration 50%; dose of drug that gives 50% maximal response
EC_{90}	Effective concentration 90%; dose of drug that gives 90% maximal response
Eotaxin/CCL11	Eosinophil chemotactic protein
ESS	Effective Sample Size
F	Fusion protein
F_0	Uncleaved precursor form of fusion protein
F_1	Cleaved active part of fusion protein 1
F_2	Cleaved active part of fusion protein 2
FBS	Fetal bovine serum
FDA	Food and Drug Administration
FDR	False discovery rate
FVP	Favipiravir
GM-CSF	Granulocyte-macrophage colony-stimulating factor
GRB2	Growth factor receptor-bound protein 2
GRO-α/CXCL1	Chemokine (C-X-C motif) ligand 1
GTP	Guanosine-5'-triphosphate
GTR	Generalised time reversible model
HAE	Human airway epithelial cell line
Hep2	Human epithelial type 2 cells
HIV	Human immunodeficiency virus
HMPV	Human metapneumovirus
HN	Haemagglutinin-neuraminidase
HPIV1	Human Parainfluenza virus type 1
HPIV2	Human parainfluenza virus type 2
HPIV3	Human parainlfuenza virus type 3
HPIV4	Human parainfluenza virus type 4
HPIVs	Human parainfluenza viruses

HR	Heptad repeat
HRP	Horseradish peroxidase
HSCT	Haemapoetic stem cell transplant
ICU	Intensive care unit
IFNα	Interferon alpha
IFNβ	Interferon beta
IFNγ	Interferon gamma
IgA	Immunoglobulin A
IgG	Immunoglobulin G
IL-xx	Interleukin xx
IMDPH	Inosine-5′-monophosphate dehydrogenase
IMP	Inosine-5′-monophosphate
IP-10/CXCL-10	Interferon gamma induced protein 10
IRF3	Interferon regulatory transcription factor 3
JIKI (trial)	Experimental Treatment with Favipiravir for Ebola Virus Disease (trial) (Jiki = hope in Kissi language)
JS	HPIV3 reference strain, first isolated in 1980s
KNIME	Konstanz Information Miner
L	Large polymerase
LLC-MK2	Rhesus monkey (macaca mulatta) kidney cell line
LRT	Lower respiratory tract
LRTI	Lower respiratory tract infection
MAPK/ERK	Mitogen-activated protein kinases (originally called ERK)/extracellular signal-regulated kinases pathway
MCMC	Markov Chain Monte Carlo
MCP-1/CCL2	Monocyte chemotactic protein 1
MDA5	MDA5 (Melanoma Differentiation-Associated protein 5), a pattern recognition receptor
MDBK	Bovine kidney cell line
MDCK	Madin-Darby Canine Kidney cell line
MeV	Measles virus
MIG	Monokine induced by gamma interferon (CXCL9)
MIP-1α	Macrophage inflammatory protein 1 alpha

MIP-1β	Macrophage inflammatory protein 1 beta
MK9	HPIV3 reference strain, supplied by PHE, UK,
MOI	Multiplicity of infection
mRNA	Messenger RNA
MuV	Mumps virus
NCBI	National Centre for Biotechnology Information
NDV	Newcastle disease virus
NGS	Next generation sequencing
NHS	National Health Service
NP	Nuclear protein
NPA	Nasopharyngeal aspirate
P	Phosphoprotein
P/C/V/D	Alternative proteins coded for by the phosphoprotein (P) genome of paramyxoviruses
PBS	Phosphate buffered saline
PCR	Polymerase chain reaction
PDU	Paediatric day unit
PFU	Plaque-forming unit
pH	Potential of hydrogen (measure of aciditiy or alkalinity of a substance)
PHE	Public Health England
PICU	Paediatric intensive care unit
PIV5	Parainfluenza virus 5
PIV5 V	Parainfluenza virus 5 protein V
PKR	Protein kinase RNA-activated interferon-induced/ double-stranded RNA-activated protein kinase
PLC/PRF5	Human Alexander hepatoma cell line
PMH	Past medical history
PS	Path Sampling
qPCR	Quantitative polymerase chain reaction
QUASR	Quantify and Annotate short reads in R
R^2	Coefficient of determination, a measure of the correlation between the dependent and independent variable

RANTES	"Regulated on activation, normal T cell expressed and secreted" (a chemokine) (also known as CCL5)
RBV	Ribavirin
RdRp	RNA-dependent RNA-polymerase
RIG-I	Retinoic acid-inducible gene I (a pattern recognition receptor)
RNA	Ribonucleic acid
RSV	Respiratory syncytial virus
RT	Reverse transcription
RT PCR	Reverse transciption PCR
SDF1α	Stromal cell derived factor 1 alpha
SEM	Standard error of the mean
SI	Standard international unit (pharmacological measure of potency)
SNAP29	Synaptosomal associated protein 29
SOP	Standard operating procedure
SP	Sialidase propeller
SQL	Structured Query Language
SS	Stepping Stone Sampling
T-705	Favipiravir
T25	Corning cell culture flask with a surface area of 25 cm^2
TICAM1	TIR-domain adapter containing molecule 1
TIR	Toll-interleukin receptor
TLR3	Toll-like receptor 3
TM	Transmembrane domain
TNFα	Tumour necrosis factor alpha
TNFβ	Lymphotoxin-alpha (LT-α) or tumor necrosis factor-beta
TRIF	TIR-domain containing adapter-inducing interferon β
TRN	Tamura-Nei model
TUFM	Tu translation elongation factor, mitochondrial
UK	United Kingdom
URT	Upper respiratory tract
URTI	Upper respiratory tract infection
USA	United States of America

UV	Ultra violet
VLP	Virus like particle
VP4/VP2	Capsid protein of rhinovirus
VUD	Volunteer unrelated donor (transplant)
WGS	Whole genome sequencing
ZNV	Zanamivir

1 Chapter 1: Introduction

1.1 HPIV3 classification, structure and replication

1.1.1 Classification

Human parainfluenza viruses (HPIVs) were originally isolated from three children with lower respiratory tract infections in the 1950s (Vainionpää and Hyypiä, 1994; Henrickson, 2003). The viruses were found to be distinct from influenza despite similarities in pathology and were subsequently classified together with other non-segmented negative sense RNA viruses in the order *Mononegavirales* (Pfaller, Cattaneo and Schnell, 2015), as shown in Figure 1-1. Viruses belonging to this order share a number of similarities and encompass a diverse range of clinically and economically relevant pathogens as well as a diverse range of hosts including humans, animals, birds and plants (King, 2012) . Within the scope of clinically relevant human disease, this order contains families such as *Filoviridae*, that includes Ebola and Marburg viruses; *Rhabdoviridae*, that includes lyssaviruses; and *Bornaviridae* that cause a diverse range of CNS infections in animals with potential cross-infections in humans. Newly emerging viruses in this order include a new family *Nyamiviridae* that contains two new species of virus that have been isolated from insects and birds (Kuhn *et al.*, 2013).

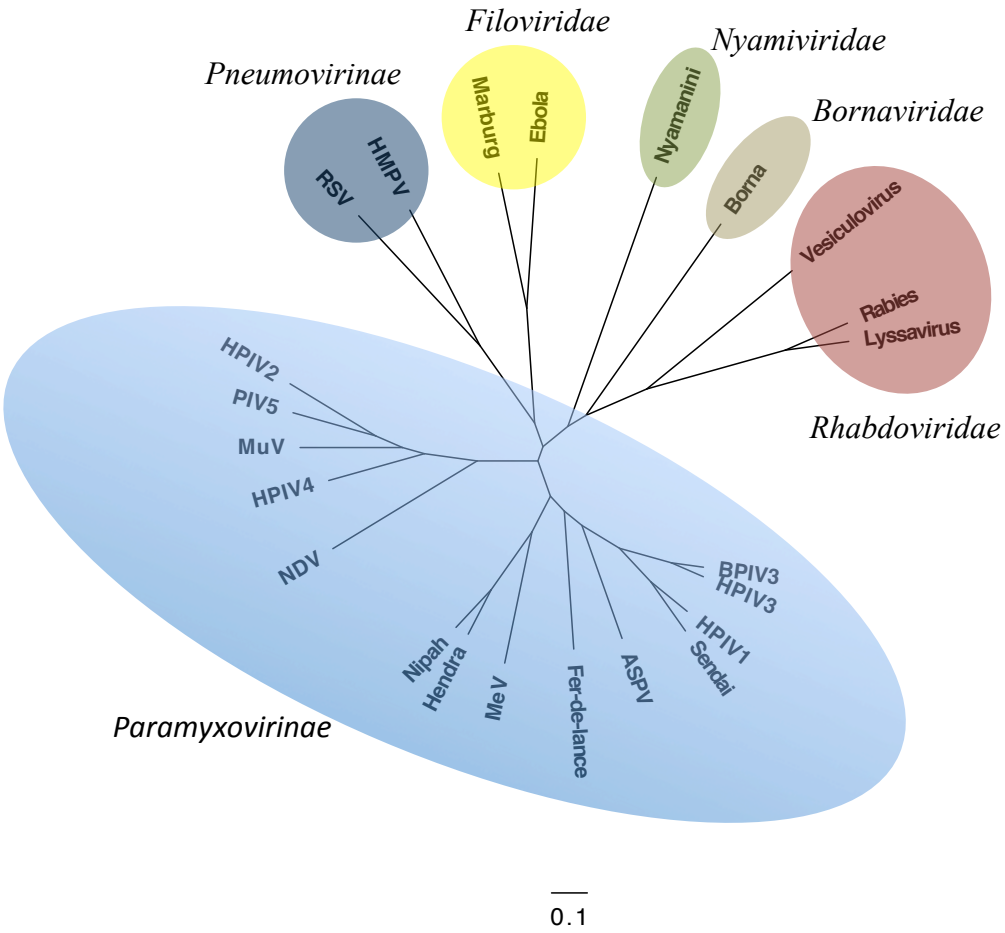

Figure 1-1 Phylogeny of genera within the order *Mononegavirales*. The tree was generated using MEGA (Tamura *et al.*, 2013) based on full genome sequences. Branch lengths are scaled to substitutions/site. Abbreviations and accession numbers: Borna - AJ311524.1; Nyamanini - NC_012703.1; Lyssa - MF187880.1; Rabies - AF499686.2; Vesiculovirus - JX569193.2; Marburg - DQ217792.1; Ebola - AF086833.2; Midway - NC_012702.1; HMPV – human metapneumovirus (MG431250.1); RSV – respiratory syncytial virus (KM360090.1); MuV – mumps virus (AF345290.1); PIV5 – parainfluenza virus 5 (NC_006430.1); NDV – Newcastle disease virus (AF375823.1); MeV – measles virus (AF266290.1); ASPV – Atlantic salmon parainfluenza virus (EF646380.1); BPIV – bovine parainfluenza virus (D84095.1); Fer-de-lance - NC_005084.2; Hendra - NC_001906.3; Nipah - NC_002728.1; Sendai - M30202.1; HPIV1-4 – human parainfluenza virus 1-4 (KX570602.1; KM190939.1; NC_001796.2; KF483663.1)

HPIVs from the Paramyxovirinae can be subdivided into four types based on antigenic and phylogenetic characteristics and these all belong to the family *Paramyxoviridae*. This comprises the largest family within the *Mononegavirales*

order, and it is broadly divided into *Paramyxovirinae* and *Pneumovirinae* (Figure 1-1). The *Pneumovirinae* contain two viruses that are known to cause significant respiratory infections in humans, namely respiratory syncytial virus (RSV) and human metapneumovirus (HMPV). The *Paramyxovirinae* comprise five main genera that encompass a range of clinically relevant viruses. These include morbillivurses (measles (MeV)), rubulaviruses (mumps (MuV), HPIV2 and 4), henipaviruses (Nipah and Hendra viruses) and respiroviruses (HPIV1 and 3). Other important members of this family have been used extensively as models for the study of the *Paramyxovirinae* either due to ease of genetic manipulation or due to the ready availability of a small animal model. These are parainfluenza virus 5 (PIV5), a rubulavirus; Sendai virus, a murine respirovirus and Newcastle Disease virus (NDV), an avian pathogen and a member of the avulaviruses.

Although all *Paramyxoviridae* share a similar genomic structure the subdivision into genera is broadly based on two factors. The first is the expression of one or more additional proteins from the polycistronic phosphoprotein (P) gene and the second is the neuraminidase activity (or lack thereof) of the main attachment glycoproteins. For instance the glycoprotein receptor of mumps and parainfluenza viruses has both haemagglutinin and the neuraminidase functions, the measles virus only has the former and the G protein of RSV – neither (Noton and Fearns, 2015; Pfaller, Cattaneo and Schnell, 2015).

1.1.2 HPIV structure

Paramyxoviruses are spherical enveloped viruses of approximately 150-350nm in diameter. HPIV3 is at the smaller end of this scale with a diameter of 150nm (Fields, Knipe and Howley, 2013). They consist of a nucleocapsid helical structure that contains the viral RNA, fully encapsidated by the nucleocapsid protein (NP). The components that form the active viral polymerase complex, namely the large polymerase (L) and the phosphoprotein (P) are associated with the nucleocapsid complex. The core is surrounded by a lipid envelope, lined with the matrix protein (M). The latter holds in place the tails of the glycoproteins: fusion (F) and haemagglutinin neuraminidase (HN) that coat the virion surface (Figure 1-2).

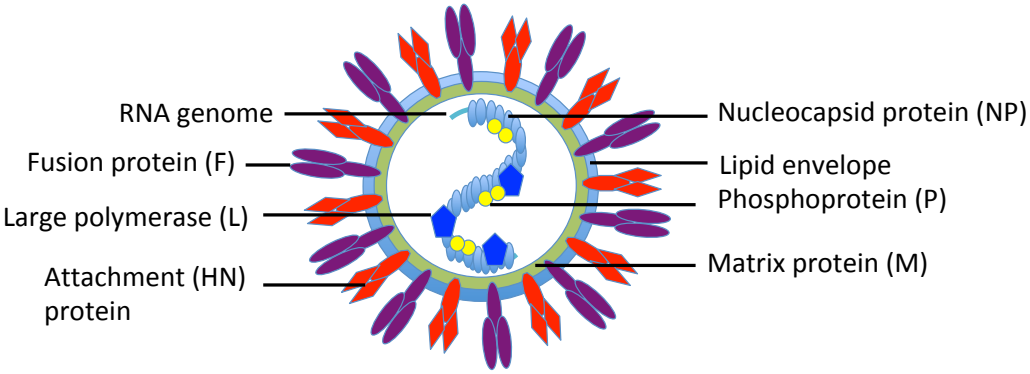

Figure 1-2 Diagrammatic structure of HPIV3 virus. The viral particle contains a core that consists of the RNA genome enclosed fully by the nucleocapsid protein (NP), with the large polymerase (L) and phosphoprotein (P) bound to the nucleocapsid. The core is surrounded by the matrix protein (M) and the lipid envelope. Attachment protein (HN) and fusion protein (F) dot the virus surface.

A.

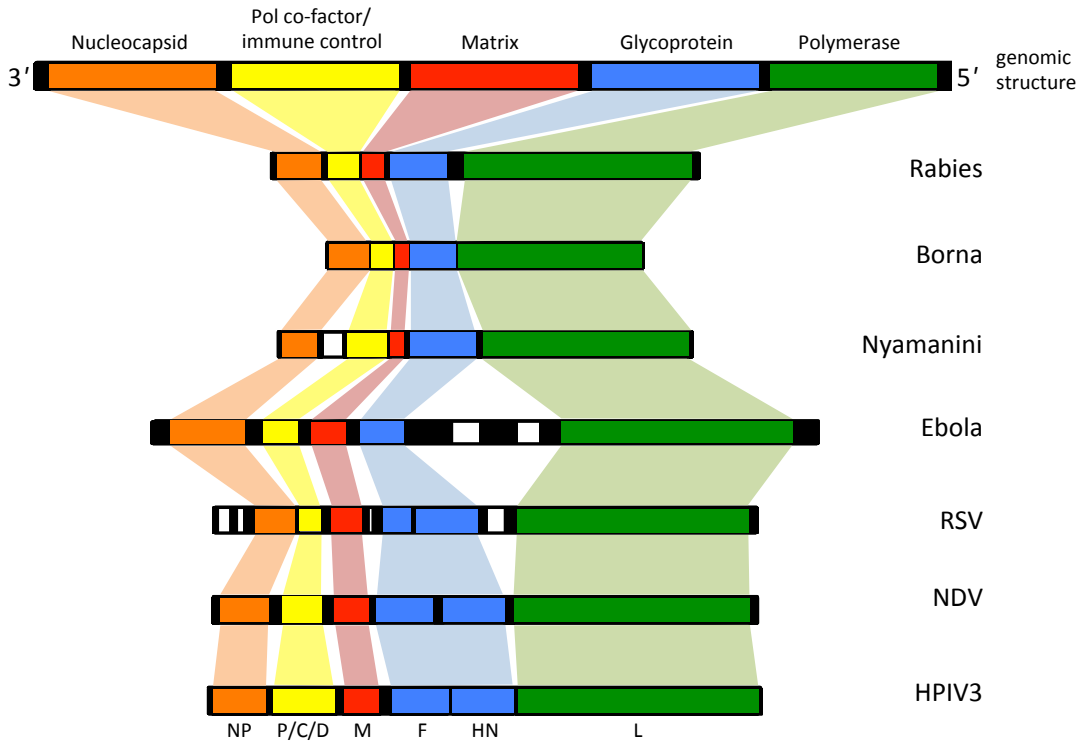

B.

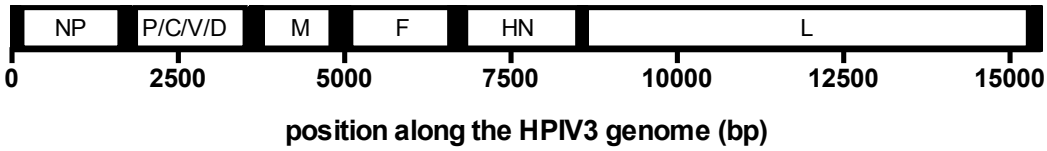

Figure 1-3 *Mononegavirales*: genome structure. A. General genomic structure of *Mononegavirales* reflects the repeated nucleocapsid (orange), polymerase co-factor/immune control (yellow), matrix (red), glycoprotein (blue), polymerase (green) structure in members of this order. The size of the genomes and individual components is scaled to their respective lengths. Adapted from (Pfaller, Cattaneo and Schnell, 2015). B. Structure of the HPIV3 genome, bp = base pairs.

The genome of HPIV3 is 15462 nucleotides long and has the following structure: 3′ - nucleocapsid protein (NP), phosphoprotein (P) - which also codes for accessory proteins C/D and V, matrix (M) protein, fusion (F) protein, haemagglutinin neuraminidase (HN) protein, large polymerase (L)-5′ (Galinski and Wechsler, 1991; Vainionpää and Hyypiä, 1994; Fields, Knipe and Howley, 2013). Each gene starts with a short conserved signal termed “gene start” and

ends with another highly conserved segment termed “gene end”, these are approximately 10-13 nucleotides in length. Genes are separated by short non-transcribed intergenic regions of approximately 40-55 nucleotides in length. Additionally a leader promoter region is found at the very three prime end of the genome and a trailer region at the five prime end. (Vainionpää and Hyypiä, 1994; Fields, Knipe and Howley, 2013; Noton and Fearns, 2015).

1.1.3 Life cycle

The lifecycle of HPIV3 is summarised in Figure 1-4. The infection is initiated when the HN protein binds to the cell surface receptor (Elango *et al.*, 1986; Suzuki *et al.*, 2001). It then triggers the F receptor to undergo a conformational change causing the virus to fuse with the host cell (Porotto *et al.*, 2011). The RNA-nucleocapsid core is then released. L and P form the polymerase complex and P chaperones the complex to the helical nucleocapsid (Chattopadhyay and Banerjee, 2009; Dochow *et al.*, 2012). The polymerase engages the RNA near the 3′ end of the genome and proceeds along it with individual N subunits being displaced and then replaced as it passes by. Transcription begins when the polymerase complex encounters the start signal and continues until the gene end segment is encountered (Noton and Fearns, 2015). Viral mRNA molecules are then modified to mimic host messenger RNAs, acquiring a 5’ methylated cap structure and a polyadenylated 3’ tail (Vainionpää and Hyypiä, 1994; Henrickson, 2003; Fields, Knipe and Howley, 2013). It has been shown that in RSV, cap methylation is essential for further elongation of the transcript. If cap methylation fails the polymerase complex aborts transcription (Barik, 1993). The polymerase then continues to scan the non-coding intergenic region until it encounters the next gene start sequence and proceeds with transcription. This process is not fully robust and therefore a gradient in the concentration of sub-genomic RNA transcribed is formed, with genes closest to the 3′ end transcribed more frequently than those closest to the 5′ end (Cox *et al.*, 2017).

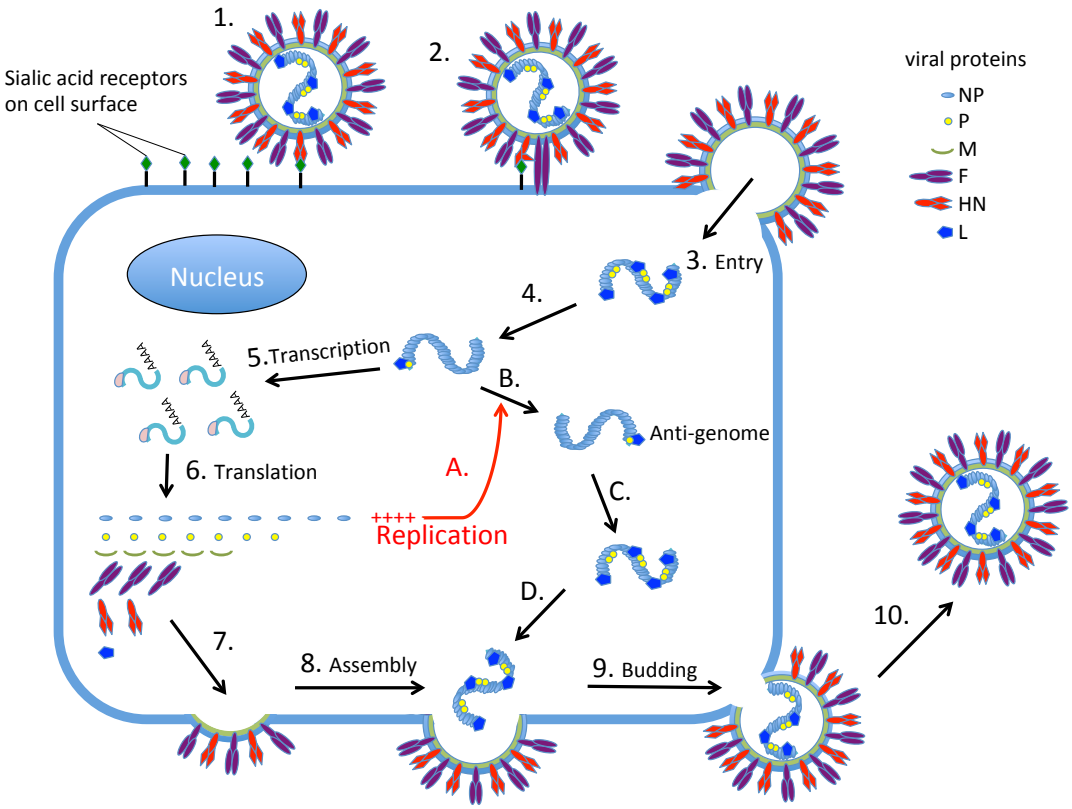

Figure 1-4 HPIV3 life cycle. The virus binds to the sialic acid receptor on the cell surface (1) via the HN protein and triggers the activation of the F protein and cell fusion (2). The viral core is released into the cytoplasm (3). Viral L and P form the polymerase complex, which binds to the RNA encased in the nucleocapsid (4) and transcription (5) begins. Viral mRNAs are capped, polyadenylated and then translated into viral proteins (6). Genes at the 3′ end of the viral RNA are transcribed more frequently, eventually leading to a concentration gradient of viral proteins (6). An increase in NP and P concentration drives the switch to viral replication (A), the polymerase complex enters a hyperprocessive state and generates the anti-genome copy (B), followed by a genome copy (C). The matrix protein guides the viral components to the cell surface (7) and helps to mediate assembly (8) and (D), and budding (9). The new virus particle is then released from the cell surface (10).

The switch between transcription and replication in paramyxoviruses has been the subject of much research and debate (Noton and Fearns, 2015). The current accepted model is as follows. During replication the polymerase must initiate on the very first nucleotide at the 3′ end of the RNA template. It must also ignore the intergenic regions and continue to elongate the positive sense anti-genome until it reaches the 5′ end. The 3′ end of the antigenome contains a sequence that then signals to the polymerase to initiate the genome RNA synthesis. Both the anti-

genome and genome RNAs are immediately encapsidated by NP, that is delivered to them in complex with P, as described above (Chattopadhyay and Banerjee, 2009). It is widely believed that this immediate encapsidation plays a crucial role in pushing the polymerase into the state where it disregards intergenic regions and proceeds with RNA replication (Fields, Knipe and Howley, 2013). It has been postulated that an excess of NP and P proteins is required for the polymerase to initiate at the very first base of the template at the 3′ end. As these are not present upon viral entry, the polymerase initiates at the start region of the first gene and commits to transcription. As the concentration of NP and P rises during infection, the polymerase gains the capacity to initiate at the 3′ end. However if the concentration of these two proteins is not sufficient for immediate encapsidation of the new anti-genomic RNA, the polymerase aborts elongation and returns to transcription. As the concentration of NP and P rises, and nascent RNA is encapsidated, the polymerase is pushed into a hyperprocessive state and commits to elongation (Noton and Fearns, 2015). The new nucleocapsids are then guided towards the cellular membrane by the M protein, that is itself associated both with the lipid bilayer as well as the cytoplasmic tails of the glycoproteins (Stone and Takimoto, 2013; Bracken *et al.*, 2016), the new viral particles bud from the cell surface and the connection is severed via the neuraminidase of the HN glycoprotein (Huberman, Peluso and Moscona, 1995).

1.2 HPIV3 protein function

1.2.1.1 Nucleocapsid protein (NP)

The HPIV3 nucleocapsid protein is 515 aa long (Figure 1-3B). It fully encapsidates the viral RNA and forms a helical nucleocapsid structure that is required for virus assembly, packaging and release of new viral particles. The symmetry inherent in this process forms the basis of the “rule of six” where the length of the genome must be a multiple of six for *Paramyxovirinae* (Henrickson, 2003; Fields, Knipe and Howley, 2013). Additionally NP serves the function of protecting the RNA from the host innate immune response and subsequent degradation (Heggeness *et al.*, 1980). It also provides a template for the

polymerase complex during viral transcription and replication (Figure 1-4). Each nucleocapsid protein has an N-terminal and a C-terminal core domain that are connected by a hinge. These interact with adjacent subunits and the RNA threads through the interface between the N terminal domain and the C terminal domain (Heggeness *et al.*, 1980; Alayyoubi *et al.*, 2015) although further research in the interaction of NP with the viral genome in ongoing (Lee *et al.*, 2017) . The importance of NP in virus assembly has been shown in the virus-like particle (VLP) formation experiments in NDV and Sendai virus. In the latter, it has been shown that the interaction of NP with the F protein on the host cellular membrane is what serves to localise the nucleocapsid complex to the plasma membrane. Abrogation of this interaction can attenuate virus production by as much as 70% (Stone and Takimoto, 2013; Bracken *et al.*, 2016).

1.2.1.2 Phosphoprotein (P)

The phosphoprotein (P) is 604 aa long (Figure 1-3B). It is a key player in the formation of the transcription and replication complex of the virus. P has the capacity to bind both NP and L. By binding NP it prevents the polymerisation of this protein as well as the encapsidation of non-viral RNA by chaperoning NP to nascent viral RNA during replication. The L protein alone, has a tendency to dimerise and is unable to bind to the nucleocapsid complex (Chattopadhyay and Banerjee, 2009). The functions of the P protein are to prevent the dimerization of the L protein and to guide it to the nucleocapsid as well as to ensure continued contact between the two during transcription or replication (Chattopadhyay and Banerjee, 2009). Solved crystal structures of L and P suggest that upon binding to L, the P protein causes a conformational change and forces the N terminal of L to protrude outwards, thus allowing it to bind to the nucleocapsid complex (Noton and Fearns, 2015). Recently an additional immunomodulatory role has been attributed to P. It was found to interact with synaptosomal associated protein 29 (SNAP29) and prevent it from binding to syntaxin 17, thereby inhibiting the fusion of autophagosomes and lysosomes during autophagy (Ding *et al.*, 2014). The authors have hypothesised that this mechanism serves to enhance extracellular viral yields by sequestering virions via a co-localisation of the M protein with the autophagosome. This, in turn, facilitates the binding of

newly formed virus particles to the membrane and ultimately the release and budding of virions. A similar subversion of this pathway is seen in other viral replication cycles such as that of influenza, rotavirus and HIV, to name a few (Ding *et al.*, 2014).

1.2.1.3 C protein/D protein/V protein

Other proteins are encoded by the P region of the genome by use of site-specific editing of P mRNA and overlapping reading frames (Figure 1-3B). Although the V protein is expressed in the Sendai virus, a well-established model for respirovirus infection (Kato *et al.*, 1997), HPIV3 does not express the full length V protein (Fields, Knipe and Howley, 2013). Instead a D protein is produced by addition of five G residues (Haller *et al.*, 2000). It has been linked to interferon beta (IFNβ) interference and its deletion has been shown to restrict viral growth, but the full extent of its role remains unclear (Roth *et al.*, 2013).

The C protein of HPIV3 is 199 aa long and has been found to be essential for virulence both *in vitro* and *in vivo* (Durbin *et al.*, 1999). It has been found to interact directly with STAT1, thereby inhibiting IFNα and β signalling (Durbin *et al.*, 1999; Caignard *et al.*, 2009) The C protein also interacts with the L protein, down regulating transcription in a dose dependent manner (Malur, Hoffman and Banerjee, 2004). The C protein has also been shown to interact directly with growth factor receptor-bound protein 2 (GRB2) and activate the MAPK/ERK signalling pathway (Caignard *et al.*, 2009) . This stimulates cell proliferation which in turn supports viral replication and blocks the interferon type I driven antiviral response (Caignard *et al.*, 2009).

1.2.1.4 Matrix protein (M)

The matrix protein is 353 aa long (Figure 1-3B). The main functions of this protein are virus assembly and trafficking to the cell membrane (Figure 1-4). Consequently, M has the capacity to interact with many proteins including itself, cellular membranes, the cytoplasmic tails of the viral glycoproteins as well as the nucleocapsid complex (El Najjar *et al.*, 2014). This allows the matrix protein to bind to the part of the cellular membrane rich in viral glycoproteins, and to guide the nucleocapsid complex to the same site. Most studies on the structure and

function of paramyxovirus M proteins have been carried out in Sendai and NDV viruses. These have included studying gene deletions (Bracken *et al.*, 2016), crystallography (Battisti *et al.*, 2012) and the formation of VLPs (Pantua *et al.*, 2006). The latter have shown that in a number of viruses including HPIV3, NDV, Sendai, and MeV, the M protein is of itself sufficient for budding of VLPs (Pantua *et al.*, 2006; Bracken *et al.*, 2016; Wang *et al.*, 2017). The binding of M to the cell membrane lipid bilayer is likely to be driven by the hydrophobic interactions in the C-terminal domain (El Najjar *et al.*, 2014). It is important to note that there is greater homology between C-terminal domains of paramyxoviruses than between the N-terminal domains, which suggests that the N-terminal domain is involved with more virus-specific interactions (El Najjar *et al.*, 2014). Recent work has also demonstrated that the matrix protein of HPIV3 initiates mitophagy by binding to mitochondrial Tu translation elongation factor (TUFM), and thus contributes to the inhibition of type I IFN response by this virus (Ding *et al.*, 2017).

1.2.1.5 Fusion protein (F)

The fusion protein of HPIV3 is 539 aa long (Figure 1-3B) and as the name suggests mediates fusion between the virus and the host cell (Figure 1-4). It is a class one viral fusion protein with a structure and function shared by many viruses (Palgen *et al.*, 2015). In short, a class one viral fusion protein is synthesised as a precursor (designated F_0 in HPIV3) and cleaved en route to the cell surface by a protease in the late compartments of the secretory pathway; into an N terminal element (F_2 in HPIV3) which contains a receptor binding domain and the C terminal element (F_1 in HPIV3), which is anchored by a transmembrane segment in the viral membrane and contains the fusion module. Other common viruses that contain this type of fusion protein are influenza, HIV and the *Filoviridae*, e.g. ebola (Morrison, 2003; Fields, Knipe and Howley, 2013).
The fusion protein of HPIV3 is additionally activated by its interaction with HN prior to cell binding (Porotto, Salah, *et al.*, 2012). Cleavage site variants have been shown to affect the fusogenicity of HPIV3 (Palmer *et al.*, 2012). During fusion the heptad repeat regions form a trimer-of-hairpins structure and this drives the fusion between the virus and the host cell (Dutch *et al.*, 2001; Yin *et al.*,

2005; Lamb, Paterson and Jardetzky, 2006). In HPIV3 the conformational change is driven and controlled by the interaction of F and HN after the latter binds to the cell surface (Porotto, Palmer, *et al.*, 2012). Other viruses require external triggers such as pH in the case of influenza (Fields, Knipe and Howley, 2013) or furin cleavage of F_0, in the case of HPIV1 and Sendai virus (Smith *et al.*, 2009).

1.2.1.6 Haemagglutinin – neuraminidase (HN)

The HN genome of HPIV3 encodes a second surface viral glycoprotein, haemagglutinin-neuraminidase. It is 572 aa long (Figure 1-3B) and fulfils a number of important functions in the viral lifecycle (Figure 1-4).

The fist step in infection is the binding of the haemagglutinin component to the sialic acid receptor on the host cell surface (Porotto *et al.*, 2001). The specificity of this interaction determines the tropism of HPIV3. It has previously been shown that both HPIV1 and 3 bind to sialic acids at the terminal branching polylactosamine structures (Suzuki *et al.*, 2001). HPIV1 has the ability to recognise α2,6-linked sialic acids, that are predominantly expressed in the human trachea, whereas HPIV3 may require a specific accessory glycochain (Fukushima *et al.*, 2014). The latter may be key to different pathologies exhibited by respiroviruses in clinical settings. This is reflected by the *in vivo* pathology of both viruses where HPIV1 predominantly infects the upper respiratory tract, whereas HPIV3 is associated with lower respiratory tract infections and pneumonia (Suzuki *et al.*, 2001; Henrickson, 2003; Fukushima *et al.*, 2014).

After binding to the cell surface the HN engages the F protein and triggers the conformational change that will lead to fusion with the host cell (Porotto *et al.*, 2011). The timing of the triggering of the F protein is essential for viral fitness both *in vivo* and *in vitro* (Prince, Ottolini and Moscona, 2001). The interaction with F is confined to the second binding site of HN and it has been shown that HN and F associate even before receptor engagement via the primary binding site when HN triggers the aggregation of HN-F complexes (Lawrence *et al.*, 2004; Porotto *et al.*, 2011).

The neuraminidase component of the HN is involved in the release of the virus from the infected cell (Huberman, Peluso and Moscona, 1995; Fields, Knipe and

Howley, 2013). A number of previous studies have shown that the balance between receptor binding and the neuraminidase function of the HN glycoprotein is essential to the virus cycle (Huberman, Peluso and Moscona, 1995; Moscona, 1997; Porotto, Salah, *et al.*, 2012). This has been linked to cell culture adaptation where a more fusogenic phenotype with reduced neuraminidase activity is observed (Palmer *et al.*, 2012). A functioning neuraminidase also mediates viral interference (Horga *et al.*, 2000): by selectively removing sialic acid receptors from the cell, the cell is rendered impervious to superinfection by another virus relying on the same cell receptor for binding and entry.

1.2.1.7 Large polymerase (L)

The L protein of HPIV3 is a large RNA-dependent RNA-polymerase (RdRp) of 2233 amino acids long (Figure 1-3B). In the absence of P protein, HPIV3 L is unstable and prone to degradation or the formation of non-functional dimers (Chattopadhyay and Banerjee, 2009; Cox and Plemper, 2015). The complex that it forms with the phosphoprotein carries out a number of functions including mRNA synthesis, 5′capping and methylation of nascent RNAs and 3′polyadenylation (Henrickson, 2003; Fields, Knipe and Howley, 2013; Cox and Plemper, 2015; Noton and Fearns, 2015) (Figure 1-4). Six highly conserved regions have been identified in the L proteins of other members of *Mononegavirales* (Cox and Plemper, 2015; Pfaller, Cattaneo and Schnell, 2015). So far, conserved region III (GDNQ sequence) has been identified as the polymerase active site, VI (GXGXG) is involved in cap methylation and region V has been linked to mRNA capping. The functions of the other three conserved regions remains to be elucidated (Dochow *et al.*, 2012; Cox and Plemper, 2015).

1.3 Clinical impact

1.3.1 Epidemiology

Human parainfluenza viruses (HPIV) are members of the *Paramyxoviridae*, a family in the order of *Mononegavirales*. There are four subtypes (1.1.1 Classification) and all four are significant causes of both upper and lower

respiratory tract infections. Human parainfluenza 3 (HPIV3) has been identified as the most prevalent circulating parainfluenza serotype in UK and Wales (Zhao *et al.*, 2017). The epidemiological pattern of HPIV in England and Wales has remained similar over the last 30 years, with HPIV3 being the dominant serotype (68.3% of circulating strains), with peaks occurring annually between March and June (Zhao *et al.*, 2017) (Figure 1-5). There is little variation from this pattern reported globally (Liu *et al.*, 2013), unlike, for example, influenza, where seasonality is known to be affected by latitude (Koul *et al.*, 2014) .

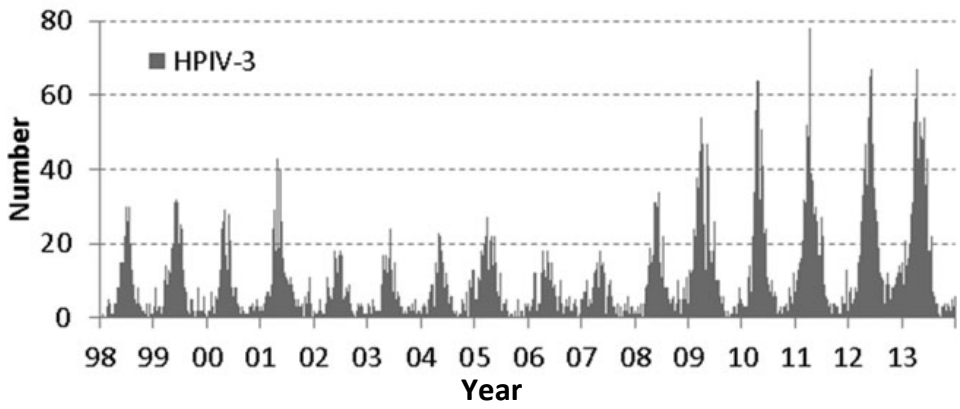

Figure 1-5 HPIV3 prevalence in UK and Wales 1998-2013. Weekly numbers of HPIV3 reported to Public Health England (PHE) show an annual peak in late spring/summer. Figure taken from (Zhao *et al.*, 2017).

HPIV is an important respiratory pathogen with a broad spectrum of presentation and a significant impact both in the paediatric and the immunocompromised cohorts. In the former it is responsible for up to 6.8% of all paediatric admissions for respiratory presentations (Weinberg *et al.*, 2009). In the immunocompromised population, the reported incidence of infection varies between 5 and 12% with lower respiratory tract infections (LRTIs) and mortality of up to 75% being reported (Seo *et al.*, 2014; Shah *et al.*, 2016). Most primary infections occur below the age of five and immunity to HPIV3 is incomplete, potentially because of various immune evasion strategies (See Section 1.5.4) (Spriggs *et al.*, 1987; Murphy *et al.*, 1988; Henrickson, 2003; Schomacker *et al.*, 2012) and re-infections occur throughout life.

1.3.2 Transmission

Transmission of HPIV3 is through respiratory droplets and fomites, where the virus can remain viable for up to 10 hours given the right conditions of temperature and humidity (Brady, Evans and Cuartas, 1990). Extensive studies conducted with respiratory syncytial virus (RSV), a closely related paramyxovirus, have also identified gloves and hospital gowns as potential sources of nosocomial transmission (Chow and Mermel, 2017). Transmission within the immunocompromised cohort is exacerbated by prolonged asymptomatic shedding (Zambon *et al.*, 1998; Jalal *et al.*, 2007), although in the paediatric cohort the evidence for this is conflicting (Piralla *et al.*, 2009; Aliyu *et al.*, 2015). Paediatric outbreaks are further complicated by complex shared transmission routes involving communal areas, toys and patterns of behavior that involve self-inoculation via eyes, nose and mouth (Chow and Mermel, 2017).

1.3.3 Morbidity and mortality

Overall there is a broad spectrum of pathology and severity that is associated with HPIV3 infection (Herzog *et al.*, 1989; Cilla *et al.*, 2008; Park *et al.*, 2009; Maeng *et al.*, 2012; Shah *et al.*, 2016). This is largely dependent on the age, previous medical history and immune status of the patient in question. Infection typically initiates in the upper respiratory tract, from where it can migrate lower causing pneumonia and secondary infections. Blocked Eustachian tubes tend to predispose to otitis media, a well reported sequela of HPIV3 infection in children (Schomacker *et al.*, 2012). In most healthy individuals HPIV3 causes self-limiting coryzal symptoms (Henrickson, 2003). In children and the elderly, HPIV3 is more likely to spread to smaller airways (Cilla *et al.*, 2008; Liu *et al.*, 2013; Shi *et al.*, 2015). In severely immunosuppressed individuals there have been reports of giant-cell pneumonia (Butnor and Sporn, 2003), transplant rejection (Herzog *et al.*, 1989; Vilchez *et al.*, 2003) and systemic viraemia with spread to other organs including CNS involvement with fatal outcomes (Madden, Burchette and Hale, 2004). The impact in the adult post-haematology transplant cohort has been widely reported (Zambon *et al.*, 1998; Cortez *et al.*, 2001; Jalal *et al.*, 2007;

Maziarz *et al.*, 2010) with conflicting reports on outcome, depending on other organisms isolated as well as the immunosuppression status of the patient.

A number of small studies have evaluated the impact of respiratory viruses including HPIV3 in the paediatric oncology cohort (Bowden, MD, 1997; Christensen, Nielsen and Hasle, 2005; Piralla *et al.*, 2009; Lindblom *et al.*, 2010; Ustun *et al.*, 2012; Berrueco *et al.*, 2013; Benites *et al.*, 2014; Söderman *et al.*, 2016; Torres *et al.*, 2016; Santolaya *et al.*, 2017). In each case, outbreaks were identified retrospectively and prospective identification of a point source was not possible (Piralla *et al.*, 2009; Berrueco *et al.*, 2013). There is limited consensus on prevalence, severity of infection and clinical outcome data. HPIV3 has been reported as a causative pathogen in 1-18% of respiratory viral infections in paediatric oncology patients, and as such has been conflictingly described as both a common as well as a relatively rare pathogen (Christensen, Nielsen and Hasle, 2005; Lindblom *et al.*, 2010; Ustun *et al.*, 2012; Benites *et al.*, 2014; Santolaya *et al.*, 2017). Increased progression to LRTI, with associated poor outcome (Bowden, MD, 1997; Christensen, Nielsen and Hasle, 2005; Ustun *et al.*, 2012; Söderman *et al.*, 2016), as well as no difference in clinical outcome (Torres *et al.*, 2016) have both been reported. Although discrepancies between studies could be attributed to confounding factors such as immunosuppression status, a separate study found that there were no additional risk factors in developing HPIV3 complications in haematopoietic stem cell transplant (HSCT) patients (Ustun *et al.*, 2012; Torres *et al.*, 2016; Santolaya *et al.*, 2017). Additionally, the prevalence of co-infections with more than one respiratory virus in this cohort has been quoted to be between 2 and 26% with both no clinical impact (Lindblom *et al.*, 2010; Torres *et al.*, 2016) and increased severity of infection reported (Cilla *et al.*, 2008; Ustun *et al.*, 2012). The above suggests that dual infections may additionally play an important role in the clinical outcome and the possibility of dual transmission in paediatric outbreaks should not be overlooked.

1.3.4 Prevention and treatment

1.3.4.1 Vaccine candidates

Currently there is no licensed vaccine for HPIV3, although due to its epidemiological impact, a number of candidates have been evaluated over the years (Murphy *et al.*, 1988; Schmidt *et al.*, 2012). A cold adapted attenuated vaccine candidate cp45 (cold passage 45) (Belshe and Hissom, 1982) has been shown to be safe and immunogenic in a small animal model (Crookshanks-Newman and Belshe, 1986) as well as in small paediatric studies (Karron *et al.*, 2003; Belshe *et al.*, 2004). Vaccines based on a related non-primate virus, such as bovine parainfluenza (Karron *et al.*, 1996; Greenberg *et al.*, 2005) have also been evaluated and found to be safe candidates in humans. Improved reverse genetic models of HPIV3 (Pfaller, Cattaneo and Schnell, 2015; Beaty *et al.*, 2017) allowing for chimeric vaccines with improved immunogenicity, cost and delivery (Haller *et al.*, 2000; Schmidt *et al.*, 2001; Greer *et al.*, 2007; Senchi *et al.*, 2013) have been successfully tested in small animal models. However, no evaluation of long-term efficacy or large clinical trials has been conducted. Therefore the emphasis remains on infection control or on potential therapeutic candidates.

1.3.4.2 Therapeutic candidates

1.3.4.2.1 Ribavirin

Currently there are no licensed treatments for HPIV3. Ribavirin is a nucleoside analogue with broad anti-viral activity *in vitro* with a number of proposed mechanisms of action including GTP depletion via IMP dehydrogenase inhibition, inhibition of viral polymerase and inhibition of RNA capping (Crotty, Cameron and Andino, 2002; Leyssen *et al.*, 2005). It has been successfully used for treatment of hepatitis C and is licensed for treatment of respiratory syncytial virus (RSV), another member of the *Paramyxoviridae*, in young children. Although ribavirin has two Food and Drug Administration (FDA) black box warnings including teratogenicity and haemolytic anaymia, it is generally well tolerated with bronchospasm (aerosolized) (Falsey, 2012) and reversible haemolytic anaemia (systemic) being among the more severe side effects reported (Karin Jorga *et al.*, 2006).

Ribavirin, either aerosolized or systemic, with or without gamma globulin, was originally seen as a promising therapeutic candidate for treatment of HPIV3 in haematopoietic stem cell transplant (HSCT) patients with mixed outcomes being reported in small, uncontrolled studies and case reports (Lewis *et al.*, 1996; Chakrabarti *et al.*, 2000). However a number of recent more systematic studies and meta analyses have shown that ribavirin had little or no effect on morbidity and mortality in patients with proven lower respiratory tract infection (LRTI) caused by HPIV3 (Seo *et al.*, 2014). High-dose intravenous gammaglobulin similarly had no effect (Falsey, 2012; Shah *et al.*, 2016) . Although the efficacy of ribavirin has been shown *in vitro* for tissue culture adapted strains, its lack of therapeutic efficacy in patients necessitates another evaluation of its inhibitory effect on clinical strains and if conclusively demonstrated, a different approach to delivery and dosing.

1.3.4.2.2 Favipiravir

Favipiravir (T-705), like ribavirin, is a nucleoside analogue with broad spectrum activity *in vitro* (Furuta *et al.*, 2013). First marketed in 2003, it is licensed against influenza in Japan. Favipiravir is a selective and potent inhibitor of RNA dependent RNA polymerases and has been shown to be virucidal by inducing catastrophic viral mutagenesis (Furuta *et al.*, 2013; Arias, Thorne and Goodfellow, 2014; Vanderlinden *et al.*, 2016). *In vitro* it has demonstrated activity against a broad range of RNA viruses, including positive stranded RNA viruses such as norovirus, *Flaviviridae* and negative stranded RNA viruses such as *Filoviridae* (including Ebola) and *Paramyxoviridae* (Jochmans *et al.*, 2016; Sissoko *et al.*, 2016; Vanderlinden *et al.*, 2016). Among the latter, the effectiveness of favipiravir has been demonstrated *in vitro* on culture adapted strains of human metapneumovirus (HMPV), RSV, HPIV and measles virus (Jochmans *et al.*, 2016). So far this antiviral has not been assayed against wild type clinical strains of HPIV3.

1.3.4.2.3 Zanamivir

Zanamivir is a neuraminidase inhibitor and is licensed for the treatment of influenza under the trademark name of relenza. It inhibits influenza by preventing the release of new viral particles from the infected cell. Although its

impact on the clinical outcome of influenza infection has recently been questioned (Jefferson *et al.*, 2014), its low toxicity profile and mechanism of action would nonetheless make it a potential candidate for the treatment of HPIV3. HPIV3 relies on a joint haemagglutinin-neuraminidase (HN) protein both for its attachment and fusion to the host cell (Figure 1-2), as well as for viral escape and for the prevention of aggregation of viral particles on the cell surface (Porotto *et al.*, 2001; Lamb, Paterson and Jardetzky, 2006). The structure of the HPIV3 HN neuraminidase binding pocket shows sufficient homology with that of the influenza neuraminidase to suggest a potential high affinity for zanamivir (Lawrence *et al.*, 2004). The role of this protein in both viral binding and fusion with the target cell, as well as in the release of the nascent virus from the cell surface, indicates the potential for zanamivir to interfere with the viral replication cycle of HPIV3 at two points. *In vitro* studies on tissue culture adapted strains have generally concluded that zanamivir has the potential to act as a binding inhibitor of HPIV3 albeit at EC_{50} values approaching milimolar concentrations, making this an unfeasible *in vivo* candidate (Greengard *et al.*, 2000). It was similarly concluded that zanamivir was poorly effective as an inhibitor at the viral release stage.

1.3.4.3 Alternative approaches: synergy and novel therapeutics

As zanamivir remains a potentially effective inhibitor of parainfluenza, albeit at unfeasible concentrations *in vivo*, a number of studies have looked at improved drug delivery (Shanmugam *et al.*, 2013) and synergy (Bailly *et al.*, 2016). In a recent study, the anti-parasitic drug suramin was discovered to be a non-competitive inhibitor of HPIV3 HN protein, synergistic with the action of zanamivir. However the concetrations required were still prohibitively high (Bailly *et al.*, 2016). Equally it has been reported that low dose ribavirin has the capacity to potentiate favipiravir in treatment of Ebola in a small animal model (Westover *et al.*, 2016). Although the pathologies of these diseases are vastly different and this has not been demonstrated in a clinical setting, this is nonetheless encouraging and provides potential avenues for further therapeutics research.

Other novel therapeutics for HPIV3 have been proposed, based both on the structure of the virus as well as on the mechanisms of infection and pathology (Hayden, 2009, 2013). Among the most promising drugs is a new sialidase fusion protein inhibitor DAS181 (Ansun BioPharma, 2017). This drug has been identified as a potential therapeutic candidate for viruses that are reliant on a sialic acid receptor for cell entry including influenza, reovirus, rotavirus, adenovirus and parainfluenza viruses (Triana-Baltzer *et al.*, 2009; Stencel-Baerenwald *et al.*, 2014). As an inhibitor of HPIV3 it has been shown to be effective both in human airway epithelial (HAE) cells and a small animal model (Moscona *et al.*, 2010), as well as in a number of clinical cases (Chalkias *et al.*, 2014; Waghmare *et al.*, 2015; Salvatore *et al.*, 2016). Phase I trial results have been encouraging, although some potential adverse side effects have been reported in patients with underlying atopy (Zenilman *et al.*, 2015; Colombo *et al.*, 2016).

Newer approaches have centered around structure guided synthesis of novel compounds (Alymova *et al.*, 2004, 2005; Tindal *et al.*, 2007) . These have been tested both *in vivo* and *in vitro* with a particular focus on finding a more efficient inhibitor for the HN of HPIV3 (Moscona, 2005). Other potential targets include the F protein (Porotto *et al.*, 2010) as well as a more targeted approach to the polymerase (Cox and Plemper, 2015; Fearns and Deval, 2016).

1.4 Experimental models

1.4.1 HPIV experimental strains

To date most of the experimental work on HPIV3 has been conducted using significantly laboratory adapted strains. Two strains, in particular have been widely used: JS strain and Washington strain.

The Washington strain is alternatively identified as C243 or strain 47885. It was originally isolated from a one year old female in 1957 in Washington DC (Galinski, Mink and Pons, 1988; Galinski and Wechsler, 1991). It was propagated in LLC-MK2 cells, and has since been used as a prototype strain for outbreak tracking (Zambon *et al.*, 1998; Jalal *et al.*, 2007), phylogenetic modeling (Goya, Mistchenko and Viegas, 2016; Košutić-Gulija *et al.*, 2017), studies of virus

evolution (Tsutsui *et al.*, 2017), therapeutic inhibitor development and evaluation (Tindal *et al.*, 2007; Guillon *et al.*, 2014; Bailly *et al.*, 2016) and vaccine research (Haller *et al.*, 2000; Senchi *et al.*, 2013) among others. An early study looking at HPIV3 diversity has identified differences in the F and HN proteins between this strain and minimally adapted (HN) and plaque purified (F) strains isolated from paediatric patients (Van Wyke Coelingh, Winter and Murphy, 1985; Coelingh and Winter, 1990) . It is noteworthy that in the F protein, some of the differences identified were located in the cleavage domain, which has since been linked to fusogenicity and potentially culture adaptation (Palmer *et al.*, 2012; Palermo *et al.*, 2016), however this connection was not made at the time.

The JS strain of the virus, alternatively known as strain 14702 or strain Z11575 was originally sourced from a one year old child with a febrile illness in the early 1980s and isolated in bovine embryonic kidney cells (BEK). It was subsequently passaged 14 times in African Green monkey kidney cells (AGKM) and plaque purified to serve as a vaccine candidate (Belshe and Hissom, 1982). Therefore the JS strain has since become the main strain for HPIV3 vaccine research (Belshe *et al.*, 1992, 2004), including recombinant vaccines (Schmidt *et al.*, 2001; Greer *et al.*, 2007) and development of reverse genetics systems (Durbin *et al.*, 1997; Roth, Li and Barnard, 2010; Beaty *et al.*, 2017) The JS strain was found to be distinct from the prototype Washington strain (Stokes *et al.*, 1992) with the majority of differences found in the F gene. However it is still a significantly culture passaged strain that cannot be considered a true reflection of circulating strains.

1.4.2 Growth in immortalised cell culture

Until recently the isolation and propagation of any virus for diagnostic or experimental purposes was reliant on its ability to proliferate in cell culture. As discussed above, heavily culture adapted strains of HPIV3 are widely used for research. HPIV3, especially in its adapted form grows readily in many immortalised culture systems. To name but a few: LLC-MK2 cells (Galinski, Mink and Pons, 1988), Vero cells (Schmidt *et al.*, 2001), BEK and AGKM cells (Belshe and Hissom, 1982), A549 (Guillon *et al.*, 2014), MDBK cells (Coelingh and Winter, 1990). Overall HPIVs are known to propagate more readily in epithelial

rather than fibroblast cell lines (Henrickson, 2003). These viruses are not known to be cytopathic in cell culture, although they are known to become more fusogenic and destructive with increased adaptation to a particular cell line (Henrickson, 2003; Palmer *et al.*, 2012; Palermo *et al.*, 2016).

1.4.3 Small animal models

The use of small animal models, particularly rodents is widespread in virus research (Adachi and Miura, 2014). These are particularly useful when a small animal equivalent of the virus exists, such as in the case of Sendai virus (murine) and HPIV1 (human) (Adderson *et al.*, 2015), as the model virus is thus able to replicate in its natural host. However no such model is available for HPIV3. Animal models of HPIV3 have included ferrets (Mascoli *et al.*, 1976), guinea pigs (Ye *et al.*, 2010), hamsters (Rydbeck, Love and Norrby, 1988) and cotton rats (Porter *et al.*, 1991). The latter, in particular is considered to be a good model for HPIV3 infection as infection in cotton rats is thought to reproduce faithfully the effects of infection as well as vaccine efficacy in humans (Ottolini *et al.*, 1996, 2002; Boukhvalova, Prince and Blanco, 2009). However these are complex to handle and no genetically specific lineages currently exist (Green, Huey and Niewiesk, 2013).

1.4.4 Human airway epithelial cells

Human airway epithelial (HAE) cells are primary cells that are sourced either from bronchial or nasal biopsies. They constitute three primary cell types: basal, goblet and ciliated; and these form tight junctions at air/liquid interface. This *ex vivo* culture system has been widely used for for efficient modeling of the human airway in oncology (Gruenert, Finkbeiner and Widdicombe, 1995), immunology (Stewart *et al.*, 2012), virology (Banach *et al.*, 2009) and others (Balloy *et al.*, 2015). In HPIV3 research it has been used to study inflammatory responses and growth kinetics of different parainfluenza subtypes (Zhang *et al.*, 2005; Schaap-Nutt *et al.*, 2012) and novel therapeutic drug testing (Moscona *et al.*, 2010). Additionally it is considered to be a very close approximation of the natural host for virus culture (Palmer *et al.*, 2012; Palermo *et al.*, 2016). The above, coupled with the current trend to reduce the use of animal in scientific research

(Regulation and Department for Business, 2014) make this model an ideal candidate for further study of HPIV3.

1.5 Pathogenesis

HPIV3 is not known to be cytopathic in tissue culture, however work in HAE cells has shown increased shedding, replacement of cells and increased mucin production (Zhang *et al.*, 2005, 2011). This is consistent with the pathology seen in clinical cases (Schomacker *et al.*, 2012). Overall the pathologenesis of HPIV3, like that of other respiratory viruses should be evaluated as a balance between the direct effects of the virus itself and that of the immune response it triggers (Meissner, 2016).

1.5.1 Direct effect of HPIV

HPIV3 has a number of mechanisms aimed at down-regulating its pathogenicity *in vivo*. Protein C of HPIV3 down-regulates viral transcription and replication (Elango *et al.*, 1986; Malur, Hoffman and Banerjee, 2004). The production of the F protein is decreased by an aberrant end signal at the end of the M gene, leading to less fusogenic phenotypes *in vivo* (Lingemann et al. 2015). There is evidence based on small animal models of HPIV3 (Moscona, 2005) and Sendai virus (Kato *et al.*, 1999) that more fusogenic variants of these viruses trigger a stronger inflammatory response, thus precipitating a more clinically adverse infection but equally contributing to faster clearing of the virus. Hence, it could be argued that a more fusogenic phenotype would constitute a more aggressive, but paradoxically less successful strain in an immunocompetent population. This is consistent with what is observed in a clinical scenario. In patients with an intact immune system the virus does not appear to be cytopathic and histology does not suggest virus related cell destruction (Porter *et al.*, 1991; Schomacker *et al.*, 2012). In patients with severe immune deficiencies, however, the virus exhibits a more fusogenic phenotype (Madden, Burchette and Hale, 2004), combined with systemic viraemia (Porter *et al.*, 1991; Schomacker *et al.*, 2012).

1.5.2 Subversion of the innate immune system and viral clearance

In addition to dampening its direct effect on the host, there are a number of ways in which HPIV3 directly subverts the immune system and ensures viral persistence. (Fields, Knipe and Howley, 2013). The C protein of HPIV3 prevents STAT1 phosphorylation with the subsequent inhibition of IFN α and β signalling (Caignard *et al.*, 2009; Shil *et al.*, 2017). Additionally the M protein has been shown to trigger mitophagy suppressing the RIG-I part of the immune pathway and abrogating the mitochondrial mediated part of the immune response (Ding *et al.*, 2017) .

Clearance of HPIV3 is impaired by creation of infection reservoirs: HPIV3 has been shown to prevent autophagy of infected cells (Ding *et al.*, 2014) and to enhance the survival of monocytes by triggering the GM-CSF autocrine loop *in vivo* (Plotnicky-Gilquin *et al.*, 2001). Additionally the C protein of HPIV3 is known to activate the MAPK/EPK pathway to create a favourable environment for viral replication (Caignard *et al.*, 2009). Clinically this leads to an increased production of mucus, blocking airways and preventing the clearance of pathogens (Vareille *et al.*, 2011; Schomacker *et al.*, 2012). This in turn, predisposes to secondary infections and adversely affects clinical outcome (Alymova *et al.*, 2005; Yamaya *et al.*, 2010).

1.5.3 Inflammatory response

In the general population, HPIV3 has been compared to RSV, another paromyxovirus, with a well-studied immune driven disease enhancement mechanism (Openshaw and Tregoning, 2005). In RSV infections, it is often not the viraemia itself, but the immune response of the host that causes the most damage and mediates disease severity. This aspect has been less well studied in HPIV3, with conflicting data on correlation of chemokine production and the severity of disease (Gern *et al.*, 2002).

Increases in pro-inflammatory chemokines such as RANTES, IL-6, MIP1 alpha and beta as well as IP10 and IL8 has been reported both in *in vitro* (Zhang *et al.*, 2005; Schaap-Nutt *et al.*, 2012; Lewandowska-Polak *et al.*, 2015) and *in vivo* (Gern *et al.*, 2002; Ottolini *et al.*, 2002; Feghaly *et al.*, 2012) studies of HPIV3 infection. The latter, in particular, have been correlated with severity of disease,

while RANTES and IFNγ have been linked to respiratory symptom exacerbation in patients with pre-existing atopy (Ye *et al.*, 2010; Johnson *et al.*, 2013; Lewandowska-Polak *et al.*, 2015). As mentioned above, it has been shown that viral phenotype can be correlated with the inflammatory response and hence clinical outcome (Kato *et al.*, 1999; Moscona, 2005; Lingemann *et al.*, 2015).

1.5.4 Adaptive immune response and re-infection

There is limited evidence that repeated previous exposure to HPIV3 can protect against mild infections (Spriggs *et al.*, 1987) and that maternal antibodies are protective to some extent in infants before the age of 6 months (Lee *et al.*, 2001). However, overall the adaptive immune response against HPIV3 is incomplete and infections occur throughout life (Fields, Knipe and Howley, 2013) for a number of reasons. Activation of dendritic cells is essential for the formation of a long -term adaptive immune response and prevention of re-infection with the same virus (Howard *et al.*, 2004). HPIV3 infects and replicates readily in dendritic cells, effectively clearing them from the site of infection (Plotnicky-Gilquin *et al.*, 2001). HPIV3 infected dendritic cells have also been shown to have very poor antigen presenting capacity (Plotnicky-Gilquin *et al.*, 2001). Therefore the formation of the adaptive immune response against HPIV3 is impaired.

When present, antibodies against HPIV3 glycoproteins are considered to be the most important in terms of long-term protection (Spriggs *et al.*, 1987). As described above, HPIV3 has a mechanism that down regulates the production of F proteins (Lingemann *et al.*, 2015) thus further down-regulating the production of neutralising antibodies. It has been shown that mutations that abolish this mechanism cause a significant increase in anti-F antibodies that is not correlated with, and therefore cannot be attributed to a rise in viral load (Lingemann *et al.*, 2015). Moreover IgG transport into the respiratory lumen is inefficient and IgA antibodies required for protection are short lived (Fields, Knipe and Howley, 2013). There is currently little experimental evidence linking HPIV3 HN and F phenotype with variations in the adaptive immune response (Kato *et al.*, 1999; Lingemann *et al.*, 2015). However it could be argued that more fusogenic strains would be not only more effective in triggering the inflammatory response but

equally in generating a more robust long-term adaptive immune response with a potential impact on clinical severity.

1.6 Thesis aims

As described above, HPIV3 is an important pathogen with significant clinical impact. Overall, to date, there is little data and consensus on the interplay between host and virus factors in the pathogenesis and disease severity caused by HPIV3 (Schomacker *et al.*, 2012). It is widely accepted that HPIV3 has a particularly significant impact in immunocompromised patients, which would indicate that host response is an important contributor to the pathogenesis of HPIV3 infection (1.3.3 Morbidity and Mortality). However it has also been shown that clinical severity can be correlated to viral phenotype and to the fusogenicity of the viral strain in particular (1.5 Pathogenesis). Despite this, there is little data on the genetic diversity of circulating strains, potential correlation with their phenotype and consequently clinical impact.

As immunity to HPIV3 is incomplete, regular peaks in cases in late spring and summer occur in the community (Zhao *et al.*, 2017). This has the potential to lead to outbreaks in healthcare settings with ensuing impacts on morbidity and mortality as well as structural and financial consequences for the health service, such as ward closures and bed shortages. Although there are a number of potential therapeutic candidates for HPIV3, there is currently neither licensed treatment nor vaccine (see Section 1.3.3). While much research has been conducted in this area, most of it has been carried out on significantly culture adapted reference strains (see Section 1.4.1). As mentioned above, there is sufficient evidence to support that these do not represent a true reflection of circulating wild type strains (Palmer *et al.*, 2012, 2014). Therefore there is a clear need for models for therapeutic candidates based on HPIV3 strains that are present in the natural host.

Therefore the goals of this thesis are summarized as follows:

1. To characterise phenotypically circulating clinical strains of HPIV3 in the UK
2. To characterise phylogenetically circulating strains of HPIV3 in the UK
3. To create a robust model for testing of therapeutic candidates for HPIV3

2 Chapter 2: Materials and methods

Full ethics statement available in Appendix 1 – Ethics approval

2.1 Sample collection

Clinical strains were obtained from HPIV3 positive respiratory patient samples collected between 2011 and 2015 by the PHE laboratory, Addenbrooke's hospital, Cambridge. This laboratory covers Cambridge University Hospitals as well as the wider geographical area of North Herfordshire, East Anglia, Lincolnshire, Watford, Milton Keynes, Peterborough & Luton. All identifiable information was removed prior to the study. Anonymous patient demographics such as age, sex, location, as well as date and type of the sample were retained where possible. For the purposes of outbreak tracing all outbreak samples were link-anonymised. Hereby the samples were anonymised for laboratory work, but were linked to codes that could be identified by the clinical laboratory and other teams. Patient demographics and immunosuppression status were retained where possible. Further patient information including patient movement, symptom onset, other organisms isolated and clinical outcome were extracted from EPIC hospital systems (www.epic.com) where required.

All patients were originally diagnosed by routine respiratory diagnostic PCR on upper respiratory tract samples (either swabs or naso-pharyngeal aspirates). The multiplex PCR diagnostic panel used has been validated for the PHE diagnostic laboratory at Addenbrooke's hospital, Cambridge and includes the following common respiratory viruses: influenza A and B, RSV, enterovirus, rhinovirus, HMPV, adenovirus and HPIV1-4. The samples were identified as belonging to human parainfluenza virus 1 and 3 by the respiratory diagnostic panel and subsequently subtyped further by the HPIV subtyping PCR panel.

2.2 Cells, virus and inhibitors

2.2.1 Reference virus strain and inhibitors.

The culture adapted HPIV3 strain (MK9) was obtained from Public Health England (PHE) culture collections (www.phe-culturecollections.org.uk). Ribavirin (RBV) and zanamivir (ZNV) were obtained from Sigma and favipiravir (FVP) from Atomax.

2.2.2 PLC/PRF5 cells

The PLC/PRF5 human Alexander hepatoma cell line was obtained from Public Health England (PHE) culture collections. HPIV3 has been cultured previously in numerous cell lines including, among others: CV-1, 293T, Hep2, MDCK and Vero (Palmer *et al.*, 2012; Jochmans *et al.*, 2016). In this case the PLC/PRF5 cell line was chosen as it was previously used for tissue culture based diagnosis of respiratory viruses in the laboratory that supplied clinical samples for this study. More importantly, it was judged, that as this line was suitable for tissue culture-based diagnostics, it would be suitable for isolation of clinical strains.

The PLC/PRF5 cell line was maintained in Dulbecco's Modified Eagle Medium (DMEM) high glucose medium supplemented with 10% fetal bovine serum (FBS), penicillin (100 SI units/ml), streptomycin (100 µg/ml) and 2 mM L-glutamine at 37°C in 5%

2.2.3 Human airway epithelial cells

Human airway epithelial (HAE) cells were obtained from Epithelix. These were nasal cells sourced from a single donor: 46-year-old Caucasian female with no recorded relevant medical history. Cell integrity, morphology, cilia beating frequency and screens for other pathogens (Mycoplasma, HIV 1 and 2, hepatitis B and C) were carried out by Epithelix prior to shipment. Proprietary media (cat number EP05MM) for cell maintenance was purchased from Epithelix. Cells were transferred into media upon arrival and were maintained at 37°C at 100% humidity, 5% CO_2. The medium was changed every 2-3 days as per the protocol supplied by Epithelix. Surface mucus was removed once a week by washing the surface of the culture three times by adding 200 µl of sterile pre-warmed PBS and incubating for five minutes at 37°C before aspirating.

2.3 Growth of virus and preparation of stock

2.3.1 PLC/PRF5 cells: infection and harvesting protocol

Cell monolayers were set up at 70% confluence in T25 flasks and each monolayer was inoculated with 20 µl clinical sample in 200 µl maintenance

medium (high glucose DMEM with 1% fetal bovine serum (FBS) and 2mM L-glutamine) supplemented with penicillin 100 U/ml, streptomycin 100 µg/ml, gentamicin 50 µg/ml, ceftazidime 50µg/ml, vancomycin 50 µg/ml and fungizone (amphotericin B) 5 µg/ml to minimise bacterial and fungal outgrowth. Infections were carried out at 37°C for 2 hours. The inoculum was then removed, the cells washed twice in PBS, covered with maintenance medium as above and incubated for 4 days at 33°C in 5% CO_2. Supernatant samples of 50 µl were collected on day zero and day four. Viral growth was evaluated by quantifying viral copy number in the supernatant samples by qPCR (see protocol below). Samples that demonstrated significant yield were freeze-thawed and aliquots were stored at -80°C for further experimental work.

2.3.2 PLC/PRF5 – growth, preparation of stock and cell culture adaptation

Growth of clinical samples in immortalised cells was carried out in two cycles. During the first cycle the cells were infected as described above and viral yield was characterized as positive (an increase of $>10^3$ viral genome copies/ml); intermediate (an increase between 5-10^3 viral genome copies/ml) and negative (an increase <5 viral genome copies/ml). Samples that were classified as positive were stored at -80°C. Samples that were classified as intermediate underwent a second passage. Additionally 11 samples were chosen at random from those classified as negative for further culture to evaluate potential yield from subsequent passages even if no growth was detected at passage 1. After second passage, positive samples were stored and those classified as either negative or intermediate were passaged one more time, afterwards positive samples were stored and all others discarded.

During the second cycle all samples that were classified as non-positive at passage one, underwent a second passage. Samples classified as positive were stored as above. Overall only samples grown at passage 1 were selected for subsequent work. These underwent an additional passage to maximize stock and to harvest RNA for whole genome sequencing. Additionally 6 clinical strains and the laboratory strain MK9 underwent repeated passage up to passage 10. To this end these strains were inoculated onto PLC/PRF5 cell monolayers in T25 flasks as described above. After each passage the cell monolayers were freeze-thawed,

the supernatant and cells were collected and clarified by centrifugation. Subsequently 20 µl of the clarified supernatant in 200 µl of maintenance media was used as inoculum for the next passage. Virus was harvested for whole genome sequencing and plaque phenotype at passage 1, 5 and 10 (see protocols below).

2.3.3 HAE cells: infection and harvesting protocol

The transwell support containing the cells was placed using sterile forceps into 0.7 ml of fresh HAE culture medium pre-warmed to 37°C. The surface of the cells was washed three times as described above. Cells were then infected with 10 µl of clinical sample in 100 µl of pre-warmed serum free medium supplemented with penicillin 100 U/ml, streptomycin 100 µg/ml, gentamicin 50 µg/ml, ceftazidime 50 µg/ml, vancomycin 50 µg/ml and fungizone (amphotericin B) 5µg/ml to minimize bacterial and fungal out growth, as above. Cells were then incubated at 37C, 5% CO_2 for 60 minutes. Following incubation the virus was removed from the apical surface by pipetting and cells were incubated as before. Apical samples were collected at 72 hours from the apical surface. 300 µl of pre-warmed PBS was added to the apical surface and cells were incubated at 37°C, 5% CO_2 for 30 min. Following the incubation the sample was removed by pipetting and viral titre was quantified by qPCR protocol (see below). Wells where growth was detected were freeze-thawed to maximize virus yield and stored at -80°C for further experimental work. Whole genome sequencing was carried out on RNA extracted from the freeze thawed sample.

2.3.4 Screening for other respiratory viral infections

A 500 µl aliquot from each viral stock was tested on the diagnostic respiratory panel (PHE laboratory, Addenbrooke's) that includes the following common viruses: influenza A and B, RSV, enterovirus, rhinovirus, HMPV, adenovirus and HPIV1, 2, 3 and 4 to exclude other viral respiratory infections. All samples that were infected by other viruses were excluded from further study.

2.4 Plaque protocol, immunostaining and analysis

2.4.1 Optimisation of immunofocal plaque assay

2.4.1.1 Overlay

2 overlays were trialed: Avicel (2.5% in H_20) and agarose (2% in PBS) diluted 1:1 in maintenance media. The plates were incubated at 33°C + 5% CO_2 for seven days. Agarose plates were inverted and Avicel plates were kept immobile for the entire incubation period. The cells were then fixed in formal saline (4% formaldehyde in PBS) for 10 min minimum, the overlays were removed and the cells were washed in PBS before staining. Cells were then stained with a primary commercial HPIV3 HRP conjugated antibody (ThermoFisher scientific, goat, anti HPIV 3 and 2, HRP conjugated; catalogue number PA1-73040) and subsequently with a secondary antibody, active in the 800 channel of the Li-Cor Odyssey imager (IRDye800CW anti-goat). These were subsequently scanned on the Li-Cor Odyssey imager.

2.4.1.2 Stain

3,3'-diaminobenzidine (DAB) stain was prepared using a previously published protocol (Thordal-Christensen *et al.*, 1997). In brief, stock solutions of 1% DAB and 0.3% hydrogen peroxide were prepared, aliquoted and stored. When required, 250 µl of 1% DAB, 250 µl of 0.3% hydrogen peroxide and 5 ml of PBS were mixed to produce a working stain. TrueBlue Peroxidase Substrate (KPL, SeraCare, catalogue number 5510-0052) stain required no prior preparation.

2.4.2 Immunofocal plaque assay

Monolayers at 80-90% confluence (1 x 10^6 cells/well) were set up in 6 well plates and infected with serial dilutions of virus stock (500 µl/well). Infections were carried out in maintenance medium (high glucose DMEM supplemented with 1% fetal bovine serum (FBS), penicillin (100 SI units/ml), streptomycin (100 µg/ml) and 2 mM L-glutamine) at 37°C for 2 hours. The inoculum was then removed and the monolayers washed twice in PBS. A 1% agarose overlay with 50% maintenance medium was applied to the infected monolayer. The plates were then incubated inverted at 33°C in 5% CO_2 for 7 days. Subsequently they were fixed with 4% formaldehyde in PBS, the agarose plugs were removed and

the monolayers were washed three times in PBS prior to immunostaining. Each titration was performed in triplicate.

The infected cells were stained with a mixture of three rabbit polyclonal anti-F HPIV3 antibodies at 1:5000 dilution in PBS containing 5% FBS at room temperature for 1 hour (500 µl/well). The antibodies were raised against the following epitopes NQESNENTDPRTERF (amino acids 96-110), NRVDQNDKPYVLTNK (amino acids 525-539), and KEWIRRSNQKLDSIG (amino acids 471-485) of the F protein. The cells were then washed three times with PBS, leaving each wash on for 5 min, and subsequently incubated with an anti-rabbit HRP conjugated secondary antibody at 1:1000 in PBS containing 5% FBS at room temperature for 1 hour (500 µl/well). The cells were washed 5 times in PBS and reacted with True Blue Peroxidase substrate (SeraCare) (500 µl/well) for 20min at room temperature. The plaques were scanned and subsequently identified and measured using the Fiji analyze particles module (Schindelin *et al.*, 2012).

2.4.3 Plaque processing and analysis

The plates were then scanned on Epson Perfection V330 Photo scanner at the following resolutions: 800 dpi for small plaque phenotype and 300 dpi and 500 dpi for large and medium plaque phenotype for plaque counting and surface area measurements respectively. The plaques were then analysed using the Fiji analyse particles module. In brief, the global scale was set by measuring the diameter of a well in pixels on the image and scaling it to the physical diameter of the well (diameter = 34.8 mm for a 6 well dish (http://csmedia2.corning.com/LifeSciences/Media/pdf/cc_surface_areas.pdf)).

The image was then transformed to 32 bit. Background was subtracted with the setting “light background” and a rolling ball radius of 50 pixels. The image was then converted to binary by using the “make binary” function and plaques were separated using the “watershed” function where required. The function “analyse particles” was then used with particle size and circularity adjusted according to the properties of the plaques measured, plaques on edges were excluded and the options “show outlines” and “display results” were selected. The outline image thus generated was then overlaid onto the original image using the “overlay”

function to confirm that all plaques were correctly identified and included by the analysis. Adjustments to particle size and circularity were then carried out to optimize the analysis if required. This protocol was adapted from the particle analysis protocol by Image J (https://imagej.net/Particle_Analysis).

2.4.4 Statistical analysis

All statistical analysis was carried out in GraphPad Prism version 6.00 for Mac OS X, GraphPad Software, La Jolla California USA, www.graphpad.com. Linear regressions from the standard curve for qPCR were fitted using the linear regression model. Dose response curves for drug inhibition assays were fitted using the 4 parameter logistic (4PL) fit. Curves with $R^2 > 0.9$ and a $p<0.05$ for replicates test for lack of fit were accepted as adequate models. First order derivatives for growth kinetics were calculated using the XY analysis function of GraphPad version 6.00 as above.

2.5 HPIV3 inhibition by ribavirin, favipiravir and zanamivir

2.5.1 Cell viability assay

Cells in 96 well plates were either mock inoculated or inoculated with serial dilutions of each inhibitor (ribavirin, favipiravir or zanamivir) starting with a concentration of 1 mM in eight biological repeats. Plates were then incubated at 33°C for 7 days and assayed with CellTiter-Blue® Cell Viability Assay (Promega) as per the manufacturer's instructions. The dose of 1mM was chosen to reflect the upper limit of a potential physiological dose in a patient.

2.5.2 Plaque reduction assay

Cell monolayers were either mock inoculated or inoculated with the MK9 reference strain stock dilutions required to produce 20-100 plaques in each well. Inhibitors at required concentrations, or an equivalent volume of diluent were added to the overlay and the monolayers were incubated for 7 days, fixed and immunostained and plaque area was measured.

2.5.3 Growth inhibition assay

Cell monolayers were either mock inoculated or inoculated with laboratory strain (MK9) virus stock in triplicate. The inoculum was then removed and the monolayers were washed, covered with maintenance medium containing the inhibitors at required concentrations, or the equivalent volume of diluent, and incubated for 24 hours. Following the incubation period both the supernatant and the cells were harvested. Subsequently the concentration of released virus in the supernatant was determined by plaque titration. Viral RNA levels in infected cells was determined by qPCR and normalised to the total RNA in the sample.

Subsequently growth kinetic inhibition experiments were carried out on clinical strains as above. Two concentrations of each inhibitor, corresponding to the 50% maximum effective concentration (EC_{50}) and 90% maximum effective concentration (EC_{90}) values, as interpolated from the dose response curve of infectious particle reduction in the supernatant using reference strain MK9, were used. The EC_{50} value for zanamivir was inferred from the dose response curve of the reduction of viral copy number by qPCR and the higher concentration was taken as the maximum concentration assayed, 1 mM.

2.5.4 Binding inhibition with zanamivir

Cell monolayers were inoculated with laboratory strain (MK9) in triplicate with the required viral dilutions in maintenance medium, with or without the indicated concentrations of zanamivir. The inoculum was then removed, the cells were washed with PBS, covered with agarose overlay and incubated, fixed and immunostained as per protocol above.

2.5.5 Pre-incubation with zanamivir

High viral titres (at least 10^5 PFU/ml) were pre-incubated with different concentrations of zanamivir or with equivalent volume of diluent (PBS) for 1 hour at 37°C. Mock controls with virus on its own, UV inactivated virus with zanamivir, and zanamivir on its own, were included. Post incubation, the remaining infectivity in the sample was determined by plaque assay. Each sample was diluted at least by a factor of 10^4, ensuring that any residual inhibitor effect was negligible.

Subsequently binding inhibition and pre-incubation with zanamivir was carried out on five clinical strains that were shown to be significantly more susceptible to EC_{50} ZNV by growth inhibition (see above). For binding inhibition two concentrations of the inhibitor were used. The lower concentration corresponded to the EC_{50} interpolated from the dose response curve of binding inhibition using laboratory strain MK9 and the higher was the maximum concentration used 1 mM. For pre-incubation with ZNV only the maximum concentration of 1 mM was used.

2.6 HPIV3 growth kinetics in HAE cells

2.6.1 Growth kinetics – sample infection and harvesting

This protocol was adapted from a protocol kindly provided by Dr Lauren Parker in the Barclay Laboratory, Imperial College, London.

The transwell support containing the cells was placed using sterile forceps into 0.7 ml of fresh HAE culture medium pre-warmed to 37°C and the cells were washed as described above.

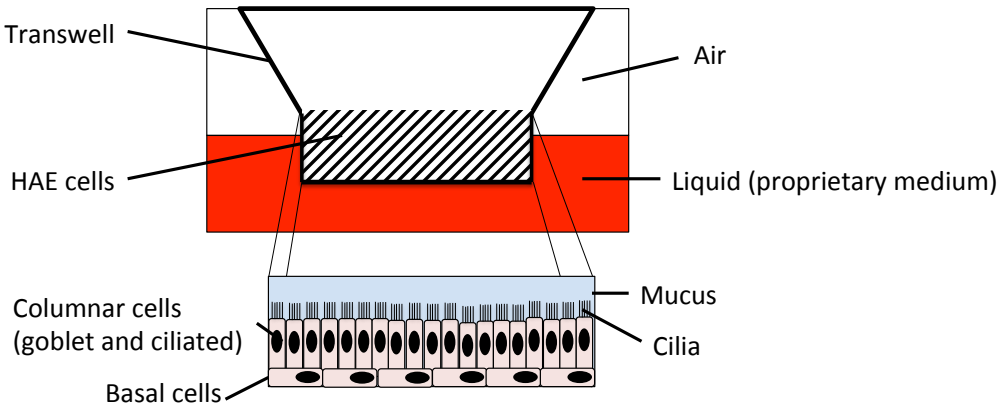

Figure 2-1 Diagram of transwell support with HAE cells. HAE cells were grown in transwell supports, each resting in 0.7 ml of HAE culture medium at an air/liquid interface. This 3D cell culture was comprised of basal and columnar (goblet and ciliated) cells forming tight junctions. The beating cilia were covered by a layer of mucus that was removed by gentle washing at regular intervals and prior to infection as described in the text.

The cells were then infected or mock-infected at 0.001 MOI (the number of $5x10^5$ cells/well was assumed) in 100 µl of pre-warmed PBS and incubated at 37°C, 5% CO_2 for 60 minutes. Following incubation the virus was removed from the apical surface by pipetting and cells were re-incubated as before. All infections were carried out in biological triplicates apart from mock-infected wells that were biological duplicates.

Samples were taken at required timepoints from both the apical surface and the basolateral surface. For apical collection 300 µl of pre-warmed PBS was added to the apical surface and the cells were incubated at 37°C, 5% CO_2 for 30min. Following the incubation the virus was removed by pipetting and stored at -80°C in 50 µl aliquots for further processing. An aliquot was then defrosted for each sample and plaque titrated to determine the virus yield in the supernatant. For collection from the basolateral surface, the transwell membrane was transferred to a new 24 well plate, containing 0.7 ml of pre-warmed culture medium. The spent medium was then harvested and stored at -80°C in 50 µl aliquots for further processing. One aliquot of each basolateral sample was then defrosted, RNA extracted and virus yield was measured by qPCR.

At the final timepoint, cells from one infected well/strain were lysed and stored in lysis buffer for further analysis. Cells from the second infected well/strain, as well as from one of the mock infected wells were fixed in 4% paraformaldehyde freshly diluted in PBS overnight at +4°C and stored in PBS. Cells from the final set of wells were freeze-thawed and plaque titrated to determine the virus titre in the cells for each sample.

2.6.2 Cytokine and chemokine measurements

Cytokine and chemokine measurements were carried out using the Cytokine & Chemokine 34-Plex Human ProcartaPlex Panel 1A kit on samples obtained from the basolateral surface or HAE cells. The kit contained the following targets: Eotaxin/CCL11; GM-CSF; GRO-α/CXCL1; IFNα; IFNγ; IL-1β; IL-1α; IL1-RA; IL-2; IL-4; IL-5; IL-6; IL-7; IL-8/CXCL-8; IL-9; IL-10; IL-12 p70; IL-13; IL-15; IL-17A; IL-18; IL-21; IL-22; IL-23; IL-27; IL-31; IP-10/CXCL-10; MCP-1/CCL2; MIP-1α; MIP-1β; RANTES; SDF1α; TNFα; TNFβ. All samples were diluted in a ratio 1:1 apart from samples taken at the final time point (72 hours) where the samples

were diluted 1:10 in DMEM. The assay was read on a Luminex 200 system Luminex xPONENT for LX100/LX200 version 3.1; the doublet discrimination (DD) gate was set at 5,000-25,000 with a timeout of 60 seconds and bead event/bead region at 50-00 as per manufacturer's instructions. The final concentrations of each target were calculated based on the standard curve generated used the Bio-Plex Manager Software version 6.1 using the standards supplied by the manufacturer. All statistical analysis was carried out using GraphPad 6.00, as described above.

2.7 Molecular methods and sequencing

2.7.1 qPCR

Total RNA from samples was extracted using the GenElute Mammalian Total RNA Miniprep kit (Sigma) according to the manufacturer's guidelines. This was amplified on the ViiA7 Real Time PCR system (Applied Biosystems) using a qPCR protocol obtained and modified from the standard operating procedure (SOP) for HPIV3 typing used by the PHE diagnostic laboratory, Addenbrooke's Hospital, Cambridge. The primers and the taqman probe used were: forward 5'-GCTCCTTTYATCTGTATCCTCAGAGATCC-3' (nucleotides 1035-1063, accession number NC_001796.2); reverse 5'-TGATCTTCCCGTCACATACTGTTGCATG-3' (nucleotides 1172-1145, accession number NC_001796.2) probe 5'-FAM-ATAGTTGCCTGGTGCGAA-TAMRA-3' (nucleotides 1094-1077, accession number NC_001796.2). The cycling conditions used were: hold at 50°C for 30 min, hold at 95°C for 2 min, followed by 45 cycles, while acquiring fluorescence data, through 95°C for 15 s and 60°C for 60 s. An amplicon from the diagnostic assay positive control was obtained and cloned by TA cloning using the PureYield™ Plasmid Midiprep System (Promega). The sequence of the amplicon aligned to 138bp of the nucleocapsid gene of HPIV3 (nucleotides 1035-1172 accession number NC_001796.2). Ten fold serial dilutions of the plasmid were subsequently used to establish a standard curve. Linear regression of the standard curve for genome copy number quantification was fitted using GraphPad Prism version 6.00.

2.7.2 Whole genome sequencing

2.7.2.1 RNA extraction and amplification for whole genome sequencing

Total RNA from samples was extracted using the GenElute Mammalian Total RNA Miniprep kit (Sigma) according to the manufacturer's guidelines. Full genome amplification was achieved using a set of twelve primers producing twelve overlapping amplicons (Figure 2-2). All primer pairs, apart from pairs 4 and 8, were generated in a pilot project conducted prior to this PhD by Dr Kyriaki Ranellou. Primers 4F and 8R were generated as part of this project. The kit used was Superscript III One-step RT-PCR System with Platinum Taq High Fidelity from Invitrogen. The RT step was performed at 50°C for 30 min. This was followed by a 2min denaturation step at 94°C, and 35 cycles of denaturation (94°C for 15 s), annealing (55°C for 30 s) and extension (68°C 3 min 30 s). After the final extension step (68°C for 5 min) the reaction was held at 4°C. Following amplification the products were ran on a 1% agarose gel for confirmation and cleaned following the Epoch Life Science Quick Protocol for EcoSpin All-in-one Mini Spin Columns.

A

Primer pair		Primer sequence	Fragment (bases)
1	F	ACCAAACAAGAGAAGARACTTGTYTG	1-520
	R	TCCAGGTCACTTCCAAATATCCA	
2	F	CAGCYGGTGGAGCTATCATT	166-2127
	R	GAGCTGCTTCTTCTCCCAGG	
3	F	AAACAARGCAGTCAACCACC	1569-2646
	R	TCTGTTTGCCCCTTTGTGTC	
4	F	CGATTGCTCTCTTCTGTATCCTTCC	2148-4212
	R	TGGCATCRAACAGCATTCCT	
5	F	ACCCCACATTAGAGTTGCCA	3860-5659
	R	TCCTGCTGCTTCACAACCTA	
6	F	GGACACAAAYAAAGCAGTGC	5527-7587
	R	AGGAGTGCTAGAGARATGACT	
7	F	ACTCAGACTTGGTACCTGACT	7500-9398
	R	TGCACTTATATTCCATCGGCC	
8	F	AYGTGCTATCRAAATTAGCCTCA	9046-11184
	R	AGCYTGAGGAAGAATTCTCCCATCATA	
9	F	ATAGGYGTGAGGGTGACTGC	10929-12433
	R	TGTGAGGCTTCCATCCAAGA	
10	F	GGACTTGAAACRCCTGACCCA	12111-14064
	R	GGAAGAGCCTGTCCTTGTCT	
11	F	GAAGGTAGRGATCTCATTTGGGA	13164-15067
	R	CCTGTAAGYAATCGAGTCGAT	
12	F	TYGGAATCAACAGCACTAGTTG	13975-15462
	R	ACCAAACAAGAGAAGAACTCTGYTTGG	

B

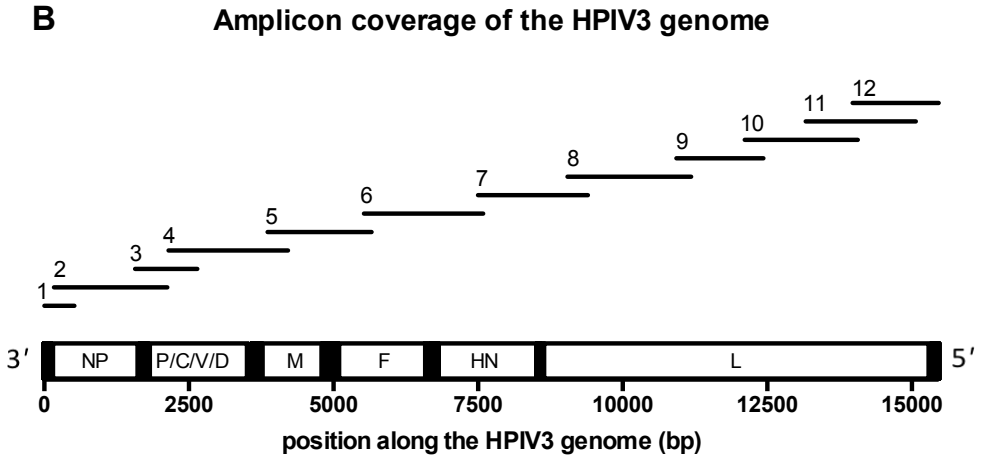

Figure 2-2 Primers used for full genome sequencing of HPIV3 (A) and the position of the amplicons along the HPIV3 genome (B) 12 primer pairs were designed (A) and used to generate overlapping amplicons covering the entire HPIV3 genome as shown in (B)

2.7.2.2 Reference sequence and validation of the pipeline

Two of the isolates, MK9 and 153, were first sequenced by Sanger sequencing to validate the NGS sequencing pipeline. Primers were originally designed using the genscript sequencing primer design tool (http://www.genscript.com). These were used for Sanger sequencing together with the amplification primers, aiming for overlapping amplicons < 700bp each. The sequence was then aligned to a consensus extracted from the following sequences: KF687321, KF530255, EU326526, KF530227, KF687319, KF530232, KF687317, KF530249, KF530245, KF530250, KF530229, KF530243, AB736166, KF530252, KF530236, KF530225, KF687340, KF530254, KF687318, KF530230, KF687346, KF530233, KF530242, KF530251, KF530241, KF530253, KF530257, KF530238, KF530231, KF530234, KF530247, EU424062, KF530256, FJ455842, KF687336, U51116, NC_001796.2 using Sequencher 5.4 from Genecodes (https://www.genecodes.com).

2.7.2.3 NGS sequencing and analysis

The amplicons generated had their concentrations determined on a nanodrop spectrophotometer (Thermo Scientific), were combined in equimolar concentrations and sequenced on the Illumina platform. Paired short reads were then processed with Trimgalore to remove the Illumina paired end library adapters (Nextera (https://support.illumina.com/)) as well as short and low quality reads to retain those with length >20bp and Phred scores >20. Terminal primer sequences were subsequently removed with Cutadapt (Martin, 2011). Alignment was performed with Bowtie2 (Langmead and Salzberg, 2012), with the alignment score "–-score-min" of -0.6, using the Sanger sequences obtained above as reference (strain 153 was used as a reference sequence for clinical strains) and the consensus was extracted with Samtools (Li *et al.*, 2009). The "–-score-min" of -0.6 meant that for a sequence length of 150bp (approximate maximum length of sequence obtained), a mismatch of 15 bases was permitted. This provided the optimum tradeoff between a high quality alignment and allowance for genome variability, which has shown only 5% overall divergence between recent clinical strains and the prototype Washington strain (MK9) (Mao *et al.*, 2012) and previously been shown not to exceed 10% at any point in the HPIV3 genome (Palermo *et al.*, 2016). The results were then compared to the

sequences obtained using Sanger sequencing of the laboratory strain MK9 and sequence 153 as well as the consensus sequences obtained using the previously published *de novo* Ebola pipeline using QUASR for quality control and Spades 3.5 for assembly (Arias *et al.*, 2016). In each case the sequences were identical to those obtained using the newly developed pipeline. Variant analysis was subsequently conducted using V-Phaser2 (Yang *et al.*, 2013). The full script for the new bioinformatics pipeline detailed here was written in perl and is shown in Appendix 3.

2.7.3 Sequencing for outbreak tracing

2.7.3.1 Extraction and amplification

Total RNA from samples was extracted using the GenElute Mammalian Total RNA Miniprep kit (Sigma) according to the manufacturer's guidelines. Amplification was carried out using nested PCR with the following primers:

		sequence	position (bp)	product size (bp)
primer set 1	forward	CAAGAGTRGATGCAATTTTCCAACC	4182-5535	1353
	reverse	GTTGACYARTACACCTACATGCTG		
primer set 2	forward	GGGCYTCATCAGTAGAGATYA	4703-5160	457
	reverse	GCACTGCYTTRTTTGTGTCC		

Table 2-1 Primers used for amplification of HPIV3 fragment for outbreak tracing. The primers used for nested PCR amplification of HPIV3 fragment for outbreak tracing for cycle 1 (primer set 1) and cycle 2 (primer set 2). The amplification products covered the hypervariable region of HPIV3 between the M and the F coding regions of the genome, as in Figure 5-3.

The first cycle (primer set 1) was performed using the Superscript III One-step RT-PCR System with Platinum Taq High Fidelity from Invitrogen. The reverse transcription (RT) step was performed at 50°C for 30 min. This was followed by a 2min denaturation step at 94°C, and 35 cycles of denaturation (94°C for 15 s), annealing (55°C for 30 s) and extension (68°C 3 min 30 s). After the final extension step (68°C for 5 min) the reaction was held at 4°C. The second cycle was performed with Taq DNA polymerase (Invitrogen) with the same cycling conditions without the RT step (5 µl of product of the first cycle amplification was used as template).

Following two cycle amplification the products were ran on a 1% agarose gel for confirmation and cleaned following the Epoch Life Science Quick Protocol for EcoSpin All-in-one Mini Spin Columns. Rhinovirus genotyping was attempted for patients 1,3,7,11,14 and 15 and was conducted according to a previously published protocol (Wang et al. 2015).

2.8 Epidemiology and phylogenetics

2.8.1 Epidemiology

The number of samples tested positive for HPIV3 was extracted from the local hospital records from January 2011 until end of August 2017. Positive samples were deduplicated by each patient's unique hospital number, their date of birth, and if they had a positive sample within 72 days of a previous positive sample (Piralla *et al.*, 2009). The data were visualized in GraphPad Prism version 6.00 for Mac, GraphPad Software, La Jolla California USA, www.graphpad.com. All samples were link-anonymised for laboratory work and patient demographics and immunosuppression status were retained where possible. Further patient information including patient movement, symptom onset, other organisms isolated and clinical outcome were extracted from the hospital electronic patient record.

2.8.2 Phylogenetics

All HPIV3 full genome sequences available on NCBI were downloaded and genomes originating from the same source and found to contain minimal variance were removed for clarity and to minimize bias. Sequences in Genbank that originated from strains that were repeatedly passaged in culture or were deliberately modified, such as strain 47885, C243, 14702 and strain JS, were also removed, leaving 36 diverse full genome sequences. These, together with the 20 sequences obtained in this project were aligned in UGENE using the Muscle algorithm (Okonechnikov, Golosova and Fursov, 2012). Subalignments were extracted using UGENE. The most suitable substitution model was selected using the JModelTest 2.0 Software (Darriba *et al.*, 2012). Position by position rates, distance matrices and maximum likelihood trees were generated using

Molecular Evolutions Genetics Analysis (MEGA) software version 7 (Tamura *et al.*, 2007). 1000 bootstrap iterations were used for maximum likelihood tree confidence estimates. Clusters were visualized using Automatic Barcode Gap Discovery (ABGD) (Puillandre *et al.*, 2012). A Bayesian Markov Chain Monte Carlo (MCMC) inference model was selected using marginal likelihood estimation using path sampling (PS) and stepping stone sampling (SS) with BEAST v1.8.4 with a chain length of one million and one hundred path steps respectively (Bryant, Holmes and Barrett, 2007; Xie *et al.*, 2011; Ayres *et al.*, 2012; Drummond *et al.*, 2012). Tracer was used to assess convergence based on the effective sample size with 10% burn-in and effective sample size (ESS) values above 200. Maximum clade credibility trees were generated with Tree Annotator and subsequently visualized and edited using FigTree v1.4.3 (http://tree.bio.ed.ac.uk/software/figtree/).

2.8.3 Outbreak - transmission mapping

15 patients involved in the outbreak were identified. Data pertaining to patient admissions was collected between 08/05/2017 and 31/08/2017. In order to visualize the respective locations of patients, a timeline incorporating admission dates, symptom onset and first confirmed HPIV3 positive sample was constructed in GraphPad Prism version 6.00 for Mac, GraphPad Software, La Jolla California USA, www.graphpad.com. Data was then organized in an SQL database. For the purposes of the model, the susceptibility period was defined as 1-7 days prior to symptom onset and the infectious period as 4 days prior to symptom onset. The patient was then considered infectious for the remaining duration of the outbreak due to the prolonged asymptomatic shedding exhibited by this patient cohort. Symptom onset was defined as any viral respiratory symptom in either the upper or lower respiratory tract including exacerbations of previously known respiratory conditions. Where no symptom onset date was available, the date of the first positive HPIV3 sample was used. The locations of patients included the paediatric oncology ward involved in the outbreak, the paediatric day unit (PDU) and the paediatric intensive care unit (PICU). Patients were in isolation at various times during their stay and freely ambulant on the wards during others. The data was subsequently visualized in KNIME 3.3.2

FoodChain-Lab (Weiser *et al.*, 2016). SQL database analysis and KNIME 3.3.2 FoodChain-Lab visualization was conducted by Callum Pearson (PHE, department of Epidemiology, Addenbrooke's Hospital, UK)

3 Chapter 3: Protocol optimisation, viral stock growth and phenotype *in vitro*

3.1 Introduction

There is a broad spectrum of pathology and severity that is associated with HPIV3 infection (Herzog *et al.*, 1989; Cilla *et al.*, 2008; Park *et al.*, 2009; Maeng *et al.*, 2012; Shah *et al.*, 2016), from coryzal symptoms in otherwise healthy adults to bronchiolitis to lower respiratory tract infection (LRTI) in the paediatric population and life-threatening pneumonia in the immunocompromised. The above notwithstanding, most studies have used well established and significantly culture adapted strains of HPIV3 and the impact of diversity of clinical strain phenotypes and genotypes on clinical outcome has not been investigated. The current project aimed to elucidate the phenotypic and genetic variation of HPIV3 as well as the sensitivity of different strains to antiviral medication.

HPIV3 positive clinical samples were collected from the PHE diagnostic laboratory, Cambridge University Hospitals and stocks of minimally passaged clinical strains of diverse provenance were grown in tissue culture. To this end protocols for viral growth and detection were optimized, using diagnostic assays as starting points. Additionally, an immunofocal plaque assay was set up and different overlays, antibodies and stains were trialled in order to create a robust infectivity-based assay to assess HPIV3 plaque phenotype. Finally, twelve sets of primers were optimized and an NGS pipeline was validated for whole genome amplification of HPIV3.

The genotypes and phenotypes of 22 clinical strains of diverse dates of collection and provenance as well as the laboratory adapted strain MK9 were then evaluated to determine whether these clinical strains were diverse and distinct from the culture adapted strains of HPIV3. Furthermore, in order to examine the effects of culture adaptation on both genotypic and phenotypic levels, 6 clinical strains of diverse plaque phenotypes were repeatedly passaged in tissue culture and their phenotypes and genotypes were evaluated at passages 1,5 and 10. It was established that the stock of clinical strains generated with minimal passage in tissue culture was sufficiently diverse and distinct from the significantly

culture-adapted strain MK9 and were therefore suitable for further work within this project.

3.2 Sample collection and provenance

The number of samples that tested positive for HPIV3 was extracted from the local hospital records from January 2011 until end of August 2017. Positive samples were deduplicated by each patient's unique hospital number, their date of birth, and if they had a positive sample within 72 days of a previous positive sample (Piralla *et al.*, 2009). The data was visualized in GraphPad Prism version 6.00 for Mac, GraphPad Software, La Jolla California USA, www.graphpad.com.

The number of samples that tested positive for HPIV3 on the respiratory virus panel in PHE Addenbrooke's (Cambridge University Hospitals (CUH)), Cambridge during the years 2011-2017 is shown in Figure 3-1. The prevalence of HPIV3 follows a cyclical pattern with peaks occurring towards the end of spring and start of summer every year.

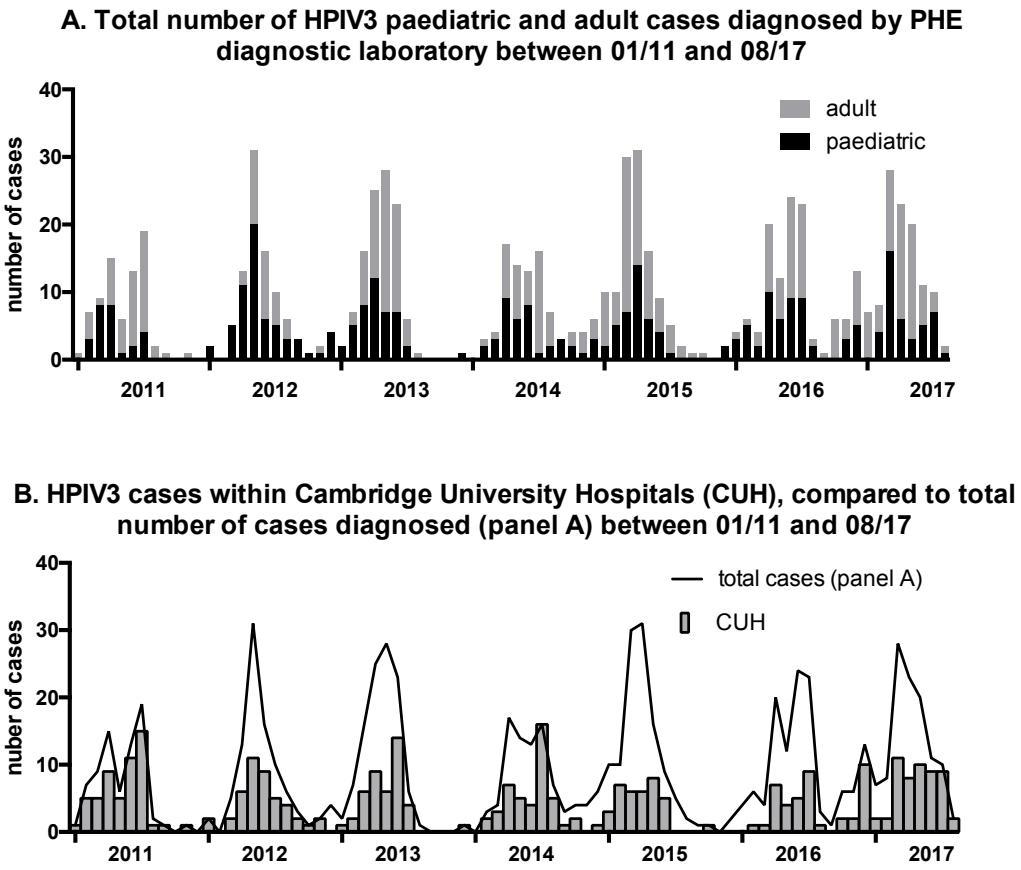

Figure 3-1 Total samples tested positive for HPIV3 by PHE diagnostic laboratory, Cambridge University Hospitals (CUH), during 2011-2017. Panel A shows the total number of samples tested positive for HPIV3 deduplicated by patient number, date of birth and previous positive sample date. The relative number of paediatric and adult cases is shown. Panel B shows the same data, divided by sample provenance, illustrating the proportion of samples originating from CUH and from the general geographical area covered by the laboratory including North Herfordshire, East Anglia, Lincolnshire, Watford, Milton Keynes, Peterborough & Luton.

3.3 Virus detection and growth protocol optimisation

3.3.1 Detection and quantification

3.3.1.1 CPE

The diagnostic criteria for HPIV in tissue culture, as stated in the original SOP, suggested that the presence of syncytia should be used as a marker for HPIV infection (Vainionpää and Hyypiä, 1994). Therefore the cytopathic effect (CPE) demonstrated by both the MK9 lab-adapted strain and a number of clinical isolates was examined to determine whether it constituted an objective and reliable diagnostic criterion.

Some of the results can be seen in Figure 3-2. CPE caused by strain MK9 included cell rounding, destruction and occasional syncytia. This result is characteristic of a tissue culture adapted strain of HPIV3 (Henrickson, 2003). However clinical isolates lack this adaptation and may also contain other pathogens and contaminants that could affect the cell monolayer. For instance, clinical isolate 581 produced CPE with larger cells (Figure 3-2C) and more syncytia, whereas 572 (Figure 3-2D) had a more intact cell sheet but greater cell fusion. Based on these observations it was concluded that CPE could not be considered a reliable marker of infection.

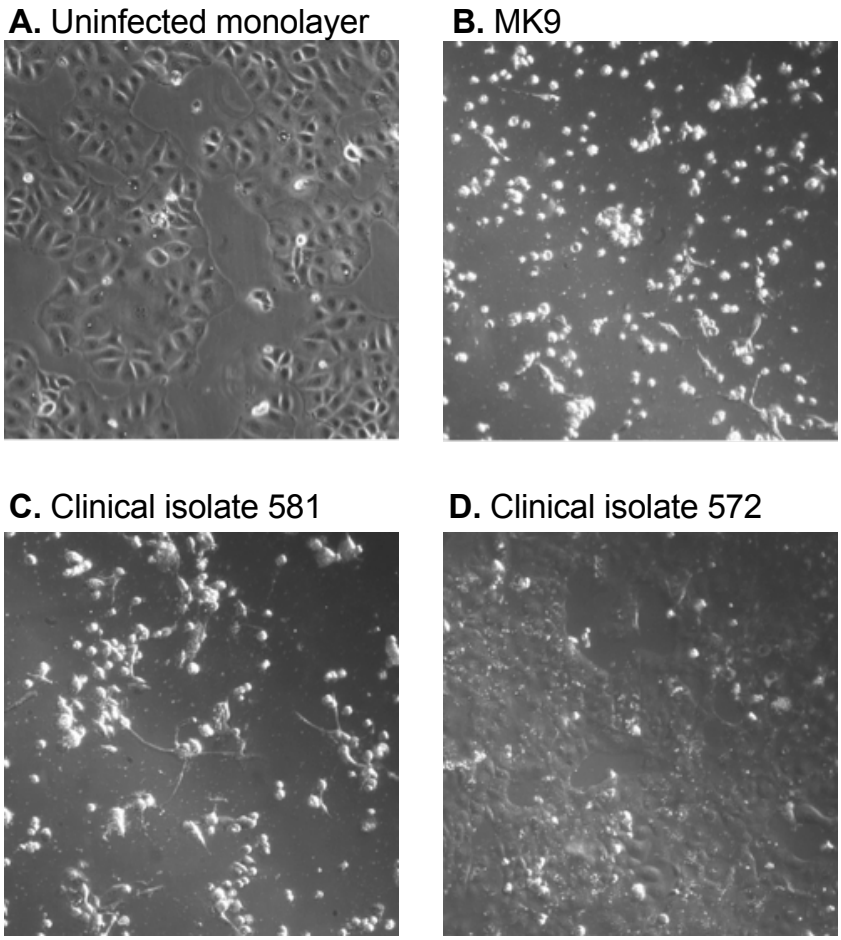

Figure 3-2 HPIV3 cytopathic effect on PLC/PRF5 cell monolayer. PLC/PRF5 cell monolayer (A) was inoculated with strains MK9 (tissue culture adapted lab strain) (B), clinical isolate 581 (C) and clinical isolate 572 (D) as described in the Materials and Methods. The cells were then incubated in maintenance media (see Materials and Methods) and pictures of the cell sheet were taken on day five at x10 magnification.

3.3.1.2 qPCR

A PCR amplicon from an HPIV3 positive sample obtained from the PHE Microbiology and Virology diagnostic laboratory was cloned by TA cloning into a plasmid and subsequently used to establish a standard curve using serial 10 fold dilutions of the plasmid. The full protocol and sequences are detailed in Materials and Methods. Sequences for primers and the taqman probe, as well as the cycling conditions were taken from the diagnostic typing SOP for human parainfluenza viruses (see Materials and Methods for details). As part of the optimization of the protocol two conditions were trialed with primer

concentrations of 100μM and 500μM respectively, the linear regressions were calculated using GraphPad and can be seen in Figure 3-3. As the RT qPCR was found to be efficient at both concentrations, the lower concentration (100 μM) was been chosen for further work.

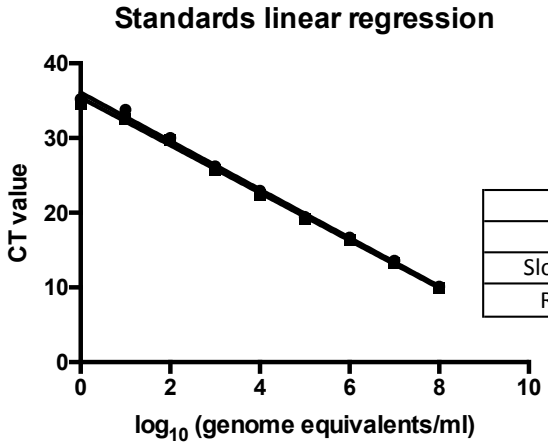

	Primer concentration	
	100nM	500nM
Slope	-3.183	-3.242
R^2	0.9976	0.9965

Figure 3-3 PCR optimization. RT qPCR standards were cloned by TA cloning into a plasmid from a positive control obtained from the PHE Microbiology and Virology diagnostic laboratory. A standard curve using 10 fold dilutions of the plasmid was then established with two primer concentrations 500 μM and 100 μM; respective linear regressions can be seen in the graph, the table shows the corresponding slope and R^2 values

3.3.1.3 Immunofocal plaque assay

Although RT qPCR allows accurate detection and quantification of the amount of viral nucleic acid within a sample, it gives no indication of the number of viable infectious units. To this end a plaque assay was established and optimized using the lab-adapted HPIV3 strain.

3.3.1.3.1 Overlay

Cell monolayers were prepared and inoculated as described in Materials and Methods. After incubation the inoculum was removed, cells were washed twice

in PBS and covered with overlay. 2 overlays were trialed: Avicel (2.5% in H_20) and agarose (2% in PBS) diluted 1:1 in maintenance media. Following 7 days incubation cells were stained with a primary commercial HPIV3 HRP conjugated antibody and subsequently with a secondary antibody, active in the 800 channel of the Li-Cor Odyssey imager as described in Materials and Methods. Our results indicated that the Avicel was not compatible with the immunofocal plaque assay as no HPIV3 plaques were observed. However the agarose overlay allowed clear plaque formation and was therefore used for all subsequent assays.

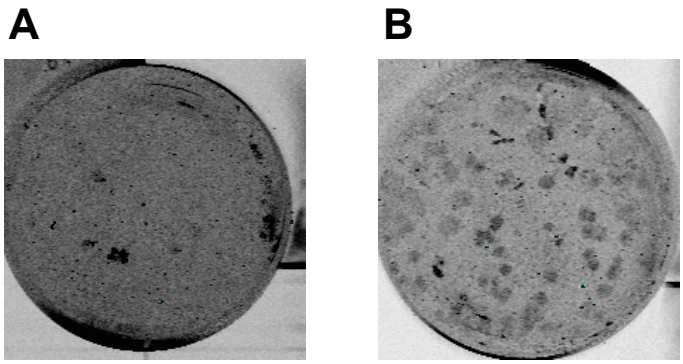

Figure 3-4 Plaque assay overlay optimization. Plaque assays were performed using two different overlays Avicel (A) and agarose (B) using the HPIV3 reference strain MK9. Cell monolayers were prepared and inoculated as described in Materials and Methods. Plaque assays were visualized using the immunostaining method as follows: cells were first incubated with primary antibody (ThermoFisher scientific, goat, anti HPIV 3 and 2) diluted 1:1000 in PBS with 5% serum, then washed three times in PBS and incubated with secondary antibody (IRDye800CW anti-goat, diluted 1:1000 in PBS with 5% serum) for another hour. The cells were then washed five times in PBS and imaged on the Li-Cor Odyssey imager**.**

3.3.1.4 Immunostaining

Due to the number of samples to be analysed further optimisation was undertaken to establish a high contrast strain and an antibody that would detect multiple isolates with equal efficiency. To this end 3,3'-diaminobenzidine (DAB) stain and TrueBlue Peroxidase Substrate were compared and the results can be seen in Figure 3-6. The contrast obtained with TrueBlue Peroxidase Substrate was sufficient for both plaque counting and area measurement as described in Materials and Methods.

However the immunostaining method was reliant on a commercially produced antibody of considerable cost that was raised against an unspecified target. Given the potential issues with the impact of sequence variation on the ability of this antibody to detect clinical isolates we developed our own anti-HPIV3 antibody against highly conserved regions of the F protein. To this end a consensus sequence of the F proteins of HPIV3 was extracted using UGENE (Okonechnikov, Golosova and Fursov, 2012) from an alignment of full protein sequences extracted from the Genbank (AAB21447.1, ABZ85672.1, BAA00012.1, NP_067151.1, BAS30451.1, ACJ70089.1, BAS30450.1) Translation of the F gene of the consensus sequence was also used as an HPIV3 reference (see Materials and Methods). The alignment of F sequences extracted from the Genbank sequences was submitted to a commercial supplier and 3 conserved epitopes for antibody generation (Figure 3-5) were identified.

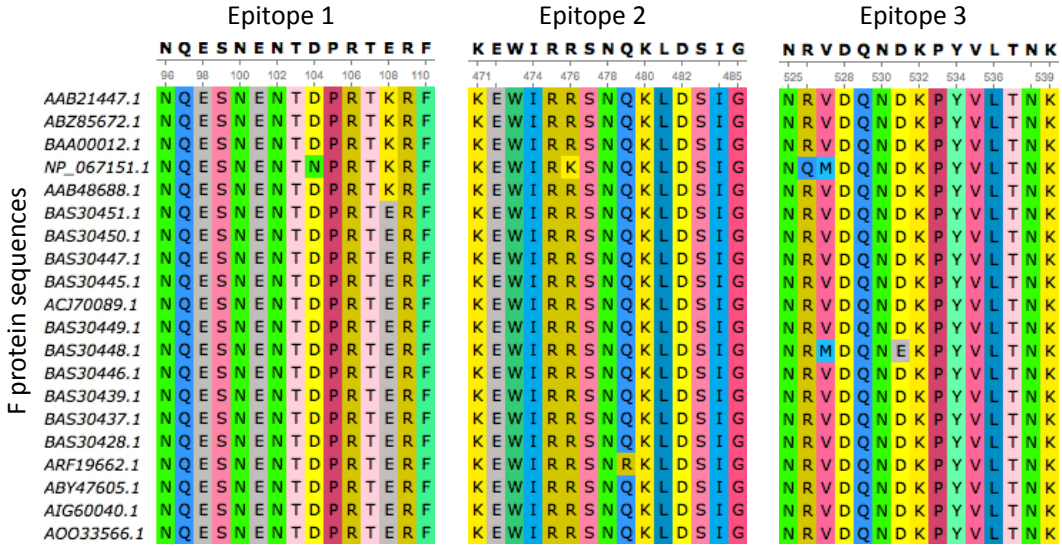

Figure 3-5 Fusion protein epitopes used for anti-HPIV3 generation. Fusion protein alignments were submitted to a commercial supplier and 3 well-conserved epitopes in the fusion protein of HPIV3 were identified. The accession numbers of sequences used are listed and the alignments for the three epitopes (aa 96-110; 471-485; 525-539) are shown as well as the consensus epitopes used for antibody generation.

The purified antibodies were then used for plaque immunostaining as described in Materials and Methods. Each antibody was originally trialled separately and in each case produced high contrast plaques using the MK9 laboratory strain of HPIV3 (results not shown). 1:1:1 mixture of three antibodies was used for the

final optimised immunostaining protocol, the results of which can be seen in Figure 3-6C.

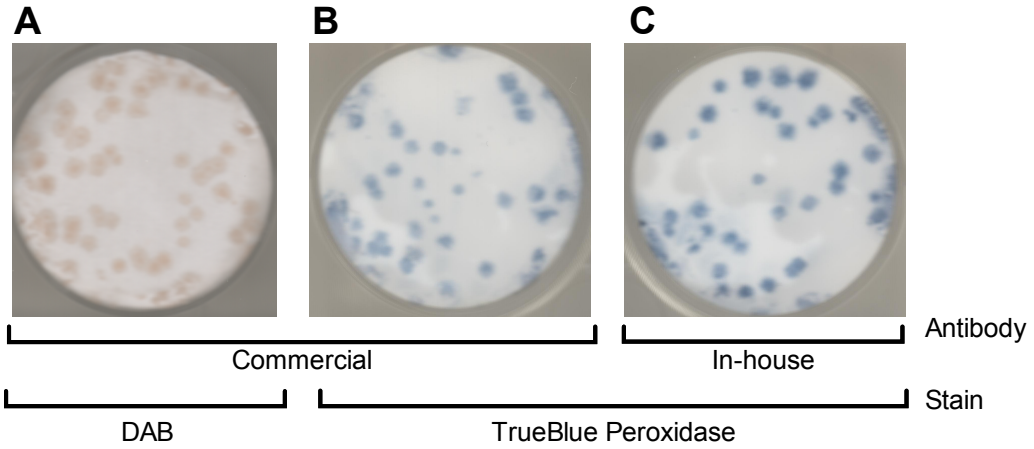

Figure 3-6 Immunostaining protocol optimization All three panels show plaques imaged against a white background produced by laboratory strain MK9. Cell monolayers were inoculated as described in Materials and Methods, plates were covered with agarose overlay and incubated inverted for 7 days. They were subsequently fixed and immunostained. Plaques were incubated with either a commercial anti-HPIV3 antibody (A and B) or a cocktail of 3 rabbit anti-HPIV3 fusion protein antibodies (C) as the primary antibody. As the in-house antibody was not HRP conjugates, the plates in (C) were additionally incubated with a secondary anti-rabbit HRP conjugated antibody prior to staining. Subsequently plaques were stained with either 3,3'-diaminobenzidine (DAB) (A) or TrueBlue Peroxidase stain (B and C).

3.3.2 Optimisation of cell lines

3.3.2.1 Generation of interferon deficient cell lines.

Interferon deficient cell lines have been generated previously in order to increase viral titres obtained in bovine, porcine and human cells of recombinant RSV, Bunyamwera and simian virus 5 (Young *et al.*, 2003), porcine sapovirus (Hosmillo *et al.*, 2014) and influenza A (Pérez-Cidoncha *et al.*, 2014). In an attempt to produce an interferon deficient cell line to improve the yield of HPIV3, the parental cell line was transduced with three lentivirus vectors: BVDV NPro, PIV5 V and empty vector (control). Both BVDV NPro and PIV5 V are known to interfere with the interferon pathway, which forms part of the innate immune response of the cell to infection. BVDV NPro polypeptide targets the interferon regulatory factor 3 (IRF3), a transcription factor essential for interferon promoter activation, for proteosomal degradation (Hilton *et al.*, 2006). The V

protein of parainfluenza virus 5 (PIV5) blocks interferon signalling in human cells by causing degradation of the STAT1 protein, a key component of IFN signalling as well as preventing nuclear translocation of IRF3, a key transcription factor and interferon β (IFNβ) promoter (Carlos *et al.*, 2009).

Therefore in order to increase the virus yield an attempt was made to attenuate the IFN response of the wild type cell line. To this effect PLC/PRF5 cells were transduced with lentiviral vectors expressing BVDV NPro, PIV5 protein or an empty vector. Subsequently the cell lines were evaluated by measuring the HPIV3 viral yield by qPCR and plaque titration, as well as evaluating the plaque phenotype of strain MK9. No differences in viral yield by qPCR (Figure 3-7A) or plaque titration (approximately $4.7x10^5$ PFU/ml, data not shown) or plaque phenotype (Figure 3-7B) were observed in either of the cell lines following infection with the laboratory strain MK9.

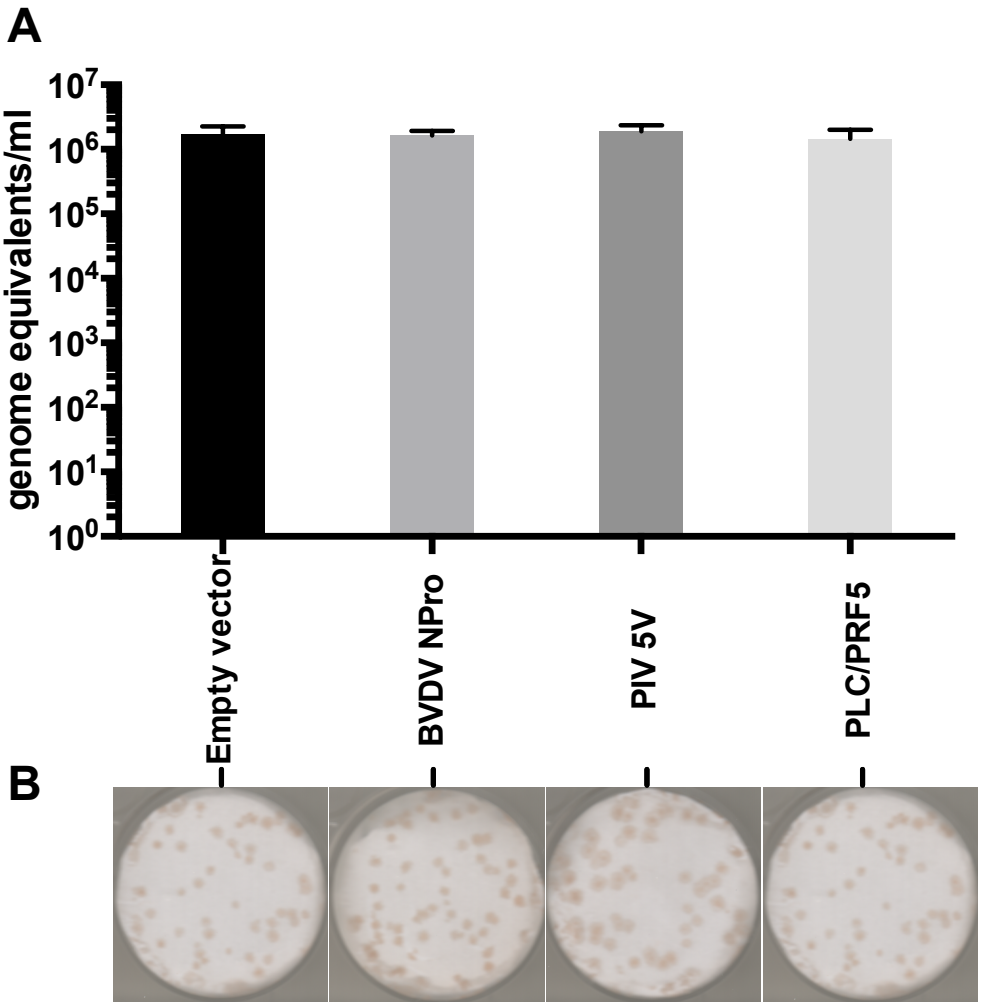

Figure 3-7 HPIV3 laboratory strain infection of the wild type cell line PLC/PRF5 and the cell lines transduced with empty vector, BVDV, NPro and PIV5V. Cell monolayers were prepared and virus was inoculated as described in Materials and Methods. A supernatant sample of 50μl was taken on day four (D4) of incubation and viral copy number was determined by one step RT-qPCR as described in Materials and Methods. Each point represents 3 biological repeats +/-SEM (A). Plaque phenotype (B) was observed at 7 days post inoculation; infection was carried out as described in Materials and Methods with agarose overlay and immunofocal staining with a commercial HPIV3 primary antibody followed by DAB staining, as described in Section 3.3.1.3 **Immunofocal plaque assay**.

As no dramatic changes in viral titre in the transformed cells was detected, the ability of the cells to respond to a mimic of viral RNA was observed. Poly I:C is a synthetic analog of double stranded RNA (ds RNA). Both natural and synthetic dsRNAs are known to induce type I IFNs, especially IFNβ. Poly I:C is recognized by Toll-like receptor 3 (TLR3), this then activates the transcription factor

interferon regulatory factor 3 (IRF3) and NF-κB protein through the adapter inducing IFNβ (TRIF, also known as TICAM-1) leading to the release of IFNβ, a simplified summary of this pathway can be seen in Figure 3-8. The outcome of poly I:C stimulation of the cell lines is shown in Figure 3-9.

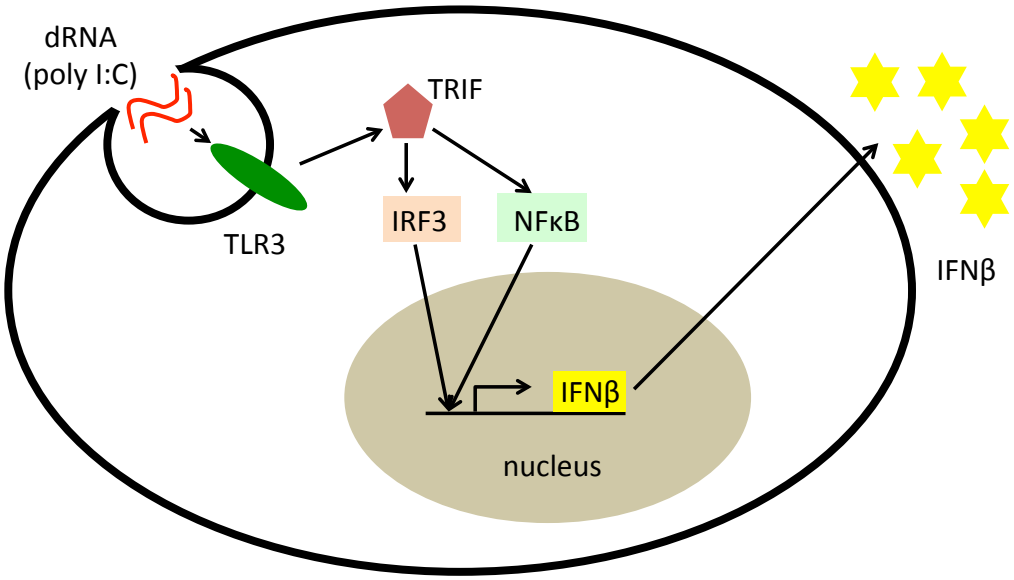

Figure 3-8 Simplified summary of IFNβ induction by poly I:C stimulation of the cell. Poly I:C, a dRNA mimic is recognized by toll-like receptor 3 (TLR3), this in turn activates TIR-domain-containing adapter-inducing interferon-β (TRIF), which in turn stimulates the transcription factor interferon regulatory factor 3 (IRF3) and the NF- κ B protein. These two pathways stimulate the transcription of the IFNβ genes, which eventually leads to the release of the interferon by the cell as part of the innate immune response. This figure has been adapted and simplified from (Suh *et al.*, 2007).

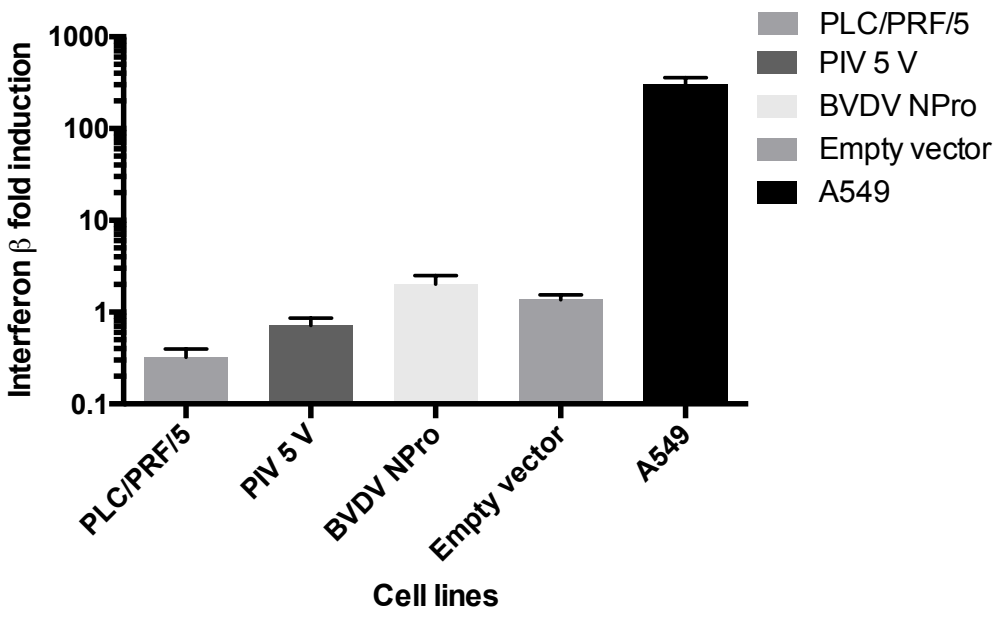

Figure 3-9 Outcome of poly I:C stimulation of the parental cell line and the three transduced cell lines. PLC/PRF5 wild type cell line and the A 549 cell line were cultured to 80-90% confluence, transfected with 10μg of poly I:C by Lipofectamine 2000 transfection according to the manufacturer's instructions and incubated for 6 hours. Total RNA was extracted as described in Materials and Methods and 50 ng was subsequently reverse transcribed. Primers against interferon β (IGUC0772 CAGAAGGAGGACGCCGCATTGAC and IGUC0773 CCAGGCACAGTGACTGTACTCC) and β actin (control) (IGUC0784 TTCTACAATGAGCTGCGTGTG and IGUC0785 GGGGTGTTGAAGGTCTCAAA) were used. The results were calculated using the ΛΛ Ct method (Applied Biosystems) and the fold change in gene expression described relative to the mock treated control.

The A549 cell line, used here as a positive control, showed a robust interferon response, which demonstrates that the stimulation was performed adequately. However neither the wild type cell line nor the empty vector transduced cell line showed any significant signs of interferon β gene induction following poly I:C transfection. This implies that the interferon response may be already attenuated in the parental cell line. A subsequent detailed literature search indicated that the PLC/PRF5 is the Alexander hepatoma cell line, that contains the integrated DNA of hepatitis B (HBV) which is known to subvert the innate immune system (Daemer *et al.*, 1980) possibly due to the homology between hepatitis B virus DNA and sequences regulating the interferon pathway (Onji *et al.*, 1989). Although some conflicting data showing that IFNβ induction by poly

I:C and Sendai virus was not downregulated in an ex-vivo model of HBV infected human hepatocytes (Suslov *et al.*, 2018), has recently been published, it is at odds with other recent work (Lebossé *et al.*, 2017) that supports the mechanism described above. Overall, it seems that interaction between chronic HBV infection and the interferon pathway is yet to be fully elucidated, but it is likely that the interferon pathway is already compromised in the PLC/PRF5 cell line and therefore further optimization in this respect was not required.

3.3.3 Optimisation of the infection protocol

The original cell-culture based respiratory virus diagnostic protocol (Cambridge PHL, Standard Operating Procedure-Virus Culture Section Methods Reference No: VIRSOP/005c, issued 20/01/12 by GM Sutehall) used in PHE laboratory Addenbrooke's Cambridge was used as a starting point for the development of the growth and infection protocol for HPIV3 clinical samples. An overnight incubation with the virus inoculum in an unspecified volume on a roller and then a subsequent incubation for up to two weeks at 33°C, was specified for diagnostic purposes. As this was considered to be both technically and temporally impractical three different conditions were trialed using different volumes of inoculum and incubation times as detailed in Figure 3-10B. Three infection protocols were established taking into account the need to allow for maximum virus binding and replication while at the same time minimizing the likelihood of contamination, which was particularly important given the nature of the inoculum. Strain MK9 and clinical isolate 600 were chosen as representative samples and growth was examined using the three conditions over a period of 5 days. Samples were removed from the culture every 24 hours and the levels of viral genome present in the sample were determined by one-step RT-qPCR as described above. The results obtained are illustrated in Figure 3-10. As can be seen, all three protocols demonstrated robust levels of virus replication, with peak viral titres obtained by day 4. Based on these results, it was decided that infection protocol II was best suited to enable a robust and efficient workflow.

A. HPIV3 lab-adapted strain (MK9)

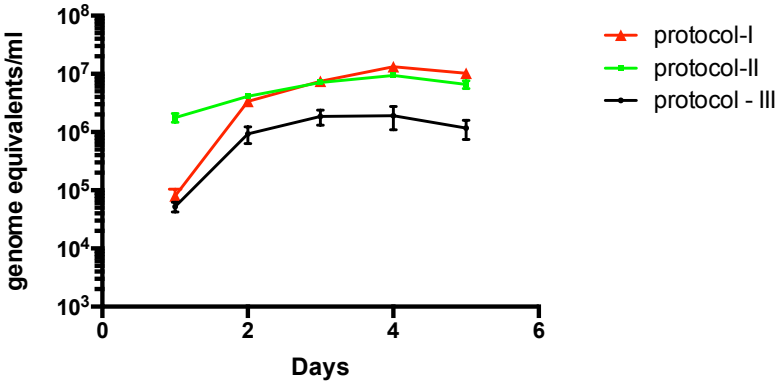

B. Clinical isolate 600

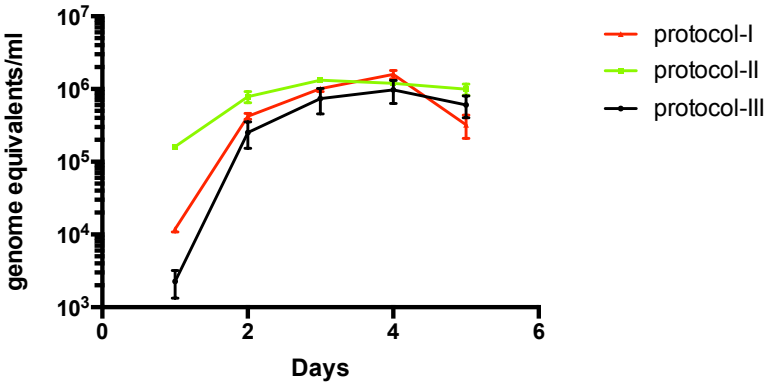

C. Infection protocols specifications

		Protocol I	Protocol II	Protocol III
Inoculum	Clinical sample (µl)	20µl	20µl	20µl
	Maintenance medium (µl)	200µl	200µl	800µl
Inoculation conditions		On rocker at 37°C for 24 hours	On rocker at 37°C for 2 hours	33°C for 24 hours
Wash		Twice in PBS	Twice in PBS	Twice in PBS
Incubation conditions		33°C for 5 days	33°C for 5 days	33°C for 5 days

Figure 3-10 Infection protocol optimization. HPIV3 (MK9) lab adapted strain (A) and clinical isolate 600 (B) were inoculated or mock inoculated and incubated according to the three infection protocols trialed (C). Supernatant samples of 50 µl were collected every day from day one to day five. Day 0 samples (protocols I and III) were collected immediately after the inoculum was removed, the cells were washed and covered with maintenance medium. Day 1 sample for protocol II was collected at the same time point, which in this case represents 22 hours of virus growth. Viral genome equivalents were quantified by one-step RT-qPCR and viral copy number was calculated by linear regression using a standard curve generated using serial, 10 fold dilutions of a cloned DNA amplicon as described in Materials and Methods. Each point represents 3 biological repeats +/- SEM.

3.4 Growth of clinical strains

3.4.1 Growth in immortalised cell culture

Clinical samples were collected between the years 2011-2016 from the diagnostic laboratory Addenbrooke's Hospital, PHE England as described above. Clinical virus strain stocks were grown using the optimized infection and growth protocol (see Section 3.3.3) as described in Materials and Methods. The success rate for each passage, as well as the workflow are summarized in Figure 3-11.

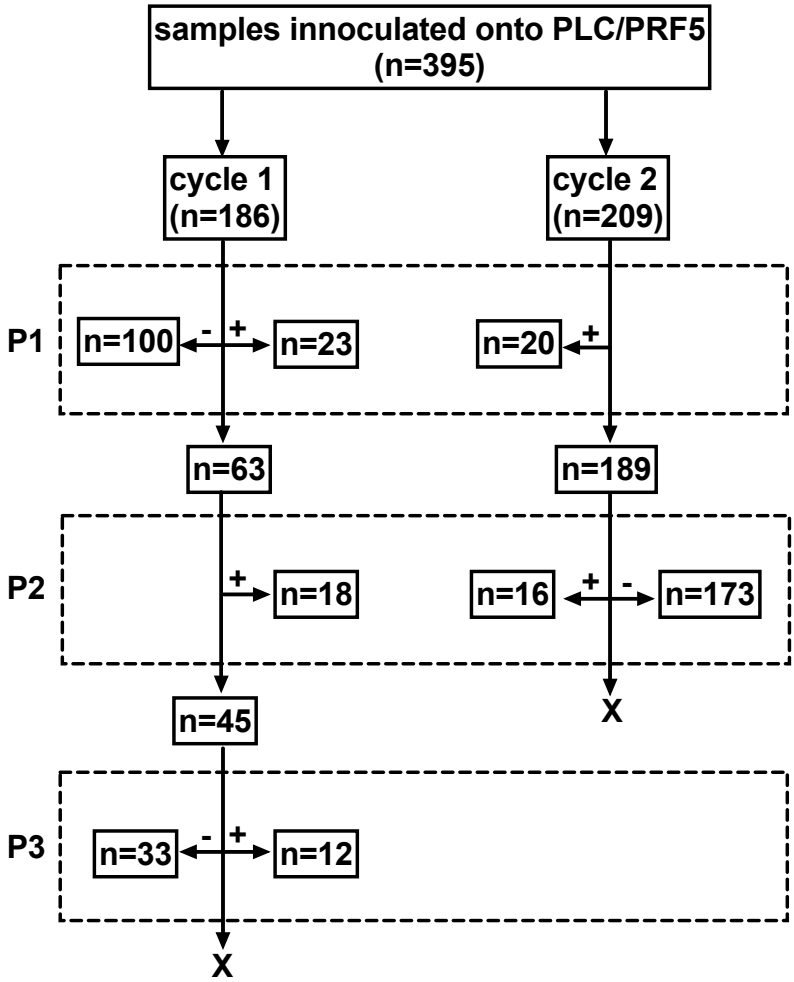

Figure 3-11 Summary of growth success rate in cell culture. 395 samples were originally inoculated onto PLC/PRF5 cells, as described in the text. The growth was carried out in two separate cycles: over 3 passages (P1, P2 and P3) for cycle 1 and 2 passages for cycle 2. The number of samples (n) used in each step is indicated, as well as the number of samples that were classed as successful/positive (+) and rejected (-) at each stage. The detailed protocol criteria involved in each cycle as well the outcomes are summarized in **Figure 3-12**.

The results according to protocols specific to each cycle are shown in Figure 3-12. Only 43/395 samples were successfully grown at passage 1 as seen in Figure 3-12. Two further samples were excluded due to co-infection with other viruses (influenza B in both cases). Additionally 34 samples were grown at passage 2 of both cycles and 11 samples were grown at passage 3 of cycle 1 (see Figure 3-12 Summary).

The low success rate was attributed to the nature of the prior storage of samples as well as the potential bottleneck introduced by growth in immortalised cell culture. A comparatively significant percentage of samples was also lost due to fungal and bacterial contamination (Figure 3-12 Summary) during passage 1 of cycle 1. This was subsequently addressed at P2 of cycle 1 by increasing antibiotic and anti-fungal concentrations in maintenance media (see Materials and Methods). The original antibiotic mix used for passage 1 of cycle 1 did not include ceftazidime and only contained 0.5 μg/ml of fungizone (amphotericin B) as opposed to 5 μg/ml.

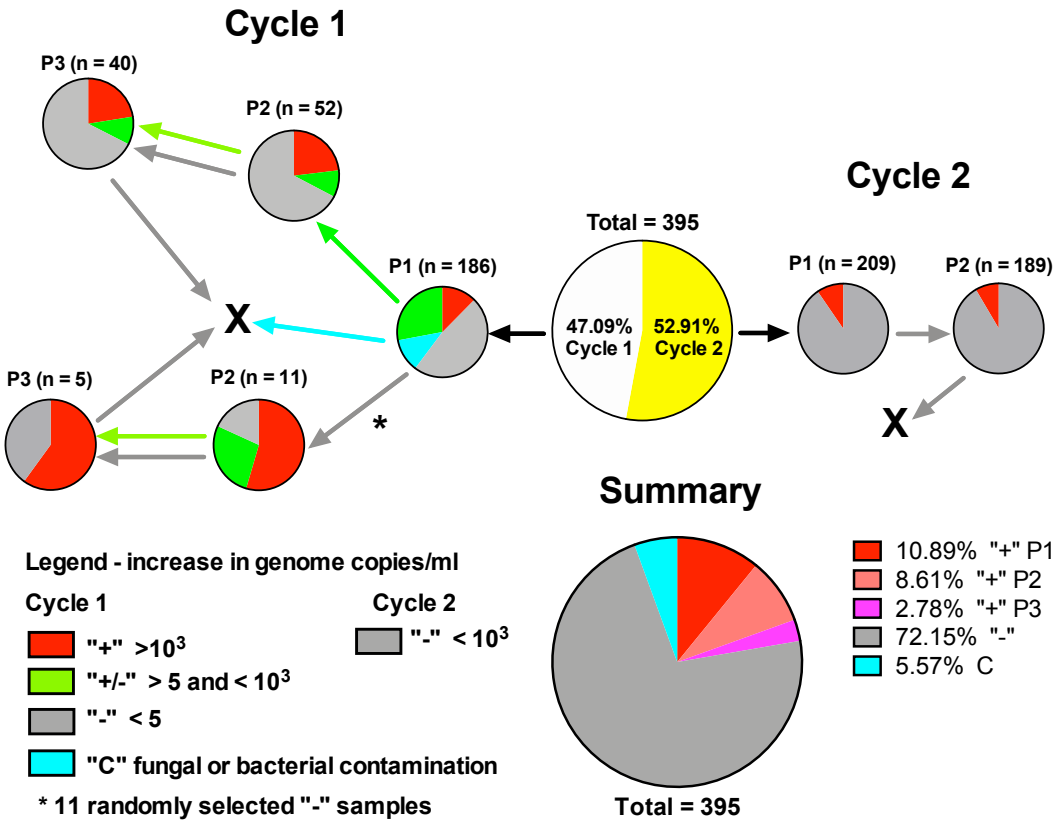

Figure 3-12 Growth of HPIV3 clinical strains in cell culture (according to protocol for each cycle). 395 clinical samples identified positive for HPIV3 between 2011-2016 were grown in two cycles**.** Cycle 1 involved 3 passages (P1, P2 and P3), where the outcome of each passage was characterized according to increase in viral load in samples between days 0 and 4 as positive (>10^3 genome copies/ml "+"), intermediate (5-10^3 genome copies/ml "+/-") and negative (<5 genome copies/ml "-"). 12% of samples at P1 of cycle 1 were lost to bacterial or fungal contamination (C). Sample selection criteria for subsequent passage are indicated by arrow colour: "-" grey; "+/-" green; "C" blue; black - all. Additionally 11 negative samples of cycle 1 P1 were randomly selected for further passage. Cycle 2 consisted of 2 passages and the outcome was characterized as for cycle 1, but only as positive (>10^3 genome copies/ml "+") or negative (<10^3 genome copies/ml "-"). As for cycle 1, sample selection criteria for subsequent passage is indicated by arrow colour. Adjusted anti-microbial concentrations ensured no contamination was seen after P1 of cycle 1. All samples that were contaminated or that failed to grow after P3 during cycle 1 or P2 during cycle 2 were discarded (X). The overall outcome of all the samples processed during both cycles in shown in Summary. (n = number of samples)

3.4.2 Growth in human airway epithelial cells

Clinical samples were collected during an outbreak in the summer of 2017: 15 samples from patients that were involved in the outbreak and 15 samples from unrelated patients were collected overall. For the purposes of phenotypic work, 9 of the samples were grown in human airway epithelial (HAE) cells. 4/9 were successfully grown and none were found not to be co-infected with any other respiratory viruses. 3 diverse strains were selected to undergo whole genome sequencing (WGS) and 2 (outbreak strain 8 and background strain D) were used for plaque phenotype in immortalised cell culture and for growth kinetics and immune response characterization in human airway epithelial cells.

3.5 Whole genome amplification and sequencing protocol optimisation

3.5.1 Primer optimization

During a pilot study undertaken prior to the start of this project 13 primer sets were identified as suitable for amplification of the entire genome of HPIV3 as described in Materials and Methods. In the majority of cases it was possible to generate overlapping amplicons in such a way that all sequenced regions were covered outside of primer binding sites, however further optimization was required for four primer pairs. The details of the original primer sets as well as those trialed as part of the optimisation can be seen in Figure 3-13 (for sequences see Appendix 2).

A

	Original primers pairs		
Amplicon	Primer F	Primer R	Region (bp)
1	KK-XF	KK-XR1	1-190
2	KK-XF	KK-XR2	1-520
3	KK-1F	KK-1R	166-2127
4	KK-NR1F	KK-NR1R	1569-2646
5	KK-NR2F	KK-NR2R	2610-4212
6	KK-3F	KK-3R	3860-5659
7	KK-4F	KK-4R	5527-7587
8	KK-5F	KK-5R	7500-9398
9	KK-6F	KK-6R	9046-10956
10	KK-7F	KK-7R	10929-12433
11	KK-8F	KK-8R	12111-14064
12	KK-9F	KK-9R	13164-15067
13	KK-10F	PIV-5R	13975-15462

B

	Trialled primers pairs		
Amplicon	Primer F	Primer R	Region (bp)
4a	KK-NR1F	NR1Ra	1569-2256
4b	KK-NR1F	NR1Rb	1569-2356
5a	NR2Fa	KK-NR2R	2046-4212
5b	NR2Fb	KK-NR2R	2148-4212
9a	KK-6F	6Ra	9046-11184
9b	KK-6F	6Rb	9046-10832
10a	7Fa	KK-7R	10757-12433
10b	7Fb	KK-7R	10728-12433

C

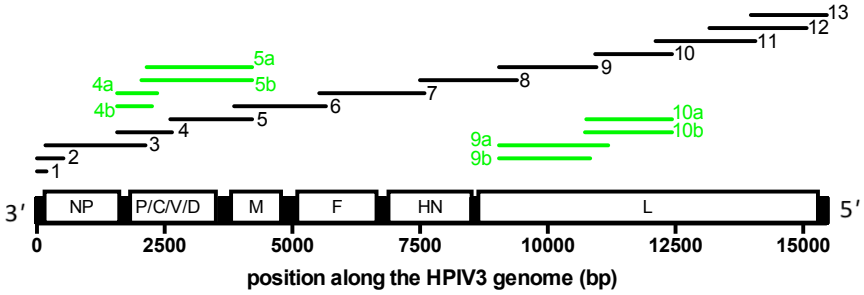

D

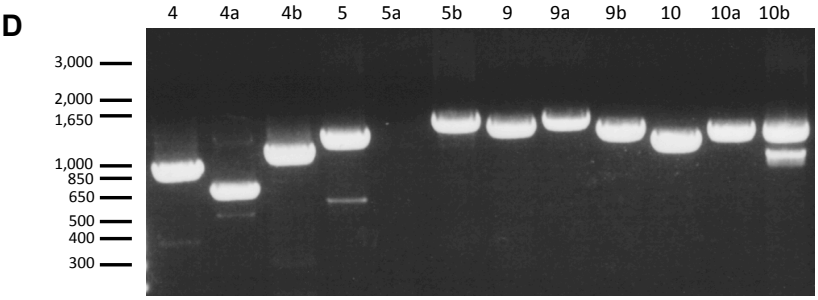

Figure 3-13 Primer optimization. 13 primer sets identified in the pilot study (A) were used for the amplification of the laboratory strain MK9 genome. The amplicons generated with respect to their position along the HPIV3 genome are shown in black in panel C, numbered 1-13 respectively. 2 areas that required further optimization were identified at the overlap between amplicons 4 and 5 and 9 and 10. To this end 8 alternative primer pairs (B) were designed covering these two regions. Their respective locations are shown in panel C in green. The new primer pairs (C) and their original counterparts were then used to amplify the relevant part of the MK9 laboratory strain genome using the protocol described in Materials and Methods. The gel with the amplicons generated is shown in (D). Based on these results primer pairs 5b and 9a (B) were chosen as alternatives for primer pairs 5 and 9 (C).

Two clinical isolates: 99 and 153 were then amplified using the primer sets shown in Figure 3-13A with optimized primer pairs 5b and 9a (Figure 3-13B) replacing their original counterparts 5 and 9 Figure 3-13A. The amplification results can be seen in Figure 3-14 and the final set of optimized primers can be seen in Table 3-1.

A. Clinical isolate 99

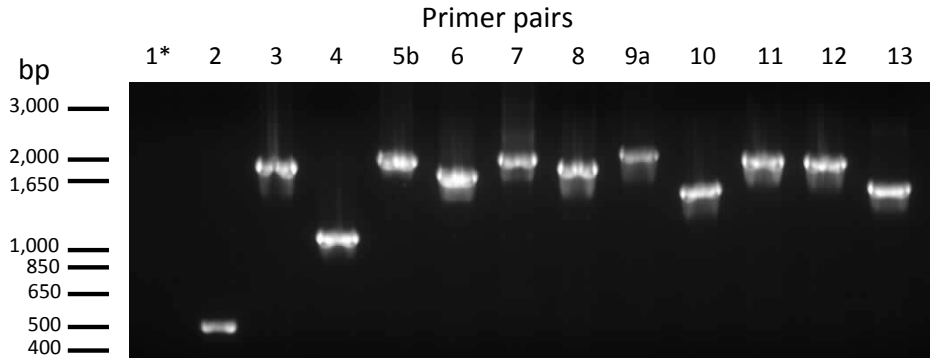

B. Clinical isolate 153

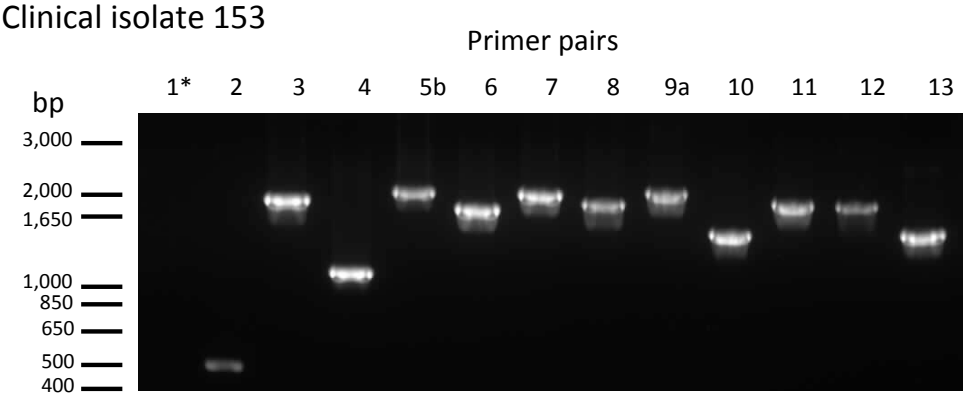

* Amplification failed

Figure 3-14 Whole genome amplification of two clinical isolates using the optimised primer set. Clinical isolates 99 (panel A) and 153 (panel B) were amplified using primer pairs detailed in **Figure 3-13**A with primer sets 5 and 9 replaced with 5b and 9a **Figure 3-13**C. No amplicon for primer set 1 was observed for either strain (not shown in figure for ease of visualization). As this region was also covered by primer set 2 (see **Figure 3-13**C), the decision was made not to use primer set 1 for further amplification work

Consequently twelve optimised primer pairs were finalized. These can be seen in Table 3-1, and, with respective genome coverage, in Figure 2-2 in Materials and Methods. Although amplification with this protocol was attempted directly from clinical samples, the results were inconsistent and never yielded the full amplicon set required for whole genome sequencing. Additionally as well characterised large viral stocks were required for further experiments, the decision was taken to continue working with minimally passaged clinical strains.

Final optimised set of primers				
Original amplicon number	New amplicon number	Primer F	Primer R	Region (bp)
2	1	KK-XF	KK-XR2	1-520
3	2	KK-1F	KK-1R	166-2127
4	3	KK-NR1F	KK-NR1R	1569-2646
5a	4	NR2Fa	KK-NR2R	2046-4212
6	5	KK-3F	KK-3R	3860-5659
7	6	KK-4F	KK-4R	5527-7587
8	7	KK-5F	KK-5R	7500-9398
9a	8	KK-6F	6Ra	9046-11184
10	9	KK-7F	KK-7R	10929-12433
11	10	KK-8F	KK-8R	12111-14064
12	11	KK-9F	KK-9R	13164-15067
13	12	KK-10F	PIV-5R	13975-15462

Table 3-1 Optimised set of primers for HPIV3 whole genome amplification. The final optimized set of primers, based on the original set designed during the pilot project, as seen in **Figure 3-13**A including two optimized primer pairs 5a and 9b **Figure 3-13**B and without original primer set 1 that failed to produce an amplicon during amplification of two clinical isolates **Figure 3-14**. The table also shows the new primer pair numbers that were used for subsequent work.

3.5.2 NGS pipeline validation

Having established an optimised set of primers, the NGS pipeline (see Materials and Methods) was validated as follows. The laboratory strain MK9 and strain 153 were first sequenced by Sanger sequencing, as described in Materials and Methods, as well as the previously published *de novo* Ebola pipeline using QUASR for quality control and Spades 3.5 for assembly (Arias *et al.*, 2016) and the optimized NGS protocol, described followed by the bioinformatics pipeline

established here. In each case the final sequences were identical to those obtained by the new pipeline. In order to control the length and quality of the sequences, all strains were analysed using FastQC (Andrews, 2018) post primer trimming and quality control (as detailed in Materials and Methods). Summary statistics for strains 153 and MK9 can be seen in Figure 3-15C. The depth of NGS coverage for strains 153, MK9 and the average of all strains sequenced with 95% CI is shown in Figure 3-15A, B and C respectively. The average Phred score for all strains was 38 The sequence lengths and overall alignment percentages as well as the depth of coverage remained consistently high apart from the very 5' and 3' ends, confirming the robustness of the pipeline.

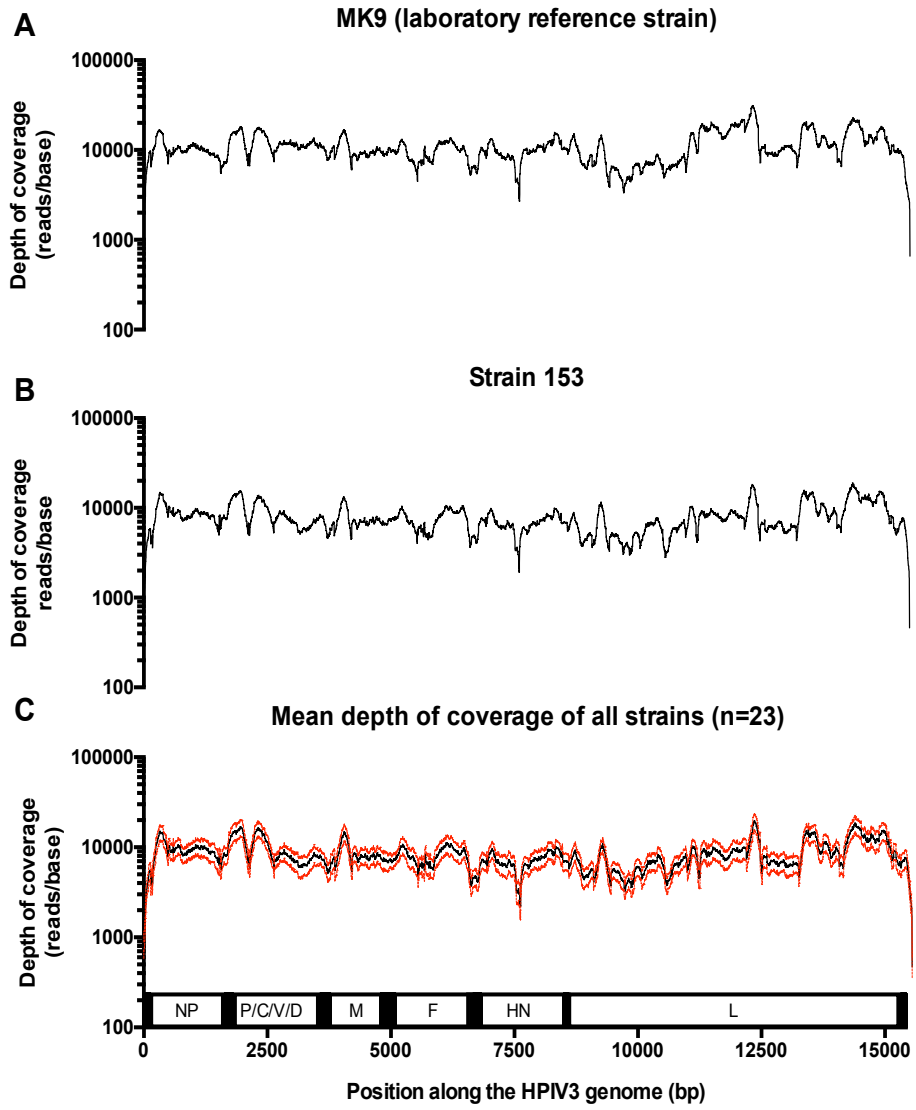

D

Strain identifier	MK9	153
Total reads	643058	460056
Sequence length (bp)	20-150	20-150
%GC	35	35
Overall alignment with Bowtie2 (%)	99.46	99.62

Figure 3-15 Depth of coverage achieved for laboratory strain (A), strain 153 (B), FastQC (Andrews, 2018) **statistics for both sequences (D) and average depth of coverage for all sequences (C).** Consistent coverage of above 1000 was achieved over the full length of the genome of both sequences excluding the very 5′ and 3′ prime ends. This is consistent with the average depth of coverage achieved for all sequences (black) shown in (D) with 95%CI (red). The length of the final sequence was 15409 base pairs, as the forward primer (26 bases) of the first amplicon, and the reverse primer of the last amplicon (27 bases) were removed in the pipeline. sequence length and overall

alignment with Bowtie 2 to the respective strains sequenced by Sanger sequencing was achieved.

3.6 Phenotypic and genotypic diversity of HPIV3 clinical strains

3.6.1 Clinical HPIV3 strains demographics.

With a robust amplification protocol and sequencing pipeline established, 23 clinical strains of diverse provenance, that were originally grown at passage 1, were selected for whole genome sequencing as described in Materials and Methods. The details of these are summarised in Table 3-2.

Sample			Patient				
Lab ID	Date collected	Source	Sex	Age	Originating hospital	In/out patient	PMH
14	Nov-14	URT swab	F	1 year	Basildon	in	unknown
16	May-14	URT swab	M	50 years	CUH	in	post allograft
21	Jun-14	URT swab	F	54 years	no data	unknown	unknown
30	Jul-14	URT swab	M	60 years	CUH	out	post VUD
53	Apr-14	URT swab	F	58 years	CUH	in	asthma
60	Jun-11	URT swab	F	56 years	CUH	in	unknown
65	Jun-11	URT swab	F	54 years	CUH	in	unknown
82	Jul-11	URT swab	M	2 months	Harlow	in	unknown
112	Jun-12	URT swab	M	84 years	CUH	out	on alemtuzumab
113	Jul-12	URT swab	M	42 years	CUH	in	unknown
121	Nov-12	URT swab	F	61 years	CUH	in	post allograft
122	Dec-12	NPA	M	9 months	Hinchingbrooke	in	unknown
128	Feb-13	NPA	F	9 months	CUH	in	unknown
129	Feb-13	TA	F	4 years	Frimley Park	in/ICU	unknown
153	Apr-13	NPA	F	12 years	Frimley Park	in	ALL relapse
180	May-13	NPA	F	3 months	CUH	out	CF
362	Mar-15	URT swab	F	80 years	Nursing home	out	unknown
371	Apr-15	URT swab	F	89 years	Nursing home	out	unknown
390	Feb-14	URT swab	F	1 year	CUH	in	unknown
395	Apr-15	URT swab	M	70 years	CUH	in	unknown
8	Jul-17	URT swab	M	1 year	CUH	in	ALL
D	Jun-17	URT swab	F	20 years	CUH	in	1° immunodeficiency
I	Jun-17	URT swab	F	28 years	CUH	in	PE

Table 3-2 Clinical strains demographics summary. The table summarises the clinical strains used in this project together with clinical and demographic information where available. Abbreviations: URT = upper respiratory tract; NPA = nasopharyngeal aspirate; TA = tracheal aspirate; M= male; F = female; CUH = Cambridge University Hospitals; ICU = intensive care unit; PMH = past medical history; ALL = acute lymphocytic leukaemia; VUD = volunteer unrelated donor (transplant); CF = cystic fibrosis; PE = pulmonary embolism.

The majority of the samples (17/23) were taken from inpatients, reflecting an unavoidable sampling bias towards cases requiring admission and potential co-morbidities. Although the majority of the cases originated from Cambridge

University Hospitals (16/23), the rest were from a more diverse geographical distribution reflecting the area covered by PHE laboratory Addenbrooke's (see Materials and Methods). Relevant past medical history (PMH) is shown where available (10/23) and in most cases includes patients with haematological oncology conditions such as relapsed acute lymphocytic leukaemia (ALL), immunosuppressive chemotherapy treatment (alemtuzumab) and post bone marrow transplant including allograft and volunteer unrelated donor (VUD). This reflects the immunosuppressed population where HPIV3 is known to have the highest impact (Nichols, 2001; Shah *et al.*, 2016). Two chronic respiratory conditions have also been identified: cystic fibrosis (CF) and asthma. Parainfluenza viruses have known to contribute to infective exacerbations of asthma (Lewandowska-Polak *et al.*, 2015), particularly in paediatrics and the clinical impact of respiratory viruses on cystic fibrosis patients is well recognised (Flight and Jones, 2017).

3.6.2 Genotypic diversity of HPIV3 clinical strains

In order to assess the degree of genotypic variability of clinical strains of HPIV3 in this study, the whole genomes of the clinical strains described above, as well as laboratory strain MK9 were sequenced. A maximum likelihood phylogenetic tree was constructed using all the clinical sequences as well as laboratory strains MK9 sequenced here and strain JS (accession number Z11575). Strain JS is a well-known laboratory reference strain that has been used extensively for vaccine research for HPIV3 (see Introduction). An attempt to include the Washington strain (accession number 47885) was also made. However it was found to be identical to strain MK9 and therefore was not included in further analysis. Figure 3-16 shows the genotypic diversity exhibited by clinical strains. It shows that laboratory adapted strains form a separate and clearly distinct cluster from the clinical strains.

This is consistent with that has previously been described in literature (Palmer *et al.*, 2012; Palermo *et al.*, 2016). However there is currently little data on the specific mutations or regions of the genome that may be involved in culture adaptation. Most of the research to date has concentrated on HN and F parts of genome as it has been observed that clinically adapted strains have fusogenic

phenotypes (Henrickson, 2003; Moscona, 2005; Lingemann *et al.*, 2015). In order to clarify this, an analysis of the differences between sequences of the clinical strains and the consensus sequence of both JS and MK9 was conducted. The results are shown in Figure 3-17. Although clear peaks around the F coding region are present, the differences were not seen to be confined to one part of the genome.

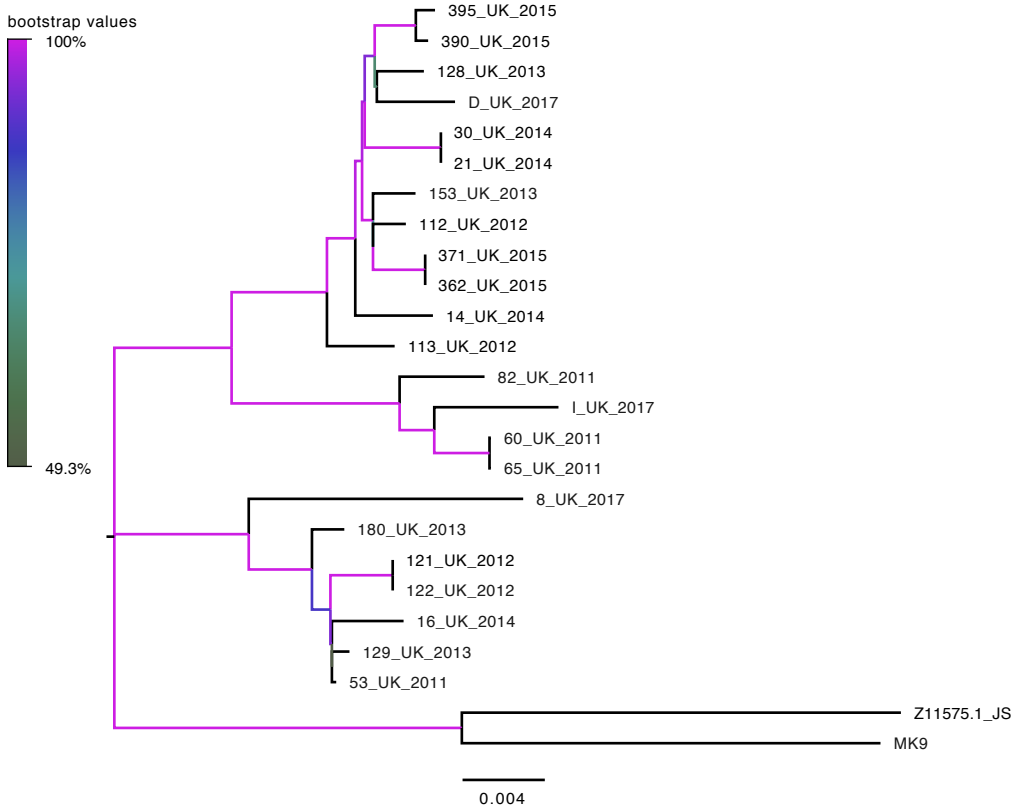

Figure 3-16 Molecular Phylogenetic analysis of clinical strains and strains MK9 and JS of HPIV3 by Maximum Likelihood method. The evolutionary history was inferred by using the Maximum Likelihood method based on the General Time Reversible model + G + I (see Materials and Methods) (Nei and Kumar, 2000) and 1000 bootstrap repetitions. The tree is drawn to scale, with branch lengths measured in the number of substitutions per site. The analysis involved 25 nucleotide sequences. Codon positions included were 1st+2nd+3rd+Noncoding. Branches are coloured by their bootstrap values as per the colour legend. Evolutionary analyses were conducted in MEGA7 (Kumar, Stecher and Tamura, 2016), figure caption adapted from MEGA7.

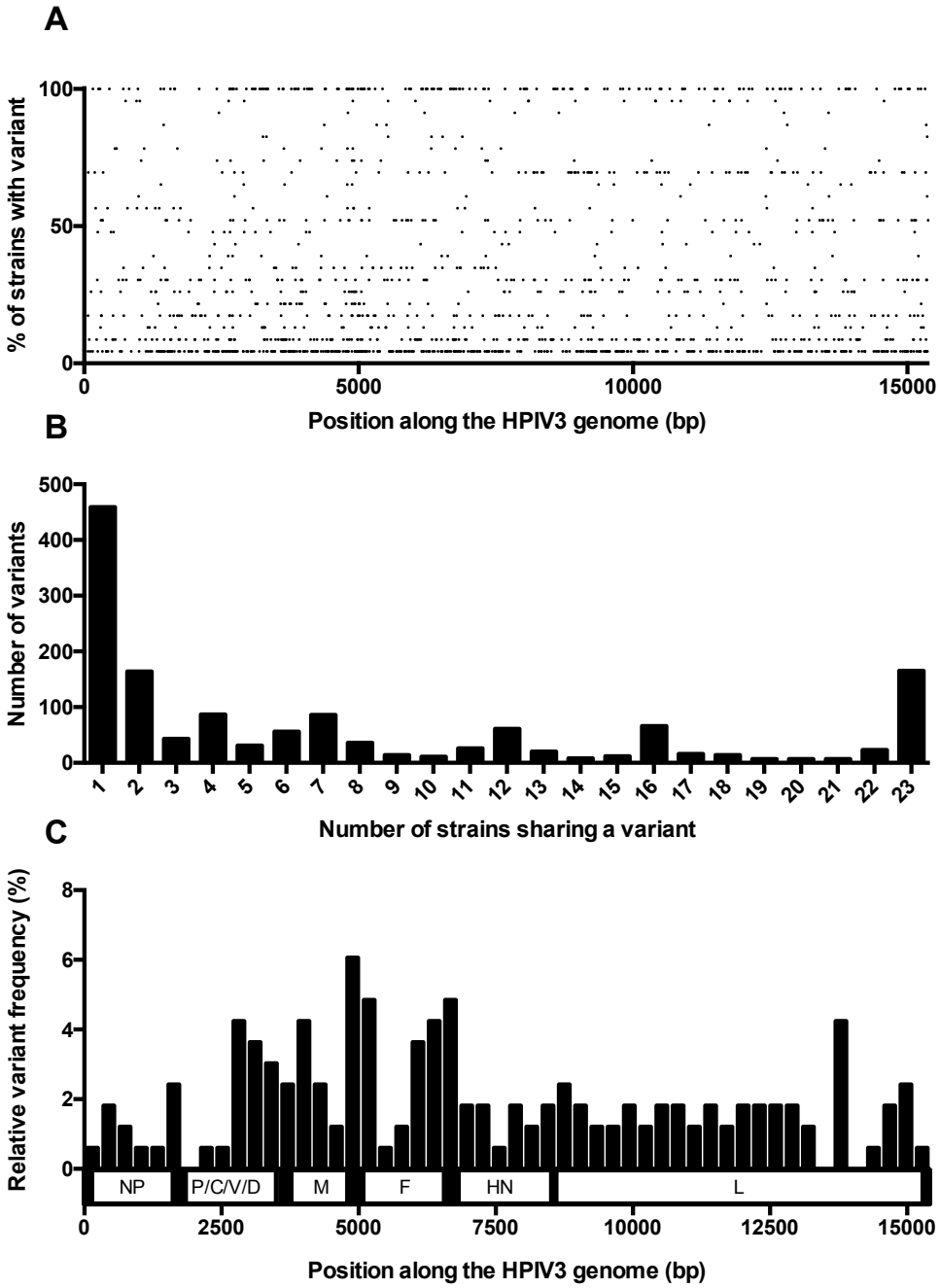

Figure 3-17 Differences between clinical HPIV3 strains and laboratory adapted JS and MK9 reference strains The differences between 23 clinical strains as detailed in **Table 3-2** and the consensus of laboratory adapted strains JS and MK9 are shown. In panel A the location of the variants along the HPIV3 genome (x axis) is shown against the percentage of the strains that contain a variant at this location (y axis). Panel B shows the histogram of the number of variants (x axis) that are shared by a specific number of strains (y axis). The relative locations of variants seen in all the 23 strains (165 variants) is shown in panel C as a histogram illustrating the relative frequency (x axis) at which these strains occur at a specific locations along the HPIV3 genome (y axis) (width of bin = 300bp). Genome differences were analysed using UGENE. All other calculations and analyses were carried out in GraphPad 6.

3.6.3 Phenotypic diversity of clinical strains

As discussed previously (see Introduction) there is evidence that connects variants in the F and HN part of the HPIV3 genome to the fusogenicity of strains and hence to plaque phenotype in immortalised cell culture. Therefore, having established the genotypic diversity of clinical strains as well as their considerable differences from the laboratory adapted strains MK9 and JS, an attempt was made to evaluate the phenotypic diversity by looking at plaque phenotype in PLC/PRF5 cells. To this end 13 diverse clinical strains drawn from the entire period of sample collection (2011-2017) that did not cluster together by full genome sequence, were selected. Their relative plaque phenotype, as well as that of the laboratory reference strain MK9 are shown below in Figure 3-18. Clinical strains were observed to exhibit considerable diversity in plaque size, while the culture adapted laboratory strain had a significantly larger plaque phenotype than the minimally passaged and HAE grown strains.

A. Plaque phenotypes of clinical strains

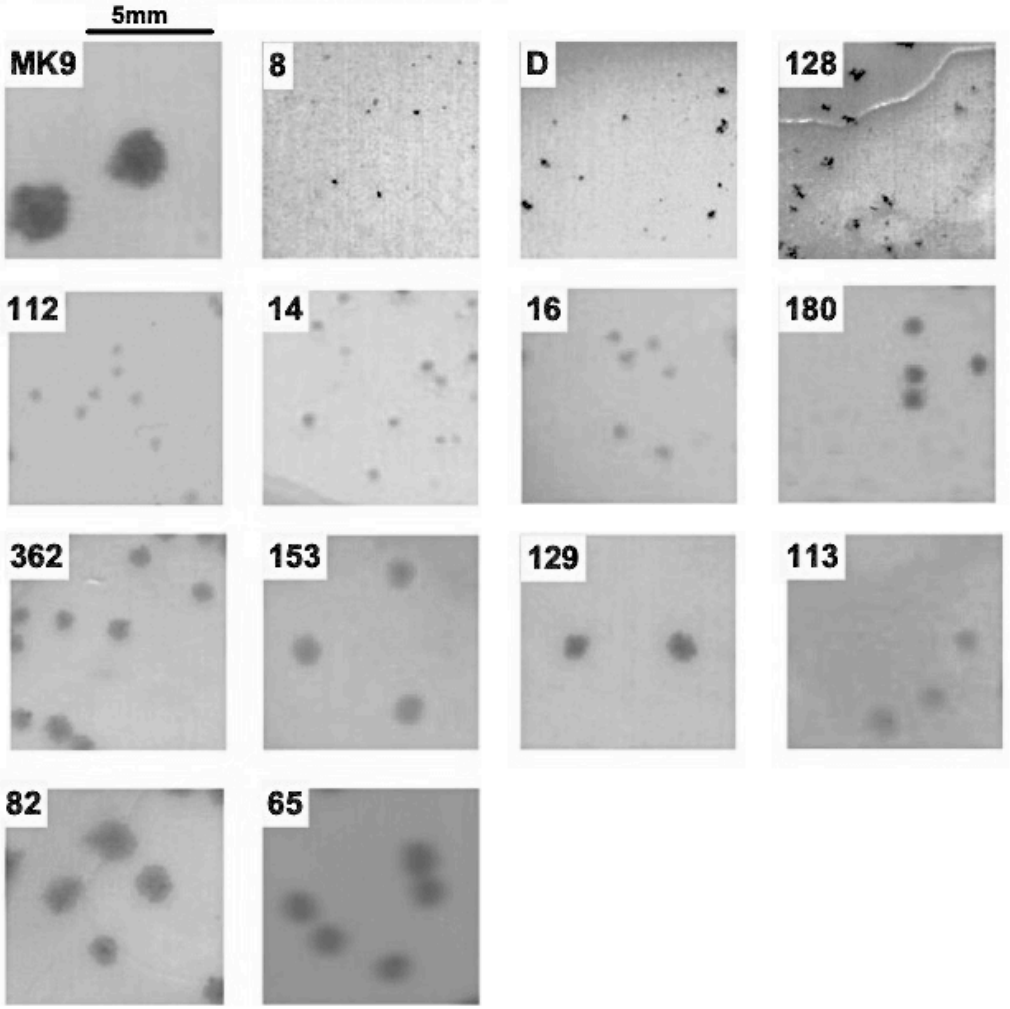

B. Summary of plaque areas of HPIV3 strains (in plaque size order)

clinical strain ID	plaque area (mm^2 +/- SEM)	clinical strain ID	plaque area (mm^2 +/- SEM)	clinical strain ID	plaque area (mm^2 +/- SEM)
MK9	3.96 +/- 0.45	14	0.30+/-0.04	129	0.92+/-0.04
8	0.02+/-0.01	16	0.33+/-0.03	113	0.94+/-0.05
D	0.04+/-0.01	180	0.57+/-0.02	82	1.46+/-0.16
128	0.07+/-0.01	362	0.59+/-0.06	65	1.47+/-0.11
112	0.16+/-0.01	153	0.83+/-0.03		

Figure 3-18 Diverse plaque phenotypes of clinical strains and reference strain MK9 Clinical strains and strain MK9 were inoculated, incubated and stained as described in Materials and Methods. The wells were then scanned against a white background with strains 8; D; 112 and 128 in 800dpi, the other strains in 500dpi resolution. All pictures were transformed into 8bit in Fiji. The figure shows these starting with MK9 and then ordered by plaque size (A). The plaque areas were calculated in Fiji and are summarized in panel B in mm^2 +/- SEM, subdivided into small (<0.5 mm^2), medium (0.5 mm^2-1 mm^2) and large (>1 mm^2) phenotype.

It could be logically hypothesized that strains exhibiting smaller plaque phenotypes would be genetically less similar to strain MK9 than strains exhibiting larger plaque phenotypes. However, this is not reflected in phylogenetic analysis (Figure 3-16), where, for example, strains 8 and D, which exhibit the smallest plaque phenotype, do not cluster together, but strains 65 and 82 that have the largest plaque phenotype do. This indicates that there may be a specific section of the genome or a number of specific genotypic changes that can be linked to plaque phenotype. To this end, clinical strains were subdivided into small, medium and large plaque phenotype according to plaque area (Figure 3-18). Consequently, in order to identify any significant regions related to plaque size phenotype, the sequences of these were grouped together and then each group was compared to the sequence of strain MK9 that has a markedly larger plaque size than any of the clinical strains.

The differences between each group and the reference strain were then extracted using UGENE (Okonechnikov, Golosova and Fursov, 2012) and the relative frequency of variants that were seen in all the strains in a particular group were plotted along the distance along the HPIV3 genome (Figure 3-19). Similarly to Figure 3-17, a peak in variability was observed at the intergenic region between M and F coding regions for all plaque phenotypes. However, as shown by a red arrow in Figure 3-19, a reduction in variants was observed towards the end of the F genome (bin centered on 6400bp) in the larger plaque phenotype group, which indicates that this region may be potentially significant for plaque phenotype.

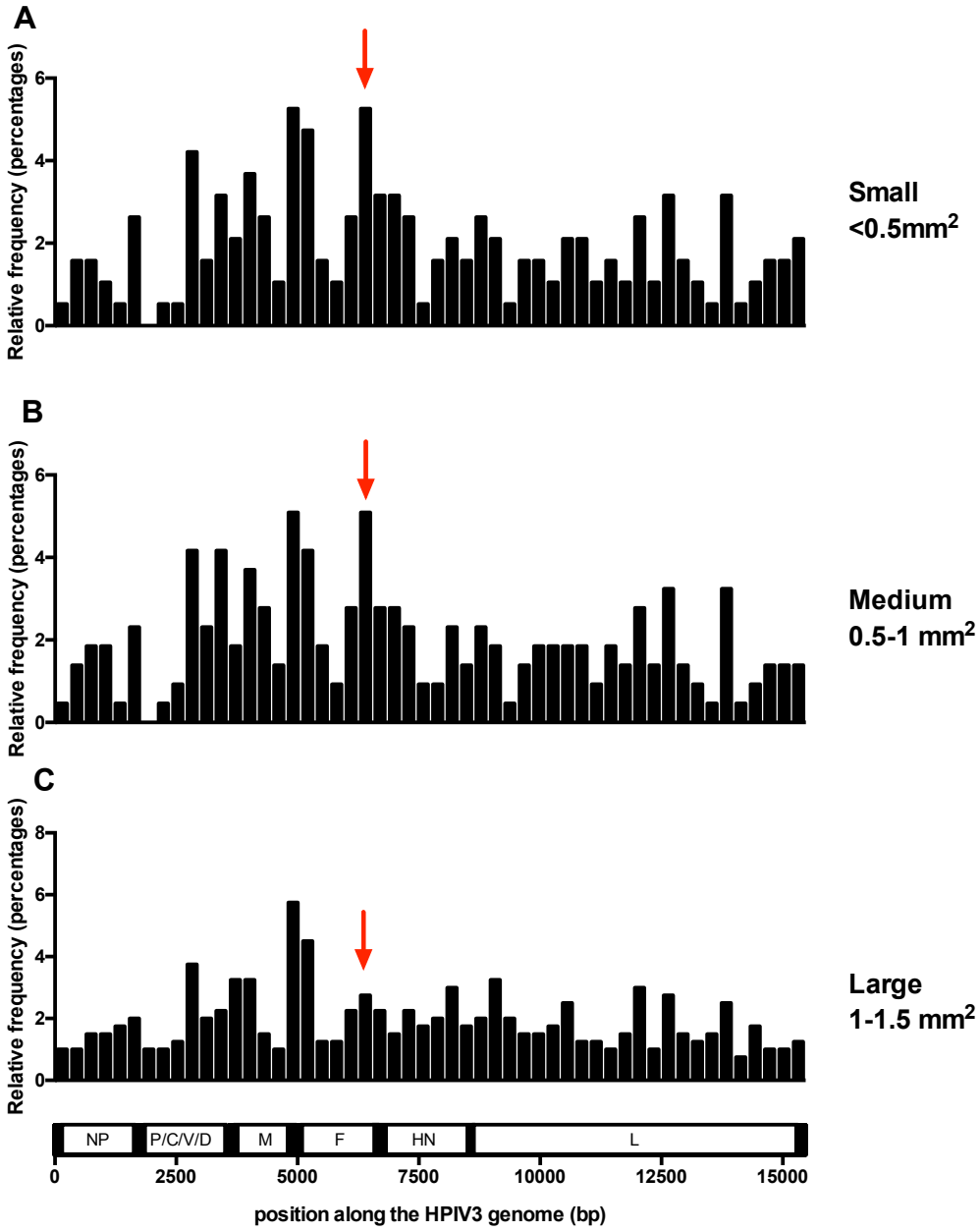

Figure 3-19 Locations of variants present in clinical strains with different plaque phenotypes. The clinical strains of HPIV3 were divided into three groups according to plaque phenotype as shown in **Figure 3-18**. The sequences of each group were aligned with strain MK9 as reference and differences extracted using UGENE. Only variants that were present in all strains were selected. The relative frequencies (%) at which variants were observed along the HPIV3 genome are shown in panel A (small phenotype: strains 8, D, 128, 112, 14 and 16); B (medium phenotype: strains 180, 362, 153, 129, 113) and C (large phenotype: strains 82 and 65). X-axes of all panels are aligned to the schematic representation of the HPIV3 genome. Bin widths are 300bp. A red arrow indicates a location at the end of F part of the genome (bin centred on 6400bp) where a significant proportion of variants in small and medium plaque phenotype, but not large plaque phenotype are concentrated.

However one must keep in mind that the numbers involved in the current project are small and strains within the larger plaque phenotype (65 and 82) group are phylogenetically closely related. Additionally this observation may be confounded by the fact that laboratory strain MK9 is significantly culture adapted and the variants detected may be a reflection of culture adaptation rather than plaque phenotype.

3.6.4 Serial passage in culture: effect on genotype and phenotype

As mentioned above, it is recognized that clinical strains of HPIV3 change their phenotypic and genotypic characteristics with adaptation to immortalised cell culture (Henrickson, 2003; Palmer *et al.*, 2012; Palermo *et al.*, 2016). This can be a confounding factor when studying phenotype and potentially drug sensitivity, as previously mentioned. More importantly, in the context of this project, the viral stock generated contained samples that were grown after 1,2 and 3 passages in tissue culture (Figure 3-12) as whole genome sequences from original clinical samples could not be obtained. Therefore an attempt was made to examine culture adaptation of 6 strains grown at passage 1 in PLC/PRF5 cells. The goal was to assess how plaque phenotype was affected by culture adaptation, as well as to determine whether samples grown at later passages could be used for further work on clinical strains. To this end, 6 clinical strains and the laboratory strain MK9 were repeatedly passaged up to passage 10 as described in Materials and Methods.

The change in plaque phenotype with passage is illustrated in Figure 3-20. Panel A of Figure 3-20 clearly shows a marked increase in plaque size with culture adaptation in all clinical strains. A number of new smaller plaque variants, were observed in strain MK9 with passage. The distributions of plaque areas at passages 1, 5 and 10 are illustrated in Figure 3-20B. There is a clear shift towards larger plaque variants exhibited by all clinical strains, although smaller plaque variants still appear to be present.

This is reflected in the genome analysis. When consensus sequences of clinical strains and strain MK9 at passage 1, 5 and 10 were compared, they were found to be near identical. All differences observed were a shift from non-ambiguous

bases to ambiguous bases or *vice versa*, meaning that no 100% change in any variant was detected. This is reflected by the presence of diverse plaque phenotypes, as shown in Figure 3-20B. The locations of variants and their frequency distribution along the HPIV3 genome are shown in Figure 3-21. At passage 5, a peak at the junction between and M and F genome (bin centered on 5200bp), showed the greatest increase (Figure 3-21B). This is potentially consistent with the abrogation of the aberrant read through between M and F parts of the genome, causing increased plaque area phenotype (Lingemann *et al.*, 2015) (see Introduction). Unlike analyses above (Figure 3-17 and Figure 3-19) this cannot be attributed in phylogenetic differences between strains (Figure 3-16). By passage 10 more variants in NP, F and HN parts of the genome were observed (Figure 3-21D), as well as a broader peak encompassing the intergenic M and F region as well as the start of the F gene.

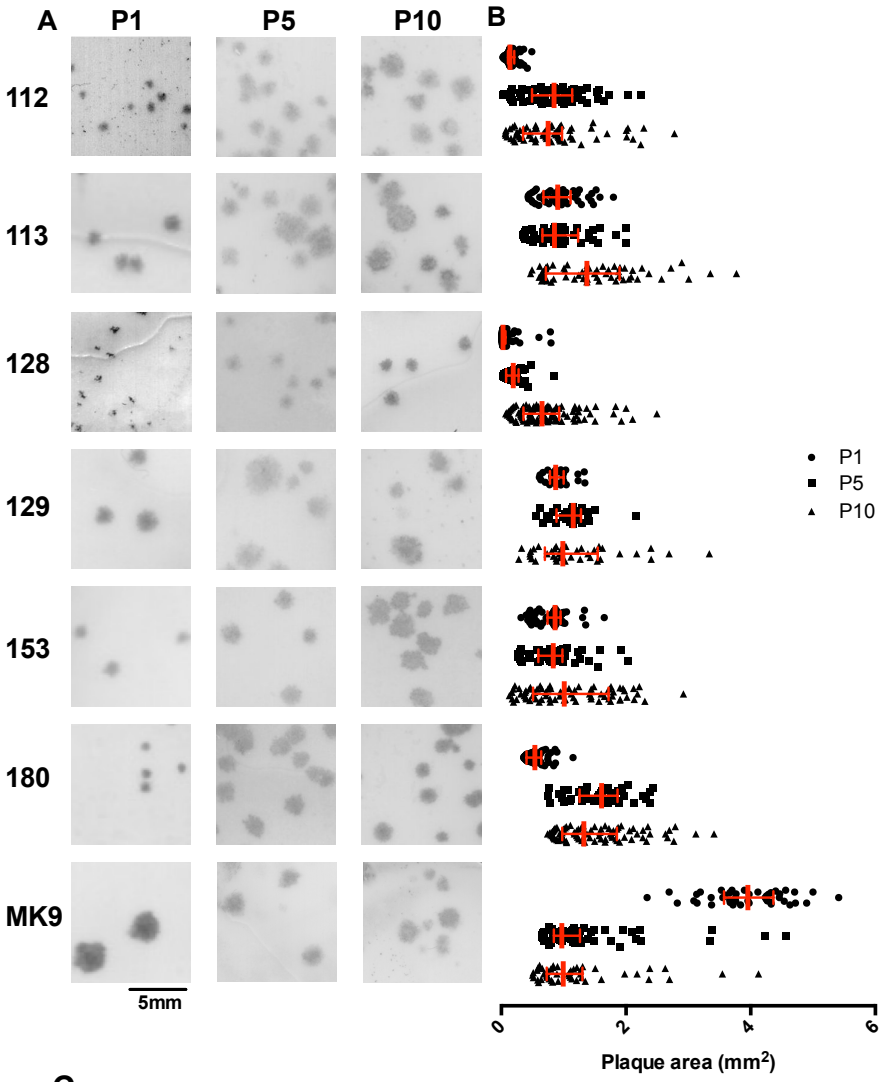

C

	Average plaque area (mm²) +/- SEM at passage		
Strain	1	5	10
MK9	3.94 +/- 0.09	1.23 +/- 0.08	1.22 +/- 0.11
180	0.56 +/- 0.02	1.57 +/- 0.07	1.49 +/- 0.07
153	0.84 +/- 0.03	0.84 +/- 0.06	1.10 +/- 0.08
129	0.91 +/- 0.04	1.11 +/- 0.06	1.19 +/- 0.11
128	0.07 +/- 0.01	0.20 +/- 0.02	0.73 +/- 0.05
113	0.92 +/- 0.05	0.94 +/- 0.06	1.44 +/- 0.10
112	0.16 +/-0.01	0.84 +/- 0.06	0.82 +/- 0.07

Figure 3-20 Clinical strains develop a larger plaque phenotype with increased passage in immortalised cell culture. Clarified supernatant was collected at passage 1, 4 and 10 (P1, P5 and P10). Cell monolayers were prepared and viral samples were inoculated, incubated and stained as described in Materials and Methods. The wells were then scanned against a white background and transformed into 8-bit images. Plaque phenotype was evaluated at passage 1, 5 and 10 (P1, P5 and P10 respectively), scanned pictures of plaques (A) show an increased phenotype with increasing passage. Panel B illustrates the plaque area measured in mm^2 with the median +/- interquartile range indicated in red. The average plaque area in mm^2 +/- SEM is summarized in C. All images processing and plaque measurement was carried out in Fiji.

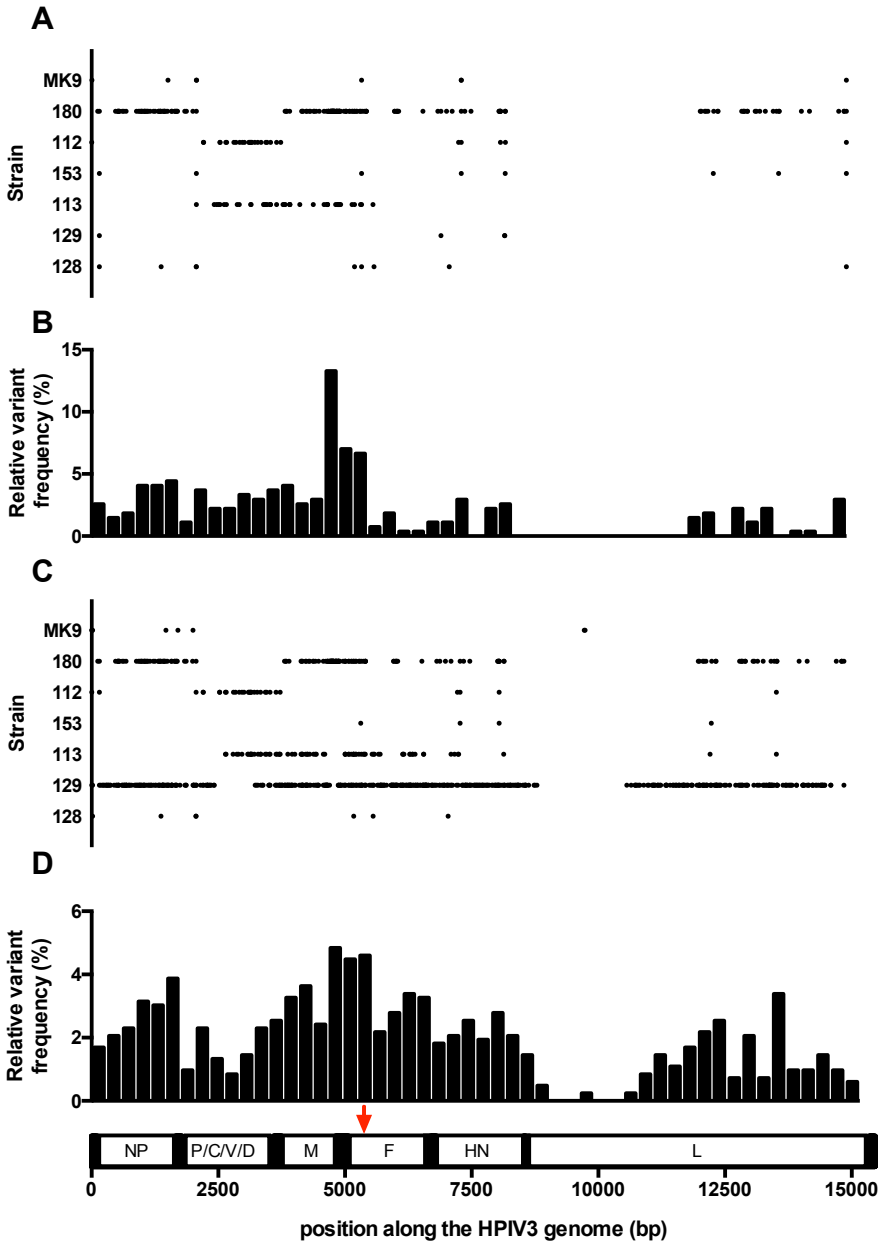

Figure 3-21 Variants observed in HPIV3 clinical strains and reference strain MK9 following repeated passage in PLC/PRF5 cell line. 6 HPIV3 clinical strains and reference strain MK9 were repeatedly passaged in PLC/PRF5 cells. Whole genome sequences were obtained at passage 1 (P1), 5 (P5) and 10 (P10). The variants observed at P5 and P10 were then extracted using UGENE using P1 sequences as reference. These were then plotted against their position along the HPIV3 genome (x axis) for each strain (y axis) at P5 (panel A) and P10 (panel C). None of the changes were found to correspond to a 100% change in a variant. The relative frequencies at which these variants were found along the length of the HPIV3 genome are plotted in panel B (P5) and panel D (P10). All x axes are aligned to a diagrammatic representation of the HPIV3 genome. The red arrow points to the location coding for the cleavage site in the F_0 protein.

Additionally there is a large increase in variants towards the end of the F genome as observed in Figure 3-19, which confirms that this area may be correlated with plaque size. Furthermore it is interesting to note that at P10 none of the variants observed in MK9 fall within F or HN parts of the genome, although smaller plaque phenotypes are seen in tissue culture. This is further evidence that parts of the genome other than F and HN are likely to be involved in tissue culture adaptation.

However, in addition to the above, a number of specific variants should be noted. In strain 128 a change from R to A at base 5367 detected at passage 5 resulted in a loss of a variant with a glutamic acid (E) at position 108 in the F protein. An E at position 108 has been associated with a smaller plaque phenotype and its replacement by lysine (K) to culture adaptation in a previous study (Palermo *et al.*, 2016). This site was considered to be of particular importance for plaque phenotype as it is located within the cleavage site between F_1 and F_2 subunits of the F protein (red arrow in Figure 3-21). This is partially consistent with observations in this project, as all clinical strains with smaller plaque phenotypes (Figure 3-18) apart from strain 16 and 112 contain an E variant at this location. Strain 16 has a K, whereas strain 112 has an arginine (R) at location 108. The latter is particularly significant, as strain 112 has been seen to retain this variant at least until passage 10, but nonetheless has demonstrated a significant increase in plaque size with passage (Figure 3-20). It is also important to note that by passage 10, there is an increase in frequency in variants within the region that encompasses the cleavage site between the F_1 and F_2 subunits (red arrow in Figure 3-21), emphasizing that this region may be important for culture adaptation.

Another significant variant correlated with culture adaptation has been attributed to position 556 of the HN protein of HPIV3 (Palermo *et al.*, 2016). A change from an asparagine (N) to aspartic acid (D) at that site has been linked to a decrease in neuraminidase activity and consequent increase in plaque size (Palermo *et al.*, 2016). It is however important to note that strain JS has an N at this location. It is of note that all clinical strains sequenced for this project contain an N at that location, whereas reference strain MK9 has a D. Changes due to culture adaptation at this site have been observed in strains 129 and 180, as

they exhibit a reduction of the N variant by 55% and 71% respectively by passage 10. This indicates that although this variant may have been linked to culture adaptation, it is not present in all cases.

It would be tempting to assume that the changes seen with passage in laboratory strain MK9 could be solely attributed to its adaptation to the PLC/PRF5 cell line (as it was previously cultured in BSC-1 cells, https://www.phe-culturecollections.org.uk) and would be shared by other strains adapting to the same cell line. In this context, a notable variant was observed at position 255 in HN protein where all strains at passage 1, including the strain MK9 contain a cysteine (C). However strain MK9 develops at serine (S) variant at that location by passage 5, which is shared by strain 112 at passage 10, strain 153 at passages 5 and 10 and strain JS. It is however important to note that this variant was not detected in strain MK9 at passage 10.

Although a number of potentially important sites and locations within the HPIV3 genome have been identified above, it is beyond the scope of this project to determine the exact significance or impact made by each variant observed. Overall it can be concluded that there is a definite increase in variants with larger plaque phenotypes exhibited by all clinical strains with increasing culture adaptation. Additionally, adaption to this particular cell line was also demonstrated by reference strain MK9. A number of specific variants were identified with potential correlation to plaque size. Most importantly, as significant culture adaptation was seen in all clinical strains it was decided that only clinical strains grown at passage 1 of both cycles should be used for further work.

3.7 Discussion

To date a number of studies on different pathogens have attempted to correlate clinical disease severity with plaque morphology *in vitro*. A distinct smaller plaque phenotype has been correlated to increased clinical pathogenesis and neuroinvasiveness of herpes simplex virus 1 (HSV1) (Mao and Rosenthal, 2003). On the other hand smaller plaque variants of West Nile virus (NWV) (Jia *et al.*, 2007) and dengue virus (Blaney *et al.*, 2002) were seen to be less neuroinvasive than their larger plaque counterparts. In respiratory viruses, plaque

morphologies were linked to different strains of rhinoviruses (Jacobs *et al.*, 2013) and different strains of RSV, with the more virulent strain A producing larger plaques (Kim *et al.*, 2015). It would therefore be logical to assume that there may be a correlation between HPIV3 phenotype *in vitro* and *in vivo*. To this end, the diversity of HPIV3 clinical strains *in vitro* had to be established.

So far, most studies on HPIV3 have been carried out on laboratory adapted strains. The small number of studies that have looked at behaviour of clinical strains of HPIV3 have concentrated on differences between a limited number of closely related clinical strains and a reference laboratory adapted strain *in vitro* and to an extent *in vivo* (Moscona, 2005; Palmer *et al.*, 2012, 2014). Unfortunately, differences between clinical strains themselves have hitherto not been explored. Therefore the first goal of this project was to create a library of highly diverse clinical samples of HPIV3. To this end HPIV3 positive clinical samples of diverse provenance were collected from the PHE laboratory, Cambridge. The number of cases of HPIV3 diagnosed by the laboratory over time was consistent with published seasonal variation (Zhao *et al.*, 2017). Samples collected contained a significant proportion of paediatric cases, which was in agreement with previous assessments of HPIV3 epidemiology in the literature (Henrickson, 2003; Mao *et al.*, 2012; F. Wang *et al.*, 2015) (Figure 3-1). Clinical samples selected for further study were also found to contain a significant proportion of immunocompromised cases, which also reflects the impact of HPIV3 described in other studies (Lindblom et al. 2010; Falsey 2012; Schomacker et al. 2012). All samples collected were from the upper respiratory tract of patients, as lower respiratory tract samples were classed as category 3 samples, and could not be transported off NHS/PHE premises for further culture. Most patients who undergo lower respiratory airway sampling, such as broncheo-alveolar lavage (BAL), would also have a matching upper respiratory airway sample processed by the laboratory, therefore it is very unlikely that no samples from these patients were obtained. Additionally there is evidence from studies with RSV that samples from both upper and lower airways in the same patient yielded the same RSV strain (Kim *et al.*, 2015). This means that, although the possibility that divergent HPIV3 strains could be found exclusively in the lower respiratory tract infection cannot be completely excluded, it is unlikely.

However, in future studies, it would be important to address this by sequencing and culturing HPIV3 samples from different sites of one patient to ensure lack of bias towards a particular subset of strains due to within host viral evolution.

At the other end of the severity spectrum, it is important to note that clinical HPIV3 samples collected for this project were mainly obtained from hospitalized patients. Patients in the community, presenting with mild symptoms, are rarely screened for respiratory viruses. This created an unavoidable bias towards more severe presentations of HPIV3. This sampling issue, however, is not unique to this project (Mao *et al.*, 2012; Košutić-Gulija *et al.*, 2017). In other respiratory studies, specifically those focusing on the pathogenesis of respiratory viruses, this drawback has previously been addressed by blindly sampling patients who were hospitalised for reasons other than respiratory presentations, for instance day surgery cases (Gern *et al.*, 2002). This approach, however would have necessitated additional financial support as well as additional ethical approval, which was deemed unfeasible, given the constraints of this project. It is however something that should be addressed in future studies focusing specifically on the pathogenesis of HPIV3 in a clinical setting.

Having obtained a representative cross-section of clinical samples, robust protocols for virus growth and detection were established. First and foremost a quick and efficient technique for measuring viral copy number was developed. Molecular techniques for HPIV detection in diagnostics and research are currently widely used (Jalal et al. 2007; Almajhdi 2015) and the assay adapted for my project forms part of a diagnostic respiratory panel that has been fully accredited (https://www.gov.uk/government/organisations/public-health-england). The primers and probe used were aligned to a part of the HPIV3 nucleocapsid gene, which is highly conserved among HPIV3 (Vainionpää and Hyypiä, 1994).

Although a PCR-based assay would facilitate a rapid evaluation of viral copy number, the study of phenotype *in vitro* required an infectivity based assay. The majority of studies (Hawthorne & Albrecht 1981; Bailly et al. 2016), that have previously used infectivity based assays of HPIV3 have focused on laboratory adapted strains that are known to be more cytopathic than HPIV3 clinical strains (Henrickson, 2003). Therefore protocols used in studies involving slow growing,

non-cytopathic viruses such as HPIV1 (Fukushima *et al.*, 2011) using solid overlays coupled with immunofocal staining techniques, were adapted for this project. For HPIV3 immunofocal staining protocols, primary antibodies directed against the HN subunit of HPIV3 (Bailly *et al.*, 2016) are most often used in literature. However the HPIV3 HN protein is known to be highly variable among HPIV3 clinical strains (Almajhdi, Alshaman and Amer, 2012; Goya, Mistchenko and Viegas, 2016; Košutić-Gulija *et al.*, 2017). Therefore for the purposes of this project an antibody against highly conserved F protein epitopes of HPIV3 was developed and an immunofocal assay for the detection of HPIV3 was successfully established.

The next step was the optimization of a growth protocol for clinical strains of HPIV3. Primary cell lines are generally considered to be superior to immortalised ones in terms of both viral yield (Yamaya *et al.*, 2002) as well as reduced culture adaptation effects (Palermo *et al.*, 2009). This is consistent with results obtained in this project, where the success rate for clinical strain growth in HAE cells was vastly superior to that obtained in immortalised tissue culture (44% vs 11% success rate). However HAE culture is not without its drawbacks. It does not allow efficient upscaling and is poorly adapted for the production of large volume stocks that were required for this project. Additionally HAE cells are obtained from a pool of donors and this may lead to heterogenous results and poor repeatability over longer time periods. Given these constraints, the decision was taken to use immortalised cell culture for the majority of viral stock growth, although we recognize this may have introduced a bias into our results.

Immortalised epithelial cell lines have previously been used to grow laboratory adapted reference strains of HPIV3 (Stokes *et al.*, 1992; Henrickson, 2003; Schmidt *et al.*, 2012). The choice of the PLC/PRF5 cell line (Alexander hepatoma cell line (Daemer *et al.*, 1980)) for this project was based on the experience with this cell line in the diagnostic field both for respiratory viruses (Nicholson *et al.*, 2014) as well as others (Jiang *et al.*, 2009).

It has previously been shown that the yield of some slow growing viruses, such as RSV, in immortalised tissue culture can be enhanced by inhibiting the interferon response of the cells (Stewart, Randall and Adamson, 2014) and that HPIV3 growth was inhibited by interferon response in the A549 cell line (Zhao *et*

al., 1996). Interferon inhibition has previously been achieved by either adding interferon inhibitors to the growth media (Stewart, Randall and Adamson, 2014) or by transducing the cells with lentiviral vectors expressing BVDV NPro and PIV 5V (Hilton *et al.*, 2006; Childs *et al.*, 2007) that are known to interfere with interferon beta production. In the current study, the latter was attempted, however the resultant cell lines did not yield higher viral titres. Poly I:C stimulation of the parental cell line and cell lines transduced with BVDV NPro, PIV 5V and empty vector confirmed that there was no difference in the interferon response of the wild type and transduced cell lines (Figure 3-9). Further literature review showed that the PLC/PRF5 cell line is chronically infected with hepatitis B (Daemer *et al.*, 1980; Koch *et al.*, 1984; Pinto, Bey and Bernstein, 1985), which has a complex and multifactorial suppressive effect on type 1 interferon (Guo, 2013) although it does not produce infectious virus (Daemer *et al.*, 1980). Therefore the PLC/PRF5 cell line was deemed to be suitable for HPIV3 culture.

However it cannot be assumed that all HPIV3 clinical strains had the capacity to grow efficiently in immortalised cell culture (Palmer *et al.*, 2014), which is likely reflected by the poor success rate achieved here. Therefore it could be argued that a proportion of clinical strains were missed and the cultured strains were biased towards those with the ability to grow in immortalised cells. In order to address this in the future, a larger scale study could be conducted with a range of clinical samples were inoculated both into single donor HAE cells and immortalised cell culture. Although this is unlikely to reach statistical significance due to the low growth success rates achieved in immortalised cell culture, it would nonetheless help to pinpoint some potential variants, that could then be explored further with a reverse genetics system (Beaty *et al.*, 2017).

When this project started there were very few whole genome sequences of HPIV3 available. Over the last few years, this number has increased, partially due to decreased cost and greater access to next generation sequencing (Kothari *et al.*, 2017) and a greater interest in viral metagenomics of respiratory infections (Madi *et al.*, 2018). However the bulk of whole genome sequences available centers on a small number of episodes or studies, yielding clusters of highly similar or identical genomes (Greninger *et al.*, 2017). Additionally there

are still no whole genome sequences from circulating UK strains. As part of this project, a robust amplicon-based sequencing pipeline was established and 23 whole genome sequences of UK clinical strains of different provenance and date of collection, as well as that of the laboratory strain MK9 were generated. The clinical stains were sourced from a diverse range of patients and were all distinct from both culture adapted strains MK9 and JS (Stokes *et al.*, 1992) .

Having established that clinical strains were significantly distinct from the laboratory strain MK9, an attempt was made to correlate this to their phenotype *in vitro*. Clinical strains were found to exhibit a diverse range of plaque sizes, which were all significantly smaller than the one demonstrated by strain MK9. A correlation between plaque phenotype *in vitro* and pathogenesis *in vivo* has previously been demonstrated in small animal studies for RSV (Stokes *et al.*, 2011) and rhinovirus (Jacobs *et al.*, 2013). It is of note that strains that were grown in HAE cells (8 and D) had the smallest plaque phenotype in PLC/PRF5 cells. This reflects that the selection of clinical strains in this project was inevitably biased towards strains that were able to grow in immortalised cell culture. To address this, a limited number of strains grown in HAE cells were included for comparison where possible.

First, clinical strains were divided into three groups according to plaque phenotype, and genomes of each group were compared to the genomes of laboratory adapted strains as reference. Subsequently, 6 clinical strains with diverse plaque phenotypes as well as laboratory strain MK9 were serially passaged in PLC/PRF5 cells with plaque phenotype and genotype recorded at passage 1, 5 and 10. Previously, HN and F genes have been implicated in culture adaptation and consequent larger plaque phenotypes (Palmer *et al.*, 2012, 2014). This is partially supported by data obtained here, as less variation in the F coding part of the genome between larger plaque phenotype strains and the laboratory culture adapted strains was recorded. However this result could have been confounded by small sample size (only two clinical strains), as well as by the fact that strains 65 and 82 were phylogenetically very similar.

All clinical strains exhibited larger plaque phenotypes with increased culture adaptation, whereas strain MK9 developed smaller sized variants, which likely reflected adaptation to the PLC/PRF5 cell line. The intergenic M –F region was

found to be a focus of culture adaptation driven change with overall more variants detected at passage 10 compared to passage 1 sequences in that region. In literature, this part of the genome has previously been connected to a smaller plaque phenotype due to aberrant transcription between M and F coding regions of the HPIV3 genome as part of the viral subversion of the immune system (Lingemann *et al.*, 2015). This leads to a decrease in the amount of F protein produced and subsequently a less immunogenic and less fusogenic phenotype *in vivo* (Lingemann *et al.*, 2015). Changes in this part of the HPIV3 genome would therefore be potentially consistent with HPIV3 adaptation to immortalised cell culture, however validation of this would require confirmation using reverse genetics. Changes in two specific variants previously identified in literature (Palmer *et al.*, 2012), namely E108K in the F protein, which has been linked to larger plaque phenotype and N556D in the HN protein, linked to a deficient neuraminidase, were also observed, although not in all strains. A new variant, potentially specifically linked to PLC/PRF5 cell adaptation, C256S in the HN protein of strain MK9 at passage 5, as well as clinical strains 112 and 153, was also identified.

It is important to note that in literature, larger plaque sizes produced by HPIV3 strains have frequently been correlated with culture adaptation and therefore with a decreased suitability for replication in the natural host (Moscona, 2005; Palmer *et al.*, 2012, 2014). However little attention has been given to the potential that the larger plaque phenotype could be a naturally occurring variant, as has been observed in other viruses (Mao and Rosenthal, 2003; Jacobs *et al.*, 2013; Kim *et al.*, 2015). Unfortunately because of this connection, most of the data on plaque size is inevitably correlated with data obtained from culture adaptation studies. In the future, an HPIV3 reverse genetics system (Pfaller, Cattaneo and Schnell, 2015; Beaty *et al.*, 2017) would help to elucidate the exact effects of these variants, although a greater numbers of clinical strains are required to establish whether other variants, specifically from other parts of the genome are involved.

Overall, in this chapter, I have demonstrated the optimization of the protocols required for reliable growth, quantification and whole genome sequencing of HPIV3. These protocols have been applied to grow a stock of minimally passaged

clinical strains from the UK, covering patient samples across a number of years. The clinical strains have been shown to be phylogenetically and phenotypically diverse, as well as significantly different from the culture-adapted reference strain MK9. Serial passage of a number of clinical strains in immortalised cell culture has helped to identify potentially important variants linked to tissue culture adaptation. Most importantly the above has shown that clinical strain stocks grown for this project are suitable for further work on phenotypic and phylogenetic diversity of HPIV3 in a wider context and potential correlation to pathogenesis. This will be addressed in further experiments carried out in a primary cell line (HAE cells) in the following chapter.

4 Chapter 4: HPIV3 clinical strain phenotypes in human airway epithelial cells and implications for clinical pathogenesis.

4.1 Introduction

As previously discussed there is a broad spectrum of pathology and severity that is associated with HPIV3 infection (Herzog *et al.*, 1989; Cilla *et al.*, 2008; Park *et al.*, 2009; Maeng *et al.*, 2012; Shah *et al.*, 2016) the underlying causes of this are unknown and are likely to include a combination of both viral and host factors.

Previously, there have been attempts to study the virulence of HPIV3 in immortalised cell lines, where culture adapted strains typically become more fusogenic and show increased cytopathic effect (Stark *et al.*, 1991; Henrickson, 2003). This has led to studies looking at particular aspects of HPIV3 that would allow it to replicate more efficiently in the natural host, including the particular attributes that would make it more successful in the host (Palermo *et al.*, 2016). Small animal models including hamsters (Crookshanks-Newman and Belshe, 1986), guinea pigs (Ye *et al.*, 2010), ferrets (Mascoli *et al.*, 1976) and cotton rats (Murphy, Dubovi and Clyde, 1981; Boukhvalova, Prince and Blanco, 2009) have also been employed to investigate the pathogenesis of HPIV3, including potential treatment strategies.

More recently, primary cell lines such as human airway epithelial (HAE) cells have become more common in the study of respiratory viruses (Zhang *et al.*, 2005). These readily support HPIV3 replication in a natural environment, including viral propagation in an environment with beating cilia and directional apical budding of new virus from cilia shafts (Zhang *et al.*, 2005, 2011). This system has also allowed the study of the innate immune responses induced by HPIV infection (Schaap-Nutt *et al.*, 2012; Lewandowska-Polak *et al.*, 2015). Both *in vitro* (Zhang *et al.*, 2005; Schaap-Nutt *et al.*, 2012; Lewandowska-Polak *et al.*, 2015) and *in vivo* studies (Gern *et al.*, 2002; Ottolini *et al.*, 2002; Feghaly *et al.*, 2012), have demonstrated increases in pro-inflammatory chemokines such as

RANTES, IL-6, MIP1 alpha and beta as well as IP10 and IL8 following HPIV3 infection.

As variation in viral pathogenesis could have important implications for clinical outcome in otherwise similar hosts, in this chapter, I have attempted to elucidate whether the behaviour of HPIV3 clinical strains in a model of the natural host (HAE cells) could be correlated with genotypic and phenotypic characteristics. As previously described, most studies have used well established and significantly culture adapted strains to study HPIV3, although it has been shown that these have distinct phenotypes and genotypes (Palmer *et al.*, 2014). Therefore, in order to look at potential diversity in naturally occurring strains, well-characterised stocks of clinical HPIV3 strains were required for this project. To this end, stocks of diverse clinical strains were grown in PLC/PRF5 cells and a small number of clinical samples were also propagated in HAE cells. Subsequently a number of these were sequenced and characterized according to their phenotype in immortalised cell culture, as discussed in the Chapter 1. Growth kinetics and cytokine responses triggered by five clinical strains with diverse plaque phenotypes and specific fusion protein variants, as well as reference strain MK9, were then evaluated in HAE cells. Although the numbers involved were small, it was nonetheless possible to demonstrate that there are potential differences in the behaviour of clinical strains in HAE cells linked to specific variants and phenotypes in immortalised cell culture. Additionally it was possible to demonstrate that although viral load is frequently used as a marker of clinical disease severity, it may not necessarily correlate with the extent of the immune response and its impact on morbidity and mortality.

4.2 Sample selection

In the previous chapter, I have described the growth of viral stocks of clinical strains of HPIV3, their characterization by plaque phenotype in PLC/PRF5 cells, as well as their phylogenetic relationship. The purpose of this chapter was to investigate whether the phenotype in cell culture as well as the genotype of a particular strain would affect its virulence as measured by growth kinetics and innate immune response triggered in HAE cells. Therefore 5 clinical strains with

different plaque phenotypes, as well as the reference laboratory strain MK9 were selected for this purpose.

A recent paper discussed the correlation of success in the natural host with an E variant at position 108 in the F protein of HPIV3 and an N at position 556 in the HN protein of HPIV3, going as far as correlating changes at these sites with cell culture adaptation (Palermo *et al.*, 2016). It was additionally argued that the E variant at 108 in the F protein was specific to clinical strains grown in HAE cells (Palermo *et al.*, 2016). To this end, strains grown both in PLC/PRF5 cells (K variant at 108 in F) as well as HAE cells (E variant at 108 in F) were chosen for analysis in HAE cells (Figure 4-1B). Additionally, the strains were paired phylogenetically, as shown in Figure 4-1A, meaning that strains with different plaque phenotypes and F 108 variants were nonetheless closely related to reduce other potential confounding factors in their behaviour. All the clinical strains had the N variant at amino acid 556 in the HN protein (linked to significantly reduced neuraminidase function (Palmer *et al.*, 2012; Palermo *et al.*, 2016)), laboratory strain MK9, had a D variant at that position.

A

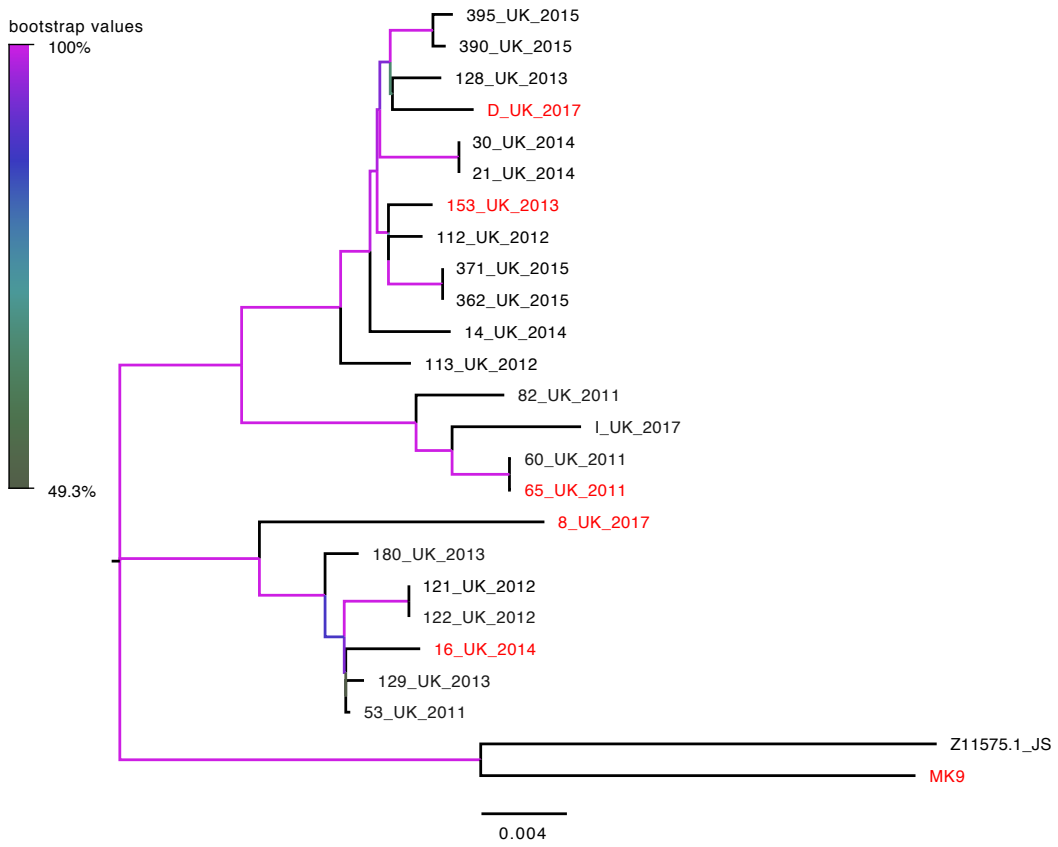

B

Lab ID	Grown from original sample in	Plaque phenotype	F 108 variant	HN 556 variant
8	HAE	small	E	N
D	HAE	small	E	N
16	PLC/PRF5	small	K	N
153	PLC/PRF5	medium	K	N
65	PLC/PRF5	large	K	N
MK9	laboratory reference strain	very large	K	D

Figure 4-1 Selection of strains for phenotype investigation in HAE cells. Panel B shows the clinical strains selected as well as laboratory reference strain MK9, including the cell type that was used for growth from original clinical sample (where applicable), plaque phenotype, as identified in the Chapter 1 and respective F 108 and HN 556 variants. The phylogenetic relationship between the strains chosen (in red) is shown in panel A. This phylogenetic tree is a copy of the one shown in **Figure 3-16** and illustrates the phylogenetic relationship between clinical strains sequenced as part of this thesis. Branches are coloured by their bootstrap values, as per the colour legend.

4.3 Growth kinetics in primary cells

In order to investigate the relative growth rates of the clinical strains and the laboratory reference strain MK9 in primary cells, five diverse clinical strains and the laboratory reference were grown in HAE cells. All strains were plaque titrated and the infection was carried out at 0.001 MOI/cell. The results are shown in Figure 4-2. Viral growth was assessed by sampling released virus and titration by plaque assay (Figure 4-2A). The laboratory strain MK9 grew slower in HAE cells compared to the clinical strains. This was consistent with previously published data (Palmer *et al.*, 2012) as the reference strain was poorly adapted for growth in primary cells. Additionally some differences were observed in clinical strain titres at 72 hours, with the smaller plaque phenotype strains 8 and D reaching a roughly 1-2 $\log_{10}$ smaller titres compared to the larger plaque phenotypes. Rate of growth was calculated by taking the first derivative at each timepoint (Figure 4-2B). A slower rate for the laboratory strain, as well as for strains 153 and 8 were observed. Due to potential differences in neuraminidase function between clinical strains and the laboratory strains that would lead to enhanced cell-associated virus in the latter, viral titres were also calculated in freeze thawed cells at 72 hours and this, together with final viral titres at 72 hours is shown in Figure 4-2C. Due to financial constraints only one biological replicate could be obtained for the viral load in cells. As expected, the cell associated viral titre for strain MK9 was observed to be significantly higher than that obtained by quantifying released virus only. This was not the case for the clinical strains, where a good positive correlation was found between the two respective titres (R^2 = 0.8, data not shown). Consistent with previous data (Zhang *et al.*, 2005), I observed that HPIV3 was only secreted from the apical surface of the cells as no virus was detected in the basal compartment (data not shown).

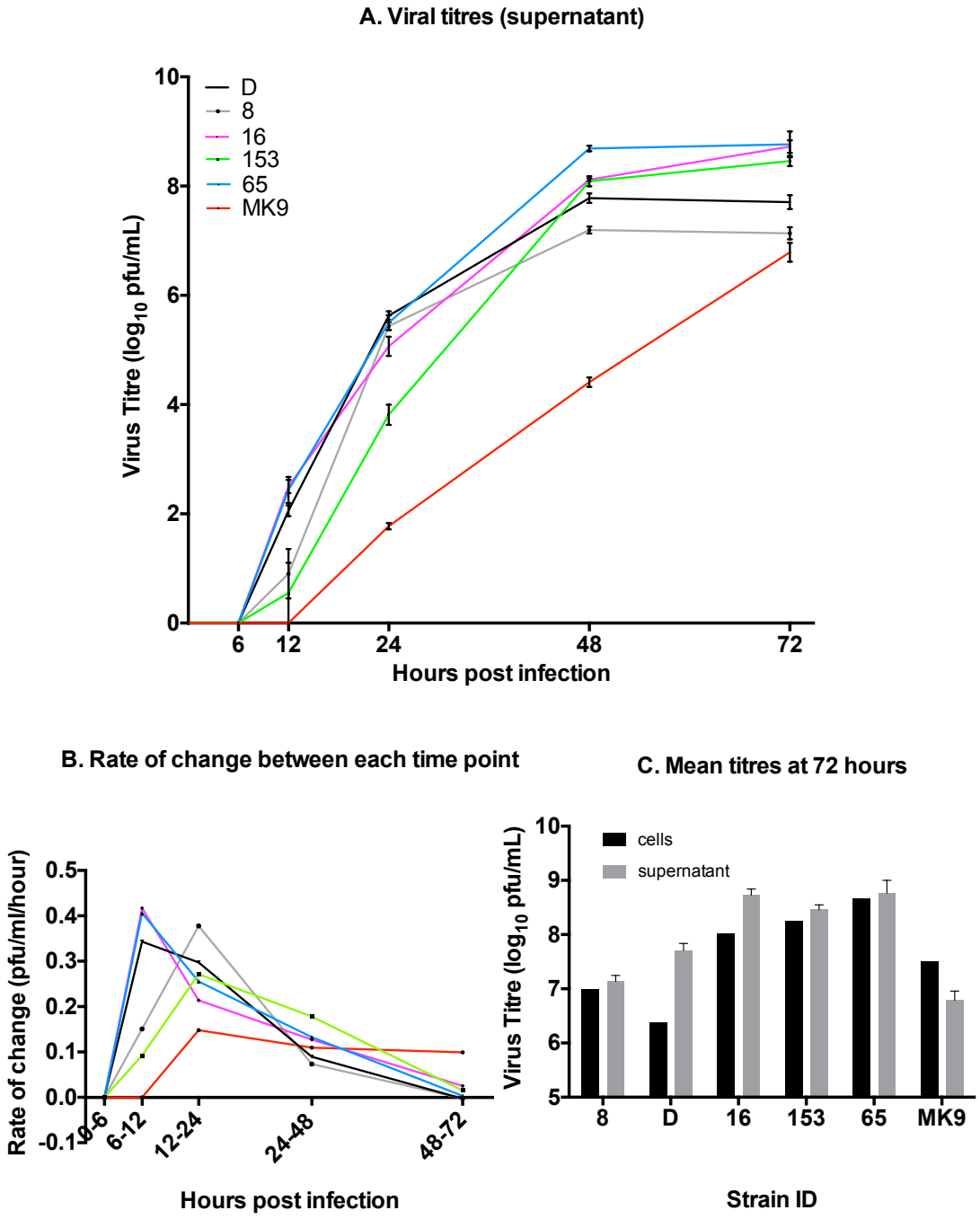

Figure 4-2 Clinical strains show diverse growth kinetics in human airway epithelial cells. Virus yields at each time point measured by plaque titration of the supernatant are shown in (A). Each point represents the mean of 3 biological repeats +/-SEM. Rate of growth (B) has been calculated by calculating the rate of viral titre increase at each time point (first derivative) in GraphPad Prism version 6. Virus yields at 72 hours (3 biological repeats +/- SEM) (A) are compared to yields in the cells (one biological repeat) at 72 hours in panel (C). For all clinical strains the titre in the supernatant exceeds that found in the cells, apart from the laboratory strain MK9 where the converse is true. Similarly, strain MK9 shows a significant growth defect compared to the clinical strains, both in absolute titres (A) and growth rate (B).

4.3.1 Immune response in human airway epithelial cells

As discussed above, the pathogenesis of HPIV3 is likely to be reliant on an interplay between host and viral factors. Having established the relative growth kinetics of selected clinical strains and strain MK9 in HAE cells, I examined the innate immune response triggered following infection. To this end the levels of select cytokines and chemokines induced during the infection timecourse were measured. A full list of the cytokines/chemokines tested can be found in Materials and Methods. A measurable response, that was significantly different from the negative control wells was detected for RANTES, IP-10, MIP1α and β, IL-1α and IL-8. The results are summarized in Figure 4-3 and Figure 4-4. The values recorded for IL-8, were out of operating range throughout the entire time course apart from the final time point (72 hours) where the samples were diluted 1:10. Four wells: 2 infected by strain 16, 1 by strain 8 and 1 by strain D were deemed to be contaminated and therefore were not evaluated for cytokine induction. Therefore cytokine induction by strain 16 is not shown and values obtained for strains 8 and D represent biological duplicates only. Induced cytokine levels are shown in Figure 4-3A. Strains 8 and D were observed to be more effective in inducing RANTES, which has been heavily implicated in asthma exacerbation linked to HPIV3 infection (Lewandowska-Polak *et al.*, 2015; Chihara *et al.*, 2018). Strain MK9, on the other hand was observed to have the least effect immunologically, potentially due to the lower viral load at 72 hours. This was an unexpected result, as previously published data suggests that fusogenic strains, although slow growing in the natural host had the capacity to cause more immune mediated damage than their less fusogenic counterparts (Moscona, 2005). Therefore, the cytokine levels observed at 72 hours were corrected for cell associated viral loads measured at the same time point for each strain (Figure 4-2C), these are shown in Figure 4-3B and Figure 4-4B. After the correction, strain MK9 was indeed seen to be more inflammogenic than clinical strains 153 and 65. Strains 8 and D, in each case, were seen to induce the highest level of response, with strains 153 and 65 showing the least per cell associated PFU.

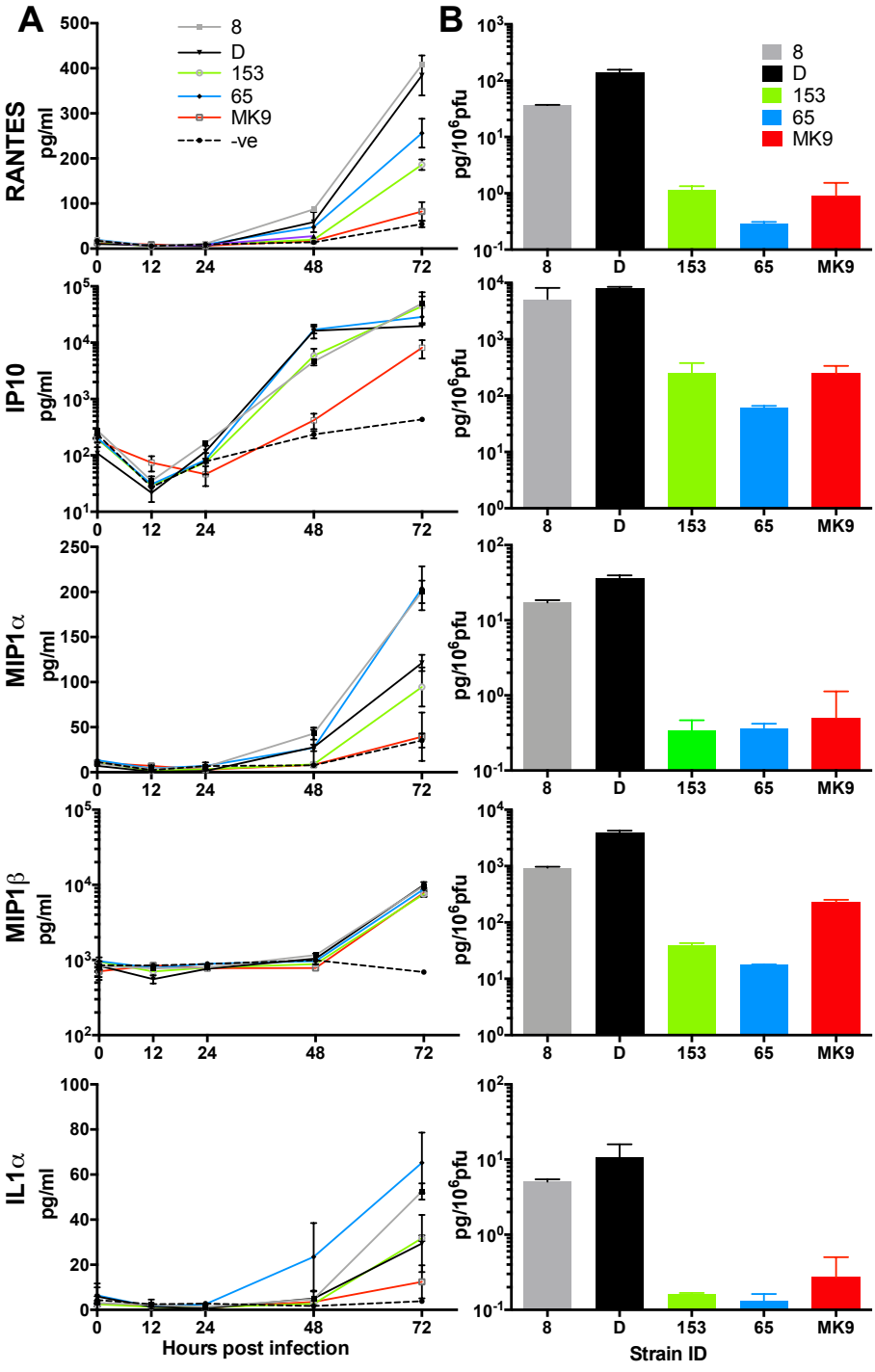

Figure 4-3 Infections with clinical strains and the culture adapted laboratory strain shows diversity of chemokine and cytokine responses in HAE cells. Absolute (pg/ml) (A) and corrected for viral load at 72 hours (pg/10^6pfu) (B) levels of RANTES, IP10, MIP1α and β, IL1α after infection with 4 clinical strains and the laboratory reference strain MK9 (LS) are shown. 65, 153 and MK9 represent the mean of 3 biological repeats +/- SEM; 8, D and uninfected (negative) controls represent 2 biological repeats +/-SEM.

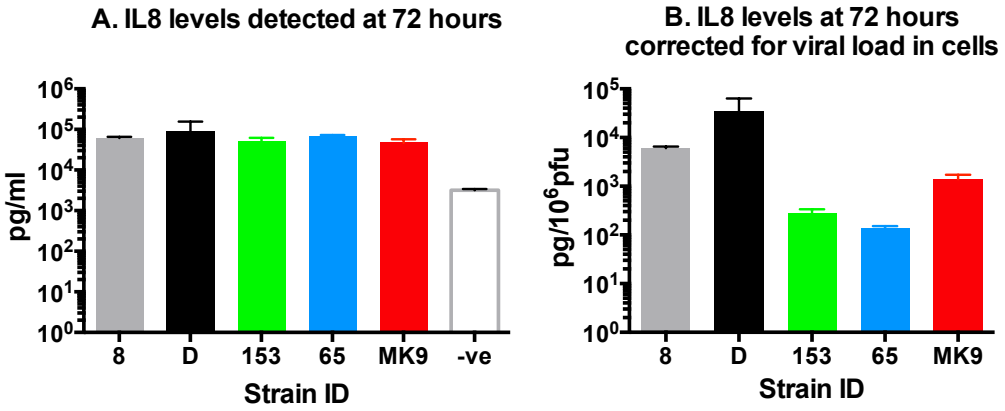

Figure 4-4 Infection with clinical strains and the culture adapted strain MK9 shows a significant increase in IL-8 levels. Absolute (pg/ml) (A) and corrected for viral load (pg/10^6pfu) levels of IL-8 induced by 4 clinical strains and the laboratory strain MK9 measured at 72 hours. Each column represents the mean of 3 biological repeats +/- SEM for strains 65, 153 and MK9 and a mean of 2 biological repeats +/- SEM for strains 8, D and negative control. All the clinical strains cause a significant increase in IL-8, with a potential significant variation when corrected for viral load (B).

4.4 Discussion

A large spectrum of pathology has been attributed to HPIV3 viruses (Madden, Burchette and Hale, 2004; Weinberg *et al.*, 2009; Schomacker *et al.*, 2012). The severity of infection has frequently been correlated to the immune status of the patient as well as their age, with HPIV3 infections being particularly significant in the very young and the very old (Henrickson, 2003; F. Wang *et al.*, 2015). This places host factors at the forefront of the clinical impact of HPIV3 infection. As a result, viral factors and their potential contribution to clinical severity have not been studied as extensively.

HAE cells are an established *ex vivo* approximation of the natural host for many respiratory viruses (Yamaya *et al.*, 2002; Fulcher *et al.*, 2005) including HPIV3 (Zhang *et al.*, 2005, 2011). A number of studies have made use of this model in an attempt to elucidate the features that make HPIV3 more successful in the natural host (Palmer *et al.*, 2012; Palermo *et al.*, 2016) as well as the growth kinetics and immune responses of different HPIV subtypes (Schaap-Nutt *et al.*, 2012) in HAE cells. Therefore this model was used to investigate the correlation between

phenotype in immortalised cell culture and genotype of 5 diverse clinical strains of HPIV3 and reference strain MK9 with their growth kinetics and cytokine response in HAE cells. Strains were chosen according to their plaque phenotype, as well as particular variants at amino acid positions 108 in the F protein and 556 in the HN protein (Figure 4-1). These were also paired phylogenetically as much as possible (Figure 4-1A) so as to reduce any other potential confounding factors, although due to small numbers of samples these could not be entirely excluded. The F proteins of clinical strains with an E at position 108 in the F protein have been previously observed to have a fusion protein cleavage defect, leading to very small plaque sizes or failure to grow in immortalised cell lines (Palermo *et al.*, 2016). This is supported by data discussed in Chapter 1, where small plaque size was correlated with this variant that was lost with culture adaptation. Additionally, it was previously observed that strains with a D at amino acid 556 of the HN protein had a 5-fold decrease in their neuraminidase activity compared to those that had an N at that position (Palmer *et al.*, 2012; Palermo *et al.*, 2016) . This was linked to culture adaptation (Palermo *et al.*, 2016) and was in agreement with data discussed in the previous chapter, where strain MK9 was found to have a D variant and two clinical strains were observed to acquire it during culture adaptation. It was, however, found that strain JS, another well-known significantly culture adapted HPIV3 strain, contained an N variant, indicating that, although potentially linked to culture adaptation, a D variant at position 556 in HN cannot be seen as a defining feature of a culture adapted strain, as discussed in Chapter 1.

A significant difference was observed between the rate of growth and final virus titres at 72 hours between clinical strains (Figure 4-2) and strain MK9. This was consistent with previous findings that the growth of significantly culture adapted strains would be impaired in the natural host (Moscona, 2005; Palmer *et al.*, 2012). This difference was less pronounced when cell-associated virus was measured (Figure 4-2B) and is consistent with a reduced neuraminidase function of strain MK9, linked with the D variant at location 556 of the HN protein. A previous study has shown that HAE grown clinical strains with E variants at amino acid 108 in the F protein grew well in HAE cells, and although some differences in the rate of growth were seen, similar viral loads by day 3

post infection were observed in all the strains (Palermo *et al.*, 2016). This is consistent with the viral titres observed in the current study for strains 8 and D (10^7-10^8 PFU/ml). It is important to note that four clinical strains used in the (Palermo *et al.*, 2016) study were all closely related, suggesting that potentially only one phenotype was studied. However, in the current study, all strains with a K variant at 108 in the F protein were observed to have yielded a higher viral titre (10^8-10^9 PFU/ml) at 72 hours (Figure 4-2). This suggests that this variant is not detrimental to virus growth kinetics in the HAE model. Additionally it was observed that clinical strains 8 and 153 exhibited a markedly slower growth rate compared to other clinical strains (Figure 4-2B). This was particularly noteworthy, as these strains were not closely phylogenetically related (Figure 4-1A) and contained different 108 F variants.

The total number of clinical strains grown in HAE cells in the (Palermo *et al.*, 2016), study was 8, here it was 3. Although all these strains were found to contain an E variant, overall the sample is too small to speculate that this variant is overwhelmingly dominant in the natural host. Equally, as growth in immortalised cell culture would predispose to the K variant, one cannot make inferences as to the frequency of this variant in the natural host from sequences grown in immortalised cells. Additionally the data on growth kinetics in HAE cell obtained here, suggests that other significant mutations, that do not significantly influence phylogenetic classification may govern the rate of growth of HPIV3 in HAE cells, however the current study lacks statistical power to speculate further.

Although growth kinetics of viral strains provide a measure of viral fitness, in clinical practice, it is often the immune response provoked by a particular virus that contributes to the severity of the disease. This has been particularly well studied in RSV, another paramyxovirus, where the severity of the disease has been linked to levels of particular chemokines (Gern *et al.*, 2002; Habibi and Openshaw, 2012). The inflammatory response caused by HPIV3 has received less attention, although it has been studied in the cotton rat model (Ottolini *et al.*, 2002), *ex vivo* in primary cells (Schaap-Nutt *et al.*, 2012; Lewandowska-Polak *et al.*, 2015) and in a clinical setting (Feghaly *et al.*, 2012). In small animal models, infection with HPIV3 has been correlated to laryngotracheal inflammation and an increase in IFNγ secretion, a potentially key pathology linked to asthma

exacerbations in paediatric cases in particular (Ottolini *et al.*, 2002; Weinberg *et al.*, 2009; Ye *et al.*, 2010). This has been confirmed by another study in a primary cell line, although in that case the infection was carried out at a significantly higher MOI than here (Lewandowska-Polak *et al.*, 2015). A similar study in HAE cells reported an increase in IFNα and β generated by HPIV3 at later timepoints (Schaap-Nutt *et al.*, 2012). It has been reported that the HPIV3 C protein binds STAT1 and inhibits its phosphorylation thereby inhibiting interferon signalling, as well as down-regulating viral RNA synthesis, and reducing the innate response, which may explain the lack of measurable interferon induction detected here (Caignard *et al.*, 2009).

In a clinical study, where inflammatory chemokines in nasal washes from children infected with parainfluenza were analysed, IL-6, IL8, MIP1α and β, RANTES and MIG (not measured in this study) were identified as specific to infection with parainfluenza viruses, with IP10 and IL1α showing less statistically significant increases over levels recorded in uninfected controls (Feghaly *et al.*, 2012). Consistent with results previously described in literature (Schaap-Nutt *et al.*, 2012; Schomacker *et al.*, 2012; Lewandowska-Polak *et al.*, 2015), I have been able to obtain measurable increases in RANTES, MIP1α and β, IP10, IL1α and IL8 (Figure 4-3 and Figure 4-4). IL6 levels were found to be high both in the infected and non-infected cells, this was potentially due to culture handling, as previously described in literature (Schaap-Nutt *et al.*, 2012). Strain MK9, although yielding the lowest viral load (Figure 4-2) was seen to be moderately inflammogenic when compared to clinical strains grown in PLC/PRF5 cells (Figure 4-3 and Figure 4-4). This is consistent with previously reported data (Moscona, 2005), that indicates that strains with greater fusogenic properties due to changes in their HN protein have the potential to trigger a greater innate immune response. In this context, unexpectedly, strains 8 and D, which exhibited the smallest plaque phenotype in immortalised cell culture, were shown to trigger the highest level of cytokine release per PFU. This was surprising, as these strains were considered to be best adapted for survival in the natural host, based on previously published data (Palmer *et al.*, 2012; Palermo *et al.*, 2016). Overall it was observed that strains with an E variant at position 108 in the F protein (strains 8 and D) yielded smaller viral loads and greater cytokine

release than strains with a K variant at F 108 (strains 65, 153). Although it is suggested that E variants are disadvantaged in immortalised cell culture (Palermo *et al.*, 2016), the data obtained here implies that the converse may not necessarily be true for K variants in the HAE model.

In clinical studies, HPIV3 infection has been distinguished from other types of HPIV by significantly increased levels of IL8, and less significant increases of IL1α and IP10 (Feghaly *et al.*, 2012; Schaap-Nutt *et al.*, 2012), with IL8 and IP10 correlated to clinical severity (Gern *et al.*, 2002; Feghaly *et al.*, 2012). This is in agreement with the results obtained here (Figure 4-3 and Figure 4-4). In this study no significant difference in IL8 or IP10 levels were recorded between strains when uncorrected for viral load (Figure 4-3A), however strains 8 and D were shown to induce higher cytokine levels per PFU, than the other strains tested. This has potential implications for the severity of disease caused by these strains. For instance, RANTES secretion (Figure 4-3A), which is implicated in asthma exacerbation caused by respiratory viral infections (Chihara *et al.*, 2018), was increased in smaller plaque phenotype strains 8 and D, even without correction for viral load (Figure 4-3B) compared to strains 65, 153 and MK9. The above may have implications for more targeted clinical treatment as cotton rat studies have previously shown that innate immune system modulation with glucocorticoids during HPIV3 infection may have a beneficial effect on outcome (Ottolini *et al.*, 2002).

Overall HPIV3 clinical strains with E variants at position 108 in their F proteins were observed to behave differently from strains with K variants, both in terms of growth kinetics and cytokine release. Within the limits of the data obtained, one cannot deduce a specific mechanism responsible for these differences. It could be argued that strains 8 and D produced smaller viral loads due to their more inflammogenic nature, which could potentially be linked to their more efficient replication in HAE cells, as suggested in the paper discussed (Palermo *et al.*, 2016). However, it could equally be argued that slower growing strains would be less adept at producing sufficient immunomodulatory proteins in the required time frame and thus trigger a greater innate immune response (Caignard *et al.*, 2009). Overall my results would suggest that strains with K variants at 108 in the F protein represented a more successful phenotype in HAE

cells, which is somewhat surprising, given that all clinical strains grown in HAE cells contained an E variant. In the future it would be informative to see whether HPIV3 strains with K variants at amino acid 108 in the F protein would develop an E variant at that location with adaptation to HAE cells.

At this stage, it is important to interpret these findings within the limitations of the current model. Although HAE cells are considered to be a close approximation of the living host, it remains a very limited model of the immune system compared to either a small animal model or a clinical study. It lacks the capacity to recruit cells, such as T lymphocytes, that would be involved in driving the cytokine response *in vivo* and naturally cannot model the adaptive immune system. The cells are collected from only one donor and from only one location within the respiratory tract, which excludes the variability introduced within and between hosts. In the study discussed (Palermo *et al.*, 2016), clinical strains with E variants were also successfully grown into cotton rats. Unfortunately no such data for closely related strains with K variants is available. Additionally the number of strains involved is very small, and although an attempt was made to exclude confounding factors by phylogenetically matching the strains, other differences, that have been unaccounted for cannot be excluded. Nonetheless, the above demonstrates that clinical strains of diverse phenotypes and genotypes have the potential to behave differently in the natural host.

Overall, in this chapter I have shown that there is sufficient evidence to suggest that different clinical strains of HPIV3 may produce a different clinical picture in otherwise similar hosts. However, as discussed previously, there is currently little data on circulating strains within the UK and little consensus on the phylogenetic characterization thereof. Although, in this chapter, a variant that was not linked to phylogenetic classification was heavily implicated in the phenotype displayed by HPIV3 clinical strains in HAE cells, it was also discussed that other variants, hereto unclassified cannot be excluded. In this context, a measure of diversity and evolution of HPIV3 is crucial to our understanding of its' impact and epidemiology and this is discussed in the following chapter.

5 Chapter 5: UK circulating strains of human parainfluenza 3: phylogenetic analysis and outbreak investigation.

5.1 Introduction

As discussed above, the clinical impact of HPIV3 is well studied in adults where studies have quoted figures ranging from 27% to 75% mortality due to lower respiratory tract infection (LRTI) attributed to HPIV3 (Seo *et al.*, 2014). This is in contrast to the paucity of data available on the impact of HPIV3 in the paediatric population, where data is frequently conflicting both in terms of risk factors (Ustun *et al.*, 2012; Torres *et al.*, 2016; Santolaya *et al.*, 2017) and outcome (Bowden, MD, 1997; Christensen, Nielsen and Hasle, 2005; Söderman *et al.*, 2016; Torres *et al.*, 2016). A number of HPIV3 outbreaks in paediatric settings have been identified, but in each case, outbreaks were identified retrospectively and prospective identification of point sources was not been possible (Piralla *et al.*, 2009; Berrueco *et al.*, 2013). In the current chapter, a cluster of HPIV3 cases identified on a paediatric oncology ward in the summer of 2017 was analysed in this context.

First and foremost, in order to establish the diversity of circulating HPIV3 UK strains, the genetic analysis of full genome sequences of twenty circulating UK strains between the years 2011-2015 was carried out. This data, together with other full genome sequences available in the Genbank, was used to conduct a phylogenetic analysis of UK circulating strains of HPIV3. Previously, phylogenetic analysis of HN gene sequences has been used to characterize emerging strains as well as tracing outbreaks (Piralla *et al.*, 2009; Almajhdi, Alshaman and Amer, 2012; Mao *et al.*, 2012; Goya, Mistchenko and Viegas, 2016; Košutić-Gulija *et al.*, 2017). The F gene has been shown to be equally valid for HPIV3 phylogenetic classification (Košutić-Gulija *et al.*, 2017). Additionally a small region directly preceding and overlapping with the start of the F gene has been historically used to trace outbreaks (Zambon *et al.*, 1998; Jalal *et al.*, 2007). For the purposes of this project, a short hypervariable region in the HPIV3 genome was identified and evaluated as a potential target for outbreak tracing by comparing

phylogenetic classification obtained using full genome sequences and those obtained using this hypervariable region. A nested PCR protocol for the amplification of this region was established and using this method, the cluster of HPIV3 cases was identified as a point source outbreak.

Subsequently molecular data obtained was combined with epidemiological information extracted from hospital records using Structured Query Language (SQL) (Weinberg *et al.*, 2010), as well as a clear visualization tool based on Konstanz Information Miner (KNIME) version 3.3.2 (Berthold *et al.*, 2008). The latter is an open source tool that has been successfully used in the pharmaceutical and food industries and clinical epidemiology analysis (Risselada *et al.*, 2009; Ratnam *et al.*, 2014; Nicola *et al.*, 2015; Weiser *et al.*, 2016).

5.2 Results

5.2.1 Outbreak identification and sample selection

A cluster of HPIV3 cases was identified on a paediatric oncology ward in the summer of 2017. In order to determine whether the activity observed represented a deviation from the norm, seasonal trends of HPIV3 in the surrounding geographical area as well as on the ward in question were analysed.

First, epidemiological trends were compared between the number of positive samples for the 6 adjoining geographical areas covered by the laboratory and those for the hospital alone for years 2014-2017 and the paediatric oncology unit for the same dates up to and including August 2017. Once the outbreak was identified, samples from the 15 outbreak cases and 15 non-outbreak parainfluenza cases were collected for further analysis.

The number of positive cases identified by the PHE laboratory at the index teaching hospital between the years 2014-2017 is summarized in Figure 5-1A. Expected seasonal fluctuations in HPIV3 prevalence, with peaks in late string and summer were observed. No unusual activity pointing to a potential outbreak was identified. This was confirmed when the number of total HPIV3 cases in the index teaching hospital was compared to the number of cases within the full geographical area covered by the laboratory (Figure 5-1B). In contrast the number of cases observed in the paediatric oncology unit clearly reflected a peak centered in June- August 2017 (Figure 5-1C). This was seen to exceed the usual

seasonal fluctuations observed on this ward during previous seasons and an outbreak was suspected on the 14th of July 2017.

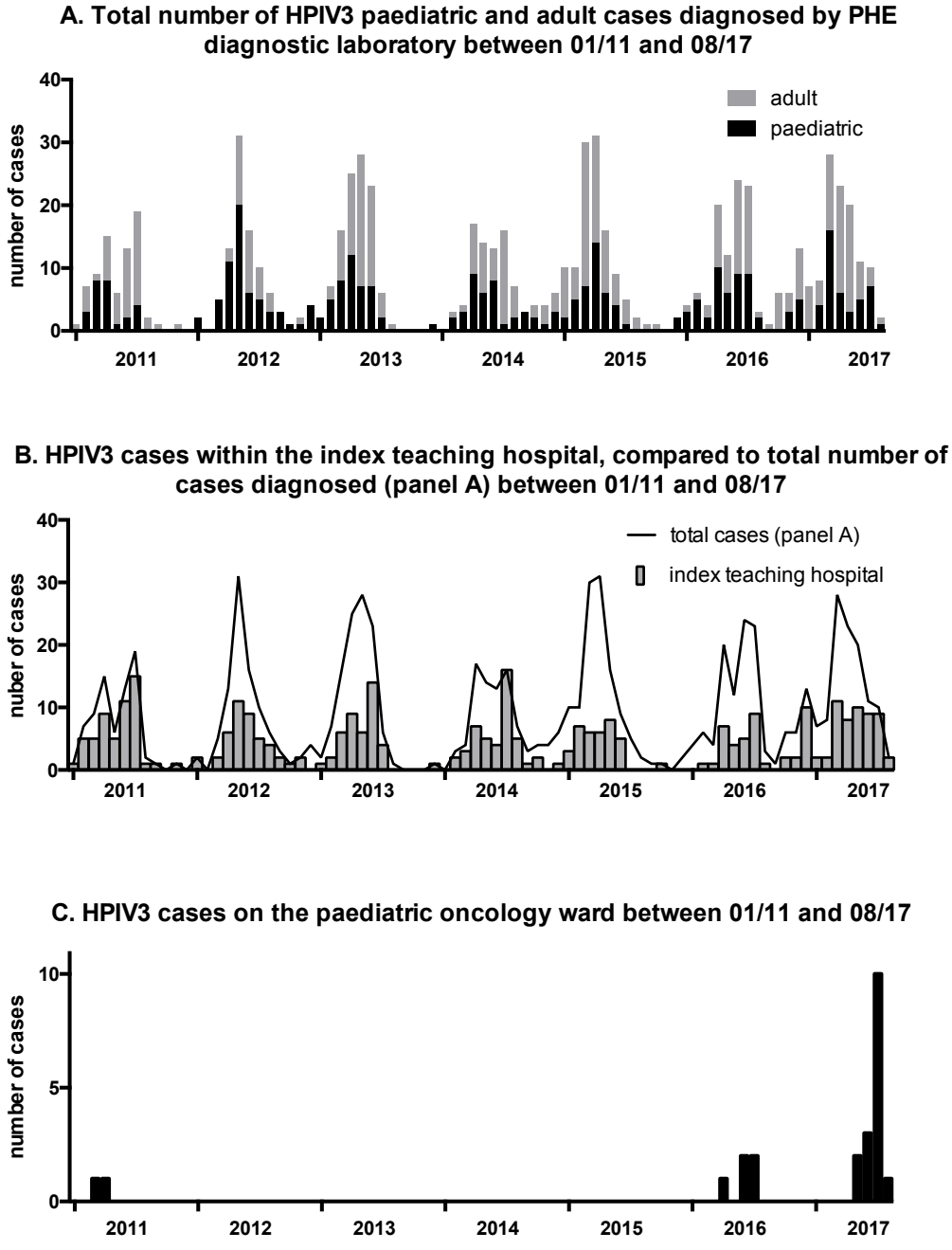

Figure 5-1 Epidemiological incidence of HPIV3 and outbreak identification. The total number of HPIV3 cases diagnosed by the PHE laboratory, at the index teaching hospital, subdivided by adult and paediatric cases during the period January 2011 to August 2017 is shown in A. Number of cases for the same time period, geographically located within the index teaching hospital itself, compared to the total number of cases diagnosed are shown in B. Cases on the paediatric oncology ward within the same time period are shown in C.

5.2.2 Clinical details of the patients

The clinical details of the patients involved, including their underlying diagnosis, any other organisms isolated and potential impact of the infection are summarized in Table 5-1.

Lab ID	Underlying diagnosis	Reason for admission	Interval between AD and SD (days)	Interval between AD and SOD (where available) (days)	Interval between SOD (where available) and SD (days)	Potential nosocomial infection?	Potential cause of admission/ prolonged stay?	Other organisms isolated
1	CNS tumour	febrile neutropenia	1	-2	3	N	Y	rhinovirus
2	CNS tumour	febrile neutropenia	2	0	2	Y	Y	adenovirus
3	CNS tumour	febrile neutropenia	4	0	4	N	Y	rhinovirus
4	AML	new diagnosis	15	13	2	Y	N	
5	ALL	elective	0			N	Y	Gram +ve cocci*
6	ALL	febrile neutropenia	33			N	N	
7	ALCL	febrile neutropenia	1	0	1	Y	Y	rhinovirus
8	ALL	elective	1	0	1	N	N	
9	ALL	relapse	18	11	7	Y	N	
10	post-transplant	post- transplant	253			N	N	
11	ALL	febrile neutropenia	2			Y	Y	rhinovirus
12	non-malignant haematology disorder	elective	0			N	N	
13	Non Hodgkin's lymphoma	elective	0	-3	3	Y	Y	
14	CNS tumour	febrile neutropenia	4			Y	Y	rhinovirus
15	ALL	febrile neutropenia	0			N	Y	rhinovirus

* blood culture

Table 5-1 Clinical details of patients involved in outbreak. This table summarises the clinical details, including the underlying diagnosis as well as other microorganisms isolated for patients 1-9 and 11-15. Patient 10 had a genetically different strain of HPIV3 and was therefore not included in the final analysis. There was only one fatality (patient 6), that was unrelated to infection with HPIV3. Negative numbers of days indicate that the patient became symptomatic before the admission when they were diagnosed for HPIV3. This does not exclude a potential nosocomial infection prior to this admission (see **Figure 5-8**). AD = admission date; SD = sample date; SOD = symptom onset date.

Although all patients involved were under some degree of immunosuppression due to their underlying condition or treatment, only one was post transplant. The most common underlying diagnosis (6/15) was acute lymphocytic leukemia (ALL) and other blood cancers such as Non Hodgkin's lymphoma, anaplastic large cell lymphoma (ALCL) and acute myeloid leukemia (AML) accounting for 3 more cases. There were four cases of CNS malignancy, one of a non-haematological malignancy and one post transplant. The most common cause of admission (8/14) was febrile neutropenia, which is defined as pyrexia with a low ($<0.5 \times 10^9$) neutrophil count (de Naurois *et al.*, 2010), the rest were either

routine admissions or admissions otherwise unrelated to infection: one relapse and one new diagnosis. The most common additional organism isolated was rhinovirus and this reflects the common occurrence of this virus within the paediatric patient cohort.

5.2.3 Phylogenetic analysis of the full genome sequence

In order to confirm whether this cluster of cases represented a point source outbreak and to determine the best method for molecular analysis, the epidemiology and evolution of HPIV3, in the context of strains circulating within the UK was assessed. To this end a phylogenetic tree of 20 full length HPIV3 clinical strains minimally passaged in PLC/PRF5 cells (see Table 3-2) and other full length genome sequences available from the Genbank was constructed using the Maximum Likelihood method (Figure 5-2). Please note three strains included in Table 3-2: I, D and 8 were obtained as part of the current outbreak investigation (see below) and were therefore not originally included in this part of the analysis.

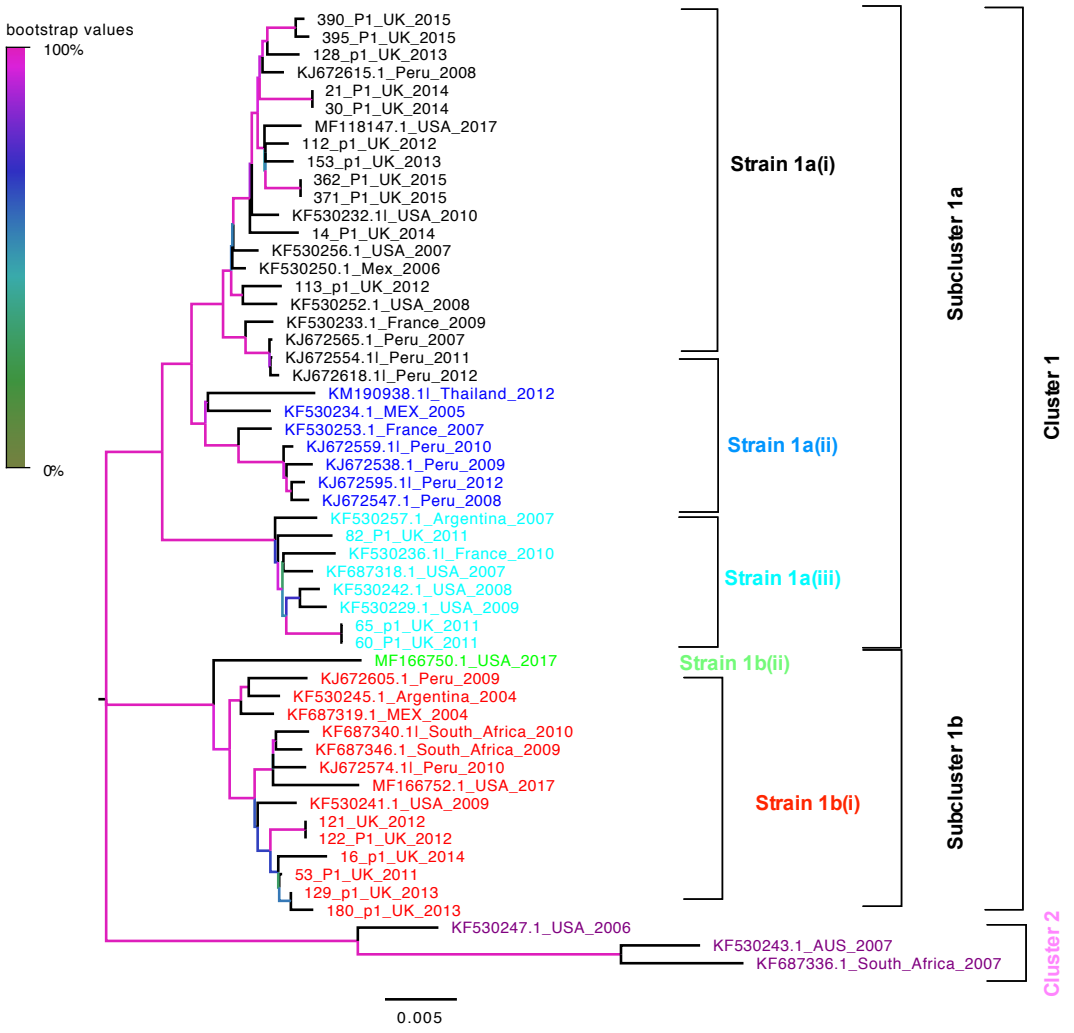

Figure 5-2 Molecular Phylogenetic analysis of HPIV3 full length genome by Maximum Likelihood method. The evolutionary history was inferred by using the Maximum Likelihood method based on the General Time Reversible + I + G model and 1000 bootstrap repetitions. The tree with the highest log likelihood (-42087.04) is shown. The tree is drawn to scale, with branch lengths measured in the number of substitutions per site. The analysis involved 56 nucleotide sequences. Evolutionary analyses were conducted in MEGA7. Clusters, subclusters and strains were identified using Automatic Barcode Gap Discovery and genetic distances of 0.043 (cluster); 0.02 (subcluster) and 0.015 (strain) were identified. All strains (and cluster 2) are coloured for ease of visualization and tracking (see **Figure 5-4** and **Figure 5-7**). Bootstrap values for each branch are colour coded as per the legend.

The automated barcode gap discovery analysis (ABGD) (Puillandre *et al.*, 2012) of the full genome sequences was used to define anything separated by more than a genetic distance of 0.043 as a cluster and 0.02 as a sub cluster. Using this method, 2 clusters were identified. Cluster 1 was further subdivided into

subclusters, 1a and 1b, with smaller subdivisions into strains, as shown in Figure 5-2. It is of note that apart from strain 1b(ii) that currently only contains one sequenced strain from the USA (2017) no temporal or geographical correlation between strains was observed. The rate of substitution/site/year has been calculated to be 4.2 $x10^{-4}$ subs/site/year using an uncorrelated relaxed clock (Drummond *et al.*, 2006), General Time Reversible model (GTR) with gamma distributed rate and invariant sites (GTR + I + G) (Tavaré, 1986; Yang, 1994; Ferreira and Suchard, 2008) and an MCMC length of 600 million, using BEASTv1.8.4 as described in Materials and Methods. This is consistent with rates observed for other RNA viruses (Jenkins *et al.*, 2002; Figlerowicz *et al.*, 2003; Sanjuán *et al.*, 2010; Tan *et al.*, 2013). The average variability across the strains available was calculated using MEGA7 (Kumar, Stecher and Tamura, 2016) and found to be 2%.

5.2.4 Analysis of variability along the genome can be used to identify a hypervariable region in HPIV3

Full genome sequencing, particularly in the context of diagnositic laboratories can be expensive and time consuming. In the current project, as previously discussed, whole genome amplification directly from clinical sample was unsuccessful and growth in immortalised cell culture yielded a very low success rate (approximately 10% at passage 1, Figure 3-12). To this end a smaller region for epidemiological and phylogenetic analysis was identified by calculating relative evolutionary rates along the HPIV3 genome (Figure 5-3).

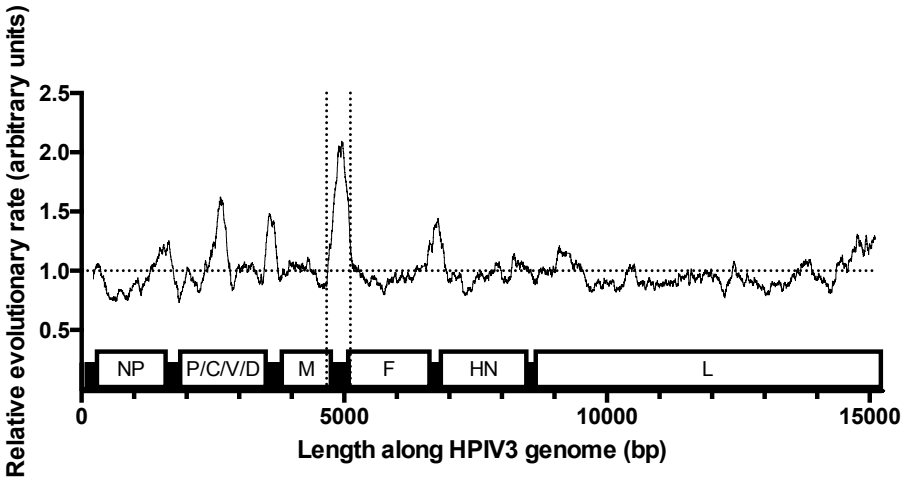

Figure 5-3 Relative site by site evolutionary rate of the HPIV3 genome. Mean (relative) evolutionary rate are shown for each site next to the site number with a window of 200. These rates are scaled such that the average evolutonary rate across all sites is 1. This means that sites showing a rate < 1 are evolving slower than average, and those with a rate > 1 are evolving faster than average. These relative rates were estimated under the GTR + I + G model. The analysis involved 56 nucleotide sequences. The position along the HPIV3 genome is shown on the x axis with the hypervariable region identified between positions 4703 to 5160. Evolutionary analyses were conducted in MEGA version 7.

The site by site relative evolutionary rate was calculated using the GTR + I= G model (Tavaré, 1986; Yang, 1994; Ferreira and Suchard, 2008) of substitution with 1000 bootstrap repetitions. A peak in evolutionary rate in the non-coding region between the M gene and the F gene was observed. For the purpose of this study this hypervariable region has been defined as a region of 457 base pairs in length from position 4703 to 5160 as shown in Figure 5-3.

5.2.5 Analysis of the hypervariable region reflects the phylogenetic profile of HPIV3.

The suitability of the hypervariable region for phylogenetic analysis was then evaluated by constructing a phylogenetic tree and comparing it to the one obtained by using full genome sequences (Figure 5-2). The BEAST (Drummond *et al.*, 2012) evolutionary tree for the hypervariable region can be seen in Figure

5-4. The rate of substitution for this region was calculated to be $1x10^{-3}$ subs/site/year with an average variability of 5%. This is markedly above the values calculated for the full genome sequence. Hence ABGD analysis (Puillandre *et al.*, 2012) was used to separate the sequences into subclusters corresponding to strains in the full genome analysis with potential for finer classification for the purposes of epidemiology. The corresponding classifications are summarized in Table 5-2.

Subdivisions identified by ABGD analysis of				
Whole genome			Hypervariable region	
Cluster	Subcluster	Strain	Cluster	Subcluster
1	1a	1a(i)	1	A
		1a(ii)		B
		1a(iii)		C
	1b	1b(i)		D
		1b(ii)		E
2			2	

Table 5-2 Subdivisions identified by ABGD analysis of whole genome sequences of HPIV3 and hypervariable region of HPIV3. The corresponding subdivisions into clusters, subclusters and strains, identified by Automatic Barcode Gap Discovery (ABGD) for whole genome sequences (**Figure 5-2**) and the hypervariable region of HPIV3 (**Figure 5-4**) are summarized. These are coloured according to the scheme used in (**Figure 5-2** and **Figure 5-4**) for ease of visualization.

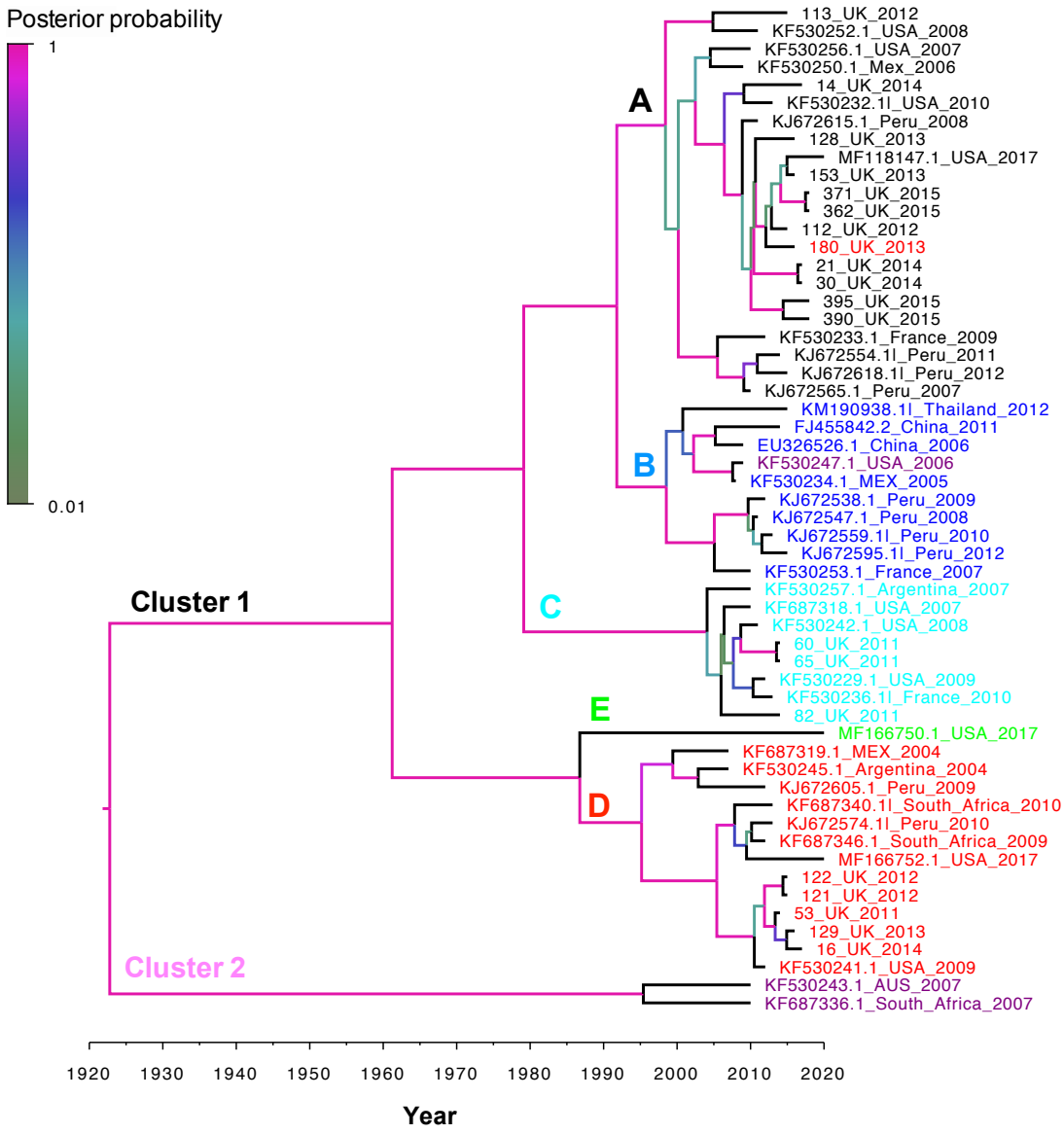

Figure 5-4 Molecular phylogenetic analysis of the HPIV3 hypervariable region using Bayesian Phylogenetics with BEAST. The evolutionary history was inferred by using Bayesian Phylogenetics based on the TRN +I model using BEAST v1.8.4. The tree with the highest log likelihood (-2020.47) using path sampling and stepping stone analysis is shown. A strict clock and a constant coalescent prior were used. The MCMC length was 10,000,000. Convergence was assessed with Tracer and the maximum clade credibility tree was generated with Tree Annotator. Dates of strain emergence (in years) are shown in the figure legend All branches are colour coded by the posterior probability as per colour legend in the figure. Automatic Barcode Gap Discovery was used to analyse genetic distances and 0.1 (cluster) and 0.04 (subcluster) were defined. Subclusters A-E are shown next to their respective branches. All strains and cluster and subcluster labels are coloured identically to the phylogenetic analysis using full genome (**Figure 5-2**) to demonstrate near identical clustering patterns.

It is of note that only two strains were not classified in the same manner by both the full genome (Figure 5-2) and hypervariable (Figure 5-4) analysis methods. Strain 180 has moved from strain 1b in Figure 5-2 to subcluster A in Figure 5-4 (see Table 5-2 for corresponding subdivisions) and strain KF530247.1 (USA2006) was noted to have moved from cluster 2 to cluster 1. It was found that strain 180 contained 3.7% ambiguous bases within its hypervariable region (0.9% R; 2.6% Y; 0.1% W). This falls just below the definition of a subcluster (genetic distance of 0.04) and would potentially place this sample into two subclusters depending on the alignment. Strain KF530247.1, on the other hand contains no ambiguities and therefore the migration between clusters cannot be explained this way. It has, however been identified as a potentially recombinant sequence in a previous study (Košutić-Gulija *et al.*, 2017). Additionally, we observed that strain 1b(ii) (MF166750.1 (USA2017)) that has been identified as an emergent strain by full genome analysis (Figure 5-2), can now be defined as a subcluster in its own right, supporting the hypothesis that this may form a new emergent strain and subsequently subcluster of HPIV3 (Figure 5-4).

5.2.6 Primer design for the amplification of the hypervariable region of HPIV3

I have demonstrated that salient phylogenetic and epidemiological analysis can be performed on a short hypervariable region of the HPIV3 genome. Although an overlapping region has been used previously for outbreak monitoring, it was a shorter segment of 244 bases, positions 4880 to 5124 (Zambon *et al.*, 1998; Jalal *et al.*, 2007). This approach would place the primer sites within the hypervariable region itself (defined here as position 4703 to 5160, Figure 5-3), potentially limiting amplification success rate. In the current analysis, the region identified was flanked by two regions of reduced variability, creating ideal locations for primer localisation (Figure 5-3). Therefore two nested sets of primers flanking this region were designed (Table 5-3).

		Sequence	Position (bp)	Product size (bp)
Primer set 1	Forward	CAAGAGTRGATGCAATTTTCCAACC	4182-5535	1353
	Reverse	GTTGACYARTACACCTACATGCTG		
Primer set 2	Forward	GGGCYTCATCAGTAGAGATYA	4703-5160	457
	Reverse	GCACTGCYTTRTTTGTGTCC		
Fragment used for phylogenetics			4753-5108	355

Table 5-3 Nested primer sets used for amplification of the HPIV3 hypervariable region. Sequences, relative positions and product sizes of two primer sets for nested amplification of the HPIV3 hypervariable region are summarized. The fragment used for phylogenetics has been cropped to allow for poor sequence quality adjacent to the primer sites.

5.2.7 Sequencing and alignment

The amplicons were subsequently sequenced by Sanger sequencing and the contigs were assembled to a reference genome using Sequencher 5.4 from Genecodes (https://www.genecodes.com). For HPIV3, a consensus sequence of the hypervariable region was extracted using alignments with the Muscle algorithm with UGENE (Okonechnikov, Golosova and Fursov, 2012). It was subsequently trimmed by 50bp and 52bp at the 3′ and 5′ prime ends respectively. The resulting fragment had good quality coverage in both directions and was therefore deemed to be suitable for further phylogenetic analysis. For rhinovirus, the alignments were done to the consensus sequence of published rhinovirus sequences KX610685; KY131965; KY645964; MF422576; MF422577; MF422578; MF422580; MF422581, as described previously (W. Wang *et al.*, 2015). The consensus was extracted as described above.

5.2.8 Phylogenetic analysis of the outbreak

In order to identify whether the cases on the paediatric oncology ward represented a point source outbreak or were merely a reflection of the circulating community strains at that point in time, 30 cases were selected for molecular analysis, where 15 constituted the suspected outbreak (Table 5-1) and 15 were control cases unrelated to the outbreak. The pertinent clinical information for all cases is summarized in Figure 5-5A and B. All patients involved in the outbreak were coded 1-15. These were all paediatric patients on the oncology unit. Samples obtained for background phylogenetic information were coded A-O. These were drawn from a wider demographic in terms of age

(range 7 months – 92 years), geographical location and immunosuppression status. It is of note that among the unrelated cases, the majority of patients (9/15) were not known to be either immunocompromised or immunosuppressed.

A. Sample dates of patients involved in outbreak

Lab ID	sample date
1	15-May
2	24-May
3	20-Jun
4	24-Jun
5	28-Jun
6	01-Jul
7	04-Jul
8	05-Jul
9	01-Jul
10	12-Jul
11	13-Jul
12	14-Jul
13	16-Jul
14	31-Jul
15	13-Aug

B. Sample dates and demographics of patients involved in outbreak

Lab ID	age (years)	Immunocompetent ?	sample date
A	67	Y	18-May
B	48	N	26-May
C*	7 months	unknown	24-Jun
D	21	N	26-Jun
E	74	Y	28-Jun
F	69	N	01-Jul
G	30	Y	05-Jul
H	35	Y	06-Jul
I	38	Y	08-Jul
J	92	Y	12-Jul
K*	1	unknown	13-Jul
L	70	N	14-Jul
M	53	Y	19-Jul
N	69	Y	31-Jul
O*	86	Y	13-Aug

* originated in the wider geographical area covered by the diagnostic laboratory

C. Molecular phylogenetic analysis of outbreak (1-15) and background (A-O) cases

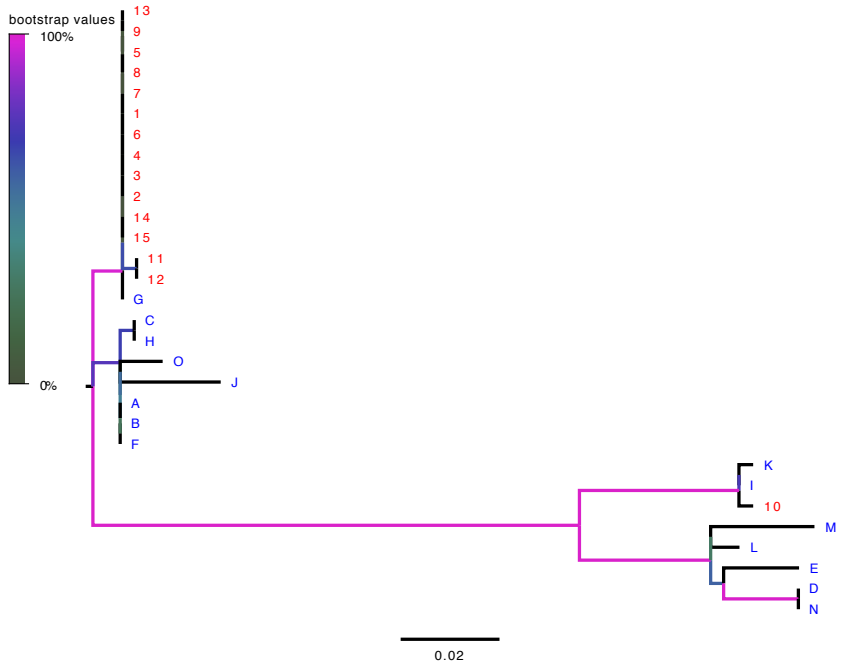

Figure 5-5 Outbreak (1-15) and non-outbreak (A-O) sample details and molecular phylogenetic analysis by Maximum Likelihood Method. Panel A summarises the dates of first HPIV3 positive samples for all patients (1-15 in red) involved in the outbreak. Demographics of patients not involved in the outbreak (A-O in blue) are shown in panel B, those marked with an asterix originated in the wider geographical area rather than at the index teaching hospital. Panel C shows the molecular phylogenetic analysis of all samples. The evolutionary history was inferred using the Maximum Likelihood method based on the Tamura-Nei + I model with 1000 bootstrap repetitions. Branches are colour coded by their respective bootstrap values as per the colour legend. The tree is drawn to scale, with branch lengths measured in the number of substitutions per site with the legend shown. There were a total of 351 positions in the final dataset. Evolutionary analyses were conducted in MEGA version 7.

The maximum likelihood tree was constructed using the Tamura-Nei model with invariant sites (Tamura and Nei, 1993) (Figure 5-5C) using MEGA version 7 (Kumar, Stecher and Tamura, 2016), as detailed in Materials and Methods. Phylogenetic analysis indicated that 12/15 outbreak strains were genetically identical, with strains 11 and 12 differing from the rest of the cohort by one nucleotide, A182C. For confirmation, strains 11 and 12 were sequenced twice to exclude sequencing errors. Background strain G was shown to be identical to the outbreak strain. This confirmed that this strain was circulating in the community rather than being unique to this outbreak. Outbreak sample 10 was seen to cluster separately from other cases involved in the outbreak. This was consistent with the clinical history of patient 10, who had been an inpatient for a number of months prior to this incident and has had no points of contact with any of the other cases (Table 5-1). Other non-related strains were shown to form two separate clusters, one being closely related to the outbreak strains (approximately 98% conformity with the outbreak strain) and the other more distinct (approximately 87% conformity with the outbreak strain).

As rhinovirus was identified as a common secondary pathogen (6/15 cases), genotyping of rhinovirus was attempted using an established protocol (W. Wang *et al.*, 2015). To this end the VP4/VP2 part of the rhinovirus genome sequence was amplified and aligned successfully for patients 7,11 and 3. All strains of the virus were found to be different and therefore no evidence of dual infection transmission was found in these cases.

5.2.9 Phylogenetic analysis in the context of other strains of HPIV3

Having confirmed a point-source outbreak, the sequences obtained were analyzed in the context of other historically circulating strains to establish whether the outbreak was caused by a newly emerging strain. To this end a Bayesian phylogenetic tree including the hypervariable region from the 30 strains identified above, as well as the 56 strains used for primer design, as detailed in Materials and Methods, was constructed using BEAST v1.8.4 (Figure 5-6). This analysis confirmed a point source outbreak and served to illustrate that the outbreak strain was closely related to USA strain MF166750 (2017),

which was identified as a potential emerging strain (Figure 5-2 and Figure 5-4). 7/15 of strains (A, B, C, F, H, O, J) not involved in the outbreak were shown to be closely related to the outbreak strain. The remaining 7 background strains and outbreak strain 10 were found in subclusters 1A (L,M,N,D.and E) and 1C (K, I and 10) and demonstrate the diversity of HPIV3 strains circulating within a given time period (Figure 5-6). Additionally outbreak strain 8 and two background strains (I and D) were grown in HAE cells as described in Materials and Methods and full sequences of these were obtained. These were then added to the phylogenetic analysis conducted above (Figure 5-2). The results are shown in Figure 5-7 and clearly show that the three strains in question were classified in the same manner by using both the full length genome (Figure 5-2) as well as the hypervariable region (Figure 5-4 and Figure 5-6).

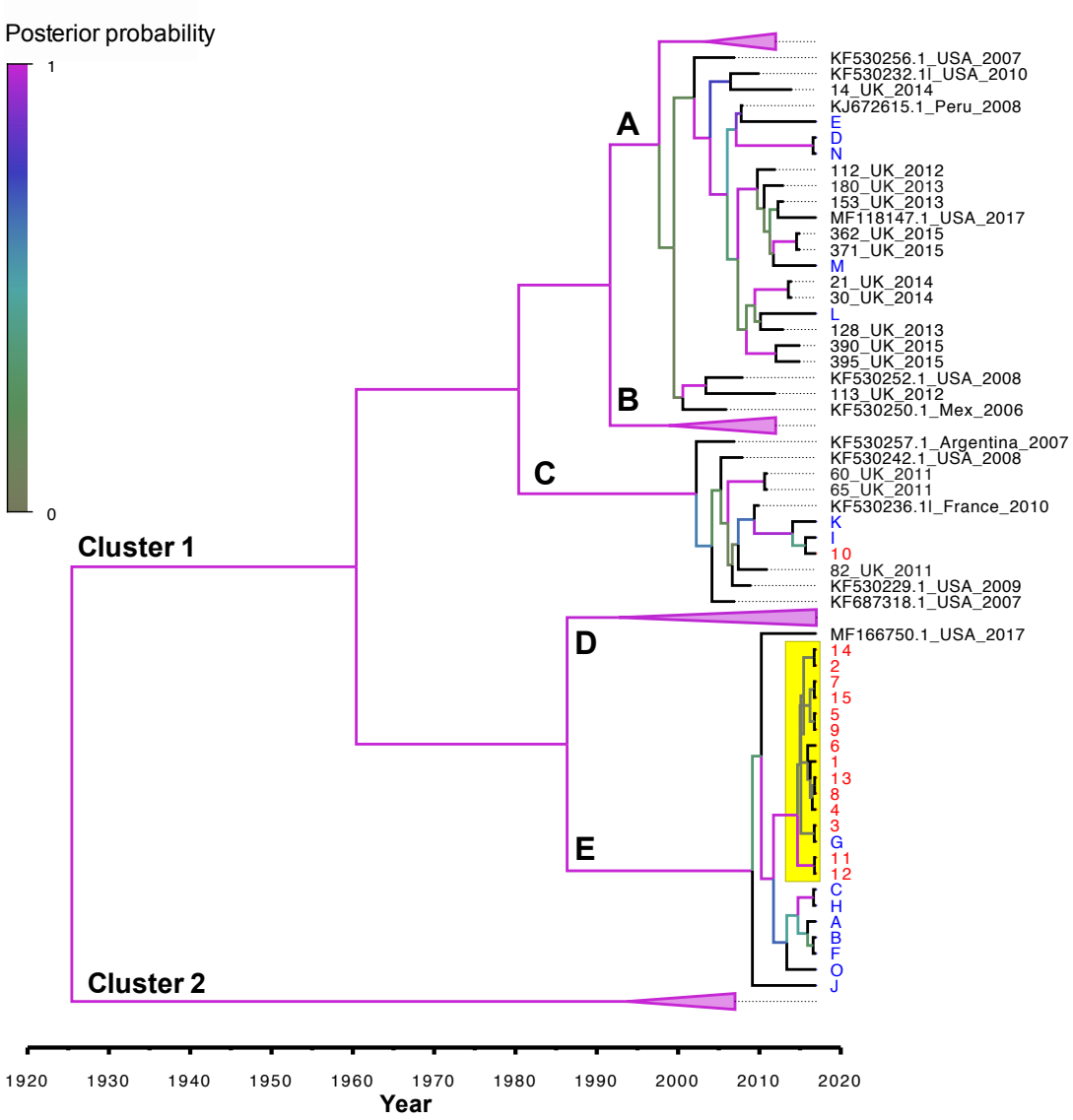

Figure 5-6 Molecular analysis of outbreak (1-15 in red) and non-outbreak (A-O in blue) strains in the context of historically circulating strains of HPIV3. The evolutionary history was inferred using Bayesian Phylogenetics based on the Tamura-Nei + I model using BEAST v1.8.4 with a strict clock and constant coalescent prior. The MCMC length was 10,000,000. Convergence was assessed with Tracer (effective sample size >200). Inferred dates of strain emergence (in years) are shown in the figure legend. All branches are coloured by their posterior probability as per the colour legend. Clusters were defined with Automatic Barcode Gap Discovery. Cluster 2, subclusters B and D and a part of cluster A have been collapsed for ease of visualization. All outbreak strains (1-15) are outlined in red and all background non-outbreak strain (A-O) in blue. The outbreak cluster is highlighted in yellow.

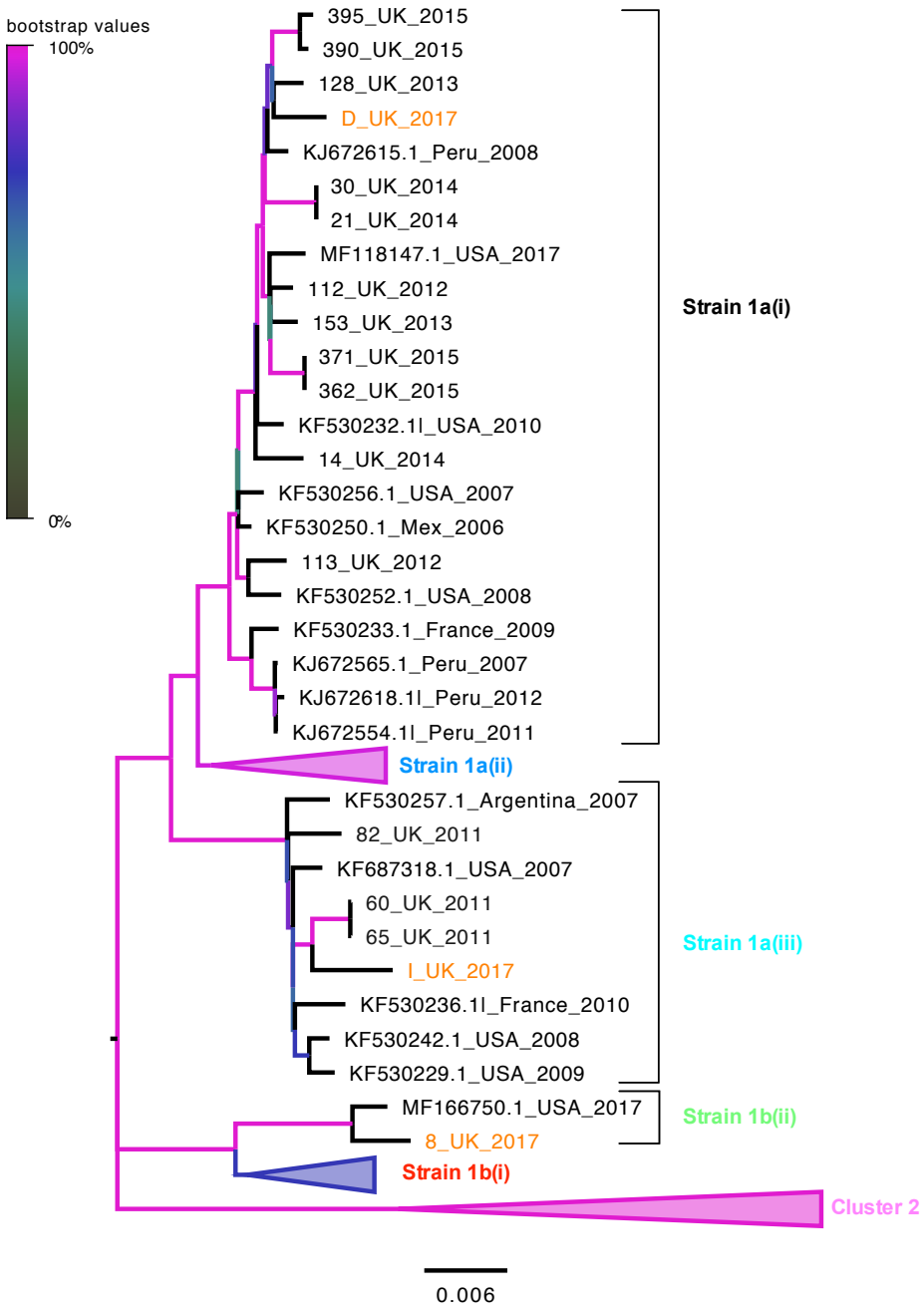

Figure 5-7 Molecular analysis of outbreak strain 8 and two background strains (I and D) in the context of other full genome sequences of HPIV3. The evolutionary history was inferred by using the Maximum Likelihood method based on the GTR + I + G model and 1000 bootstrap repetitions. The tree with the highest log likelihood (-43462.08) is shown. The tree is drawn to scale, with branch lengths measured in the number of substitutions per site. The analysis involved 59 nucleotide sequences. Evolutionary analyses were conducted in MEGA version 7. Cluster 2, and strains 1a(ii) and 1b(i) have been collapsed for ease of visualization. Clinical strains 8, I and D are shown in orange; subdivisions into strains and clusters are coloured according to the scheme used in **Figure 5-2** and **Figure 5-4** to illustrate identical clustering of these strains using both full genome and hypervariable region data. All branches are coloured according to their bootstrap values as per the colour legend.

5.2.10 Epidemiological analysis – timeline

After identifying the cluster as a point source outbreak the potential transmission routes between patients were investigated. First an attempt was made to identify the overlap of patients in space and time, to this end a timeline was constructed based on admission dates, symptom onset and first positive sample date for the patients involved (Figure 5-8A). This clearly demonstrated a significant temporal overlap between patients involved in the outbreak as well as potential delays between symptom onset and a sample being taken, where available (8/15 cases). The number of cumulative new cases at the end of each week is shown in Figure 5-8B, together with the date when the outbreak was suspected. It is clear that the outbreak was declared as the number of cases was already on the decline and therefore the window for meaningful intervention had passed.

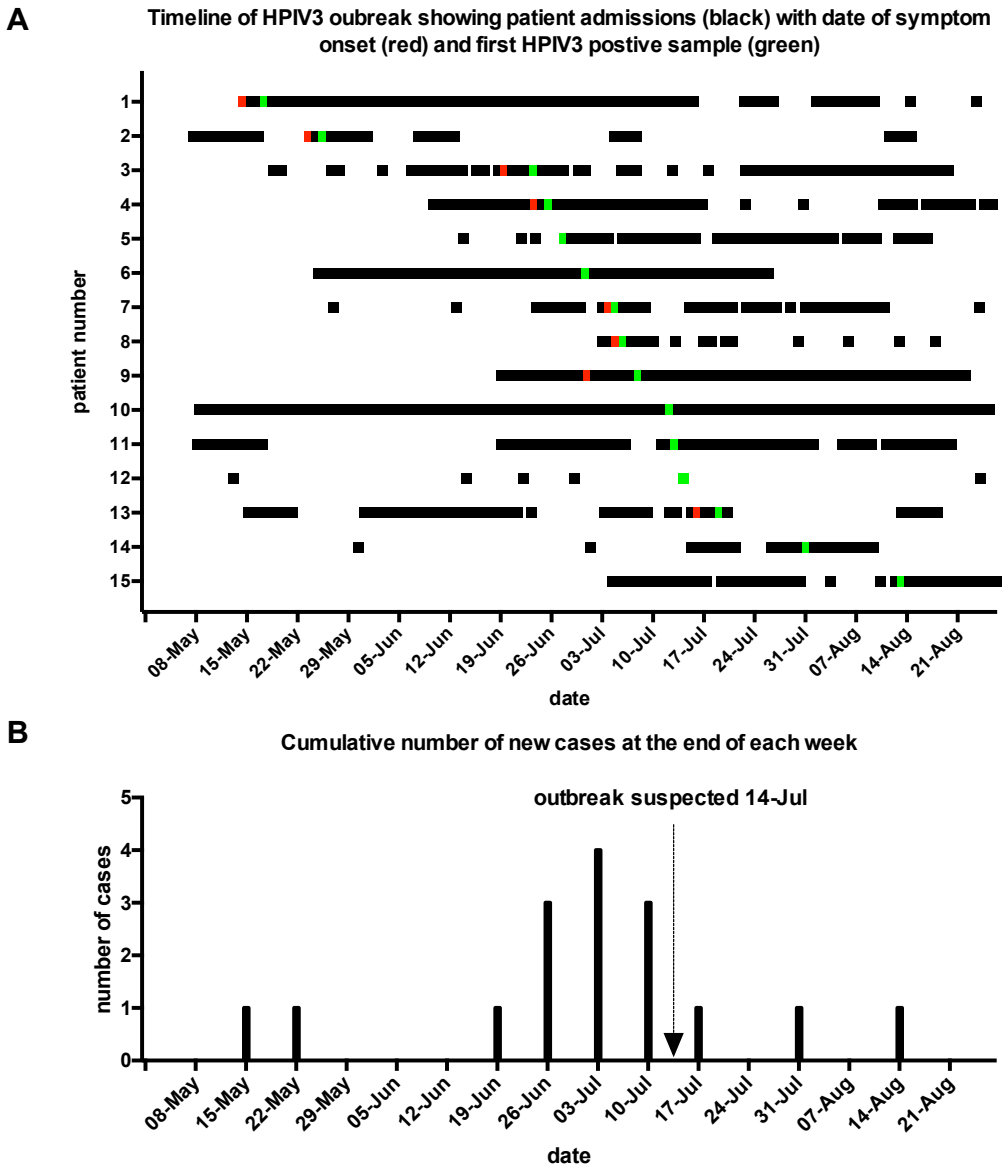

Figure 5-8 Timeline of patients' admissions to the hospital including the date (A) and cumulative number of new cases of HPIV3 at the end of each week (B) during May-August 2017. Panel A shows the movements in and out of hospital of 15 patients (coded 1-15 on the y axis) involved in the outbreak during the period encompassing a week before the first confirmed positive sample (15 May; patient 1) and until two weeks after the resolution of the outbreak in the end of August (last positive sample date 13 August; patient 15). Corresponding dates are shown on the x axis. Patient's inpatient admissions are shown in black. Where a day visit was recorded in the notes, it is reflected as an admission of 1 day on the timeline. Symptom onset dates, if available, are shown in red. Dates of confirmed positive samples are shown in green. Panel B shows the cumulative number of new cases of HPIV3 at the end of each week for the same period. The date that the outbreak was recognized (14 July) is marked with an arrow.

5.2.11 Epidemiological analysis – transmission

In order to map the potential transmission of infection, further data including the exact patient location, was then extracted and summarized in SQL together with the defined periods of potential susceptibility (1-7 days prior to symptom onset, as defined by PHE England (Couch R. B. and Englund Janet A., 1997; Zambon *et al.*, 1998; Englund, 2001) infectivity (4 days prior to symptom onset and for the duration of the outbreak (Piralla *et al.*, 2009)) and phylogenetic plausibility. Based on molecular data, Patient 10 was identified as not being part of the outbreak. Patients 11 and 12, that had a strain that differed by one identical nucleotide from the main outbreak strain, remained as part of the outbreak. This was because the possibility of an original infection by the main outbreak strain or the acquisition of their unique strain from another patient could not be excluded. It was however considered impossible for them to infect another patient with a strain that lacked this unique nucleotide difference.

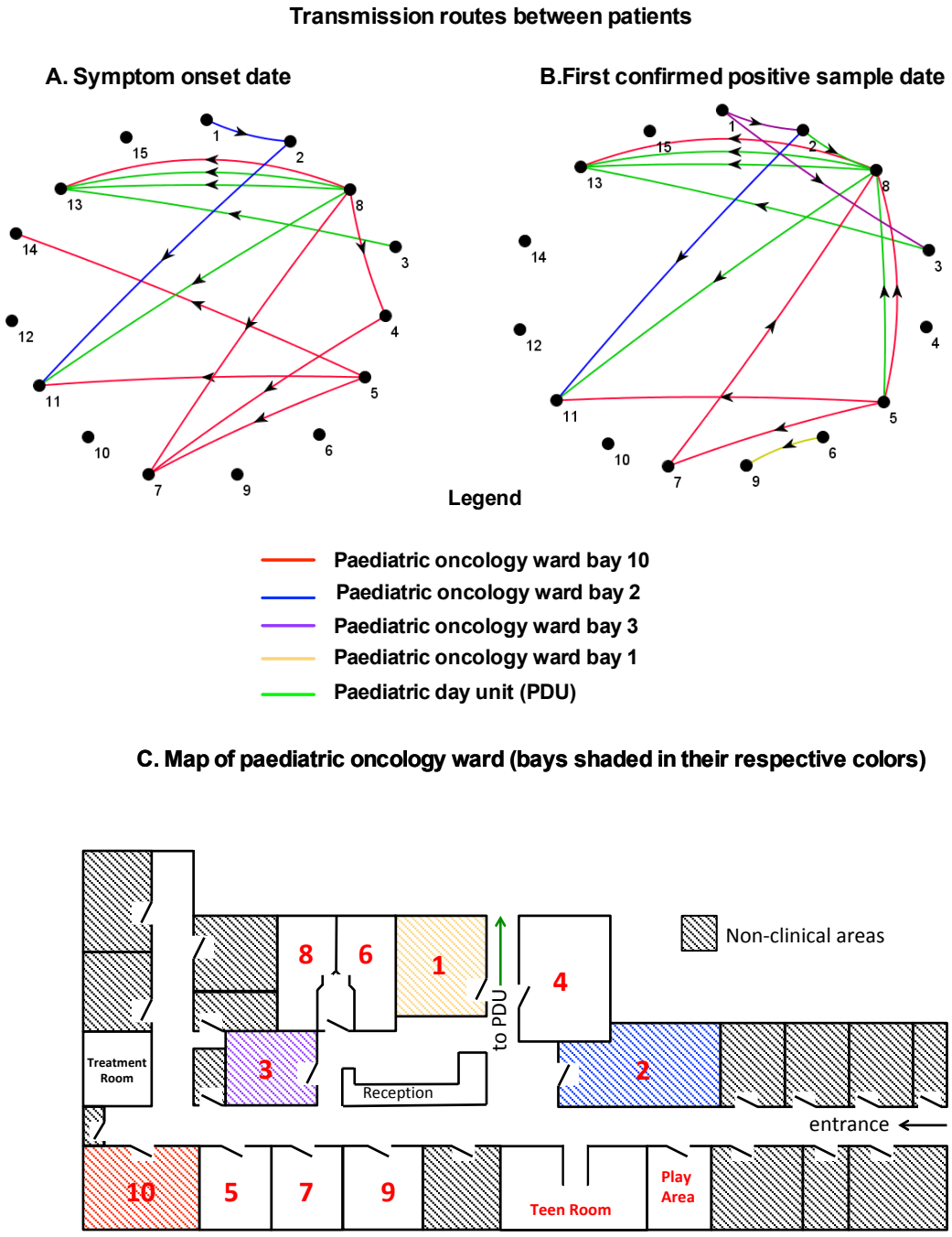

Figure 5-9 Inferred infection transmission routes between patients. Transmission routes between patients were analysed with SQL and visualized using KNIME 3.3.2. Patient location, as well as symptom onset date where available (A) and first positive HPIV3 sample date (B) were used. All phylogenetically implausible connections have been removed. The connectors between patients are colour coded according to patient location as shown in the legend and the direction of the arrow conforms to the direction of infection spread. The map of the unit with locations shaded in corresponding colours is shown in panel C (bays were numbers arbitrarily 1-10).

KNIME visualization for potential transmissions using the date of symptom onset and confirmed HPIV3 positive sample is summarized in Figure 5-9. KNIME analysis by symptom onset date (Figure 5-9A) has identified 12 phylogenetically plausible transmission events, linking 10/14 patients involved in the outbreak, and identifying a potential source of infection in 6/14 cases. Analysis by first positive sample date (Figure 5-9B) identified 15 phylogenetically plausible transmission events, linking 10/14 patients and identifying a potential source of infection in 7/14 patients. It is interesting to note that although these highly complex patients were periodically admitted onto a number of different wards, the paediatric oncology unit (ward and day unit) were the main hotspots for transmission. It is also of interest that despite extensive data mining and the flexibility of the model, we were unable to identify a clear chain of infection from the index case connecting all the patients. This indicates that an external source of infection, that has not been accounted for within the model, was involved.

5.3 Discussion

Outbreaks of respiratory viral infections are common causes of ward closures causing disruption as well as increased cost to the National Health Service (NHS) (Elliot, Cross and Fleming, 2008). These are statistically more common on paediatric wards (Chow and Mermel, 2017). This is due to a combination of factors: first and foremost children are at increased risk of infection due to immature immune systems (Maddux and Douglas, 2015; Simon, Hollander and McMichael, 2015). Additionally, many unique transmission routes including toys, eyes, aerosolisation of droplets and increased socializing that is normally encouraged on children's wards should be taken into account (Koutlakis-Barron and Hayden, 2016). HPIV3 has in turn been described as both a prevalent (Torres *et al.*, 2016) and a rare (Meidani and Mirmohammad Sadeghi, 2018) cause of nosocomial respiratory infection outbreaks on paediatric wards with additional conflicting evidence as to the potential impact in the immunocompromised paediatric cohort (Ustun *et al.*, 2012; Santolaya *et al.*, 2017). In this chapter, I discuss one such outbreak that took place in the summer of 2017. As with most outbreaks in literature, this was identified retrospectively (Liao *et al.*, 2017). One could argue that increased vigilance would allow these

outbreaks to be identified contemporaneously with potential timely intervention. However this requires a good understanding of epidemiological trends, communication between health care teams and increased vigilance.

The outbreak was originally identified by reviewing annual trends of HPIV3 on the paediatric ward in question. This allowed to pinpoint an unusual increase in the number of cases occurring on the ward between May and July 2017. In order to determine whether this peak was due to the nosocomial transmission of a single strain, sequence analysis of the respiratory samples was performed. Although rapid metagenomic sequencing has been conducted previously in a small HPIV3 outbreak (Greninger *et al.*, 2017), sequencing directly from sample is normally costly and time consuming, especially in a clinical setting. Therefore, in literature, regions of the genome are typically used to determine whether the outbreak represents a point source outbreak (Jalal *et al.*, 2007; Kiang *et al.*, 2007; Piralla *et al.*, 2009; Baier *et al.*, 2018). The most common approach to HPIV3 investigations has previously been the amplification of the HN coding region of the genome (Piralla *et al.*, 2009). As this part of the genome is considered to be an important antigenic site (Van *et al.*, 1987), it has been surmised that this region of the genome would show the greatest variation. This is also consistent with previous phylogenetic analysis of HPIV3, that relied solely on the HN sequence (Almajhdi, Alshaman and Amer, 2012; Shi *et al.*, 2015; Košutić-Gulija *et al.*, 2017). An alternative approach that has previously been used was to concentrate on a small region at the beginning and immediately preceding of the F coding region (Zambon *et al.*, 1998; Jalal *et al.*, 2007) that has previously been identified as having high variability (Storey *et al.*, 1987).

In order to approach the selection of the region for epidemiological studies in a more systematic way, in this project, the evolutionary rate of HPIV3 along the entire length of the genome was examined and a hypervariable region located within the intergenic region between M and F was identified. The suitability of this region for phylogenetic analysis was examined by comparing the clustering achieved with whole genome sequences and that using only the hypervariable region. To this end whole genome sequences from this project were combined with others obtained from Genbank and a Maximum Likelihood phylogenetic tree of the resulting 56 sequences was generated as described in the Materials

and Methods. All duplicate and highly similar sequences as well as significantly culture adapted strains were excluded leaving 56 unique sequences. Consequently only two clusters, as opposed to three previously identified in literature (Mao *et al.*, 2012; Almajhdi, 2015; Košutić-Gulija *et al.*, 2017) were observed. This was most likely due to the exclusion of strains from the middle of last century that are known to be heavily culture adapted and have therefore not been included in this analysis. Automatic Barcode Gap Discovery (ABGD) was used to separate the sequences into clusters, subclusters and strains (Puillandre *et al.*, 2012). This method has previously been used in literature to classify HPIV3 sequences (Mao *et al.*, 2012; Košutić-Gulija *et al.*, 2017) and is generally considered to be one of the best options for classification of organisms, where the correlation between genotype and phenotype has not been established (Kekkonen *et al.*, 2015). It does, however, rely purely on sequence similarity and therefore the correlation between strain classification and phenotype *in vivo* may be poor (Kekkonen *et al.*, 2015). More information on the clinical impact of HPIV3 and correlation to genotype would allow for a more informed classification concentrating on the parts of the genome with the highest impact on *in vivo* phenotype, such as has previously been carried out for RSV (Sullender, 2000).

The approach adapted in this thesis, where the region of highest variability is identified and the phylogenetic classification is then compared to the results achieved with whole genome sequences, is significantly different from those adapted in previous studies (Jalal *et al.*, 2007; Almajhdi, Alshaman and Amer, 2012; Goya, Mistchenko and Viegas, 2016), where only a fragment of the genome was analysed. One study compared the phylogenetic analysis of the HN coding region of the genome and the F coding region of the genome (Košutić-Gulija *et al.*, 2017), coming to the conclusion that either region of the genome could be used for phylogenetic classification. Additionally strain KF530247.1 was identified as a potential recombinant strain, which was in agreement with the results obtained here. However the hypervariable region identified in this thesis was significantly smaller (457bp) than the HN (1795bp) and F coding regions of HPIV3 (1850bp), which increases the likelihood of successful amplification

directly from sample as well as the efficiency and rapidity of phylogenetic analysis.

However a number of drawbacks inherent in this method should be considered. The region identified shows the highest variability within the HPIV3 genome. The rate of substitution calculated for the entire HPIV3 genome was $4.2x10^{-4}$ subs/site/year and this is consistent with other RNA viruses (Jenkins *et al.*, 2002; Sanjuán *et al.*, 2010). A faster substitution rate of $1x10^{-3}$ subs/site/year was calculated for the hypervariable region. This implies that new emerging strains could be identified earlier when analyzing only the hypervariable region, as exemplified by outbreak strains 11 and 12 that differed from the other outbreak strains by a single mutation (A182C). Although this serves as a more sensitive system, it may nonetheless be less specific, as the significance of a single mutation within the hypervariable region would be difficult to interpret in the context of the entire genome, although this does constitute a very sensitive system for outbreak tracing. Equally, as no correlation with *in vivo* phenotype has been established, a mutation within that region may have profound consequences for the behaviour of this strain *in vivo*. It is also important to note that the M-F intergenic region has been identified as a significant area both for plaque phenotype *in vitro* and culture adaptation, as previously discussed. Therefore this segment of the HPIV3 genome should be investigated further in terms of its correlation with *in vivo* and *in vitro* phenotype and implications for viral evolution. This would provide a different approach to studies that tend to center on specific HPIV3 proteins (Lamb, Paterson and Jardetzky, 2006; Battisti *et al.*, 2012; Dirr *et al.*, 2015) for the phylogenetic analysis of HPIV3.

Using the method described above, the cluster of HPIV3 cases on the paediatric oncology ward was therefore confirmed as a point-source outbreak. The clinical and infection control implications of this can be approached logically by analyzing potential preventative measures, early identification and isolation of cases as well as early recognition of nosocomial transmission and outbreak. One could also argue that an outbreak that has been identified post factum has failed on all of these accounts. Therefore each of these points should be addressed separately in the current context.

Preventative measures during seasonal peaks have previously been described for viruses such as RSV (Baier *et al.*, 2018), however the evidence base for their utility has been called into question (Beuvink, 2018). Measures such as healthcare workers wearing masks, limiting the number of visitors, particularly siblings, limiting the amount of social interaction on the ward and twice weekly screening for respiratory viruses have been proposed (Baier *et al.*, 2018). Some of these measures, particularly visitor restrictions, good hand washing practices and cough etiquette are well established (Beuvink, 2018). However others, such as limiting social interaction and play areas on wards as well as restricting sibling contact would most likely have a deleterious effect on the psychological wellbeing of the patients (Baier *et al.*, 2018) with questionable infection control benefits overall (Beuvink, 2018). However, in the current project, it is clear that there has been a breakdown in the preventative measures of infection control. The transmission analysis could not successfully be used to determine the chain of infection spread and it could therefore be surmised that either another source of infection or other points of contact between patients were present.

Cases of health care workers contributing to nosocomial outbreaks are well documented (Aitken and Jeffries, 2001; Goins, Talbot and Talbot, 2011; Danzmann *et al.*, 2013; Kim *et al.*, 2017) and cannot be excluded by the current analysis. Therefore, in order to address this point, measures such as staff screening and personal protective equipment for staff in areas, where patients are at an increased risk of hospital acquired infections, should be discussed both with the clinical and infection control teams.

Measures that ensure rapid identification and isolation of potentially infectious cases are also well established, especially on wards for immunosuppressed patients (Beuvink, 2018). However in the context of nosocomial outbreaks, symptom onset data is frequently not available and the date of first positive sample is used for all epidemiological modeling (Piralla *et al.*, 2009; Berrueco *et al.*, 2013). Although sufficient for outbreak tracing, this can potentially underestimate the impact of early symptom identification and prompt screening on outbreak prevention. To this end, this data, together with data on patient admission was collected where possible (Figure 5-8). Subsequently, transmission models involving both dates, if available, were included in this

study (Figure 5-9). Twelve transmission events, linking 10 patients were identified using the symptom onset date, whereas 15 potential transmission events were identified by the model using the positive sample date. It is important to note that data on symptom onset was only available in 8 out of 14 cases involved in the outbreak and this was further confounded by secondary infections (Table 5-1). Overall within the limitations of the data available, the current analysis identified 3 potential transmission events and 1 potential infection that could have been prevented if screening were carried out when symptoms were first identified. One could argue that this could be addressed by increasing awareness and more specific definitions of what constitutes a symptomatic individual among health care workers. However within the constraints of ward designs and lack of isolation rooms and facilities, patients are frequently prioritized by severity of symptoms. In this case, the onus falls back on good infection control practices and the fine balance between the pros and cons of limiting contact between patients (Koutlakis-Barron and Hayden, 2016; Baier *et al.*, 2018).

In the case where both of the above stages have failed and a nosocomial transmission does occur, the outbreak could be identified at an earlier stage by ensuring a greater awareness of a rising number of cases and integration of information across different clinical teams. In the current study, the correlation of an increased number of cases within space and time was masked by the seasonality of HPIV3. Seasonal bias is a well-recognized confounder in public health reporting and failures to identify outbreaks have previously been described in viral diseases with a strong seasonal bias (Pelecanos, Ryan and Gatton, 2010; Li *et al.*, 2012). Usually it is overcome by an outbreak surveillance system that takes into account information on the background level of virus activity (Enki *et al.*, 2016). There are a number of complex algorithms that are employed for this purpose for country wide surveillance (Enki *et al.*, 2016; Liao *et al.*, 2017; Wang *et al.*, 2018). These methods are usually not employed on a smaller scale in hospitals and therefore integration of information between the clinical team, infection control and the laboratory-based team is crucial. In order to address this in the future, a simple graphical interface that allows the visualization of trends of cases due to a particular microorganism within a

specific location has been introduced. This is not the first time that such a system has been proposed and although this is a step in the right direction, there is currently no clear evidence that this would have a significant impact on early detection of hospital outbreaks (Leclère *et al.*, 2017).

The clinical impact of this outbreak is difficult to assess. No fatalities that could be related to HPIV3 infection were identified. A recent investigation of an HPIV3 outbreak in a similar setting also failed to identify any fatalities associated with this virus (Piralla *et al.*, 2009). However, HPIV3 was recognized as a potential cause of an admission or prolonged stay in 9 out of 14 cases, although in 8 out of 9 cases a potential secondary pathogen was also identified, emphasizing the potential importance of dual infections (Table 5-1) Rhinovirus, a highly prevalent infection in the paediatric cohort (Söderman *et al.*, 2016) was a notable secondary viral respiratory pathogen, isolated in six of the cases. Although no instances of dual infection transmission were identified in this study, the incidence of dual infection was broadly in keeping with some previous reports (Benites *et al.*, 2014). Overall a much wider review of the impact of HPIV3 in the paediatric population is required in order to determine the exact clinical impact of HPIV3 in this setting (Santolaya *et al.*, 2017). It is important to emphasize further that currently, good infection control policies are the only approach to HPIV3 management and although root cause analysis is important it does not alleviate the clinical impact of outbreaks and infections. Therefore there is a clear and urgent need for models for therapeutic agents for HPIV3, as discussed in the following chapter.

6 Chapter 6: *In vitro* sensitivity of human parainfluenza 3 clinical isolates to ribavirin, favipiravir and zanamivir.

6.1 Introduction

As described above, HPIV3 has a significant clinical impact, particularly in the vulnerable patient cohort where it has been linked to increased morbidity and mortality (Seo *et al.*, 2014; Shah *et al.*, 2016). As immunity to HPIV3 is incomplete, its incidence follows a seasonal pattern with yearly peaks in late spring and summer (Zhao *et al.*, 2017). Transmission of HPIV is through respiratory droplets and the virus can remain viable for up to 10 hours on non-absorbent surfaces (Brady, Evans and Cuartas, 1990). Prolonged shedding by immunocompromised patients (Piralla *et al.*, 2009; Aliyu *et al.*, 2015) causes outbreaks resulting in ward closures. This disruption to clinical services is not only harmful to patients but constitutes a significant financial burden for the National Health Service (NHS) (Jalal *et al.*, 2007) as described in the previous chapter .

Although a number of potential therapeutic candidates exist, there is currently no licensed therapy or vaccine. Hence there is a clear and urgent need to develop robust therapeutic models to evaluate potential candidates for the treatment of this virus. A sizeable amount of work on HPIV3 has been conducted with a view to elucidating potential therapeutic targets for the virus, but the majority of the research has concentrated on tissue culture adapted strains.

In this chapter an infectivity based *in vitro* model for the evaluation of potential therapeutic candidates for HPIV3 based on a tissue culture adapted reference strain and a panel of minimally passaged clinical strains is presented. This model represents a significant departure from previous *in vitro* models that have used only laboratory adapted strains.

Ribavirin has previously been used to treat human parainfluenza 3 infections in HSCT patients (Lewis *et al.*, 1996; Chakrabarti *et al.*, 2000; Nichols, 2001). This approach was partially encouraged by the limited success in RSV treatment in young children, for which ribavirin is a licensed therapy (Hall *et al.*, 1983; Smith

et al., 1991), as well as experience with other viral infections such as hepatitis C (Thomas, Ghany and Liang, 2012). Additionally ribavirin has shown to be effective against parainfluenza viruses *in vitro* (Leyssen *et al.*, 2005; Kihira *et al.*, 2014). However a recent meta analyses have shown that ribavirin has no effect on patient outcome in severe HPIV3 infection in the HSCT cohort (Falsey, 2012; Seo *et al.*, 2014). It is worth noting that ribavirin was equally seen as promising candidate for treatment of haemorragic fever viruses including CCHF (Crimean Congo Haemorragic Fever) and Lassa fever (Watts *et al.*, 1989; Günther and Lenz, 2004) however despite encouraging results *in vitro*, it has been a lot less successful *in vivo* (Ceylan *et al.*, 2013; Carrillo-Bustamante *et al.*, 2017). The latter, coupled with the ribavirin toxicity profile and its teratogenic effects (Thomas, Ghany and Liang, 2012), which make aerosolized delivery for respiratory infections highly complex and impractical, has meant that its use for treatment of HPIV3 has declined. One possible reason for the lack of efficacy could be that clinical stains are more resistant to ribavirin and therefore a detailed evaluation of its inhibitory effect on clinical strains is necessary.

Favipiravir (T-705) has a similar mechanism of action to ribavirin (Vanderlinden *et al.*, 2016) and functions by inducing lethal mutagenesis (Furuta *et al.*, 2013; Arias, Thorne and Goodfellow, 2014; Vanderlinden *et al.*, 2016). It has demonstrated good inhibitory activity against a broad range of viruses including *Paramyxoviridae in vitro* and in small animal models, as well as laboratory-adapted strains of HPIV3 in particular (Jochmans *et al.*, 2016; Madelain *et al.*, 2016; Vanderlinden *et al.*, 2016). It has an excellent toxicity profile and therefore can be considered as a promising potential inhibitor of HPIV3 in a clinical setting (Madelain *et al.*, 2016).

Zanamivir is a neuraminidase inhibitor commonly prescribed for the treatment of influenza, although its efficacy in this capacity has recently been called into question (Jefferson *et al.*, 2014). *In vitro* it has shown to be effective against laboratory adapted strains of HPIV3, although at therapeutically unattainable 50% maximum effective concentrations (EC_{50}) values (Greengard *et al.*, 2000). However, given the structural similarities between the HPIV3 HN and influenza neuraminidase binding pockets (Lawrence *et al.*, 2004), as well as the ability of the HN protein of HPIV3 to influence the viral life cycle at binding, fusion and

release stages, zanamivir remains a tempting candidate for HPIV3 inhibition. To date the potential of zanamivir as a therapeutic candidate for HPIV3 has yet to be evaluated systematically for clinical strains.

6.2 Results

6.2.1 Isolation and cell culture growth of HPIV3 clinical isolates

As described previously, residual clinical samples were collected between 2011 and 2015 from the PHE diagnostic laboratory, Addenbrooke's hospital, Cambridge. Nine clinical strains collected from different years from diverse patient demographics and plaque phenotype were chosen for susceptibility testing (Table 6-1).

Sample				Patient			
Lab ID	Date collected	Source	Plaque area mm^2 +/- SEM	Sex	Age	Location	In/out patient
14	Nov-14	URT swab	0.30+/-0.04	F	1 year	Basildon hospital	in
16	May-14	URT swab	0.33+/-0.03	M	50 years	Addenbrooke's hospital	in
65	Jun-11	URT swab	1.47+/-0.11	F	54 years	Addenbrooke's hospital	in
82	Jul-11	URT swab	1.46+/-0.16	M	2 months	Harlow hospital	in
113	Jul-12	URT swab	0.94+/-0.05	M	42 years	Addenbrooke's hospital	in
129	Feb-13	Tracheal aspirate	0.92+/-0.04	F	4 years	Frimley Park hospital	in/ICU
153	Apr-13	NPA	0.83+/-0.03	F	12 years	Frimley Park hospital	in
180	May-13	NPA	0.57+/-0.02	F	3 months	Addenbrooke's hospital	out
362	Mar-15	URT swab	0.59+/-0.06	F	80 years	Essex nursing home	out
LS MK9	n/a	n/a	3.96+/-0.45	n/a	n/a	n/a	n/a

Table 6-1 Clinical strains selected for susceptibility testing. Clinical strains were collected between 2011 and 2015, all originated from the upper airway of patients. Plaque area for the clinical strains averaged 0.82 mm^2 +/- (SEM) with a range between 0.3 mm^2 and 1.47 mm^2, with strains from 2011 (65 and 82), demonstrating a comparatively large plaque phenotype. Strain MK9 is a laboratory adapted strain obtained from PHE cell culture collections.

All 9 strains were collected from the upper respiratory tract (URT) of patients including nasopharyngeal aspirates (NPAs), tracheal aspirates and swabs. Four samples originated in Addenbrooke's hospital, Cambridge, and the remaining were from East of England and London geographical areas. Seven samples were collected in an inpatient setting with one sample (129) from an intensive care unit (ICU) and 2 samples (180 and 362) from an outpatient setting. The mean age of patients sampled was approximately 27 years with a range from 3 months to 80 years. Although 6/9 were female and only 3/9 were male this represents a diverse sample of patient demographics albeit within a constrained geographical area serviced by PHE diagnostic laboratory Addenbrooke's Hospital, Cambridge. The source of samples also reflects the general pattern of the clinical impact of HPIV3, with the majority (2/9) coming from an inpatient setting, one originating from ICU and two from outpatient sources. The significant difference between the plaque area of clinical strains and strain MK9 likely reflects the culture adaptation of the laboratory strain.

The toxicity of all inhibitors was first examined in PLC/PRF5 cells and no significant reduction in cell viability was observed within the range of the concentrations used for the experiments (Figure 6-1) with ribavirin showing the highest toxicity of approximately 30% at 1 mM.

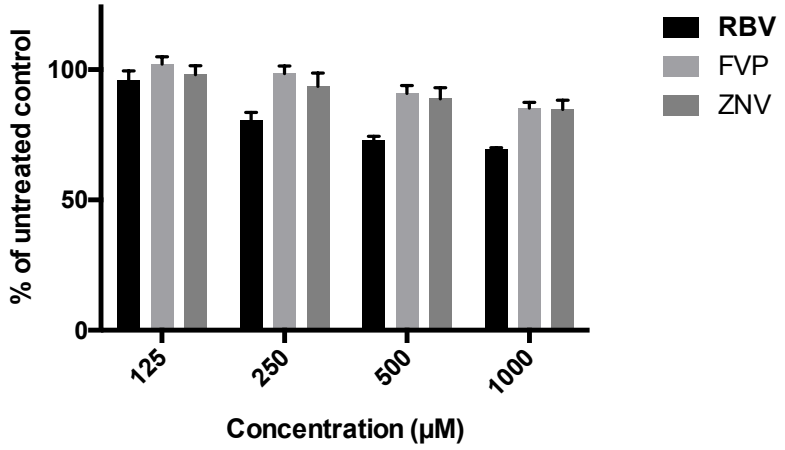

Figure 6-1 Cell viability assay of PLC/PRF5 cells with ribavirin (RBV), favipiravir (FVP) and zanamivir (ZNV). The three inhibitors have been tested in a range of 0-1 mM concentrations on PLC/PRF5 cells. Cells in 96 well plates were either mock inoculated or inoculated with serial dilutions of each inhibitor starting with a concentration of 1 mM in 8 biological repeats. Plates were then incubated at 33°C for 7 days and assayed with CellTiter-Blue® Cell Viability Assay (Promega) as per the manufacturer's instructions. Cell viability is shown as a percentage of untreated control +/-SEM.

6.2.2 Sensitivity of laboratory adapted strain MK9 to zanamivir, ribavirin and favipiravir on culture adapted HPIV3

To determine more accurately the effective concentration of each inhibitor against the lab adapted HPIV3 strain MK9, the EC_{50} was determined using plaque reduction assay where the inhibitor was present in the overlay (Figure 6-2).

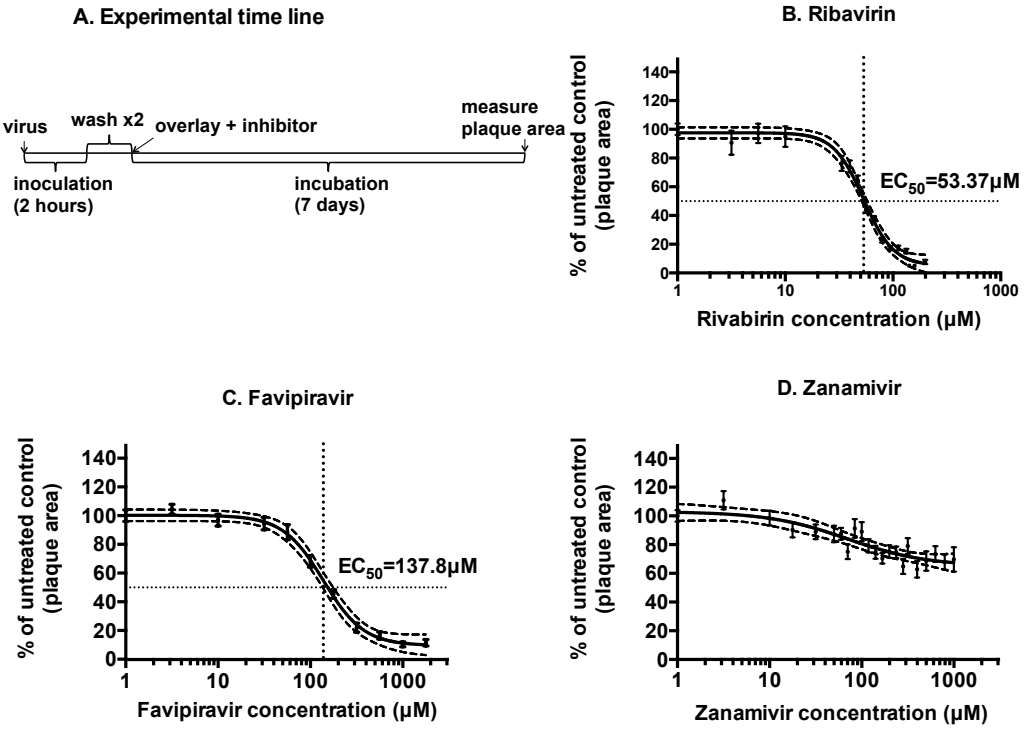

Figure 6-2 Laboratory adapted HPIV3 strain MK9 is sensitive to ribavirin and favipiravir but not zanamivir, as measured by plaque area reduction. Figure shows mean plaque area reduction as percentage of the plaque area of untreated control +/- SEM for ribavirin (B), favipiravir (C) and zanamivir (D). Experimental design is shown in (A). All plaque areas were measured using Fiji. Curves were fitted using GraphPad Prism version 6.00 with R^2>0.9. Dashed lines represent the 95% confidence intervals. Each point represents three biological repeats.

Ribavirin and favipiravir, but not zanamivir were shown to be effective inhibitors of HPIV3 strain MK9 by this method with an EC_{50} of 53.37 µM for ribavirin and 137.8 µM for favipiravir (Figure 6-2B and C). This is consistent with the mode of action of zanamivir as a neuraminidase inhibitor affecting viral attachment and release (Porotto *et al.*, 2001; Lamb, Paterson and Jardetzky, 2006). As inhibitors were only present at the growth stage of the viral life cycle in this assay (Figure

6-2A), we would expect zanamivir not to show a significant inhibitory effect in this case.

In order to determine the effect of the inhibitors on a different part of the lifecycle of HPIV3, the effect of each inhibitor on the growth kinetics of HPIV3 was evaluated. Ribavirin (Figure 6-3B and C) and favipiravir (Figure 6-3D and E) were observed to be effective inhibitors of HPIV3. Due to the mutagenic nature of favipiravir an EC_{90} was not achieved with this inhibitor when measured by the reduction in genome copy number in cells (Figure 6-3E). Zanamivir appeared to be the least effective of these inhibitors, achieving a maximum of 10% inhibition of released virus and approximately 70% reduction in genome copy number in cells at the maximum concentration assayed (1 mM) (Figure 6-3F and G).

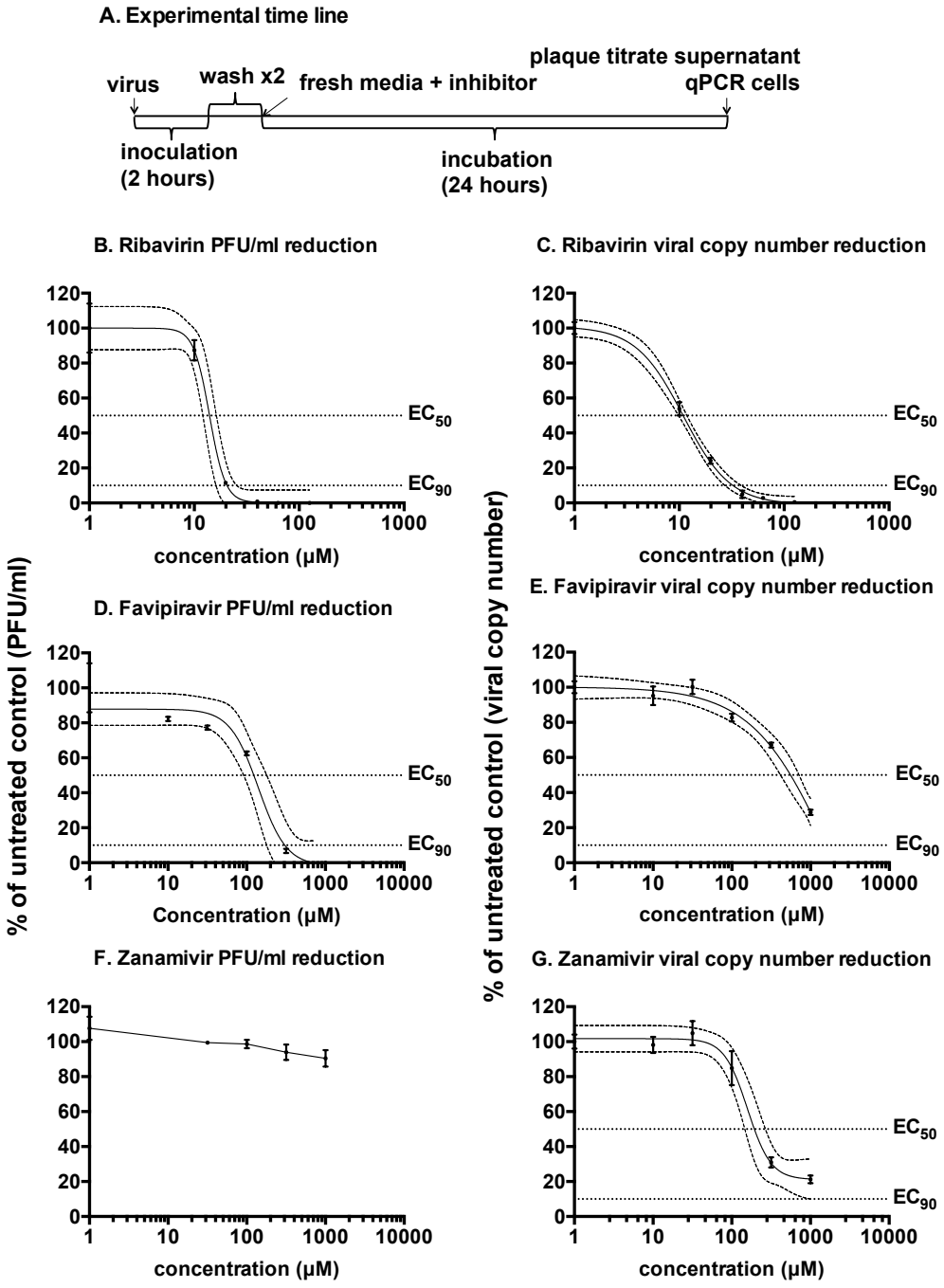

Figure 6-3 Growth of HPIV3 laboratory strain MK9 is effectively inhibited at 24 hours in the presence of ribavirin and favipiravir but not zanamivir. Experimental design is shown in A. For each inhibitor concentration, the reduction of infectious units in the supernatant is shown as a percentage of untreated control quantified by plaque titration (panels B, D and F). The reduction in viral copy number is shown as a percentage of untreated control by qPCR (panels C, E and G). All points are averages of three biological replicates +/- SEM. All plaques were counted using Fiji. All curves were fitted using GraphPad Prism version 6 with R^2>0.9. Dashed lines represent 95% confidence intervals.

6.2.3 Zanamivir inhibits HPIV3 at the level of virus binding.

The ability of zanamivir to act as an inhibitor of HPIV3 binding to host cells and its effect on the viral particle was assessed by adding the inhibitor during the inoculation and pre-incubating stages respectively. Zanamivir was found to inhibit HPIV3 at a high concentration (EC_{50} of 295 μM) when added during the inoculation stage (Figure 6-4). This is consistent with previous studies that have concentrated on the effect of zanamivir during receptor binding (Greengard *et al.*, 2000). Pre-incubation of HPIV3 with zanamivir has had no effect on the reduction of infectious units, confirming that zanamivir has no direct anti-viral activity.

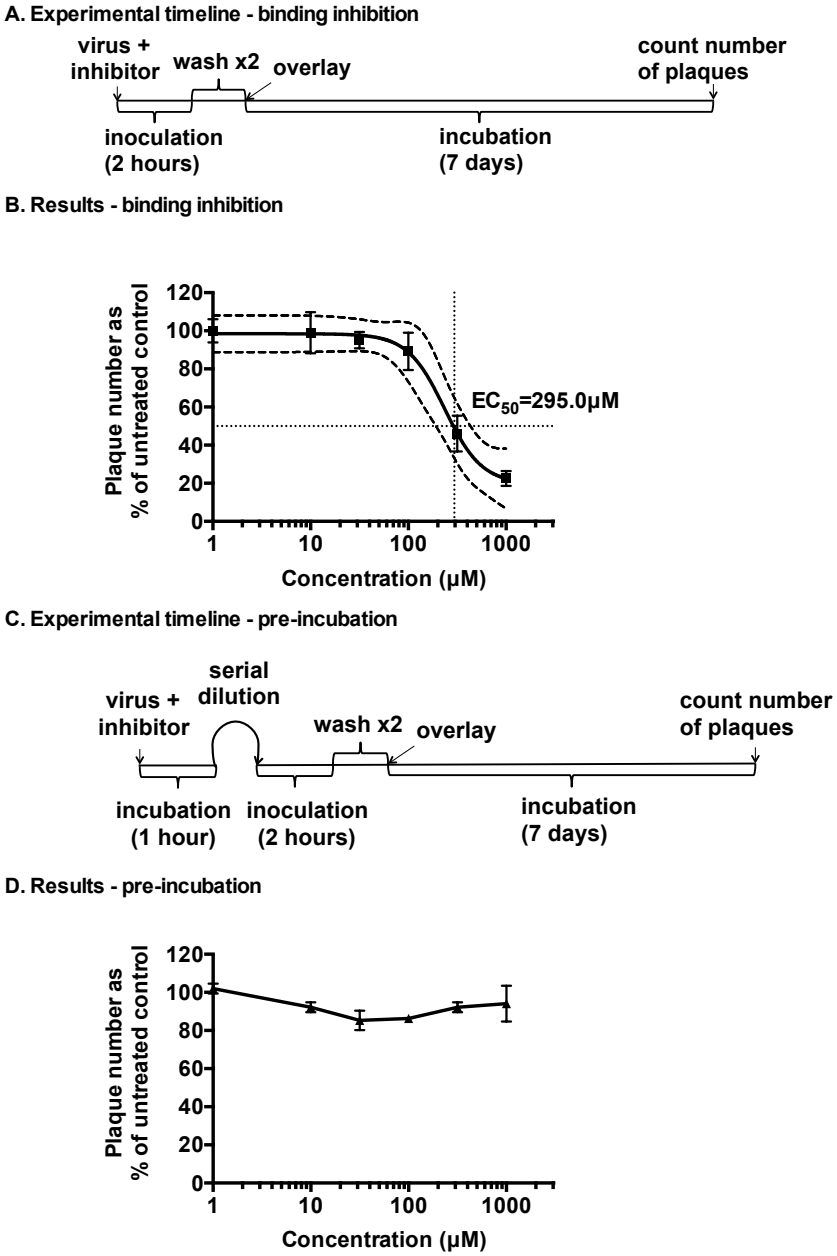

Figure 6-4 Zanamivir inhibits HPIV3 binding to host cells. Experimental design is shown in A (binding inhibition) and C (pre-incubation). The figure shows the effect on laboratory strain MK9 when zanamivir is present during inoculation (B) and when pre-incubated with zanamivir (D) to exclude the possibility of direct effects on virus particles. Panel D (pre-incubation) shows no significant effect on viral replication. In both cases the figure shows the reduction of the number of infectious units as a percentage of untreated control by plaque titration +/- SEM. All plaques were counted using Fiji. All curves were fitted using GraphPad Prism version 6.00 with R^2>0.9. Dashed lines represent 95% confidence intervals.

6.2.4 Clinical strains of HPIV3 are susceptible to ribavirin, favipiravir and zanamivir

In order to assess the sensitivity of clinical isolates to ribavirin, favipiravir and zanamivir, we selected 2 concentrations of each inhibitor. The EC_{50} and EC_{90} for ribavirin and favipiravir were interpolated using the dose response curves fitted to the reduction of released infectious viral particles data for the laboratory strain (Figure 6-3B and D). As no equivalent dose response curve could be fitted for the sensitivity of the laboratory strain to zanamivir (Figure 6-3F), the EC_{50} value was calculated from the dose response curve fitted to the reduction of viral copy number data (Figure 6-3G). The maximum concentration assayed (1 mM) was used instead of the EC_{90} for zanamivir. These inhibitor concentrations were then assayed against clinical strains of HPIV3. All clinical strains were shown to be sensitive to the three inhibitors (Figure 6-5) with the majority of the clinical strains typically being at least as susceptible as the reference strain (Table 6-2). 8/9 clinical strains were inhibited by more than 50% at the ribavirin EC_{50} concentration for the reference strain, although only 4/9 were inhibited by more than 90% at EC_{90} with 1/9 less inhibited and 4/9 showing no difference (Figure 6-5B). A similar pattern was observed for favipiravir with 4/9 strains inhibited by more than 50% at EC_{50} and 3/9 strains more than 90% at EC_{90} (Figure 6-5C). Although zanamivir was shown to be ineffective against the laboratory strain by the growth kinetic inhibition assay (Figure 6-3), at 200 μM (lower concentration) 5/9 of clinical strains were more sensitive to zanamivir than the laboratory strain. At 1 mM (higher concentration) all clinical strains are shown to be more sensitive, 9/9 achieving at least 50% inhibition and 3/9 90% inhibition (Table 6-2).

		Average percentage of untreated control (PFU/ml) +/- SEM		Number of clinical strains with significant deviation from the laboratory strain (FDR 1%)		
Inhibitor	Concentration	Lab strain (MK9)	Clinical strains	Less sensitive	More sensitive	No difference
ribavirin	$RBVIC_{50}$	47.94+/-5.97	21.5+/-2.08	0 (0%)	8 (89%)	1 (11%)
	$RBVIC_{90}$	9.12+/-0.76	5.15+/-0.78	1 (11%)	4 (44.5%)	4 (44.5%)
favipiravir	FVP IC_{50}	47.95+/-1.37	39.77+/-3.69	1 (11%)	4 (44.5%)	4 (44.5%)
	FVP IC_{90}	13.56+/-0.23	14.03+/-1.73	1 (11%)	3 (33%)	5 (56%)
zanamivir	ZNV 200µM	98.63+/-4.11	75.86+/-3.21	0 (0%)	5 (55.5%)	4 (44.5%)
	ZNV 1mM	90.41+/-4.75	25.94+/-3.72	0 (0%)	9 (100%)	0 (0%)

Table 6-2 Clinical strain susceptibility to favipiravir, ribavirin and zanamivir. Average EC_{50} and EC_{90} values for each clinical strain and for the laboratory strain MK9 (PHE cultures) determined by plaque titration of supernatant after 24 hour incubation (**Figure 6-5**) are summarized. A summary of how many clinical strains were more, less or equally susceptible to each inhibitor is included for each inhibitory concentration. All plaques were counted using Fiji.

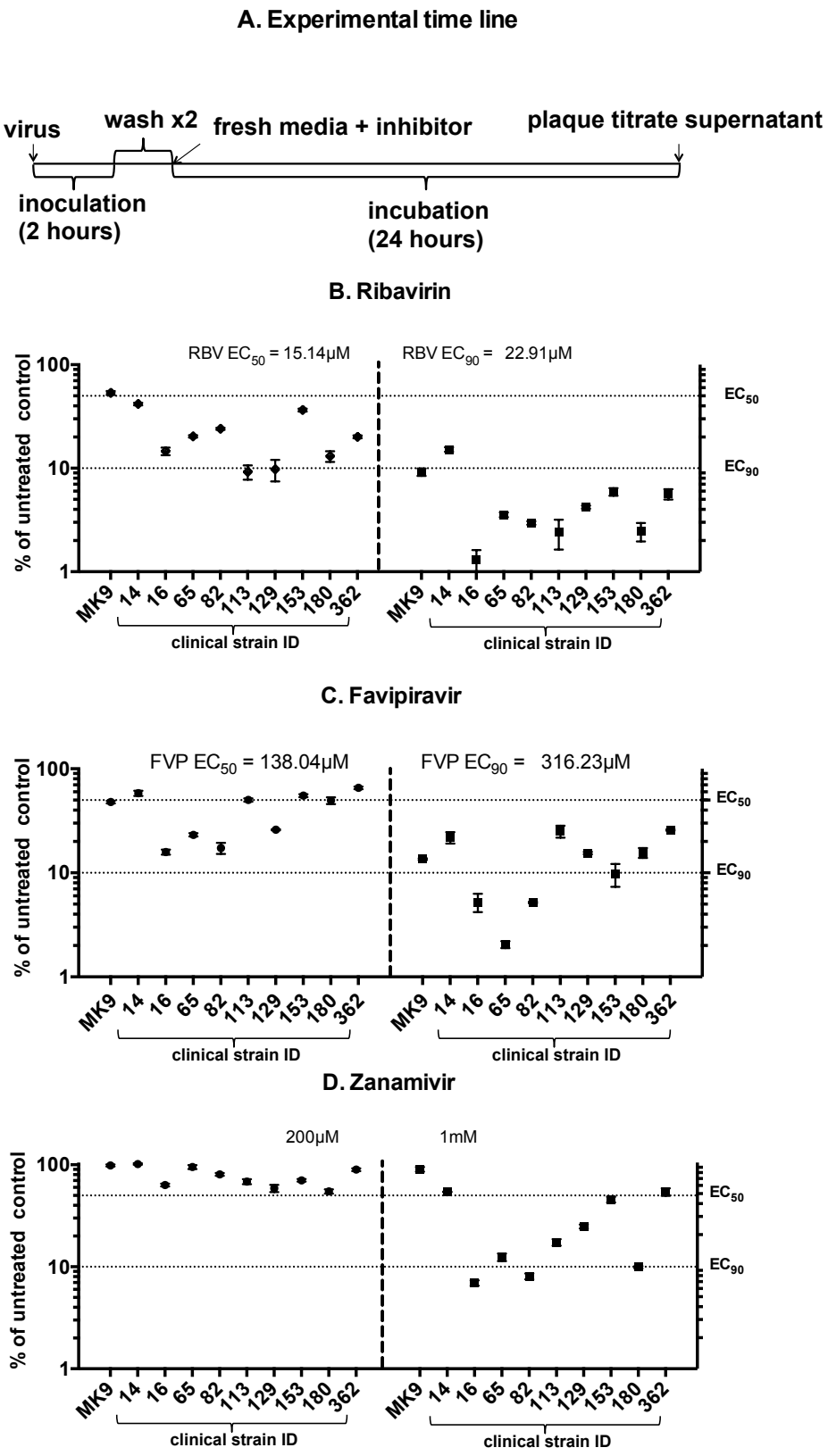

Figure 6-5 Clinical strains of HPIV3 are susceptible to ribavirin, favipiravir and zanamivir. Experimental design is shown in (A). For each clinical strain the figure shows the reduction of infectious units in the supernatant assessed by plaque titration as a percentage of the untreated control +/- SEM. 9 clinical strains and strain MK9 were inoculated at low MOI (0.01 PFU/cell) and incubated for 24 hours in triplicate with two concentrations of each inhibitor. All plaques were counted using Fiji.

6.2.5 Zanamivir inhibits binding of HPIV3 clinical strains to the host cell.

In order to investigate further the effect of ZNV on HPIV3 during binding, the above experiment was repeated with the five clinical strains that were significantly susceptible to ZNV at 200μM. All the clinical strains were shown to be as sensitive to ZNV as reference strain MK9 by this method (Figure 6-6).

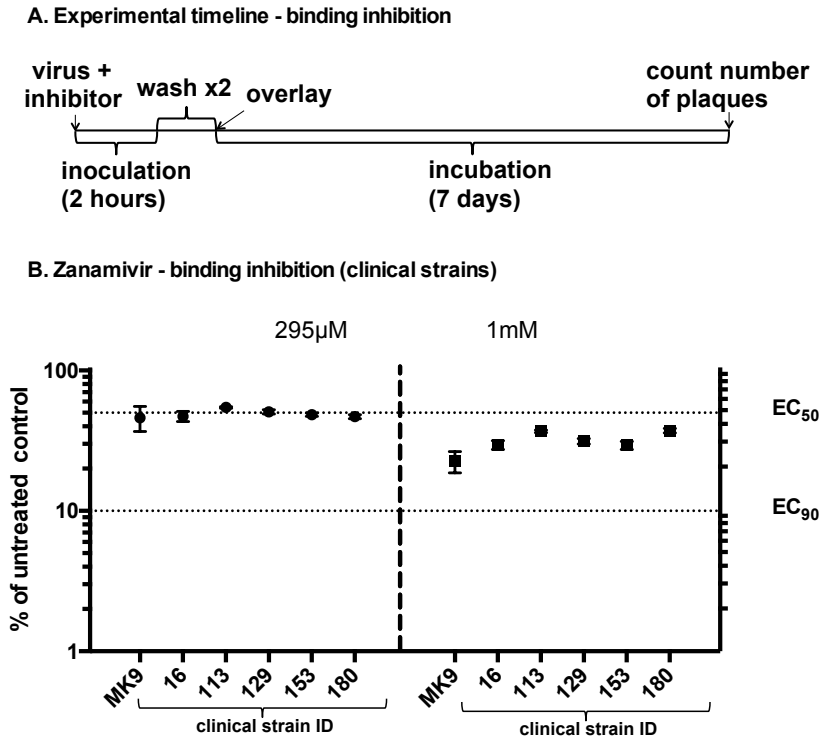

Figure 6-6 Clinical strains are susceptible to zanamivir at the level of virus binding. Experimental design is shown in (A) 5 clinical strains were inoculated in the presence of 2 difference concentrations of zanamivir. For each clinical strain the figure shows the reduction in infectious units by plaque titration as a percentage of the untreated control +/- SEM. All plaques were counted using Fiji.

Similarly to the laboratory strain, pre-incubation with ZNV was shown to have no effect on the reduction in infectious particle number of these clinical strains (data not shown).

6.3 Discussion

In this chapter ribavirin, favipiravir and zanamivir were evaluated as potential inhibitors of HPIV3 using both a laboratory adapted strain and nine distinct minimally passaged clinical strains. The clinical strains selected originated from a diverse population of patients and can therefore be considered representative

of the population covered by the PHE diagnostic laboratory Addenbrooke's Hospital, Cambridge.

The results confirmed that ribavirin is an effective inhibitor of HPIV3 *in vitro* both by plaque reduction and by growth inhibition assays (Figure 6-2 and Figure 6-3). The results are consistent with the mode of action of ribavirin (Leyssen *et al.*, 2005; Vanderlinden *et al.*, 2016) by inoside 5′ monophosphate dehydrogenase (IMDPH) and subsequent guanosine triphosphate (GTP) depletion during viral replication. An approximately 4-fold decrease in EC_{50} value against laboratory strain MK9 between the one obtained by plaque titration (53.37 μM) (Figure 6-2) and by growth kinetics inhibition (15.14 μM) (Figure 6-3) was noted. This discrepancy was likely due to differences in methodology including the stability of the inhibitor in the overlay (7 days vs 24 hour incubation), the timing of data collection and viral spread confined to cell to cell fusion in plaque assays. Clinical strains were at least as susceptible to ribavirin as the laboratory strain with a potential lower EC_{50} for clinical strains (Figure 6-5). It is important to note, however that some clinical strains do not show this effect, with 1/9 observed being less sensitive (Table 6-2).

The EC_{50} and EC_{90} levels determined in this chapter are within levels achieved in human subjects during hepatitis C treatment, where an average level of 8.19 μM, with a potential correlation with haemoglobin drop above 4 μM (Karin Jorga *et al.*, 2006) during hepatitis C therapy was recorded. The most common method of delivery for severe cases of LRTI, as is the case for HPIV3 infection, is inhaled aerosolized ribavirin. It is currently indicated as the treatment of choice for RSV infection in children and there is some evidence that it is effective, although the studies are very small (Hall *et al.*, 1983; Smith *et al.*, 1991). The most common side effect with this method of delivery is bronchospasm. Plasma levels achieved, as reported by the manufacturers (Virazole) range from 0.76μM to 6.8μM, depending on the length of delivery (2.5 hours/day, n=4, and 20 hours/day n=3, respectively) (ICN Pharmaceuticals, Inc, Costa Mesa, California, USA, no date) . This is significantly lower than the EC_{50} for ribavirin reported here in other *in vitro* studies. It is likely that concentrations in respiratory secretions exceed these, although unfortunately no data on this is available. Furthermore the aerosolized method of delivery remains problematic due to risk

of teratogenicity, as well as being time consuming. As such, although ribavirin remains an effective inhibitor of HPIV3 *in vitro*, further optimization of drug design or combination therapy is required to yield a regimen capable of delivering therapeutically useful concentrations at the site of infection. Current results, at least partially, explain the lack of clinical efficacy of ribavirin *in vivo*.

Favipiravir is a nucleoside analogue with a broad spectrum of action, and has been shown to be effective against other RNA viruses such as influenza, ebola and laboratory adapted parainfluenza strains *in vitro* (Mentré *et al.*, 2015; Jochmans *et al.*, 2016; Madelain *et al.*, 2016; Nguyen *et al.*, 2017). Given the similarities in the RNA dependent RNA polymerase, it is a promising inhibitor of HPIV3. It has been shown that favipiravir acts both by inhibiting RNA dependent RNA polymerase directly (Furuta *et al.*, 2013; Vanderlinden *et al.*, 2016) and by inducing viral mutagenesis (Arias, Thorne and Goodfellow, 2014; Vanderlinden *et al.*, 2016), giving rise to abundant non-infectious particles at lower concentrations. Overall we observed that favipiravir is an effective inhibitor of HPIV3 both by plaque reduction and growth inhibition assay (Figure 6-2 and Figure 6-3), with 8 out of 9 clinical strains tested being at least as sensitive to favipiravir as the laboratory strain MK9 (Figure 6-5). In this thesis an EC_{50} of approximately 138 μM was determined for HPIV3 by both plaque reduction and growth inhibition assay (Figure 6-3).

As favipiravir is a relatively novel therapeutic drug, very limited *in vivo* data on plasma concentrations achieved in humans is available (Madelain *et al.*, 2016), although a number of *in vivo* studies using small rodent models (Mendenhall *et al.*, 2011; Gowen *et al.*, 2015; Jochmans *et al.*, 2016) and well as non-human primates (Madelain *et al.*, 2017) have been conducted. Recently released data from the JIKI trial (Efficacy of favipiravir against ebola trial) quoted trough plasma levels of 293 μM on day 2 and 165 μM on day 4 of treatment (Nguyen *et al.*, 2017). Additionally, a theoretical dose regimen derived from murine and theoretical pharmacokinetic models provided by the manufacturers (Toyama Chemical) was used to estimate that plasma levels as high as 855 μM on average can be achieved, while remaining within well-tolerated levels in humans (Mentré *et al.*, 2015). This exceeds the EC_{50} and EC_{90} values observed here. Although encouraging, this should be interpreted with caution, as no data on favipiravir

concentration in respiratory secretions and in the lungs is currently available.

Zanamivir was observed to be ineffective against the laboratory strain of HPIV3 by two assays (Figure 6-2 and Figure 6-3). All of the clinical strains demonstrated at least a 50% reduction in infectious units in the supernatant at 1 mM ZNV and 2 out of 9 strains tested demonstrated ~ 50% inhibition at 200 μM (Figure 6-5). We have also demonstrated that zanamivir prevents HPIV3 binding to host cells at EC_{50} of 295 μM (Figure 6-4). No difference was observed between the sensitivity to ZNV in its capacity as a binding inhibitor of the laboratory strain MK9 and the clinical strains tested (Figure 6-6). This is consistent with previous data that indicates that the HN protein of HPIV3 contains two host cell binding sites and is responsible for the binding, fusion triggering and release of the new viral particle (Porotto *et al.*, 2007). In its capacity as a binding inhibitor, ZNV is known to bind to site I with a non-specific distortion of site II of the fusion protein (Porotto *et al.*, 2007). The fusion and release processes, on the other hand have been linked to binding site II (Porotto *et al.*, 2007; Palmer *et al.*, 2012). Moreover a specific mutation (N556D) at binding site II, has been linked to culture adaptation and has been shown to confer a 5-fold decrease in neuraminidase activity between a wild type strain and a significantly culture adapted strain (Palermo *et al.*, 2016). This has been linked to a more robust interaction with the cell receptor (Murrell *et al.*, 2003) and a larger plaque phenotype (Table 6-1) in culture adapted strains (Palermo *et al.*, 2016). It is of note that the reference strain MK9 contains that mutation and hence the reduced neuraminidase activity, whereas the clinical strains used in this study do not. This is concordant with the results of this study, where clinical strains have been shown to be more susceptible to ZNV than the laboratory strain MK9 as assessed by growth inhibition but not at the level of binding.

Data on the bioavalability of zanamivir is widely available in the context of its clinical use against influenza. It is found to be a well-tolerated drug with few side-effects and no drug-drug interactions reported. Oral bioavailability of zanamivir is 2%, although studies with permeability enhacers (Shanmugam *et al.*, 2013) are aiming to improve this. A correlation between intravenous administration and concentration in nasal secretions has been established with approximately 300 μM achieved 4 hours after a 600 mg infusion, dropping to

200 μM 12 hours post drug administration, but no measurements were taken from the lower respiratory tract (Cass, Efthymiopoulos and Bye, 1999). In either case these values are significantly below inhibitory EC_{50} and EC_{90} of zanamivir as determined in the current set of experiments. Nonetheless the observed susceptibility of clinical strains to zanamivir confirms the importance of conducting further studies in this area on clinical strains with minimal culture adaptation.

In this chapter an *in vitro* infectivity based model for evaluating HPIV3 susceptibility to potential therapeutic candidates using a tissue culture adapted reference strain MK9 and 9 diverse clinical strains has been presented. A necessary limiting factor in methodologies that involve immortalised cell culture is the reliance on viruses that are able to grow in this environment. A markedly larger plaque phenotype is associated with significant culture adaptation as demonstrated by the laboratory strain (Palermo *et al.*, 2016). Within these constraints, and as all clinical samples have been minimally and equally passaged in cell culture, the diversity in plaque size is an indication of diversity of phenotype of the clinical samples used. There is good evidence that heavily laboratory adapted HPIV3 strains are non-representative of the currently circulating clinical strains (Palmer *et al.*, 2012; Palermo *et al.*, 2016). Despite recent advances in human airway epithelial (HAE) culture systems (Palermo *et al.*, 2016), these are often not suitable when large volume, high titre stocks are required for subsequent downstream analysis. Ribavirin and favipiravir, but not zanamivir were found to be effective inhibitors of both the tissue culture adapted strain and clinical strains of HPIV3. Overall clinical strains were significantly more susceptible to zanamivir. Further work on clinical circulating strains, optimized methods of delivery and targeted clinical trials are required to formulate treatment for this important pathogen.

7 Chapter 7: Conclusion

HPIV3 is an important respiratory virus with the potential to cause significant pathology, particularly in immunosuppressed patients or those with a past respiratory medical history (Herzog *et al.*, 1989; Schomacker *et al.*, 2012; Ustun *et al.*, 2012; Liu *et al.*, 2013). Moreover, to date neither a licensed treatment nor vaccine is available. Hence further research is required into both the pathology as well as methods of prevention and treatment of this virus (Henrickson, 2003; Zhao *et al.*, 2017). Consequently the aims of the current project, as set out in Introduction, were to characterise the currently circulating clinical strains of HPIV3 both phenotypically and phylogenetically, as well as to evaluate the clinical significance thereof. The final aim was to study therapeutic candidates against this virus using a panel of diverse clinical strains.

Most previous research into HPIV3 has been conducted on significantly laboratory-adapted strains. Although these are readily available and grow well in immortalised cell culture, it is recognized that culture adapted strains of HPIV3 behave very differently from wild type (Moscona *et al.*, 2010; Palmer *et al.*, 2012; Palermo *et al.*, 2016). Therefore a library of diverse clinical strains was established for this project. 395 clinical samples diagnosed positive for HPIV3 by two rounds of diagnostic qPCR between 2011-2015 were grown in PLC/PRF5 cells using a growth protocol developed within this project. Consequently 43 diverse clinical strains lacking detectable co-infections with other respiratory viruses were grown successfully at first passage. In order to evaluate clinical strains that had not been exposed to immortalised cell culture and within the financial constraints of this project, 3 clinical strains, collected as part of the outbreak investigation in summer 2017, were grown in human airway epithelial cells. The limited stock obtained was used for further work on phenotype characterization to meet the first objective of this thesis.

Phenotype *in vitro* was evaluated both by examining clinical strain plaque phenotype and the effect of culture adaptation on clinical stains. There is sufficient data from studies on other viruses (Blaney *et al.*, 2002; Mao and Rosenthal, 2003; Jia *et al.*, 2007; Kim *et al.*, 2015) to suggest that there may be a correlation between viral phenotype *in vitro* and virulence *in vivo*. In this

literature, larger HPIV3 plaque phenotypes have been correlated with culture adaptation and most of the focus has centered on the HN and F proteins (Palmer *et al.*, 2012, 2014). This is in line with data obtained in this project as all clinical strains developed larger plaque phenotypes following extended passage in cell culture. However the majority of variants were found to be located within the M-F intergenic region (Lingemann *et al.*, 2015), that has previously been linked to both virulence and plaque size, rather that exclusively within the HN and F coding segments of the HPIV3 genome. The above indicates that culture adaptation studies of HPIV3 should be expanded to encompass the potential effect on the entire genome and that there is sufficient evidence to show that diverse strains of HPIV3 demonstrate different phenotype *in vitro*.

Having demonstrated a diverse plaque phenotype in clinical strains of HPIV3 in immortalised cell culture, the next aim was to demonstrate a variation in growth kinetics and immunogenicity of clinical strains in a model more representative of the natural host. There have been a number of small animal models of HPIV3 infection (Mascoli *et al.*, 1976; Murphy, Dubovi and Clyde, 1981; Ye *et al.*, 2010; Jochmans *et al.*, 2016) however a primary cell line *ex vivo* model has been shown to be ideal for growth of this virus (Ottolini *et al.*, 1996; Yamaya *et al.*, 2002; Zhang *et al.*, 2005). Therefore, as a close approximation of the natural host (Yamaya *et al.*, 2002), a primary cell model, using HAE cells was used for characterization of this virus in this project. In line with prior observations, the laboratory strain (Palmer *et al.*, 2012; Palermo *et al.*, 2016), has a significant growth defect in a more natural model, although surprisingly it is not the least immune-stimulatory when viral load is corrected for. Other results obtained at this stage were contrary to what was expected from previously published data. It could be hypothesized that strains with small plaque phenotypes, potentially correlated with the least culture adaptation, would be expected to grow best in an *ex vivo* model (Moscona, 2005; Palmer *et al.*, 2012; Palermo *et al.*, 2016). However in the current project the strains with the smallest plaque phenotype were found to exhibit neither the highest growth rate nor the highest viral titres at the final time point. Additionally no significant difference in final viral titre was detected for strains grown in immortalised cell culture regardless of plaque size *in vitro*. One could argue that this is consistent with a previous study, where

a small number of clinical strains were found to demonstrate the same growth kinetics in HAE cells (Palermo *et al.*, 2016), however in this case clinical strains were not closely related and were found to exhibit different plaque phenotypes *in vitro*.

It is essential to remember that the clinical impact of a particular pathogen is inevitably a combination of both host and pathogen factors (Openshaw and Tregoning, 2005; Schomacker *et al.*, 2012). In this project the response of the host was evaluated by measuring the cytokine release triggered by different strains of HPIV3 in HAE cells (Zhang *et al.*, 2005). At this stage of the project the clinical strains with the smallest plaque phenotype were observed to trigger the highest cytokine response, especially when corrected for relative viral load. This was particularly noted in two specific cytokines, that have previously been identified as markers of clinical severity in paramyxovirus infection: RANTES (Chihara *et al.*, 2018) and IL8 (Gern *et al.*, 2002). Although it was impossible, at this stage, to determine whether the correlation was due to the slower growth of these strains and hence to their consequent reduced inhibitory effect on the immune system (Caignard *et al.*, 2009; Ding *et al.*, 2017; Shil *et al.*, 2017) or *vise versa*, it nonetheless served to demonstrate that there was a potential correlation between *in vitro* and *in vivo* phenotype of HPIV3 with possible clinical implications.

In this project, a very limited number of clinical strains have been used. Furthermore a proportion of them were minimally passaged in immortalised cell culture, and thus exposed to artificial selective pressure prior to experimentation. The generation of large volume of well-characterised viral stocks necessitated the growth and selection of clinical samples in cell culture models. In literature, primary cell lines, such as HAEs have been described as well suited for this purpose (Palmer *et al.*, 2012, 2014). However within practical and financial constraints, it would be unfeasible to use these cells if large quantities of viral stock were required. An alternative approach would be to use the data collected in this project and apply it in a reverse genetics model of HPIV3 (Beaty *et al.*, 2017). This would further our understanding of the link between genotype and phenotype of the virus with a view to understand better its mechanisms of pathology.

In order to address the second objective of this thesis, phylogenetic classification, a new amplicon-based protocol and bioinformatics pipeline for whole genome amplification of HPIV3 was developed and validated. It was shown that the clinical strain library generated during this project was phylogenetically diverse, however no whole genome data could be obtained directly from clinical sample. Therefore as part of further investigation into the phylogenetic diversity of this virus, and with new cheaper sequencing techniques becoming more available (Jain *et al.*, 2016; Faria *et al.*, 2017), the aim in the future would be to develop a protocol to obtain whole length genome sequences directly from clinical samples and compare these with the sequences obtained in this project. It is likely that limited variability detected in the samples in this project is a reflection of a genetic bottleneck encountered during initial limited cell culture passage. Recent advances in nanopore sequencing technology could be used to obtain high quality sequences in samples as well as to identify sites of nucleoside analogue incorporation for detailed inhibitor research (Garalde *et al.*, 2018; Keller *et al.*, 2018).

As whole genome amplification is procedurally and financially difficult in a clinical setting, a method for epidemiological and phylogenetic classification of HPIV3 was developed. Unlike previously published methods (Almajhdi, Alshaman and Amer, 2012; Goya, Mistchenko and Viegas, 2016; Košutić-Gulija *et al.*, 2017), it did not rely on a protein coding region of the genome but on the most variable one. It is interesting to note that the region of the genome thus identified was the intergenic M-F region and the phylogenetic analysis carried out with it yielded the same clustering results as that obtained using the whole genome sequence. This approach was markedly different from previously published studies (Almajhdi, Alshaman and Amer, 2012; Goya, Mistchenko and Viegas, 2016; Košutić-Gulija *et al.*, 2017), as it directly compared the phylogenetic analysis between the fragment of the genome and whole genome data. However it did not provide any insights into a more meaningful function-based classification of HPIV3, relying instead on clustering based on sequence similarity as before (Mao *et al.*, 2012; Puillandre *et al.*, 2012; Kekkonen *et al.*, 2015). A more meaningful approach would require a greater understanding of the relationship between genotype and phenotype *in vivo* potentially involving

both a greater library of clinical strains as well as a more controlled system involving reverse genetics.

Nonetheless the method developed in this project was successfully applied to identify a point source outbreak on a paediatric oncology ward. Infection control approaches as well as outbreak identification tools were evaluated in this context. In addition to well established infection control procedures, supplementary measures centered on limiting social contact and play areas, that would inevitably have a deleterious effect on the mental wellbeing of paediatric patients (Baier *et al.*, 2018) were discussed. These additional interventions would necessitate a re-evaluation of the benefits and drawbacks of such an arrangement (Koutlakis-Barron and Hayden, 2016; Beuvink, 2018). A review of literature available on the morbidity and mortality of HPIV3 in the paediatric immunocompromised cohort has shown that there is no consensus on the severity of HPIV3 impact in this patient population (Piralla *et al.*, 2009; Ustun *et al.*, 2012; Torres *et al.*, 2016; Santolaya *et al.*, 2017). The scarcity of data available, combined with different conclusions presented, provides additional evidence that there may be different circulating strains with different clinical impact. Therefore any fundamental change to infection control procedures would entail a more systematic re-evaluation of the data available on the clinical impact of HPIV3 in the paediatric population against the potential benefit of introducing additional measures for the prevention and control of HPIV3 in the hospital setting.

The final goal of this project was to evaluate potential therapeutic candidates for HPIV3. The inhibitors chosen for this purpose were ribavirin, favipiravir and zanamivir. Previous research on HPIV3 inhibitors has been conducted on significantly laboratory adapted strains with no data on the susceptibility of clinical strains available. Consequently in this project, an *in vivo* model using diverse clinical strains was set up. Ribavirin has been shown to be a good inhibitor of culture adapted strains of HPIV3 *in vitro* in numerous studies (Leyssen *et al.*, 2005) and has previously been used to treat respiratory infections with this virus (Chakrabarti *et al.*, 2000; Falsey, 2012), although recent data does not suggest a significant impact on morbidity and mortality in a clinical setting (Seo *et al.*, 2014). Favipiravir, like ribavirin is a nucleoside analogue

(Vanderlinden *et al.*, 2016). It has been shown to be effective against laboratory strains of HPIV3 in small animal models as well as *in vitro* (Mentré *et al.*, 2015; Jochmans *et al.*, 2016; Madelain *et al.*, 2016; Nguyen *et al.*, 2017). Zanamivir is a neuraminidase inhibitor, licensed against influenza (Mckimm-Breschkin, 2013). It has previously been evaluated against laboratory strains of HPIV3 and has been considered a candidate for treatment because of the similarities in the structure of the neuraminidase binding pockets of influenza and parainfluenza (Greengard *et al.*, 2000; Lawrence *et al.*, 2004). Overall, all of these inhibitors appeared to be promising therapeutic candidates. Therefore, in this project, they were evaluated against 9 diverse clinical strains of HPIV3, as well as in the laboratory adapted strain. Additionally a review of the data available on the bioavalability of these drugs was conducted in order to evaluate their suitability for clinical use.

Clinical strains were shown to be at least as susceptible to favipiravir and ribavirin as the laboratory strain. However the clinical bioavailability of ribavirin quoted in the literature may be insufficient to reach the required EC_{50} and EC_{90} values in a clinical scenario (ICN Pharmaceuticals, Inc, Costa Mesa, California, USA, no date). This is reflected by its lack of efficacy as treatment against HPIV3 in a clinical setting (Seo *et al.*, 2014). On the other hand, although there is limited data on the bioavailablity of favipiravir, studies on the pharmacokinetics of this drug in Ebola virus infection demonstrate that there is a potential to reach required therapeutic levels in patients (Sissoko *et al.*, 2016; Nguyen *et al.*, 2017). Coupled with an excellent toxicity profile, favipiravir should be considered as a potential therapeutic candidate for HPIV3 in the future. It is important to remember that nucleoside analogues such as favipiravir have the potential to affect target viruses through both direct mutagenic (Arias, Thorne and Goodfellow, 2014) and indirect mechanisms (Vanderlinden *et al.*, 2016). Further investigations such as, for example, direct RNA sequencing (Garalde *et al.*, 2018) would be required to elucidate the relative contribution of each.

Interestingly, it was observed that clinical strains, on the whole, were more susceptible to zanamivir that the laboratory adapted reference strain. This was attributed to the impaired neuraminidase function of the laboratory strain. This hypothesis was based on the significantly larger plaque phenotype exhibited by

this strain as well as by the N556D variant in the HN protein, that is associated with a five fold decrease in neuraminidase function (Murrell *et al.*, 2003; Palermo *et al.*, 2016). Unfortunately the levels required for clinical strain inhibition *in vitro* would be unattainable *in vivo* (Cass, Efthymiopoulos and Bye, 1999) and therefore without further advances in drug absorbance or delivery, this drug was not considered to be a viable option. However it is worth noting that zanamivir was developed against a similar but not identical protein in a different virus (Mckimm-Breschkin, 2013), as such its efficacy against HPIV3 suggests that inhibitors designed to target HPIV3 HN specifically would be a fruitful avenue for future research (Guillon *et al.*, 2014).

It is important to have a robust model for trialing of potential therapeutic candidates for any pathogen. In this project an *in vitro* model, using cell culture was described. Other options would include an *ex vivo* model using primary cell lines or small animal models. Hamsters (Crookshanks-Newman and Belshe, 1986; Greer *et al.*, 2007; Jochmans *et al.*, 2016), cotton rats (Porter *et al.*, 1991; Prince and Porter, 1996; Ottolini *et al.*, 2002) and ferrets (Mascoli *et al.*, 1976) have previously been used for this purpose for HPIV3. However, so far there have been no models based on HAE cells, although some work has been done on the benefits of antibiotic treatment in influenza A (Yamaya *et al.*, 2010) and on immunomodulatory treatment of rhinovirus infections (Jiang *et al.*, 2016). As these are considered a very powerful *ex vivo* model for respiratory viral replication (Yamaya *et al.*, 2002) the next logical step would be to repeat the work described above in this model. Additionally, as HAE cells provide both an apical and basolateral approach, it would provide the opportunity to look for different methods of drug delivery and correlate the basolateral concentrations achieved (systemic delivery) with the apical ones (topical/inhaled delivery). This model would also allow to trial other approaches to treatment including immunomodulation and provide a more complete review of the pathology in the lung, focusing on mucus production, cilia motility and cell shedding (Zhang *et al.*, 2005; Schaap-Nutt *et al.*, 2012).

Overall in this project, diverse UK circulating strains of HPIV3 were characterized according to phenotype and genotype. We have found evidence that clinical strains demonstrate different plaque phenotypes in immortalised

cell culture and in an *ex vivo* model, both in terms of growth kinetics as well as in terms of the immune response triggered. It was also observed that the phenotype exhibited by the clinical strains was markedly different from that of the significantly culture adapted laboratory strain MK9. A phylogenetic analysis did not identify a specific UK strain, but confirmed that many different strains circulate at any one time with new strains emerging. An evolutionary rate site by site analysis of the HPIV3 genome was used to identify a hypervariable region. This region was shown to be suitable for phylogenetic and epidemiological monitoring of this virus. These results were then used to develop a nested PCR protocol that was applied to outbreak tracking on a paediatric oncology unit. Finally, three therapeutic candidates were evaluated against 9 diverse clinical strains of HPIV3 and favipiravir was identified as a good potential candidate for further research and trial in this area.

In the future, as outlined above, I would like to take advantage of the stock of well-characterised clinical strains that have been generated as part of this project to continue to study the correlation between genotype and phenotype in a primary cell model. I would like to concentrate on the clinical pathology caused by diverse strains of this virus by working with HAE cell culture models reflecting both the healthy population as well as more vulnerable cohorts such as asthma, COPD or smoking. Additionally, I would like to work with a reverse genetic model of HPIV3 (Beaty *et al.*, 2017) in order to correlate pathogenicity and fitness in specific hosts. My aim would be to elucidate whether particular strains of HPIV3 would have the potential to be more pathogenic depending on clinical background.

A further future goal would be to optimise the sequencing protocol employed in this thesis with the aim of ultimately sequencing directly from clinical samples. To start with, I would like to evaluate different methods of extracting RNA including magnetic bead extraction to maximise RNA yield (He *et al.*, 2017), followed by 3rd generation sequencing strategies, such as Oxford Nanopore (Lu, Giordano and Ning, 2016). Data, thus obtained would greatly enhance the phylogenetic analysis conducted in this thesis that relied on minimally passaged clinical strains. This approach would also provide a different perspective on outbreak tracking, particularly when using Phyloscanner (Wymant *et al.*, 2018),

which would allow to infer transmission within and between hosts in larger outbreaks.

In the long run, I would like to work on therapeutics for HPIV3, looking at new therapies (Chen *et al.*, 2011) as well potential synergistic approaches (Bailly *et al.*, 2016), using the above to refine the model developed in this project.

References

Adachi, A. and Miura, T. (2014) 'Animal model studies on viral infections', *Frontiers in Microbiology*, 5(DEC), pp. 2013–2014. doi: 10.3389/fmicb.2014.00672.

Adderson, E. *et al.* (2015) 'Safety and immunogenicity of an intranasal sendai virus-based human parainfluenza virus type 1 vaccine in 3- to 6-year-old children.', *Clinical and vaccine immunology : CVI*, 22(3), pp. 298–303. doi: 10.1128/CVI.00618-14.

Aitken, C. and Jeffries, D. J. (2001) 'Nosocomial spread of viral disease.', *Clinical microbiology reviews*, 14(3), pp. 528–46. doi: 10.1128/CMR.14.3.528-546.2001.

Alayyoubi, M. *et al.* (2015) 'Structure of the paramyxovirus parainfluenza virus 5 nucleoprotein–RNA complex', *Proceedings of the National Academy of Sciences*, 112(14), pp. E1792–E1799. doi: 10.1073/pnas.1503941112.

Aliyu, Z. Y. *et al.* (2015) 'Low Morbidity but Prolonged Viral Shedding Characterize Parainfluenza Virus 3 Infections in Allogeneic Peripheral Stem Cell Transplant Recipients.', *Blood*, 104(11). Available at: http://www.bloodjournal.org/content/104/11/2234?sso-checked=true (Accessed: 18 October 2017).

Almajhdi, F. N. (2015) 'Hemagglutinin-neuraminidase gene sequence-based reclassification of human parainfluenza virus 3 variants.', *Intervirology*, 58(1), pp. 35–40. doi: 10.1159/000369208.

Almajhdi, F. N., Alshaman, M. S. and Amer, H. M. (2012) 'Molecular Characterization and Phylogenetic Analysis of Human Parainfluenza Virus Type 3 Isolated From Saudi Arabia', *Journal of medical virology*, 84(84), pp. 1304–11. doi: 10.1002/jmv.23326.

Alymova, I. V. *et al.* (2004) 'Efficacy of Novel Hemagglutinin-Neuraminidase Inhibitors BCX 2798 and BCX 2855 against Human Parainfluenza Viruses In Vitro and In Vivo', *Antimicrobial Agents and Chemotherapy*, 48(5), pp. 1495–1502. doi: 10.1128/AAC.48.5.1495-1502.2004.

Alymova, I. V. *et al.* (2005) 'The novel parainfluenza virus hemagglutinin-neuraminidase inhibitor BCX 2798 prevents lethal synergism between a paramyxovirus and Streptococcus pneumoniae', *Antimicrobial Agents and Chemotherapy*, 49(1), pp. 398–405. doi: 10.1128/AAC.49.1.398-405.2005.

Andrews, S. (2018) 'FastQC A Quality Control tool for High Throughput Sequence Data', *http://www.bioinformatics.babraham.ac.uk/projects/fastqc/*, p. Version 0.11.7. Available at: citeulike-article-id:11583827.

Ansun BioPharma, S. D. (2017) *Ansun BioPharma Announces Breakthrough Designation for its Experimental Drug DAS181*, *October 10*. Available at: https://www.prnewswire.com/news-releases/ansun-biopharma-announces-breakthrough-designation-for-its-experimental-drug-das181-300533677.html (Accessed: 20 February 2018).

Arias, A. *et al.* (2016) 'Rapid outbreak sequencing of Ebola virus in Sierra Leone identifies transmission chains linked to sporadic cases', *Virus Evolution*. Oxford University Press, 2(1), p. vew016. doi: 10.1093/ve/vew016.

Arias, A., Thorne, L. and Goodfellow, I. (2014) 'Favipiravir elicits antiviral mutagenesis during virus replication in vivo', *eLife*. eLife Sciences Publications Limited, 3, p. e03679. doi: 10.7554/eLife.03679.

Ayres, D. L. *et al.* (2012) 'BEAGLE: An Application Programming Interface and High-Performance Computing Library for Statistical Phylogenetics', *Systematic Biology*, 61(1), pp. 170–173. doi: 10.1093/sysbio/syr100.

Baier, C. *et al.* (2018) 'Molecular characteristics and successful management of a respiratory syncytial virus outbreak among pediatric patients with hemato-oncological disease', *Antimicrobial Resistance and Infection Control*. Antimicrobial Resistance & Infection Control, 7(1), pp. 1–10. doi: 10.1186/s13756-018-0316-2.

Bailly, B. *et al.* (2016) 'A dual drug regimen synergistically blocks human parainfluenza virus infection.', *Scientific reports*. Nature Publishing Group, 6, p. 24138. doi: 10.1038/srep24138.

Balloy, V. *et al.* (2015) 'Normal and Cystic Fibrosis Human Bronchial Epithelial

Cells Infected with Pseudomonas aeruginosa Exhibit Distinct Gene Activation Patterns.', *PloS one*, 10(10), p. e0140979. doi: 10.1371/journal.pone.0140979.

Banach, B. *et al.* (2009) 'Human airway epithelial cell culture to identify new respiratory viruses: Coronavirus NL63 as a model', *Journal of Virological Methods*, 156(1–2), pp. 19–26. doi: 10.1016/j.jviromet.2008.10.022.

Barik, S. (1993) 'The structure of the 5' terminal cap of the respiratory syncytial virus mRNA', *Journal of General Virology*, 74(3), pp. 485–490. doi: 10.1099/0022-1317-74-3-485.

Battisti, A. J. *et al.* (2012) 'Structure and assembly of a paramyxovirus matrix protein', *Proceedings of the National Academy of Sciences*, 109(35), pp. 13996–14000. doi: 10.1073/pnas.1210275109.

Beaty, S. M. *et al.* (2017) 'Efficient and Robust Paramyxoviridae Reverse Genetics Systems', *mSphere*, 2(2), p. 16. doi: 10.1128/mSphere.00376-16.

Belshe, R. B. *et al.* (1992) 'Evaluation of a live attenuated, cold-adapted parainfluenza virus type 3 vaccine in children', *Journal of Clinical Microbiology*, 30(8), pp. 2064–2070.

Belshe, R. B. *et al.* (2004) 'Phase 2 evaluation of parainfluenza type 3 cold passage mutant 45 live attenuated vaccine in healthy children 6-18 months old', *The Journal of Infectious Diseases*, 189(3), pp. 462–470. doi: 10.1086/381184.

Belshe, R. B. and Hissom, F. K. (1982) 'Cold adaptation of parainfluenza virus type 3: Induction of three phenotypic markers', *Journal of Medical Virology*. Wiley Subscription Services, Inc., A Wiley Company, 10(4), pp. 235–242. doi: 10.1002/jmv.1890100403.

Benites, E. C. A. *et al.* (2014) 'Acute respiratory viral infections in pediatric cancer patients undergoing chemotherapy', *Jornal de Pediatria*. Sociedade Brasileira de Pediatria, 90(4), pp. 370–376. doi: 10.1016/j.jped.2014.01.006.

Berrueco, R. *et al.* (2013) 'Multiplex real-time PCR for prompt diagnosis of an outbreak of human parainfluenza 3 virus in children with acute leukemia', *Infection*, 41(6), pp. 1171–1175. doi: 10.1007/s15010-013-0498-8.

Berthold, M. R. *et al.* (2008) 'KNIME: The Konstanz Information Miner BT - Data Analysis, Machine Learning and Applications', in Preisach, C. et al. (eds). Berlin, Heidelberg: Springer Berlin Heidelberg, pp. 319–326.

Beuvink, Y. (2018) 'Are infection control measures helpful in reducing paediatric ward infections ?', *Paediatrics and Child Health*. Elsevier Ltd, pp. 1–7. doi: 10.1016/j.paed.2018.04.004.

Blaney, J. E. *et al.* (2002) 'Genetic Basis of Attenuation of Dengue Virus Type 4 Small Plaque Mutants with Restricted Replication in Suckling Mice and in SCID Mice Transplanted with Human Liver Cells', *Virology*, 300(1), pp. 125–139. doi: https://doi.org/10.1006/viro.2002.1528.

Boukhvalova, M. S., Prince, G. A. and Blanco, J. C. G. (2009) 'The cotton rat model of respiratory viral infections.', *Biologicals : journal of the International Association of Biological Standardization*, 37(3), pp. 152–9. doi: 10.1016/j.biologicals.2009.02.017.

Bowden, MD, R. A. (1997) 'Respiratory Virus Infections After Marrow Transplant: The Fred Hutchinson Cancer Research Center Experience', *The American Journal of Medicine*, 102(3), pp. 27–30. doi: 10.1016/S0002-9343(97)00007-7.

Bracken, M. K. *et al.* (2016) 'Viral protein requirements for assembly and release of human parainfluenza virus type 3 viruslike particles', *Journal of General Virology*, 97(6), pp. 1305–1310. doi: 10.1099/jgv.0.000449.

Brady, M. T., Evans, J. and Cuartas, J. (1990) 'Survival and disinfection of parainfluenza viruses on environmental surfaces', *American Journal of Infection Control*. Mosby, 18(1), pp. 18–23. doi: 10.1016/0196-6553(90)90206-8.

Bryant, J. E., Holmes, E. C. and Barrett, A. D. T. (2007) 'Out of Africa: a molecular perspective on the introduction of yellow fever virus into the Americas.', *PLoS pathogens*, 3(5), p. e75. doi: 10.1371/journal.ppat.0030075.

Butnor, K. J. and Sporn, T. A. (2003) 'Human parainfluenza virus giant cell pneumonia following cord blood transplant associated with pulmonary alveolar proteinosis', *Archives of Pathology and Laboratory Medicine*, 127(2), pp. 235–238.

doi: 10.1043/0003-9985(2003)127<235:HPVGCP>2.0.CO;2.

Caignard, G. *et al.* (2009) 'Differential regulation of type I interferon and epidermal growth factor pathways by a human Respirovirus virulence factor', *PLoS Pathogens*, 5(9). doi: 10.1371/journal.ppat.1000587.

Carlos, T. S. *et al.* (2009) 'Parainfluenza virus 5 genomes are located in viral cytoplasmic bodies whilst the virus dismantles the interferon-induced antiviral state of cells', *Journal of General Virology*, 90(9), pp. 2147–2156. doi: 10.1099/vir.0.012047-0.

Carrillo-Bustamante, P. *et al.* (2017) 'Determining Ribavirin's mechanism of action against Lassa virus infection', *Scientific Reports*, 7(1), pp. 1–12. doi: 10.1038/s41598-017-10198-0.

Cass, L. M., Efthymiopoulos, C. and Bye, A. (1999) 'Pharmacokinetics of zanamivir after intravenous, oral, inhaled or intranasal administration to healthy volunteers.', *Clinical pharmacokinetics*, 36 Suppl 1, pp. 1–11. doi: 10.2165/00003088-199936001-00001.

Ceylan, B. *et al.* (2013) 'Ribavirin is not effective against Crimean-Congo hemorrhagic fever: Observations from the Turkish experience', *International Journal of Infectious Diseases*. International Society for Infectious Diseases, 17(10), pp. e799–e801. doi: 10.1016/j.ijid.2013.02.030.

Chakrabarti, S. *et al.* (2000) 'Parainfluenza virus type 3 infections in hematopoetic stem cell transplant recipients: response to ribavirin therapy', *Clin Infect Dis*. Oxford University Press, 31(6), pp. 1516–1518. doi: CID000101 [pii]\r10.1086/317482.

Chalkias, S. *et al.* (2014) 'DAS181 treatment of hematopoietic stem cell transplant patients with parainfluenza virus lung disease requiring mechanical ventilation', *Transplant Infectious Disease*, 16(1), pp. 141–144. doi: 10.1111/tid.12177.

Chattopadhyay, S. and Banerjee, A. K. (2009) 'Phosphoprotein, P of human parainfluenza virus type 3 prevents self-association of RNA-dependent RNA

polymerase, L.', *Virology*. NIH Public Access, 383(2), pp. 226–36. doi: 10.1016/j.virol.2008.10.019.

Chen, Y. Bin *et al.* (2011) 'Treatment of parainfluenza 3 infection with das181 in a patient after allogeneic stem cell transplantation', *Clinical Infectious Diseases*, 53(7). doi: 10.1093/cid/cir501.

Chihara, J. *et al.* (2018) 'Elevation of the plasma level of RANTES during asthma attacks', *Journal of Allergy and Clinical Immunology*. Elsevier, 100(6), pp. S52–S55. doi: 10.1016/S0091-6749(97)70005-8.

Childs, K. *et al.* (2007) 'mda-5, but not RIG-I, is a common target for paramyxovirus V proteins', *Virology*, 359(1), pp. 190–200. doi: 10.1016/j.virol.2006.09.023.

Chow, E. J. and Mermel, L. A. (2017) 'Hospital-Acquired Respiratory Viral Infections: Incidence, Morbidity, and Mortality in Pediatric and Adult Patients.', *Open forum infectious diseases*. Oxford University Press, 4(1), p. ofx006. doi: 10.1093/ofid/ofx006.

Christensen, M. S., Nielsen, L. P. and Hasle, H. (2005) 'Few but severe viral infections in children with cancer: A prospective RT-PCR and PCR-based 12-month study', *Pediatric Blood and Cancer*. Wiley Subscription Services, Inc., A Wiley Company, 45(7), pp. 945–951. doi: 10.1002/pbc.20469.

Cilla, G. *et al.* (2008) 'Viruses in community-acquired pneumonia in children aged less than 3 years old: High rate of viral coinfection', *Journal of Medical Virology*, 80(10), pp. 1843–1849. doi: 10.1002/jmv.21271.

Coelingh, K. V and Winter, C. C. (1990) 'Naturally occurring human parainfluenza type 3 viruses exhibit divergence in amino acid sequence of their fusion protein neutralization epitopes and cleavage sites', *Journal of Virology*, 64(3), pp. 1329–1334. Available at: http://www.ncbi.nlm.nih.gov/pubmed/1689394.

Colombo, R. E. *et al.* (2016) 'A phase 1 randomized, double-blind, placebo-controlled, crossover trial of DAS181 (Fludase®) in adult subjects with well-controlled asthma', *BMC Infectious Diseases*, 16(1). doi: 10.1186/s12879-016-

1358-9.

Cortez, K. J. *et al.* (2001) 'Outbreak of Human Parainfluenza Virus 3 Infections in a Hematopoietic Stem Cell Transplant Population', *The Journal of Infectious Diseases*. Oxford University Press, 184(9), pp. 1093–1097. doi: 10.1086/322041.

Couch R. B., M. D. and Englund Janet A., M. D. (1997) 'Respiratory Viral Infections in Immunocompetent and Immunocompromised Persons', *The American Journal of Medicine*, 102(3, Supplement 1), pp. 2–9. doi: https://doi.org/10.1016/S0002-9343(97)00003-X.

Cox, R. M. *et al.* (2017) 'The structurally disordered paramyxovirus nucleocapsid protein tail domain is a regulator of the mRNA transcription gradient', *Science Advances*, 3(2), p. e1602350. doi: 10.1126/sciadv.1602350.

Cox, R. and Plemper, R. K. (2015) 'The paramyxovirus polymerase complex as a target for next-generation anti-paramyxovirus therapeutics.', *Frontiers in microbiology*. Frontiers Media SA, 6, p. 459. doi: 10.3389/fmicb.2015.00459.

Crookshanks-Newman, F. K. and Belshe, R. B. (1986) 'Protection of weanling hamsters from experimental infection with wild-type parainfluenza virus type 3 (para 3) by cold-adapted mutants of para 3.', *Journal of medical virology*, 18(2), pp. 131–7. Available at: http://www.ncbi.nlm.nih.gov/pubmed/3005486 (Accessed: 2 January 2016).

Crotty, S., Cameron, C. and Andino, R. (2002) 'Ribavirin's antiviral mechanism of action: Lethal mutagenesis?', *Journal of Molecular Medicine*, 80(2), pp. 86–95. doi: 10.1007/s00109-001-0308-0.

Daemer, R. J. *et al.* (1980) 'NOTES PLC / PRF / 5 (Alexander) Hepatoma Cell Line : Further', *Cell*, 30(2), pp. 607–611.

Danzmann, L. *et al.* (2013) 'Health care workers causing large nosocomial outbreaks: a systematic review.', *BMC infectious diseases*. BioMed Central, 13, p. 98. doi: 10.1186/1471-2334-13-98.

Darriba, D. *et al.* (2012) 'jModelTest 2: more models, new heuristics and parallel computing', *Nature Methods*, 9(8), pp. 772–772. doi: 10.1038/nmeth.2109.

Ding, B. *et al.* (2014) 'Phosphoprotein of human parainfluenza virus type 3 blocks autophagosome-lysosome fusion to increase virus production', *Cell Host and Microbe*. Cell Press, 15(5), pp. 564–577. doi: 10.1016/j.chom.2014.04.004.

Ding, B. *et al.* (2017) 'The Matrix Protein of Human Parainfluenza Virus Type 3 Induces Mitophagy that Suppresses Interferon Responses', *Cell Host & Microbe*. Elsevier, 21(4), p. 538–547.e4. doi: 10.1016/j.chom.2017.03.004.

Dirr, L. *et al.* (2015) 'The catalytic mechanism of human parainfluenza virus type 3 haemagglutinin-neuraminidase revealed.', *Angewandte Chemie (International ed. in English)*, 54(10), pp. 2936–40. doi: 10.1002/anie.201412243.

Dochow, M. *et al.* (2012) 'Independent structural domains in Paramyxovirus polymerase protein', *Journal of Biological Chemistry*, 287(9), pp. 6878–6891. doi: 10.1074/jbc.M111.325258.

Drummond, A. J. *et al.* (2006) 'Relaxed Phylogenetics and Dating with Confidence', *PLoS Biology*. Edited by D. Penny. Public Library of Science, 4(5), p. e88. doi: 10.1371/journal.pbio.0040088.

Drummond, A. J. *et al.* (2012) 'Bayesian phylogenetics with BEAUti and the BEAST 1.7.', *Molecular biology and evolution*. Oxford University Press, 29(8), pp. 1969–73. doi: 10.1093/molbev/mss075.

Durbin, A. P. *et al.* (1997) 'Recovery of Infectious Human Parainfluenza Virus Type 3 from cDNA', *Virology*. Academic Press, 235(2), pp. 323–332. doi: 10.1006/viro.1997.8697.

Durbin, A. P. *et al.* (1999) 'Mutations in the C, D, and V open reading frames of human parainfluenza virus type 3 attenuate replication in rodents and primates', *Virology*, 261(2), pp. 319–330. doi: 10.1006/viro.1999.9878.

Dutch, R. E. *et al.* (2001) 'Paramyxovirus fusion (F) protein: a conformational change on cleavage activation.', *Virology*, 281(1), pp. 138–50. doi: 10.1006/viro.2000.0817.

Elango, N. *et al.* (1986) 'Human parainfluenza type 3 virus hemagglutinin-neuraminidase glycoprotein: nucleotide sequence of mRNA and limited amino

acid sequence of the purified protein.', *Journal of virology*, 57(2), pp. 481–9. Available at: http://jvi.asm.org/content/57/2/481.full.pdf (Accessed: 4 October 2017).

Elliot, A. J., Cross, K. W. and Fleming, D. M. (2008) 'Acute respiratory infections and winter pressures on hospital admissions in England and Wales 1990-2005', *Journal of Public Health*, 30(1), pp. 91–98. doi: 10.1093/pubmed/fdn003.

Englund, J. A. (2001) 'Diagnosis and epidemiology of community-acquired respiratory virus infections in the immunocompromised host.', *Biology of blood and marrow transplantation : journal of the American Society for Blood and Marrow Transplantation*. United States, 7 Suppl, p. 2S–4S.

Enki, D. G. *et al.* (2016) 'Comparison of statistical algorithms for the detection of infectious disease outbreaks in large multiple surveillance systems', *PLoS ONE*, 11(8), pp. 1–25. doi: 10.1371/journal.pone.0160759.

Falsey, A. (2012) 'Current management of parainfluenza pneumonitis in immunocompromised patients: a review', *Infection and Drug Resistance*, p. 121. doi: 10.2147/IDR.S25874.

Faria, N. R. *et al.* (2017) 'Epidemic establishment and cryptic transmission of Zika virus in Brazil and the Americas', *BioRxiv*. Cold Spring Harbor Laboratory, pp. 1–39. doi: 10.1101/105171.

Fearns, R. and Deval, J. (2016) 'New antiviral approaches for respiratory syncytial virus and other mononegaviruses: Inhibiting the RNA polymerase', *Antiviral Research*, 134, pp. 63–76. doi: https://doi.org/10.1016/j.antiviral.2016.08.006.

Feghaly, R. E. El *et al.* (2012) 'Local production of inflammatory mediators during childhood parainfluenza virus infection', *Pediatric Infectious Disease Journal*, 29(4), pp. 1–17. doi: 10.1097/INF.0b013e3181d5da2a.Local.

Ferreira, M. A. R. and Suchard, M. A. (2008) 'Bayesian analysis of elapsed times in continuous-time Markov chains', *Canadian Journal of Statistics*. Wiley-Blackwell, 36(3), pp. 355–368. doi: 10.1002/cjs.5550360302.

Fields, B. N., Knipe, D. M. and Howley, P. M. (2013) *Fields virology*. Philadelphia: Wolters Kluwer Health/Lippincott Williams & Wilkins.

Figlerowicz, M. *et al.* (2003) 'Genetic variability: The key problem in the prevention and therapy of RNA-based virus infections', *Medicinal Research Reviews*. Wiley Subscription Services, Inc., A Wiley Company, 23(4), pp. 488–518. doi: 10.1002/med.10045.

Flight, W. and Jones, A. (2017) 'The diagnosis and management of respiratory viral infections in cystic fibrosis', *Expert Review of Respiratory Medicine*, 11(3), pp. 221–227. doi: 10.1080/17476348.2017.1288102.

Fukushima, K. *et al.* (2011) 'Plaque formation assay for human parainfluenza virus type 1.', *Biological & pharmaceutical bulletin*, 34(7), pp. 996–1000. Available at: http://www.ncbi.nlm.nih.gov/pubmed/21720003 (Accessed: 2 January 2016).

Fukushima, K. *et al.* (2014) 'Terminal sialic acid linkages determine different cell infectivities of human parainfluenza virus type 1 and type 3.', *Virology*. Elsevier, 464–465, pp. 424–431. doi: 10.1016/j.virol.2014.07.033.

Fulcher, M. L. *et al.* (2005) 'Well-Differentiated Human Airway Epithelial Cell Cultures BT - Human Cell Culture Protocols', in Picot, J. (ed.). Totowa, NJ: Humana Press, pp. 183–206. doi: 10.1385/1-59259-861-7:183.

Furuta, Y. *et al.* (2013) 'Favipiravir (T-705), a novel viral RNA polymerase inhibitor', *Antiviral Research*. Elsevier B.V., 100(2), pp. 446–454. doi: 10.1016/j.antiviral.2013.09.015.

Galinski, M. S., Mink, M. A. and Pons, M. W. (1988) 'Molecular cloning and sequence analysis of the human parainfluenza 3 virus gene encoding the L protein', *Virology*, 165(2), pp. 499–510. doi: 10.1016/0042-6822(88)90594-6.

Galinski, M. S. and Wechsler, S. L. (1991) 'The Molecular Biology of the Paramyxovirus Genus BT - The Paramyxoviruses', in Kingsbury, D. W. (ed.). Boston, MA: Springer US, pp. 41–82. doi: 10.1007/978-1-4615-3790-8_2.

Garalde, D. R. *et al.* (2018) 'Highly parallel direct RN A sequencing on an array of

nanopores', *Nature Methods*. Nature Publishing Group, 15(3), pp. 201–206. doi: 10.1038/nmeth.4577.

Gern, J. E. *et al.* (2002) 'Relationships among specific viral pathogens, virus-induced interleukin-8, and respiratory symptoms in infancy', *Pediatric Allergy and Immunology*, 13(6), pp. 386–393. doi: 10.1034/j.1399-3038.2002.01093.x.

Goins, W. P., Talbot, H. K. and Talbot, T. R. (2011) 'Health Care–Acquired Viral Respiratory Diseases', *Infectious Disease Clinics of North America*. Elsevier, 25(1), pp. 227–244. doi: 10.1016/J.IDC.2010.11.010.

Gowen, B. B. *et al.* (2015) 'Alterations in favipiravir (T-705) pharmacokinetics and biodistribution in a hamster model of viral hemorrhagic fever', *Antiviral Research*. Elsevier, 121, pp. 132–137. doi: 10.1016/j.antiviral.2015.07.003.

Goya, S., Mistchenko, A. S. and Viegas, M. (2016) 'Phylogenetic and molecular analyses of human parainfluenza type 3 virus in Buenos Aires, Argentina, between 2009 and 2013: The emergence of new genetic lineages', *Infection, Genetics and Evolution*, 39, pp. 85–91. doi: 10.1016/j.meegid.2016.01.002.

Green, M. G., Huey, D. and Niewiesk, S. (2013) 'The cotton rat (Sigmodon hispidus) as an animal model for respiratory tract infections with human pathogens.', *Lab animal*. Nature Publishing Group, 42(5), pp. 170–6. doi: 10.1038/laban.188.

Greenberg, D. P. *et al.* (2005) 'A Bovine Parainfluenza Virus Type 3 Vaccine Is Safe and Immunogenic in Early Infancy', *The Journal of Infectious Diseases*, 191(7), pp. 1116–1122. doi: 10.1086/428092.

Greengard, O. *et al.* (2000) 'The anti-influenza virus agent 4-GU-DANA (zanamivir) inhibits cell fusion mediated by human parainfluenza virus and influenza virus HA.', *Journal of virology*. American Society for Microbiology, 74(23), pp. 11108–11114. doi: 10.1128/JVI.74.23.11108-11114.2000.

Greer, C. E. *et al.* (2007) 'Long-term protection in hamsters against human parainfluenza virus type 3 following mucosal or combinations of mucosal and systemic immunizations with chimeric alphavirus-based replicon particles.',

Scandinavian journal of immunology, 66(6), pp. 645–53. doi: 10.1111/j.1365-3083.2007.02019.x.

Greninger, A. L. *et al.* (2017) 'Rapid Metagenomic Next-Generation Sequencing during an Investigation of Hospital-Acquired Human Parainfluenza Virus 3 Infections', *Journal of Clinical Microbiology*. Edited by A. J. McAdam, 55(1), pp. 177–182. doi: 10.1128/JCM.01881-16.

Gruenert, D. C., Finkbeiner, W. E. and Widdicombe, J. H. (1995) 'Culture and transformation of human airway epithelial cells.', *The American journal of physiology*, 268(3 Pt 1), pp. L347-60. Available at: file://i/Chercheurs/Brochiero_Emmanuelle/Brochiero/Ref Manager/1400/1463.pdf%5Cnhttp://www.ncbi.nlm.nih.gov/pubmed/7900815.

Guillon, P. *et al.* (2014) 'Structure-guided discovery of potent and dual-acting human parainfluenza virus haemagglutinin–neuraminidase inhibitors', *Nature Communications*. Nature Publishing Group, 5, p. 5268. doi: 10.1038/ncomms6268.

Günther, S. and Lenz, O. (2004) 'Lassa Virus', *Critical Reviews in Clinical Laboratory Sciences*. Taylor & Francis, 41(4), pp. 339–390. doi: 10.1080/10408360490497456.

Guo, P. (2013) 'Suppression of Interferon-Mediated Antiviral Immunity by Hepatitis B Virus: An Overview of Research Progress', *Scandinavian Journal of Immunology*, 78(3), pp. 230–237. doi: 10.1111/sji.12086.

Habibi, M. S. and Openshaw, P. J. M. (2012) 'Benefit and harm from immunity to respiratory syncytial virus: implications for treatment.', *Current opinion in infectious diseases*, 25(6), pp. 687–94. doi: 10.1097/QCO.0b013e32835a1d92.

Hall, C. B. *et al.* (1983) 'Aerosolized Ribavirin Treatment of Infants with Respiratory Syncytial Viral Infection', *New England Journal of Medicine*. Massachusetts Medical Society , 308(24), pp. 1443–1447. doi: 10.1056/NEJM198306163082403.

Haller, A. A. *et al.* (2000) 'Expression of the surface glycoproteins of human

parainfluenza virus type 3 by bovine parainfluenza virus type 3, a novel attenuated virus vaccine vector.', *Journal of virology*, 74(24), pp. 11626–35. doi: 10.1128/JVI.74.24.11626-11635.2000.

Hawthorne, J. D. and Albrecht, P. (1981) 'Sensitive plaque neutralization assay for parainfluenza virus types 1, 2, and 3 and respiratory syncytial virus.', *Journal of clinical microbiology*, 13(4), pp. 730–7. Available at: http://www.pubmedcentral.nih.gov/articlerender.fcgi?artid=273869&tool=pmcentrez&rendertype=abstract (Accessed: 2 January 2016).

Hayden, F. (2009) 'Developing new antiviral agents for influenza treatment: what does the future hold?', *Clinical infectious diseases : an official publication of the Infectious Diseases Society of America*, 48 Suppl 1, pp. S3-13. doi: 10.1086/591851.

Hayden, F. G. (2013) 'Advances in antivirals for non-influenza respiratory virus infections.', *Influenza and other respiratory viruses*, 7 Suppl 3, pp. 36–43. doi: 10.1111/irv.12173.

He, H. *et al.* (2017) 'Integrated DNA and RNA extraction using magnetic beads from viral pathogens causing acute respiratory infections', *Scientific Reports*. Nature Publishing Group, 7(February), pp. 1–8. doi: 10.1038/srep45199.

Heggeness, M. H. *et al.* (1980) 'Conformation of the helical nucleocapsids of paramyxoviruses and vesicular stomatitis virus: reversible coiling and uncoiling induced by changes in salt concentration.', *Proceedings of the National Academy of Sciences of the United States of America*. National Academy of Sciences, 77(5), pp. 2631–5. doi: 10.1073/pnas.77.5.2631.

Henrickson, K. J. (2003) 'Parainfluenza viruses.', *Clinical microbiology reviews*, 16(2), pp. 242–64. doi: 10.1128/CMR.16.2.242-264.2003.

Herzog, K. D. *et al.* (1989) 'Association of parainfluenza virus type 3 infection with allograft rejection in a liver transplant recipient.', *The Pediatric infectious disease journal*, 8(8), pp. 534–6. Available at: http://www.ncbi.nlm.nih.gov/pubmed/2549495 (Accessed: 13 December 2017).

Hilton, L. *et al.* (2006) 'The NPro product of bovine viral diarrhea virus inhibits DNA binding by interferon regulatory factor 3 and targets it for proteasomal degradation.', *Journal of virology*, 80(23), pp. 11723–32. doi: 10.1128/JVI.01145-06.

Horga, M. a *et al.* (2000) 'Mechanism of interference mediated by human parainfluenza virus type 3 infection.', *Journal of virology*, 74(24), pp. 11792–11799. doi: 10.1128/JVI.74.24.11792-11799.2000.

Hosmillo, M. *et al.* (2014) 'Porcine sapovirus replication is restricted by the type I interferon response in cell culture', *Journal of General Virology*, 96(Pt_1), pp. 74–84. doi: 10.1099/vir.0.071365-0.

Howard, C. J. *et al.* (2004) 'The role of dendritic cells in shaping the immune response', *Animal Health Research Reviews*. 2007/02/01. Cambridge University Press, 5(2), pp. 191–195. doi: DOI: 10.1079/AHR200468.

Huberman, K., Peluso, R. W. and Moscona, A. (1995) 'Hemagglutinin-Neuraminidase of Human Parainfluenza 3: Role of the Neuraminidase in the Viral Life Cycle', *Virology*, 214(1), pp. 294–300. doi: 10.1006/viro.1995.9925.

ICN Pharmaceuticals, Inc, Costa Mesa, California, USA, 2000 (no date) *VIRAZOLE® (Ribavirin for Inhalation Solution, USP) [package insert],*. Available at: https://dailymed.nlm.nih.gov/dailymed/fda/fdaDrugXsl.cfm?setid=ADF16E64-345F-469A-B987-3FBDD17E0AC2&type=display (Accessed: 15 July 2017).

Jacobs, S. E. *et al.* (2013) 'Human Rhinoviruses', *Clinical Microbiology Reviews*. 1752 N St., N.W., Washington, DC: American Society for Microbiology, 26(1), pp. 135–162. doi: 10.1128/CMR.00077-12.

Jain, M. *et al.* (2016) 'The Oxford Nanopore MinION: delivery of nanopore sequencing to the genomics community', *Genome Biology*, 17(1), p. 239. doi: 10.1186/s13059-016-1103-0.

Jalal, H. *et al.* (2007) 'Molecular investigations of an outbreak of parainfluenza virus type 3 and respiratory syncytial virus infections in a hematology unit.',

Journal of clinical microbiology, 45(6), pp. 1690–6. doi: 10.1128/JCM.01912-06.

Jefferson, T. *et al.* (2014) 'Neuraminidase inhibitors for preventing and treating influenza in adults and children', in Jefferson, T. (ed.) *Cochrane Database of Systematic Reviews*. Chichester, UK: John Wiley & Sons, Ltd. doi: 10.1002/14651858.CD008965.pub4.

Jenkins, G. M. *et al.* (2002) 'Rates of molecular evolution in RNA viruses: A quantitative phylogenetic analysis', *Journal of Molecular Evolution*, 54(2), pp. 156–165. doi: 10.1007/s00239-001-0064-3.

Jia, Y. *et al.* (2007) 'Characterization of a small plaque variant of West Nile virus isolated in New York in 2000', *Virology*, 367(2), pp. 339–347. doi: https://doi.org/10.1016/j.virol.2007.06.008.

Jiang, D. *et al.* (2016) 'The Anti-inflammatory Effect of Alpha-1 Antitrypsin in Rhinovirus-infected Human Airway Epithelial Cells', *Journal of Clinical & Cellular Immunology*. OMICS International, 07(06), pp. 1–7. doi: 10.4172/2155-9899.1000475.

Jiang, S. C. *et al.* (2009) 'Evaluation of four cell lines for assay of infectious adenoviruses in water samples', *Journal of Water and Health*, 7(4), pp. 650–656. doi: 10.2166/wh.2009.088.

Jochmans, D. *et al.* (2016) 'Antiviral activity of favipiravir (T-705) against a broad range of paramyxoviruses in vitro and against human metapneumovirus in hamsters', *Antimicrobial Agents and Chemotherapy*, 60(8), pp. 4620–4629. doi: 10.1128/AAC.00709-16.

Johnson, L. *et al.* (2013) 'MUC5AC and inflammatory mediators associated with respiratory outcomes in the British 1946 birth cohort.', *Respirology (Carlton, Vic.)*. Wiley-Blackwell, 18(6), pp. 1003–10. doi: 10.1111/resp.12092.

Karin Jorga, C. *et al.* (2006) 'Pharmacokinetics of ribavirin in patients with hepatitis C virus', *British Journal of Clinical Pharmacology Br J Clin Pharmacol*, 626, pp. 710–714. doi: 10.1111/j.1365-2125.2006.02704.x.

Karron, R. A. *et al.* (1996) 'Evaluation of a live attenuated bovine parainfluenza

type 3 vaccine in two- to six-month-old infants', *The Pediatric Infectious Disease Journal*, 15(8). Available at: https://journals.lww.com/pidj/Fulltext/1996/08000/Evaluation_of_a_live_attenuated_bovine.3.aspx.

Karron, R. A. *et al.* (2003) 'A live human parainfluenza type 3 virus vaccine is attenuated and immunogenic in young infants', *Pediatric Infectious Disease Journal*, 22(5), pp. 394–405. doi: 10.1097/00006454-200305000-00002.

Kato, A. *et al.* (1997) 'The paramyxovirus, Sendai virus, V protein encodes a luxury function required for viral pathogenesis.', *The EMBO Journal*, 16(3), pp. 578–587. doi: 10.1093/emboj/16.3.578.

Kato, A. *et al.* (1999) 'Sendai virus gene start signals are not equivalent in reinitiation capacity: moderation at the fusion protein gene', *J Virol*, 73(11), p. 9237–46.

Kekkonen, M. *et al.* (2015) 'Delineating species with DNA barcodes: A case of Taxon dependent method performance in moths', *PLoS ONE*, 10(4). doi: 10.1371/journal.pone.0122481.

Keller, M. W. *et al.* (2018) 'Complete genome direct RNA sequencing of influenza A virus', *bioRxiv*, p. 300384. doi: 10.1101/300384.

Kiang, D. *et al.* (2007) 'Molecular characterization of a variant rhinovirus from an outbreak associated with uncommonly high mortality', *Journal of Clinical Virology*. Elsevier, 38(3), pp. 227–237. doi: 10.1016/j.jcv.2006.12.016.

Kihira, S. *et al.* (2014) 'Ribavirin inhibits human parainfluenza virus type 2 replication in vitro', *Microbiology and Immunology*, 58(11), pp. 628–635. doi: 10.1111/1348-0421.12192.

Kim, T. *et al.* (2017) 'Molecular epidemiology and environmental contamination during an outbreak of parainfluenza virus 3 in a haematology ward', *Journal of Hospital Infection*, 97(4), pp. 403–413. doi: 10.1016/j.jhin.2017.09.003.

Kim, Y.-I. *et al.* (2015) 'Relating plaque morphology to respiratory syncytial virus subgroup, viral load, and disease severity in children', *Pediatric research*, 78(4),

pp. 380–388. doi: 10.1038/pr.2015.122.

King, A. M. Q. (2012) *Virus taxonomy : classification and nomenclature of viruses : ninth report of the International Committee on Taxonomy of Viruses*. London: Academic Press.

Koch, S. *et al.* (1984) 'The genetic organization of integrated hepatitis B virus DNA in the human hepatoma cell line PLC/PRF/5.', *Nucleic Acids Research*, 12(17), pp. 6871–6886. Available at: http://www.ncbi.nlm.nih.gov/pmc/articles/PMC320123/.

Košutić-Gulija, T. *et al.* (2017) 'Genetic analysis of human parainfluenza virus type 3 obtained in Croatia, 2011–2015', *Journal of Medical Microbiology*. Microbiology Society, 66(4), pp. 502–510. doi: 10.1099/jmm.0.000459.

Kothari, A. *et al.* (2017) 'The role of next generation sequencing in infection prevention in human parainfluenza virus 3 infections in immunocompromised patients', *Journal of Clinical Virology*, 92, pp. 53–55. doi: 10.1016/j.jcv.2017.05.010.

Koul, P. A. *et al.* (2014) 'Differences in influenza seasonality by latitude, Northern India', *Emerging Infectious Diseases*, 20(10), pp. 1723–1726. doi: 10.3201/eid2010.140431.

Koutlakis-Barron, I. and Hayden, T. A. (2016) 'Essentials of infection prevention in the pediatric population', *International Journal of Pediatrics and Adolescent Medicine*. Elsevier Ltd, 3(4), pp. 143–152. doi: 10.1016/j.ijpam.2016.10.002.

Kuhn, J. H. *et al.* (2013) 'Nyamiviridae: Proposal for a new family in the order Mononegavirales', *Archives of Virology*, 158(10), pp. 2209–2226. doi: 10.1007/s00705-013-1674-y.

Kumar, S., Stecher, G. and Tamura, K. (2016) 'MEGA7: Molecular Evolutionary Genetics Analysis Version 7.0 for Bigger Datasets', *Molecular Biology and Evolution*, 33(7), pp. 1870–1874. Available at: http://dx.doi.org/10.1093/molbev/msw054.

Lamb, R. a., Paterson, R. G. and Jardetzky, T. S. (2006) 'Paramyxovirus membrane

fusion: Lessons from the F and HN atomic structures', *Virology*, 344(1), pp. 30–37. doi: 10.1016/j.virol.2005.09.007.

Langmead, B. and Salzberg, S. L. (2012) 'Fast gapped-read alignment with Bowtie 2', *Nature Methods*. Nature Research, 9(4), pp. 357–359. doi: 10.1038/nmeth.1923.

Lawrence, M. C. *et al.* (2004) 'Structure of the Haemagglutinin-neuraminidase from Human Parainfluenza Virus Type III', *Journal of Molecular Biology*, 335(5), pp. 1343–1357. doi: 10.1016/j.jmb.2003.11.032.

Lebossé, F. *et al.* (2017) 'Intrahepatic innate immune response pathways are downregulated in untreated chronic hepatitis B', *Journal of Hepatology*, 66(5), pp. 897–909. doi: https://doi.org/10.1016/j.jhep.2016.12.024.

Leclère, B. *et al.* (2017) 'Automated detection of hospital outbreaks: A systematic review of methods', *PLoS ONE*, 12(4), pp. 1–16. doi: 10.1371/journal.pone.0176438.

Lee, M. S. *et al.* (2001) 'Half-life of human parainfluenza virus type 3 (hPIV3) maternal antibody and cumulative proportion of hPIV3 infection in young infants.', *The Journal of infectious diseases*, 183(8), pp. 1281–4. doi: 10.1086/319690.

Lee, N. *et al.* (2017) 'Genome-wide analysis of influenza viral RNA and nucleoprotein association', *Nucleic Acids Research*. Oxford University Press, 45(15), pp. 8968–8977. doi: 10.1093/nar/gkx584.

Lewandowska-Polak, A. *et al.* (2015) 'Human parainfluenza virus type 3 (HPIV3) induces production of IFNγ and RANTES in human nasal epithelial cells (HNECs).', *Journal of inflammation (London, England)*, 12, p. 16. doi: 10.1186/s12950-015-0054-7.

Lewis, V. A. *et al.* (1996) 'Respiratory disease due to parainfluenza virus in adult bone marrow transplant recipients.', *Clinical infectious diseases : an official publication of the Infectious Diseases Society of America*, 23(5), pp. 1033–7. Available at: http://www.ncbi.nlm.nih.gov/pubmed/8922798 (Accessed: 11

October 2017).

Leyssen, P. *et al.* (2005) 'The predominant mechanism by which ribavirin exerts its antiviral activity in vitro against flaviviruses and paramyxoviruses is mediated by inhibition of IMP dehydrogenase.', *Journal of virology*, 79(3), pp. 1943–7. doi: 10.1128/JVI.79.3.1943-1947.2005.

Li, H. *et al.* (2009) 'The Sequence Alignment/Map format and SAMtools', *Bioinformatics*. Oxford University Press, 25(16), pp. 2078–2079. doi: 10.1093/bioinformatics/btp352.

Li, Z. *et al.* (2012) 'Adjusting outbreak detection algorithms for surveillance during epidemic and non-epidemic periods', *Journal of the American Medical Informatics Association*, 19(E1), pp. e51–e53. doi: 10.1136/amiajnl-2011-000126.

Liao, Y. *et al.* (2017) 'A new method for assessing the risk of infectious disease outbreak', *Scientific Reports*, 7. doi: 10.1038/srep40084.

Lindblom, A. *et al.* (2010) 'Respiratory viruses, a common microbiological finding in neutropenic children with fever', *Journal of Clinical Virology*, 47(3), pp. 234–237. doi: 10.1016/j.jcv.2009.11.026.

Lingemann, M. *et al.* (2015) 'The aberrant gene-end transcription signal of the matrix M gene of human parainfluenza virus type 3 downregulates fusion F protein expression and the F-specific antibody response in vivo.', *Journal of virology*, 89(6), pp. 3318–31. doi: 10.1128/JVI.03148-14.

Liu, W.-K. *et al.* (2013) 'Epidemiology and clinical presentation of the four human parainfluenza virus types.', *BMC infectious diseases*, 13(1), p. 28. doi: 10.1186/1471-2334-13-28.

Lu, H., Giordano, F. and Ning, Z. (2016) 'Oxford Nanopore MinION Sequencing and Genome Assembly', *Genomics, Proteomics and Bioinformatics*. Beijing Institute of Genomics, Chinese Academy of Sciences and Genetics Society of China, 14(5), pp. 265–279. doi: 10.1016/j.gpb.2016.05.004.

Madden, J. F., Burchette, J. L. and Hale, L. P. (2004) 'Pathology of parainfluenza

virus infection in patients with congenital immunodeficiency syndromes', *Human Pathology*, 35(5), pp. 594–603. doi: 10.1016/j.humpath.2003.11.012.

Maddux, A. B. and Douglas, I. S. (2015) 'Is the developmentally immature immune response in paediatric sepsis a recapitulation of immune tolerance?', *Immunology*, 145(1), pp. 1–10. doi: 10.1111/imm.12454.

Madelain, V. *et al.* (2016) 'Ebola Virus Infection: Review of the Pharmacokinetic and Pharmacodynamic Properties of Drugs Considered for Testing in Human Efficacy Trials', *Clinical Pharmacokinetics*, pp. 907–923. doi: 10.1007/s40262-015-0364-1.

Madelain, V. *et al.* (2017) 'Favipiravir pharmacokinetics in nonhuman primates and insights for future efficacy studies of hemorrhagic fever viruses', *Antimicrobial Agents and Chemotherapy*. American Society for Microbiology, 61(1), pp. e01305-16. doi: 10.1128/AAC.01305-16.

Madi, N. *et al.* (2018) 'Metagenomic analysis of viral diversity in respiratory samples from patients with respiratory tract infections in Kuwait', *Journal of Medical Virology*. Wiley Online Library, 90(3), pp. 412–420. doi: 10.1002/jmv.24984.

Maeng, S. H. *et al.* (2012) 'Impact of parainfluenza virus infection in pediatric cancer patients', *Pediatric Blood & Cancer*. Wiley Subscription Services, Inc., A Wiley Company, 59(4), pp. 708–710. doi: 10.1002/pbc.23390.

Malur, A. G., Hoffman, M. A. and Banerjee, A. K. (2004) 'The human parainfluenza virus type 3 (HPIV 3) C protein inhibits viral transcription', in *Virus Research*, pp. 199–204. doi: 10.1016/j.virusres.2003.11.009.

Mao, H. and Rosenthal, K. S. (2003) 'Strain-Dependent Structural Variants of Herpes Simplex Virus Type 1 ICP34.5 Determine Viral Plaque Size, Efficiency of Glycoprotein Processing, and Viral Release and Neuroinvasive Disease Potential', *Journal of Virology*. American Society for Microbiology, 77(6), pp. 3409–3417. doi: 10.1128/JVI.77.6.3409-3417.2003.

Mao, N. *et al.* (2012) 'Human parainfluenza virus-associated respiratory tract

infection among children and genetic analysis of HPIV-3 strains in Beijing, China.', *PloS one*, 7(8), p. e43893. doi: 10.1371/journal.pone.0043893.

Martin, M. (2011) 'Cutadapt removes adapter sequences from high-throughput sequencing reads', *EMBnet.journal*, 17(1), p. 10. doi: 10.14806/ej.17.1.200.

Mascoli, C. C. *et al.* (1976) 'Further studies on the neonatal ferret model of infection and immunity to and attenuation of human parainfluenza viruses.', *Developments in biological standardization*, 33, pp. 384–90. Available at: http://www.ncbi.nlm.nih.gov/pubmed/182598 (Accessed: 15 February 2018).

Maziarz, R. T. *et al.* (2010) 'Control of an Outbreak of Human Parainfluenza Virus 3 in Hematopoietic Stem Cell Transplant Recipients', *Biology of Blood and Marrow Transplantation*. Elsevier, 16(2), pp. 192–198. doi: 10.1016/j.bbmt.2009.09.014.

Mckimm-Breschkin, J. L. (2013) 'Influenza neuraminidase inhibitors: Antiviral action and mechanisms of resistance', *Influenza and other Respiratory Viruses*, pp. 25–36. doi: 10.1111/irv.12047.

Meidani, M. and Mirmohammad Sadeghi, S. A. (2018) 'Respiratory Viruses in Febrile Neutropenic Patients with Respiratory Symptoms.', *Advanced biomedical research*. Wolters Kluwer -- Medknow Publications, 7, p. 5. doi: 10.4103/abr.abr_433_15.

Meissner, H. C. (2016) 'Viral Bronchiolitis in Children', *New England Journal of Medicine*. Edited by J. R. Ingelfinger. Massachusetts Medical Society, 374(1), pp. 62–72. doi: 10.1056/NEJMra1413456.

Mendenhall, M. *et al.* (2011) 'Effective Oral Favipiravir (T-705) Therapy Initiated after the Onset of Clinical Disease in a Model of Arenavirus Hemorrhagic Fever', *PLoS Neglected Tropical Diseases*. Edited by D. G. Bausch. Public Library of Science, 5(10), p. e1342. doi: 10.1371/journal.pntd.0001342.

Mentré, F. *et al.* (2015) 'Dose regimen of favipiravir for Ebola virus disease.', *The Lancet. Infectious diseases*. Elsevier, 15(2), pp. 150–1. doi: 10.1016/S1473-3099(14)71047-3.

Morrison, T. G. (2003) 'Structure and function of a paramyxovirus fusion protein', *Biochimica et Biophysica Acta (BBA) - Biomembranes*, 1614(1), pp. 73–84. doi: https://doi.org/10.1016/S0005-2736(03)00164-0.

Moscona, A. (1997) 'Interaction of human parainfluenza virus type 3 with the host cell surface', *Pediatr Infect Dis J*, 16(10), pp. 917–924. doi: 10.1128/JVI.02324-15.Editor.

Moscona, A. (2005) 'Entry of parainfluenza virus into cells as a target for interrupting childhood respiratory disease', *Journal of Clinical Investigation*, 115(7), pp. 1688–1698. doi: 10.1172/JCI25669.

Moscona, A. *et al.* (2010) 'A recombinant sialidase fusion protein effectively inhibits human parainfluenza viral infection in vitro and in vivo.', *The Journal of infectious diseases*. NIH Public Access, 202(2), pp. 234–41. doi: 10.1086/653621.

Murphy, B. R. *et al.* (1988) 'Current approaches to the development of vaccines effective against parainfluenza and respiratory syncytial viruses', *Virus Research*, 11(1), pp. 1–15. doi: 10.1016/0168-1702(88)90063-9.

Murphy, T. F., Dubovi, E. J. and Clyde, W. A. (1981) 'The cotton rat as an experimental model of human parainfluenza virus type 3 disease.', *Experimental lung research*, 2(2), pp. 97–109. Available at: http://www.ncbi.nlm.nih.gov/pubmed/6268401 (Accessed: 30 December 2015).

Murrell, M. *et al.* (2003) 'Mutations in human parainfluenza virus type 3 hemagglutinin-neuraminidase causing increased receptor binding activity and resistance to the transition state sialic acid analog 4-GU-DANA (Zanamivir).', *Journal of virology*, 77(1), pp. 309–317. doi: 10.1128/JVI.77.1.309-317.2003.

El Najjar, F. *et al.* (2014) 'Paramyxovirus Glycoprotein Incorporation, Assembly and Budding: A Three Way Dance for Infectious Particle Production', *Viruses*, 6(8), pp. 3019–3054. doi: 10.3390/v6083019.

de Naurois, J. *et al.* (2010) 'Management of febrile neutropenia: ESMO Clinical Practice Guidelines', *Annals of Oncology*. Oxford University Press, 21(Supplement

5), pp. v252–v256. doi: 10.1093/annonc/mdq196.

Nei, M. and Kumar, S. (2000) *Kumar, S.: Molecular Evolution and Phylogenetics*, *Oxford University Press, New York*.

Nguyen, T. H. T. *et al.* (2017) 'Favipiravir pharmacokinetics in Ebola-Infected patients of the JIKI trial reveals concentrations lower than targeted', *PLOS Neglected Tropical Diseases*. Edited by P. W. Horby. Public Library of Science, 11(2), p. e0005389. doi: 10.1371/journal.pntd.0005389.

Nichols, W. G. (2001) 'Parainfluenza virus infections after hematopoietic stem cell transplantation: risk factors, response to antiviral therapy, and effect on transplant outcome', *Blood*. American Society of Hematology, 98(3), pp. 573–578. doi: 10.1182/blood.V98.3.573.

Nicholson, K. G. *et al.* (2014) 'Randomised controlled trial and health economic evaluation of the impact of diagnostic testing for influenza, respiratory syncytial virus and Streptococcus pneumoniae infection on the management of acute admissions in the elderly and high-risk 18- to 64-y', *Health Technology Assessment*, 18(36), pp. 1–274. doi: 10.3310/hta18360.

Nicola, G. *et al.* (2015) 'Connecting proteins with drug-like compounds: Open source drug discovery workflows with BindingDB and KNIME.', *Database : the journal of biological databases and curation*. Oxford University Press, 2015. doi: 10.1093/database/bav087.

Noton, S. L. and Fearns, R. (2015) 'Initiation and regulation of paramyxovirus transcription and replication', *Virology*, pp. 545–554. doi: 10.1016/j.virol.2015.01.014.

Okonechnikov, K., Golosova, O. and Fursov, M. (2012) 'Unipro UGENE: a unified bioinformatics toolkit', *Bioinformatics*. Oxford University Press, 28(8), pp. 1166–1167. doi: 10.1093/bioinformatics/bts091.

Onji, M. *et al.* (1989) 'Defective response to interferons in cells transfected with the hepatitis B virus genome', *Hepatology*. Wiley-Blackwell, 9(1), pp. 92–96. doi: 10.1002/hep.1840090115.

Openshaw, P. J. and Tregoning, J. S. (2005) 'Immune responses and disease enhancement during respiratory syncytial virus infection', *Clinical microbiology reviews*, 18(3), pp. 541–555. doi: 10.1128/CMR.18.3.541.

Ottolini, M. G. *et al.* (1996) 'Semi-permissive replication and functional aspects of the immune response in a cotton rat model of human parainfluenza virus type 3 infection', *Journal of General Virology*, 77, pp. 1739–1743. doi: Doi 10.1099/0022-1317-77-8-1739.

Ottolini, M. G. *et al.* (2002) 'A cotton rat model of human parainfluenza 3 laryngotracheitis: virus growth, pathology, and therapy.', *The Journal of infectious diseases*, 186(12), pp. 1713–7. doi: 10.1086/345834.

Palermo, L. M. *et al.* (2009) 'Human Parainfluenza Virus Infection of the Airway Epithelium: Viral Hemagglutinin-Neuraminidase Regulates Fusion Protein Activation and Modulates Infectivity', *Journal of Virology*, 83(13), pp. 6900–6908. doi: 10.1128/JVI.00475-09.

Palermo, L. M. *et al.* (2016) 'Features of Circulating Parainfluenza Virus Required for Growth in Human Airway', *mBio*. American Society for Microbiology (ASM), 7(2), p. e00235. doi: 10.1128/mBio.00235-16.

Palgen, J.-L. *et al.* (2015) 'Unity in diversity: shared mechanism of entry among paramyxoviruses.', *Progress in molecular biology and translational science*, 129, pp. 1–32. doi: 10.1016/bs.pmbts.2014.10.001.

Palmer, S. G. *et al.* (2012) 'Adaptation of human parainfluenza virus to airway epithelium reveals fusion properties required for growth in host tissue.', *mBio*, 3(3), p. e00137-12-. doi: 10.1128/mBio.00137-12.

Palmer, S. G. *et al.* (2014) 'Circulating clinical strains of human parainfluenza virus reveal viral entry requirements for in vivo infection.', *Journal of virology*, 88(22), pp. 13495–502. doi: 10.1128/JVI.01965-14.

Pantua, H. D. *et al.* (2006) 'Requirements for the Assembly and Release of Newcastle Disease Virus-Like Particles', *Journal of Virology*, 80(22), pp. 11062–11073. doi: 10.1128/JVI.00726-06.

Park, S. Y. *et al.* (2009) 'Parainfluenza virus 3 pneumonia in a kidney transplant recipient', *Transplant Infectious Disease*, 11(4), pp. 333–336. doi: 10.1111/j.1399-3062.2009.00387.x.

Pelecanos, A. M., Ryan, P. A. and Gatton, M. L. (2010) 'Outbreak detection algorithms for seasonal disease data: A case study using ross river virus disease', *BMC Medical Informatics and Decision Making*. BioMed Central, 10(1), p. 74. doi: 10.1186/1472-6947-10-74.

Pérez-Cidoncha, M. *et al.* (2014) 'An unbiased genetic screen reveals the polygenic nature of the influenza virus anti-interferon response.', *Journal of virology*, 88(9), pp. 4632–46. doi: 10.1128/JVI.00014-14.

Pfaller, C. K., Cattaneo, R. and Schnell, M. J. (2015) 'Reverse genetics of Mononegavirales: How they work, new vaccines, and new cancer therapeutics', *Virology*. Academic Press, 479–480, pp. 331–344. Available at: https://www.sciencedirect.com/science/article/pii/S0042682215000410 (Accessed: 20 February 2018).

Pinto, M. R., Bey, E. and Bernstein, R. (1985) 'The PLC/PRF/5 human hepatoma cell line. I. Reevaluation of the karyotype', *Cancer Genetics and Cytogenetics*, 18(1), pp. 11–18. doi: 10.1016/0165-4608(85)90033-0.

Piralla, A. *et al.* (2009) 'Multicluster nosocomial outbreak of parainfluenza virus type 3 infection in a pediatric oncohematology unit: a phylogenetic study.', *Haematologica*. Ferrata Storti Foundation, 94(6), pp. 833–9. doi: 10.3324/haematol.2008.003319.

Plotnicky-Gilquin, H. *et al.* (2001) 'Differential effects of parainfluenza virus type 3 on human monocytes and dendritic cells', *Virology*, 285(1), pp. 82–90. doi: 10.1006/viro.2001.0933.

Porotto, M. *et al.* (2001) 'Human parainfluenza virus type 3 HN-receptor interaction: effect of 4-guanidino-Neu5Ac2en on a neuraminidase-deficient variant.', *Journal of virology*, 75(16), pp. 7481–7488. doi: 10.1128/JVI.75.16.7481-7488.2001.

Porotto, M. *et al.* (2007) 'A second receptor binding site on human parainfluenza virus type 3 hemagglutinin-neuraminidase contributes to activation of the fusion mechanism.', *Journal of virology*. American Society for Microbiology, 81(7), pp. 3216–28. doi: 10.1128/JVI.02617-06.

Porotto, M. *et al.* (2010) 'Viral Entry Inhibitors Targeted to the Membrane Site of Action', *Journal of Virology*, 84(13), pp. 6760–6768. doi: 10.1128/JVI.00135-10.

Porotto, M. *et al.* (2011) 'Spring-Loaded Model Revisited: Paramyxovirus Fusion Requires Engagement of a Receptor Binding Protein beyond Initial Triggering of the Fusion Protein', *Journal of Virology*. American Society for Microbiology (ASM), 85(24), pp. 12867–12880. doi: 10.1128/JVI.05873-11.

Porotto, M., Palmer, S. G., *et al.* (2012) 'Mechanism of fusion triggering by human parainfluenza virus type III: Communication between viral glycoproteins during entry', *Journal of Biological Chemistry*, 287(1), pp. 778–793. doi: 10.1074/jbc.M111.298059.

Porotto, M., Salah, Z. W., *et al.* (2012) 'Regulation of Paramyxovirus Fusion Activation: the Hemagglutinin-Neuraminidase Protein Stabilizes the Fusion Protein in a Pretriggered State', *Journal of Virology*. American Society for Microbiology, 86(23), pp. 12838–12848. doi: 10.1128/JVI.01965-12.

Porter, D. D. *et al.* (1991) 'Pathogenesis of human parainfluenza virus 3 infection in two species of cotton rats: Sigmodon hispidus develops bronchiolitis, while Sigmodon fulviventer develops interstitial pneumonia.', *Journal of virology*, 65(1), pp. 103–11. Available at: http://www.ncbi.nlm.nih.gov/pubmed/1845878%5Cnhttp://www.pubmedcentral.nih.gov/articlerender.fcgi?artid=PMC240494.

Prince, G. A., Ottolini, M. G. and Moscona, A. (2001) 'Contribution of the human parainfluenza virus type 3 HN-receptor interaction to pathogenesis in vivo', *J Virol*, 75(24), pp. 12446–12451. doi: 10.1128/JVI.75.24.12446.

Prince, G. A. and Porter, D. D. (1996) 'Treatment of parainfluenza virus type 3 bronchiolitis and pneumonia in a cotton rat model using topical antibody and glucocorticosteroid', *Journal of Infectious Diseases*, 173(3), pp. 598–608. doi:

10.1093/infdis/173.3.598.

Puillandre, N. *et al.* (2012) 'ABGD, Automatic Barcode Gap Discovery for primary species delimitation', *Molecular Ecology*. Blackwell Publishing Ltd, 21(8), pp. 1864–1877. doi: 10.1111/j.1365-294X.2011.05239.x.

Ratnam, J. *et al.* (2014) 'The Application of the Open Pharmacological Concepts Triple Store (Open PHACTS) to Support Drug Discovery Research', *PLoS ONE*. Edited by A. Gursoy. Public Library of Science, 9(12), p. e115460. doi: 10.1371/journal.pone.0115460.

Regulation, H. O. A. in S. U. (Asru) and Department for Business, I. and S. (Bis) (2014) *Working to reduce the use of animals in scientific research*.

Risselada, R. *et al.* (2009) 'Workflows for Data Mining in Integrated multi-modal Data of Intracranial Aneurysms using KNIME', *Book of Abstracts of the R User Conference (useR!)*. Available at: https://pub.uni-bielefeld.de/publication/2603517 (Accessed: 15 December 2017).

Roth, J. P. *et al.* (2013) 'Deletion of the D domain of the human parainfluenza virus type 3 (HPIV3) PD protein results in decreased viral RNA synthesis and beta interferon (IFN-β) expression', *Virus Genes*, 47(1), pp. 10–19. doi: 10.1007/s11262-013-0919-x.

Roth, J. P., Li, J. K.-K. and Barnard, D. L. (2010) 'Human parainfluenza virus type 3 (HPIV-3): construction and rescue of an infectious, recombinant virus expressing the enhanced green fluorescent protein (EGFP).', *Current protocols in microbiology*, Chapter 15, p. Unit 15F.1. doi: 10.1002/9780471729259.mc15f01s17.

Rydbeck, R., Love, A. and Norrby, E. (1988) 'Protective effects of monoclonal antibodies against parainfluenza virus type 3-induced brain infection in hamsters', *Journal of General Virology*, 69(5), pp. 1019–1024. doi: 10.1099/0022-1317-69-5-1019.

Salvatore, M. *et al.* (2016) 'DAS181 for Treatment of Parainfluenza Virus Infections in Hematopoietic Stem Cell Transplant Recipients at a Single Center',

Biology of Blood and Marrow Transplantation, 22, pp. 965–970. doi: 10.1016/j.bbmt.2016.02.011.

Sanjuán, R. *et al.* (2010) 'Viral mutation rates.', *Journal of virology*. American Society for Microbiology, 84(19), pp. 9733–48. doi: 10.1128/JVI.00694-10.

Santolaya, M. E. E. *et al.* (2017) 'Efficacy and safety of withholding antimicrobial treatment in children with cancer, fever and neutropenia, with a demonstrated viral respiratory infection: a randomized clinical trial.', *Clinical microbiology and infection : the official publication of the European Society of Clinical Microbiology and Infectious Diseases*. Elsevier, 23(3), pp. 173–178. doi: 10.1016/j.cmi.2016.11.001.

Schaap-Nutt, A. *et al.* (2012) 'Human parainfluenza virus serotypes differ in their kinetics of replication and cytokine secretion in human tracheobronchial airway epithelium.', *Virology*. NIH Public Access, 433(2), pp. 320–8. doi: 10.1016/j.virol.2012.08.027.

Schindelin, J. *et al.* (2012) 'Fiji: an open-source platform for biological-image analysis', *Nature Methods*. Nature Research, 9(7), pp. 676–682. doi: 10.1038/nmeth.2019.

Schmidt, A. C. *et al.* (2001) 'Recombinant Bovine / Human Parainfluenza Virus Type 3 (B / HPIV3) Expressing the Respiratory Syncytial Virus (RSV) G and F Proteins Can Be Used To Achieve Simultaneous Mucosal Immunization against RSV and HPIV3', *Journal of Virology*, 75(10), pp. 4594–4603. doi: 10.1128/JVI.75.10.4594.

Schmidt, A. C. *et al.* (2012) 'Progress in the development of human parainfluenza virus vaccines', *Expert Rev Respir Med*. NIH Public Access, 5(4), pp. 515–526. doi: 10.1586/ers.11.32.Progress.

Schomacker, H. *et al.* (2012) 'Pathogenesis of acute respiratory illness caused by human parainfluenza viruses', *Current Opinion in Virology*. Elsevier B.V., 2(3), pp. 294–299. doi: 10.1016/j.coviro.2012.02.001.

Senchi, K. *et al.* (2013) 'Development of oligomannose-coated liposome-based

nasal vaccine against human parainfluenza virus type 3', *Frontiers in Microbiology*, 4(NOV), pp. 1–9. doi: 10.3389/fmicb.2013.00346.

Seo, S. *et al.* (2014) 'Parainfluenza Virus Lower Respiratory Tract Disease After Hematopoietic Cell Transplant: Viral Detection in the Lung Predicts Outcome', *Clinical Infectious Diseases*. Oxford University Press, 58(10), pp. 1357–1368. doi: 10.1093/cid/ciu134.

Shah, D. P. *et al.* (2016) 'Parainfluenza virus infections in hematopoietic cell transplant recipients and hematologic malignancy patients: A systematic review', *Cancer Letters*. Elsevier Ireland Ltd, 370(2), pp. 358–364. doi: 10.1016/j.canlet.2015.11.014.

Shanmugam, S. *et al.* (2013) 'Zanamivir oral delivery: enhanced plasma and lung bioavailability in rats.', *Biomolecules & therapeutics*. Korean Society of Applied Pharmacology, 21(2), pp. 161–9. doi: 10.4062/biomolther.2013.010.

Shi, W. *et al.* (2015) 'Prevalence of human parainfluenza virus in patients with acute respiratory tract infections in Beijing, 2011-2014', *Influenza and other Respiratory Viruses*, 9(6), pp. 305–307. doi: 10.1111/irv.12336.

Shil, N. K. *et al.* (2017) 'Inflammasome antagonism by human parainfluenza virus type 3 C protein', *Journal of Virology*, (November), p. JVI.01776-17. doi: 10.1128/JVI.01776-17.

Simon, A. K., Hollander, G. A. and McMichael, A. (2015) 'Evolution of the immune system in humans from infancy to old age', *Proceedings of the Royal Society B: Biological Sciences*, 282(1821), p. 20143085. doi: 10.1098/rspb.2014.3085.

Sissoko, D. *et al.* (2016) 'Experimental Treatment with Favipiravir for Ebola Virus Disease (the JIKI Trial): A Historically Controlled, Single-Arm Proof-of-Concept Trial in Guinea', *PLoS Medicine*, 13(3). doi: 10.1371/journal.pmed.1001967.

Smith, D. W. *et al.* (1991) 'A Controlled Trial of Aerosolized Ribavirin in Infants Receiving Mechanical Ventilation for Severe Respiratory Syncytial Virus Infection', *New England Journal of Medicine*. Massachusetts Medical Society,

325(1), pp. 24–29. doi: 10.1056/NEJM199107043250105.

Smith, E. C. *et al.* (2009) 'Viral entry mechanisms: the increasing diversity of paramyxovirus entry', *The FEBS journal*, 276(24), pp. 7217–7227. doi: 10.1111/j.1742-4658.2009.07401.x.

Söderman, M. *et al.* (2016) 'Frequent Respiratory Viral Infections in Children with Febrile Neutropenia - A Prospective Follow-Up Study', *PloS one*. Edited by O. Schildgen. Public Library of Science, 11(6), p. e0157398. doi: 10.1371/journal.pone.0157398.

Spriggs, M. K. *et al.* (1987) 'Expression of the F and HN glycoproteins of human parainfluenza virus type 3 by recombinant vaccinia viruses: contributions of the individual proteins to host immunity', *Journal of Virology*, 61(11), pp. 3416–3423.

Stark, J. M. *et al.* (1991) 'Infection of cultured human tracheal epithelial cells by human parainfluenza virus types 2 and 3', *J Virol Methods*, 31(1), pp. 31–45. Available at: http://www.ncbi.nlm.nih.gov/pubmed/1849915.

Stencel-Baerenwald, J. E. *et al.* (2014) 'The sweet spot: Defining virus-sialic acid interactions', *Nature Reviews Microbiology*, pp. 739–749. doi: 10.1038/nrmicro3346.

Stewart, C. E. *et al.* (2012) 'Evaluation of Differentiated Human Bronchial Epithelial Cell Culture Systems for Asthma Research', *Journal of Allergy*, 2012(di), pp. 1–11. doi: 10.1155/2012/943982.

Stewart, C. E., Randall, R. E. and Adamson, C. S. (2014) 'Inhibitors of the Interferon Response Enhance Virus Replication In Vitro ', *PLoS ONE*. Edited by S. A. Cormier. San Francisco, USA: Public Library of Science, 9(11), p. e112014. doi: 10.1371/journal.pone.0112014.

Stokes, A. *et al.* (1992) 'The complete nucleotide sequence of the JS strain of human parainfluenza virus type 3: comparison with the Wash/47885/57 prototype strain', *Virus Research*. Elsevier, 25(1–2), pp. 91–103. doi: 10.1016/0168-1702(92)90102-F.

Stokes, K. L. *et al.* (2011) 'Differential Pathogenesis of Respiratory Syncytial Virus Clinical Isolates in BALB/c Mice', *Journal of Virology*, 85(12), pp. 5782–5793. doi: 10.1128/JVI.01693-10.

Stone, R. and Takimoto, T. (2013) 'Critical Role of the Fusion Protein Cytoplasmic Tail Sequence in Parainfluenza Virus Assembly', *PLoS ONE*, 8(4). doi: 10.1371/journal.pone.0061281.

Storey, D. G. *et al.* (1987) 'Nucleotide sequence of the coding and flanking regions of the human parainfluenza virus 3 hemagglutinin-neuraminidase gene: Comparison with other paramyxoviruses', *Intervirology*, 27(May), pp. 69–80.

Suh, H.-S. *et al.* (2007) 'Astrocyte Indoleamine 2,3-Dioxygenase Is Induced by the TLR3 Ligand Poly(I:C): Mechanism of Induction and Role in Antiviral Response', *Journal of Virology*, 81(18), pp. 9838–9850. doi: 10.1128/JVI.00792-07.

Sullender, W. M. (2000) 'Respiratory syncytial virus genetic and antigenic diversity 36', *Clin.Microbiol.Rev.*, 13(0893–8512 (Print)), p. 1–15, table.

Suslov, A. *et al.* (2018) 'Hepatitis B Virus Does Not Interfere With Innate Immune Responses in the Human Liver', *Gastroenterology*. Elsevier, Inc, 154(6), pp. 1778–1790. doi: 10.1053/j.gastro.2018.01.034.

Suzuki, T. *et al.* (2001) 'Receptor Specificities of Human Respiroviruses', *Journal of Virology*, 75(10), pp. 4604–4613. doi: 10.1128/JVI.75.10.4604-4613.2001.

Tamura, K. *et al.* (2007) 'MEGA4: Molecular Evolutionary Genetics Analysis (MEGA) Software Version 4.0', *Molecular Biology and Evolution*. Oxford University Press, 24(8), pp. 1596–1599. doi: 10.1093/molbev/msm092.

Tamura, K. *et al.* (2013) 'MEGA6: Molecular Evolutionary Genetics Analysis Version 6.0', *Molecular Biology and Evolution*, 30(12), pp. 2725–2729. doi: 10.1093/molbev/mst197.

Tamura, K. and Nei, M. (1993) 'Estimation of the number of nucleotide substitutions in the control region of mitochondrial DNA in humans and chimpanzees.', *Molecular Biology and Evolution*. Oxford University Press, 10(3), pp. 512–526. doi: 10.1093/oxfordjournals.molbev.a040023.

Tan, L. *et al.* (2013) 'The comparative genomics of human respiratory syncytial virus subgroups A and B: genetic variability and molecular evolutionary dynamics.', *Journal of virology*. American Society for Microbiology, 87(14), pp. 8213–26. doi: 10.1128/JVI.03278-12.

Tavaré, S. (1986) 'Some Probabilistic and Statistical Problems in the Analysis of DNA Sequences', in *American Mathematical Society: Lectures on Mathematics in the Life Sciences*. Amer Mathematical Society, pp. 57–86. Available at: citeulike-article-id:4801403.

Thomas, E., Ghany, M. G. and Liang, T. J. (2012) 'The Application and Mechanism of Action of Ribavirin in Therapy of Hepatitis C', *Antiviral Chemistry and Chemotherapy*, 23(1), pp. 1–12. doi: 10.3851/IMP2125.

Thordal-Christensen, H. *et al.* (1997) 'Subcellular localization of H2O2 in plants. H2O2 accumulation in papillae and hypersensitive response during the barley-powdery mildew interaction', *The Plant Journal 11(6): 1187-1194.*, 11, pp. 1187–1194. doi: 10.1046/j.1365-313X.1997.11061187.x.

Tindal, D. J. *et al.* (2007) 'Synthesis and evaluation of 4-O-alkylated 2-deoxy-2,3-didehydro-N-acetylneuraminic acid derivatives as inhibitors of human parainfluenza virus type-3 sialidase activity', *Bioorganic and Medicinal Chemistry Letters*, 17(6), pp. 1655–1658. doi: 10.1016/j.bmcl.2006.12.105.

Torres, J. P. *et al.* (2016) 'Respiratory Viral Infections and Coinfections in Children With Cancer, Fever and Neutropenia', *The Pediatric Infectious Disease Journal*, 35(9), pp. 949–954. doi: 10.1097/INF.0000000000001209.

Triana-Baltzer, G. B. *et al.* (2009) 'Novel pandemic influenza A(H1N1) viruses are potently inhibited by DAS181, a sialidase fusion protein.', *PloS one*, 4(11), p. e7788. doi: 10.1371/journal.pone.0007788.

Tsutsui, R. *et al.* (2017) 'Genetic analyses of the fusion protein genes in human parainfluenza virus types 1 and 3 among patients with acute respiratory infections in Eastern Japan from 2011 to 2015', *Journal of Medical Microbiology*, 66(2), pp. 160–168. doi: 10.1099/jmm.0.000431.

Ustun, C. *et al.* (2012) 'Human Parainfluenza Virus Infection after Hematopoietic Stem Cell Transplantation: Risk Factors, Management, Mortality, and Changes over Time', *Biol Blood Marrow Transplant*, 18, pp. 1580–1588. doi: 10.1016/j.bbmt.2012.04.012.

Vainionpää, R. and Hyypiä, T. (1994) 'Biology of parainfluenza viruses.', *Clinical microbiology reviews*, 7(2), pp. 265–75. doi: 10.1128/CMR.7.2.265.Updated.

Van, K. L. *et al.* (1987) 'Antigenic and Structural Properties of the Hemagglutinin-Neuraminidase Glycoprotein of Human Parainfluenza Virus Type 3: Sequence Analysis of Variants Selected with Monoclonal Antibodies Which Inhibit Infectivity, Hemagglutination, and Neuraminidase Acti', *Journal of Virology*, 61(5), pp. 1473–1477. doi: 61(5):1473–1477.

Vanderlinden, E. *et al.* (2016) 'Distinct Effects of T-705 (Favipiravir) and ribavirin on influenza virus replication and Viral RNA Synthesis', *Antimicrobial Agents and Chemotherapy*. American Society for Microbiology, 60(11), pp. 6679–6691. doi: 10.1128/AAC.01156-16.

Vareille, M. *et al.* (2011) 'The airway epithelium: soldier in the fight against respiratory viruses.', *Clinical microbiology reviews*. American Society for Microbiology, 24(1), pp. 210–29. doi: 10.1128/CMR.00014-10.

Vilchez, R. A. *et al.* (2003) 'Parainfluenza Virus Infection in Adult Lung Transplant Recipients: An Emergent Clinical Syndrome with Implications on Allograft Function', *American Journal of Transplantation*. Munksgaard International Publishers, 3(2), pp. 116–120. doi: 10.1034/j.1600-6143.2003.00024.x.

Waghmare, A. *et al.* (2015) 'Successful treatment of parainfluenza virus respiratory tract infection with DAS181 in 4 immunocompromised children', *Journal of the Pediatric Infectious Diseases Society*. Oxford University Press, 4(2), pp. 114–118. doi: 10.1093/jpids/piu039.

Wang, F. *et al.* (2015) 'Parainfluenza Virus Types 1, 2, and 3 in Pediatric Patients with Acute Respiratory Infections in Beijing During 2004 to 2012', *Chinese Medical Journal*, 128(20), p. 2726. doi: 10.4103/0366-6999.167297.

Wang, Q. *et al.* (2017) 'M protein is sufficient for assembly and release of Peste des petits ruminants virus-like particles', *Microbial Pathogenesis*, 107, pp. 81–87. doi: https://doi.org/10.1016/j.micpath.2017.03.021.

Wang, R. *et al.* (2018) 'Influence of infectious disease seasonality on the performance of the outbreak detection algorithm in the China Infectious Disease Automated-alert and Response System', *Journal of International Medical Research*, 46(1), pp. 98–106. doi: 10.1177/0300060517718770.

Wang, W. *et al.* (2015) 'Molecular Genotyping of Human Rhinovirus by Using PCR and Sanger Sequencing', in Jans, D. A. and Ghildyal, R. (eds) *Rhinoviruses: Methods and Protocols*. New York, NY: Springer New York, pp. 39–47. doi: 10.1007/978-1-4939-1571-2_4.

Watts, D. M. *et al.* (1989) 'Inhibition of Crimean-Congo Hemorrhagic-Fever Viral Infectivity Yields Invitro By Ribavirin', *American Journal of Tropical Medicine and Hygiene*, 41(5), pp. 581–585.

Weinberg, G. A. *et al.* (2009) 'Parainfluenza virus infection of young children: estimates of the population-based burden of hospitalization.', *The Journal of pediatrics*, 154(5), pp. 694–9. doi: 10.1016/j.jpeds.2008.11.034.

Weinberg, P. N. *et al.* (2010) *SQL, the complete reference*. McGraw-Hill.

Weiser, A. A. *et al.* (2016) 'FoodChain-Lab: A Trace-Back and Trace-Forward Tool Developed and Applied during Food-Borne Disease Outbreak Investigations in Germany and Europe', *PLOS ONE*. Edited by P. R. Cleary. Public Library of Science, 11(3), p. e0151977. doi: 10.1371/journal.pone.0151977.

Westover, J. B. *et al.* (2016) 'Low-dose ribavirin potentiates the antiviral activity of favipiravir against hemorrhagic fever viruses', *Antiviral Research*, 126, pp. 62–68. doi: 10.1016/j.antiviral.2015.12.006.

Van Wyke Coelingh, K. L., Winter, C. and Murphy, B. R. (1985) 'Antigenic variation in the hemagglutinin-neuraminidase protein of human parainfluenza type 3 virus', *Virology*, 143(2), pp. 569–582. doi: 10.1016/0042-6822(85)90395-2.

Wymant, C. *et al.* (2018) 'PHYLOSCANNER: Inferring transmission from within- and between-host pathogen genetic diversity', *Molecular Biology and Evolution*, 35(3), pp. 719–733. doi: 10.1093/molbev/msx304.

Xie, W. *et al.* (2011) 'Improving Marginal Likelihood Estimation for Bayesian Phylogenetic Model Selection', *Systematic Biology*. Oxford University Press, 60(2), pp. 150–60. doi: 10.1093/sysbio/syq085.

Yamaya, M. *et al.* (2002) 'Human airway epithelial cell culture.', *Methods in molecular biology (Clifton, N.J.)*, 188, pp. 7–16. doi: 10.1385/1-59259-185-X:07.

Yamaya, M. *et al.* (2010) 'Clarithromycin Inhibits Type A Seasonal Influenza Virus Infection in Human Airway Epithelial Cells', *Journal of Pharmacology and Experimental Therapeutics*. American Society for Pharmacology and Experimental Therapeutics, 333(1), pp. 81–90. doi: 10.1124/jpet.109.162149.

Yang, X. *et al.* (2013) 'V-Phaser 2: variant inference for viral populations', *BMC Genomics*. BioMed Central, 14(1), p. 674. doi: 10.1186/1471-2164-14-674.

Yang, Z. (1994) 'Maximum likelihood phylogenetic estimation from DNA sequences with variable rates over sites: approximate methods.', *Journal of molecular evolution*, 39(3), pp. 306–14. Available at: http://www.ncbi.nlm.nih.gov/pubmed/7932792 (Accessed: 28 November 2017).

Ye, X. *et al.* (2010) '[A guinea pig model of parainfluenza virus type 3 infection-induced acute and postinfectious cough].', *Zhonghua jie he he hu xi za zhi = Zhonghua jiehe he huxi zazhi = Chinese journal of tuberculosis and respiratory diseases*, 33(12), pp. 907–11. Available at: http://www.ncbi.nlm.nih.gov/pubmed/21211410 (Accessed: 30 December 2015).

Yin, H.-S. *et al.* (2005) 'Structure of the uncleaved ectodomain of the paramyxovirus (hPIV3) fusion protein.', *Proceedings of the National Academy of Sciences of the United States of America*, 102(26), pp. 9288–93. doi: 10.1073/pnas.0503989102.

Young, D. F. *et al.* (2003) 'Virus Replication in Engineered Human Cells That Do Not Respond to Interferons Virus Replication in Engineered Human Cells That Do Not Respond to Interferons', *Journal of Virology*, 77(3), pp. 2174–2181. doi: 10.1128/JVI.77.3.2174.

Zambon, M. *et al.* (1998) 'Molecular epidemiology of two consecutive outbreaks of parainfluenza 3 in a bone marrow transplant unit', *Journal of Clinical Microbiology*. American Society for Microbiology, 36(8), pp. 2289–2293. Available at: http://www.ncbi.nlm.nih.gov/pubmed/9666007 (Accessed: 24 July 2017).

Zenilman, J. M. *et al.* (2015) 'Phase 1 clinical trials of DAS181, an inhaled sialidase, in healthy adults', *Antiviral Research*, 123, pp. 114–119. doi: 10.1016/j.antiviral.2015.09.008.

Zhang, L. *et al.* (2005) 'Infection of ciliated cells by human parainfluenza virus type 3 in an in vitro model of human airway epithelium.', *Journal of virology*, 79(2), pp. 1113–24. doi: 10.1128/JVI.79.2.1113-1124.2005.

Zhang, L. *et al.* (2011) 'Comparison of differing cytopathic effects in human airway epithelium of parainfluenza virus 5 (W3A), parainfluenza virus type 3, and respiratory syncytial virus', *Virology*. Academic Press, 421(1), pp. 67–77. doi: 10.1016/j.virol.2011.08.020.

Zhao, H. *et al.* (1996) 'Inhibition of Human Parainfluenza Virus-3 Replication by Interferon and Human MxA', *Virology*, 220(2), pp. 330–338. doi: https://doi.org/10.1006/viro.1996.0321.

Zhao, H. *et al.* (2017) 'Epidemiology of parainfluenza infection in England and Wales, 1998-2013: Any evidence of change?', *Epidemiology and Infection*, pp. 1210–1220. doi: 10.1017/S095026881600323X.

ppendix 1: Ethics approval

NHS
Health Research Authority

NRES Committee East of England - Norfolk
Victoria House
Capital Park
Fulbourn
Cambridge
CB21 5XB

Telephone: 01223 597733
Facsimile: 01223 597645

09 February 2012

Dr Hamid Jalal
Consultant Medical Virologist
Health Protection Agency
Box 236, Addenbrooke's Hospital
Hills Road, Cambridge
CB2 0QW

Dear Dr Jalal

Study title: **Genetic Diversity and Virulence of Human Parainfluenza Viruses**
REC reference: **12/EE/0069**

The Proportionate Review Sub-committee of the NRES Committee East of England - Norfolk reviewed the above application on 06 February 2012.

Ethical opinion

On behalf of the Committee, the sub-committee gave a favourable ethical opinion of the above research on the basis described in the application form, protocol and supporting documentation, subject to the conditions specified below.

Ethical review of research sites

The favourable opinion applies to all NHS sites taking part in the study, subject to management permission being obtained from the NHS/HSC R&D office prior to the start of the study (see "Conditions of the favourable opinion" below).

Conditions of the favourable opinion

The favourable opinion is subject to the following conditions being met prior to the start of the study.

Management permission or approval must be obtained from each host organisation prior to the start of the study at the site concerned.

Management permission ("R&D approval") should be sought from all NHS organisations involved in the study in accordance with NHS research governance arrangements.

Guidance on applying for NHS permission for research is available in the Integrated Research Application System or at http://www.rdforum.nhs.uk.

Where a NHS organisation's role in the study is limited to identifying and referring potential participants to research sites ("participant identification centre"), guidance should be sought from the R&D office on the information it requires to give permission for this activity.

For non-NHS sites, site management permission should be obtained in accordance with the procedures of the relevant host organisation.

Sponsors are not required to notify the Committee of approvals from host organisations.

It is the responsibility of the sponsor to ensure that all the conditions are complied with before the start of the study or its initiation at a particular site (as applicable).

You should notify the REC in writing once all conditions have been met (except for site approvals from host organisations) and provide copies of any revised documentation with updated version numbers. Confirmation should also be provided to host organisations together with relevant documentation.

Approved documents

The documents reviewed and approved were:

Document	*Version*	*Date*
Covering Letter from Dr Hamid Jalal		27 January 2012
REC application - IRAS Parts A&B	98588/287387/1/863	27 January 2012
Investigator CV - Dr Hamid Jalal		January 2012
Protocol	4	06 January 2012
Evidence of insurance or indemnity - NHS Litigation Authority		01 April 2011
Letter from Sponsor from Professor Paul Bosely		26 January 2012
Referees or other scientific critique report from Dr Mark Farrington		06 January 2012

Membership of the Proportionate Review Sub-Committee

The members of the Sub-Committee who took part in the review are listed on the attached sheet.

Statement of compliance

The Committee is constituted in accordance with the Governance Arrangements for Research Ethics Committees and complies fully with the Standard Operating Procedures for Research Ethics Committees in the UK.

After ethical review

Reporting requirements

The attached document "After ethical review – guidance for researchers" gives detailed guidance on reporting requirements for studies with a favourable opinion, including:

- Notifying substantial amendments
- Adding new sites and investigators
- Notification of serious breaches of the protocol
- Progress and safety reports
- Notifying the end of the study

The NRES website also provides guidance on these topics, which is updated in the light of changes in reporting requirements or procedures.

Feedback

You are invited to give your view of the service that you have received from the National Research Ethics Service and the application procedure. If you wish to make your views known please use the feedback form available on the website.

Further information is available at National Research Ethics Service website > After Review

12/EE/0069	**Please quote this number on all correspondence**

With the Committee's best wishes for the success of this project

Yours sincerely

pp **Dr Elizabeth Lund**
Chair

Email: Anna.Bradnam@eoe.nhs.uk

Enclosures: *List of names and professions of members who took part in the review*

"After ethical review – guidance for researchers" [SL-AR2]

Cc: Professor Paul Boseley (Sponsor Contact)
Health Protection Agency R&D Office
Porton Down
Salisbury
SP4 0JG

Mr Stephen Kelleher, (NHS R&D Contact)
Cambridge University Hospitals NHS Foundation Trust
R&D Unit, Box 277
Hills Road
Cambridge
CB2 0QQ

NRES Committee East of England - Norfolk

Attendance at PRS Sub-Committee of the REC meeting on 06 February 2012

Committee Members:

Name	*Profession*	*Present*	*Notes*
Mr Ron Driver	University Lecturer	Yes	
Ms Leanne Groves	Psychological Therapist/Occupational Therapist	Yes	
Mrs Pamela Keeley	Retired East Anglian Eye Bank Nurse Manager	Yes	
Dr Elizabeth Lund (Chair)	Independent Consultant, Nutrition and Gastrointestinal Health	Yes	

Also in attendance:

Name	*Position (or reason for attending)*
Miss Anna Bradnam	Committee Co-ordinator

Appendix 2 – Full sequences for primer optimization

A

Oligo Name	Sequence (5'-3')
KK-XF	ACCAAACAAGAGAAGARACTTGTYTG
KK-XR2	TCCAGGTCACTTCCAAATATCCA
KK-1F	CAGCYGGTGGAGCTATCATT
KK-1R	GAGCTGCTTCTTCTCCCAGG
KK-NR1F	AAACAARGCAGTCAACCACC
KK-NR1R	TCTGTTTGCCCCTTTGTGTC
KK-NR2R	TGGCATCRAACAGCATTCCT
KK-3F	ACCCCACATTAGAGTTGCCA
KK-3R	TCCTGCTGCTTCACAACCTA
KK-4F	GGACACAAAYAAAGCAGTGC
KK-4R	AGGAGTGCTAGAGARATGACT
KK-5F	ACTCAGACTTGGTACCTGACT
KK-5R	TGCACTTATATTCCATCGGCC
KK-6F	AYGTGCTATCRAAATTAGCCTCA
KK-7F	ATAGGYGTGAGGGTGACTGC
KK-7R	TGTGAGGCTTCCATCCAAGA
KK-8F	GGACTTGAAACRCCTGACCCA
KK-8R	GGAAGAGCCTGTCCTTGTCT
KK-9F	GAAGGTAGRGATCTCATTTGGGA
KK-9R	CCTGTAAGYAATCGAGTCGAT
KK-10F	TYGGAATCAACAGCACTAGTTG
PIV-5R	ACCAAACAAGAGAAGAACTCTGYTTGG

B

Oligo Name	Sequence (5'-3')
NR1Ra	GCYTCTTCCATRATCACTGTTTCTAC
NR1Rb	CGATTGCTCTCTTCTGTATCCTTCC
NR2Fa	CACACGAATRTACAACRGAAGG
NR2Fb	TGGTCYCTRGAGGAATCYCC
6Ra	AGCYTGAGGAAGAATTCTCCCATCATA
6Rb	CCAGARTCAGGGTGATCCTCYAATGA
7Fa	TTGGTTACAYCCTCGTCTTGAAGGAAG
7Fb	CAATCTATGTAGGTGATCCTTACTGYCCT

Full primer sequences for primer optimization. Sequences for primers identified in the pilot study (panel A) as well as those used for further optimization (panel B) are shown. Primer sets used for the amplification of the MK9 genome, together with the respective amplicons generated are shown in **Figure 3-13**.

Appendix 3 – Pipeline and primers for sequencing of full HPIV3 genome

Full pipeline used for NGS sequencing of full HPIV3 genome

```
#! /usr/bin/perl -w

#
#
#
# command line switches
# -h                    - prints out the syntax and exits
# -s                    - only prints out the commands of the pipelines, without running
them
# -c <config file>      - configuration file name
# -i <input file>
# -r <reference>
# -w <working directory>  - if not specified a directory with name derived from
the input file name will be used
# -l <log file>         - if not specified STDOUT will be used
#
# tools used:
#
# cutadapt
# trim_galore
# FastQC
# bowtie2
# samtools
# Picard
# GATK
# VPhaser2
#
#
# 09 Dec 2016
```

```
use strict;

use File::Copy;
use Cwd;

####################################
#
# declare some global variables
#
####################################

# store the current perl working dir
my $curdir = cwd();

# declare variables to keep the command line options
my($input, $reference, $working_dir, $logfile, $cfgfile);

# this variable will control if the actual tools are called or just the commands
printed out
use vars qw($simul_only);

# this is the log file handle variable
use vars qw($logfh);

####################################
#
# process the commmand line switches
#
####################################

use Getopt::Std;
```

```
# declare the perl command line flags/options we want to allow
my %cfg=();
getopts("hsc:i:r:w:l:", \%cfg);

# prepare usage help string
my $syntax_help = "$0 -c <config file> -i <input file stub (no extension)> -r
<reference file stub (no extension)> -w <work folder> -l <log file>";

# print the help and die if -h switch is provided
# die $syntax_help if defined $cfg{h};
if (defined $cfg{h}) {
  print "Usage:\n$syntax_help.\n";
  exit;
}

# retrieve the command line options
$simul_only = 1 if defined $cfg{s};
($cfgfile = $cfg{c}) or die "Configuration file name parameter missing, syntax:\n
$syntax_help";
($input = $cfg{i}) or die "Input file name parameter missing, syntax:\n
$syntax_help";
($reference = $cfg{r}) or die "Reference file name parameter missing, syntax:\n
$syntax_help";
if (defined $cfg{w}) {
   $working_dir = $cfg{w};
}
else {
   $working_dir = "$curdir/${input}.wd";
}
$logfile = $cfg{l};

# Create the working directory if it does not exist
if (! -e $working_dir) {
```

```
   mkdir $working_dir || die "Could not create folder $working_dir";
}

# Prepare the log file
if ($logfile) {
   open( $logfh, ">", $logfile );
}



#################################
# Load configuration from a povided cfg file
#
# we are expecting a file with <name>=<value> pairs, one in each line containing
the following parameters:
#   input =              # this is the input file name stub, without .1.fq, etc
#   reference =          # this is the reference.fa file without fa extension
#   working_folder =     # this is where the various temporary files will be
created
#   forward_primers_file =   # this is the file name containing a list of forward
primers, one per line
#   reverse_primers_file =   # this is the file name containing a list of reverse
primers, one per line
#################################

open( CONFIG, "<", $cfgfile ) or die "Could not load the configuration file $cfgfile";

my $cfg;
while (<CONFIG>) {
   chomp;               # no newline
   s/#.*//;             # no comments
   s/^\s+//;            # no leading white
   s/\s+$//;            # no trailing white
   next unless length;     # anything left?
```

```
   my ($var, $value) = split(/\s*=\s*/, $_, 2);
   $cfg{$var} = $value;
}

close (CONFIG);

#########
#
# Paths to various tools to use
#
#########

sub repltilda {
  my $orgname = shift;
  $orgname =~ s/~/$ENV{HOME}/;
  return $orgname;
}

my $cutadapt_master_bin_dir = repltilda($cfg{cutadapt_master_bin_dir}) if
defined $cfg{cutadapt_master_bin_dir};
my $cutadapt_dir = repltilda($cfg{cutadapt_dir})  if defined $cfg{cutadapt_dir};
my $FastQC_dir  = repltilda($cfg{FastQC_dir})  if defined $cfg{FastQC_dir};
my $trim_galore_dir = repltilda($cfg{trim_galore_dir})  if defined
$cfg{trim_galore_dir};
my $picard_dir = repltilda($cfg{picard_dir})  if defined $cfg{picard_dir};
my $gatk_dir = repltilda($cfg{gatk_dir})  if defined $cfg{gatk_dir};
my $vphaser2_dir = repltilda($cfg{vphaser2_dir})  if defined $cfg{vphaser2_dir};

# these are the file names containing lists of forward and reverse primers
(respectively), one primer per line
my $forward_primers_file = repltilda($cfg{forward_primers_file}) if defined
$cfg{forward_primers_file};
```

```
my $reverse_primers_file = repltilda($cfg{reverse_primers_file}) if defined
$cfg{reverse_primers_file};


#########
#
# check if the required settings are there
#
#########

die 'variable cutadapt_master_bin_dir not set in the config file' if !
$cutadapt_master_bin_dir;
die 'variable cutadapt_dir not set in the config file' if ! $cutadapt_dir;
die 'variable FastQC_dir not set in the config file' if ! $FastQC_dir;
die 'variable trim_galore_dir not set in the config file' if ! $trim_galore_dir;
die 'variable picard_dir not set in the config file' if !$picard_dir;
die 'variable gatk_dir not set in the config file' if ! $gatk_dir;
die 'variable vphaser2_dir not set in the config file' if ! $vphaser2_dir;

# these are the file names containing lists of forward and reverse primers
(respectively), one primer per line
die 'variable forward_primers_file not set in the config file' if !
$forward_primers_file;
die 'variable reverse_primers_file not set in the config file' if !
$reverse_primers_file;

###############
#
# define cmd_run function
#
##############

sub cmd_run {
```

```
    my $cmd_to_run = shift;
    my $title = shift;
    my $run_regardless = shift;

    my $logmsg = "\n######### $title  ######\n";
    $logmsg .= "$cmd_to_run\n";

    # print to the log file
    if ($logfh) {
            print $logfh $logmsg;
    }

    # print to STDOUT
    print $logmsg;

    if ((! $simul_only) || ($run_regardless)) {
      $logmsg = `$cmd_to_run` . "\n";

      # print to the log file
      if ($logfh) {
              print $logfh $logmsg;
      }

      # print to STDOUT
      print $logmsg;
    }
}


###############
#
# define log_msg function
#
```

```
###############

sub log_msg {
   my $msg = shift;
   my $fh = shift;

   my $logmsg = "\n###### $msg\n";

   # print to the log file
   if ($fh) {
         print $fh $logmsg;
   }

   # print to STDOUT
   print $logmsg;
}



################
#
# define get_primers function
#
# procedure takes the primers file name and the switch to use with them and
produces one string of primers ready to be used in a cmd
#
###############
sub get_primers {
   my $primers_file = shift;
   my $prefix = shift;
   my $primers = '';

   open( PRMFILE, "<", "$primers_file" ) or die "Cannot open primers file
$primers_file: " . $!;
```

```
  while (<PRMFILE>) {
        chomp;              # no newline
        s/#.*//;            # no comments
    s/^\s+//;           # no leading white
        s/\s+$//;           # no trailing white
    next unless length;     # anything left?
    $primers .= " -$prefix $_";
  }
  return $primers;
}


#########################
#
#   Start the pipepline
#
#########################

my $cmd;


###
# STEP 0: read the forward and reverse primers list
###

log_msg("Reading primers from $forward_primers_file and
$reverse_primers_file");
my $forward_primers = get_primers("$forward_primers_file",'a');
my $reverse_primers = get_primers("$reverse_primers_file",'G');

###
# STEP 1: go to trip galore folder for initial calculations
###
```

```
chdir $trim_galore_dir or die $! . ":  trim_galore_dir = $trim_galore_dir";
cmd_run("pwd","change directory to $trim_galore_dir",1);

###
# STEP 2: export paths
###

# these should not be neeed
# $ENV{PATH} = "/usr/local/bin:$ENV{PATH}";
# $ENV{PATH} = "/usr/bin:$ENV{PATH}";

#$ENV{PATH} = "$cutadapt_master_bin_dir:$ENV{PATH}";
#$ENV{PATH} = "$cutadapt_dir:$ENV{PATH}";
#$ENV{PATH} = "$FastQC_dir:$ENV{PATH}";

log_msg( "PATH=" .$ENV{PATH} );



###
# STEP 3:  remove NEXTERA adapters
# produces 2 files: output.1.fq, output.2.fq
###
$cmd = "cutadapt -a CTGTCTCTTATA -G TATAAGAGACAG -o output.1.fq -p
output.2.fq ${input}.1.fq ${input}.2.fq";
cmd_run($cmd,"remove NEXTERA adapters");

###
# STEP 4  remove amplicon primers
# produces 2 files:  output.1f.fq, output.2f.fq
###

# run the removal tool
```

```
$cmd = "cutadapt $forward_primers $reverse_primers -o output.1f.fq -p
output.2f.fq output.1.fq output.2.fq";
cmd_run($cmd,"Remove amplicon primers ");



###
# STEP 5   run final check fastQC
#
# output of this is output.1f_val_1.fq  output.2f_val_2.fq
##
$cmd = "./trim_galore --paired --trim1 output.1f.fq output.2f.fq";
cmd_run($cmd,"run final check fastQC ");

# move  output.1f_val_1.fq  output.2f_val_2.fq to $working_dir
log_msg("move  output.1f_val_1.fq output.2f_val_2.fq to $working_dir");
if (! $simul_only) {
  move( "output.1f_val_1.fq", "$working_dir/output.1f_val_1.fq") or die $!;
  move( "output.2f_val_2.fq", "$working_dir/output.2f_val_2.fq") or die $!;
}

# cd ~/$working_dir
chdir $working_dir;
cmd_run("pwd","change directory to $working_dir",1);

##
# STEP 8 build sequence index using Bowtie
##
$cmd = "bowtie2-build ${reference}.fa $reference";
cmd_run($cmd,"build sequence index using Bowtie  ");

##
# STEP 9 index reference sequence (samtools)
#
```

```
# This will create ${reference}.fa.fai
##
$cmd = "samtools faidx ${reference}.fa";
cmd_run($cmd,"index reference sequence (samtools)  ");

##
# Step 10 create sequence dictionary (picard)
##

# copy reference.fa and reference.fa.bai to ~/picard
log_msg("copy ${reference}.fa and ${reference}.fa.fai to $picard_dir");
if (! $simul_only) {
  copy( "${reference}.fa",  $picard_dir ) or die $!;
  copy( "${reference}.fa.fai",  $picard_dir ) or die $!;
}

#cd ~/picard
chdir $picard_dir;
cmd_run("pwd","change directory to $picard_dir",1);

$cmd = "java -jar picard.jar CreateSequenceDictionary R= ${reference}.fa
O=${reference}.dict";
cmd_run($cmd,"create sequence dictionary (picard) ");



##
# align using bowtie2
#
# will create alignedoutput.sam
#
##

# cd ~/$working_dir
```

```
chdir $working_dir;
cmd_run("pwd","change directory to $working_dir",1);

$cmd = "bowtie2 -x $reference -1 output.1f_val_1.fq -2 output.2f_val_2.fq -S
alignedoutput.sam";
cmd_run($cmd,"align using bowtie2 ");

##
# step 14 convert alignment from sam to bam
#
# will create alignedoutput.bam
#
##

$cmd = "samtools view -bSo alignedoutput.bam alignedoutput.sam";
cmd_run($cmd,"convert alignment from sam to bam ");

##
# step 15 sort bam file
#
# will create ${input}.sorted.bam
##

$cmd = "samtools sort -o ${input}.sorted.bam alignedoutput.bam";
cmd_run($cmd,"sort bam file  ");

##
# step 16 index bamfile
#
# will create ${input}.sorted.bam.bai
##

$cmd = "samtools index  ${input}.sorted.bam";
```

```
cmd_run($cmd,"index bamfile ");

##
# step 17 mark duplicates in picard
#
# will create output.dups.bam and output.dups.txt
##

# copy the files needed
log_msg( "copy  ${input}.sorted.bam and ${input}.sorted.bam.bai to
$picard_dir");
if (! $simul_only) {
  copy(  "${input}.sorted.bam", $picard_dir ) or die $!;
  copy(  "${input}.sorted.bam.bai", $picard_dir)  or die $!;
}

# Change to the right directory
chdir $picard_dir;
cmd_run("pwd","change directory to $picard_dir",1);

# Run the command
$cmd = "java -jar picard.jar MarkDuplicates I=${input}.sorted.bam
O=output.dups.bam METRICS_FILE=output.dups.txt REMOVE_DUPLICATES=true
VALIDATION_STRINGENCY=LENIENT";
cmd_run($cmd,"mark duplicates in picard ");



##
# removed addorreplace groups and fixmate with PICARD
# see full annapipeline for full flow
##
```

```
$cmd = "samtools sort -o output.dups.sorted.bam output.dups.bam";
cmd_run($cmd,"sort file ");

##
# step 23 index file
#
# this will produce output.dups.sorted.bam.bai
##

$cmd = "samtools index output.dups.sorted.bam";
cmd_run($cmd,"index the file  ");

##
# removed realign for indels, as conflict with VPhaser2
#
#
##




# copy the output files to ~/VPhaser-2-02112013 and to the working directory
log_msg( "Copy output.dups.sorted.bam and output.dups.sorted.bam.bai to
$vphaser2_dir and $working_dir");
if (! $simul_only) {
  copy( "output.dups.sorted.bam", $vphaser2_dir) or die $!;
  copy( "output.dups.sorted.bam.bai", $vphaser2_dir) or die $!;
  copy( "output.dups.sorted.bam", $working_dir) or die $!;
  copy( "output.dups.sorted.bam.bai", $working_dir) or die $!;
}

# change to the vphaser directory
chdir $vphaser2_dir;
```

```
cmd_run("pwd","change directory to $vphaser2_dir",1);

# create folder $input in ~/ VPhaser-2-02112013
log_msg( "Creating output folder $vphaser2_dir/$input" );
mkdir "$input" || die "Could not create folder $vphaser2_dir/$input";

# launch VPhaser
$cmd = "OMP_NUM_THREADS=8  bin/variant_caller -i output.dups.sorted.bam  -
o ${input}";
cmd_run($cmd,"run VPhaser ");

# cleanup - important as it messes up next runs
log_msg( "Deleting temorary files output.dups.sorted.bam,
output.dups.sorted.bam.bai and output.dups.sorted.bam.bti from
$vphaser2_dir");
if (! $simul_only) {
  unlink("$vphaser2_dir/output.dups.sorted.bam");
  unlink("$vphaser2_dir/output.dups.sorted.bam.bai");
  unlink("$vphaser2_dir/output.dups.sorted.bam.bti");
}

##
#  Closing tasks
##

# Print finish message
log_msg( "All Done. Phew!" );

# close the log file
if ($logfh) {
   close $logfh;
}
```

Forward primers list

ACCAAACAAGAGAAGAAACTTGTCTG

ACCAAACAAGAGAAGAGACTTGTCTG

ACCAAACAAGAGAAGAGACTTGTTTG

CAGCCGGTGGAGCTATCATT

CAGCTGGTGGAGCTATCATT

AAACAAAGCAGTCAACCACC

ACCCCACATTAGAGTTGCCA

GGACACAAACAAAGCAGTGC

GGACACAAATAAAGCAGTGC

ACTCAGACTTGGTACCTGACT

ACGTGCTATCAAAATTAGCCTCA

ACGTGCTATCGAAATTAGCCTCA

ATGTGCTATCAAAATTAGCCTCA

ATGTGCTATCGAAATTAGCCTCA

ATAGGCGTGAGGGTGACTGC

ATAGGTGTGAGGGTGACTGC

GGACTTGAAACACCTGACCCA

GGACTTGAAACGCCTGACCCA

GAAGGTAGAGATCTCATTTGGGA

GAAGGTAGGGATCTCATTTGGGA

TCGGAATCAACAGCACTAGTTG

TTGGAATCAACAGCACTAGTTG

ACCAAACAAGAGAAGAAACTTGTTTG

AAACAAGGCAGTCAACCACC

TGGTCCCTAGAGGAATCCCC

TGGTCCCTAGAGGAATCTCC

TGGTCCCTGGAGGAATCCCC

TGGTCCCTGGAGGAATCTCC

TGGTCTCTGGAGGAATCTCC

TGGTCTCTGGAGGAATCCCC

TGGTCTCTAGAGGAATCCCC

TGGTCTCTAGAGGAATCTCC

Reverse primers list

TGGATATTTGGAAGTGACCTGGA

CCTGGGAGAAGAAGCAGCTC

GACACAAAGGGGCAAACAGA

AGGAATGCTGTTTGATGCCA

AGGAATGCTGTTCGATGCCA

TAGGTTGTGAAGCAGCAGGA

AGTCATCTCTCTAGCACTCCT

GGCCGATGGAATATAAGTGCA

TATGATGGGAGAATTCTTCCTCAGGCT

TATGATGGGAGAATTCTTCCTCAAGCT

TCTTGGATGGAAGCCTCACA

AGACAAGGACAGGCTCTTCC

ATCGACTCGATTGCTTACAGG

ATCGACTCGATTACTTACAGG

CCAAGCAGAGTTCTTCTCTTGTTTGGT

CCAAACAGAGTTCTTCTCTTGTTTGGT

GGACACAAATAAAGCAGTGC